ROBUST STATISTICAL SUBSPACE-BASED DAMAGE ASSESSMENT

by

Saeid Allahdadian

B.Sc., Isfahan University of Technology, 2008

M.Sc., Isfahan University of Technology, 2011

A THESIS SUBMITTED IN PARTIAL FULFILLMENT OF

THE REQUIREMENTS FOR THE DEGREE OF

DOCTOR OF PHILOSOPHY

in

THE FACULTY OF GRADUATE AND POSTDOCTORAL STUDIES

(Civil Engineering)

THE UNIVERSITY OF BRITISH COLUMBIA

(Vancouver)

July 2017

Abstract

The rapid spread and increasing affordability of sensors, are encouraging the government and stake-holders to instrument important infra-structures and structures. These sensors generate vast amount of data which can be used in real-time health monitoring of the instrumented structures by using damage identification methods.

A significant component of structural health monitoring is damage identification methods which process the data with the purpose of detecting damages in the structures. One of these methods with a theoretical background is the statistical subspace damage identification method (SSDI). The overarching goal in this thesis is to close the gap between theory and practice, in order to have a method with a strong theoretical background and a credible applicability at the same time.

In order to achieve this goal several contributions are motivated in this thesis, which are presented as follows:

Firstly, the effect of two challenges faced in the damage detection of structures under real test conditions, namely the measurement noise and duration (length), are theoretically evaluated. It is demonstrated that the measurement noise and length have considerable influence on the statistical subspace damage detection method and they need to be considered based on these proposed theories.

Secondly, the statistical subspace damage localization (SSDL) method, is assessed for the first time, in localizing the damage of a real experimental structure, i.e. the Yellow frame, established on the course of this research at UBC. Several methods and theories are developed in order to enable this method in identifying the damage under real test conditions. It was

demonstrated that by employing the proposed theories, the SSDL method can robustly locate the damage in a real structure such as the Yellow frame.

Finally, two indexes are proposed in predicting the detectability of damage in each element of a structure. These indexes provide valuable information on the sensitivity of SSDL method to the damage in each element.

All the proposed theories and methods are demonstrated theoretically; subsequently, they are verified by simple and sophisticated analytical models, and finally, they are validated by real-test data.

Lay Summary

Structural health monitoring is regarded as the main tool in assessing the functionality of existing structures. The importance of these techniques emerges by considering that failure of an infrastructure results in catastrophic loss. With such techniques, damages in a structure can be detected, before reaching dangerous levels. One of the robust damage detection techniques with strong theoretical background is the statistical subspace damage identification (SSDI) method.

In this thesis, the goal is to enable the SSDI method to detect damages in existing structures not only in theory but also in practice. Therefore, several theories and methods are developed and validated to assist the SSDI method in detection and localization (finding the existence and location) of damages in practice. These theories and methods not only help in predicting and treating the problems faced under real testing conditions, but also they provide valuable insight into the method and interpretation of the results.

Preface

This thesis presents the research conducted by Saeid Allahdadian under the supervision of Dr. Carlos E. Ventura from the University of British Columbia and Dr. Michael Döhler from INRIA research centre at France. Several publications are resulted from this work which are listed at the end of this section.

The contents of this thesis are drafted by the author and finalized in an iterative manner with Dr. Michael Döhler and Dr. Carlos E. Ventura. The contents of Chapters 4 and 6 and Appendix A are published in four conference papers (P1-4); a Journal paper (P5) is also in submission from these chapters and appendix. The contents of Chapters 5 and 7 are used in preparing one accepted conference paper (P6) and one Journal paper (P7).

The work presented in this thesis is performed by Saeid Allahdadian, including the literature review, designing and implementing the proposed theories and methods, designing and implementing the analytical tests (Chapter 6), building and assembling the experimental test, i.e. the Yellow frame, experimenting and analyzing the data (Chapter 7), and writing this manuscript. The theories presented in Chapters 4 and 5 and Appendix A were developed collaboratively by the author of this thesis and Dr. Laurent Mevel, and Dr. Michael Döhler, during the visit of Saeid Allahdadian to INRIA research centre. The basic coding related to the damage detection and localization method was provided by INRIA research centre. The proposed theories and methods are designed and implemented in coding by Saeid Allahdadian.

The FE model of the S101 bridge used in this thesis is created by Dr. Carlos E. Ventura. The structure and materials of the Yellow frame test were provided by Dr. Carlos E. Ventura. The entire work was conducted by Saeid Allahdadian under the supervision and editorial input from Dr. Carlos E. Ventura and Dr. Michael Döhler.

[P1] Allahdadian, S., Döhler, M., Ventura, C. E., and Mevel, L. (2016). "On the Influence of Sample Length and Measurement Noise on the Stochastic Subspace Damage Detection Technique." *SHM, Damage Detection & Mechatronics, Volume 7. Conference Proceedings of the Society for Experimental Mechanics Series, IMAC*. Springer, Cham, 35–46.

[P2] Allahdadian, S., Ventura, C., Andersen, P., Mevel, L., and Döhler, M. (2015). "Subspace based damage detection technique: investigation on the effect of number of samples." *CCEE-11th Canadian Conference on Earthquake Engineering*.

[P3] Allahdadian, S., Ventura, C., Andersen, P., Mevel, L., and Döhler, M. (2015). "Investigation on the sensitivity of subspace based damage detection technique to damage and noise levels." *IOMAC-International Operational Modal Analysis Conference*.

[P4] Allahdadian, S., Ventura, C. E., Andersen, P., Mevel, L., and Döhler, M. (2015). "Sensitivity Evaluation of Subspace-Based Damage Detection Method to Different Types of Damage." *SHM and Damage Detection*, Volume 7. *Conference Proceedings of the Society for Experimental Mechanics Series*, *IMAC*. Springer, Cham, 11–18.

[P5] Allahdadian, S., Ventura, C. E., Andersen, P., Mevel, L., and Döhler, M., "Theoretical investigation of the effect of measurement noise and length on the statistical subspace damage detection method." to be submitted.

[P6] Allahdadian, S., Ventura, C. E., Andersen, P., Mevel, L., and Döhler, M., (2017) "Practical investigation of the statistical subspace damage localization method." accpeted in *The 11th International Workshop on Structural Health Monitoring IWSHM 11, Stanford, CA*.

[P7] Allahdadian, S., Ventura, C. E., Andersen, P., Mevel, L., and Döhler, M., "Practical investigation of the statistical subspace damage localization method." To be submitted.

Table of Contents

List of Tables

List of Figures

Acknowledgments

I would like to express my sincere gratitude towards my supervisor Dr. Carlos Ventura for his constant support and guidance throughout my PhD studies. I have been gratefully fortunate to have his unwavering support on the despair moments of life. I am profoundly grateful to him for giving me the freedom and guidance in choosing and exploring the way in the ocean of knowledge while providing me with fruitful opportunities on this adventurous journey. I would like to extend my profound gratitude to my co-supervisor Dr. Michael Döhler for his generous and welcoming support. I am deeply indebted to Dr. Döhler for his continuous support and warm encouragements. Indeed, this thesis was not possible without his insightful comments and helps.

I take this opportunity to acknowledge Dr. Laurent Mevel from the INRIA research centre at France, for his welcoming support and enlightening discussions we had together with Dr. Döhler, during my joyful visit to France. His brilliance was unforgettably delightful whenever I had the pleasure of our conversation.

I would also like to wholeheartedly extend my appreciation to the members of my PhD supervisory committee: Dr. Rune Brincker from the Faculty of Civil engineering at the Technical University of Denmark for his inspiring and enlightening discussions, deep interest and tremendous support, and Dr. Ricardo Foschi for his dedication, insightful discussions and warmheartedly comments during our meetings. I am vastly honored of having the opportunity of working with them.

My appreciation extends to all of my colleagues and friends for their helps and joyful company during this journey. Many thanks go to Hamed Taheri, Neda Afghari, Salman Soleimani, Meraj Afshord, Sima Valizadeh, Abbas Javaherian, Sardaar Malek, Ilaria Capraro and Andres Barrero.

Special thanks are owed to my parents and sisters, to whom this thesis is dedicated. Despite the long distance between us, my family has been a constant source of unconditional love, support, endless patience and encouragement in every step of my life. Words cannot express my heartfelt appreciation to them.

Finally, I would like to thank gratefully the George third and sons company Ltd for their generous donation of three accurately customized foundation beams for the Yellow frame structure, the financial support from the office of Graduate and Postdoctoral Studies at the University of British Columbia (Four Year Doctoral Fellowship), and the Natural Science and Engineering Research Council of Canada (NSERC), and MITACS-INRIA (Globalink) for providing me the opportunity of a research-collaboration-trip to INRIA research centre at Rennes in France.

Dedication

To my beloved family

Chapter 1: Introduction

Structural health monitoring is regarded as the main tool in assessing the functionality of existing structures. The importance of the research on this technique becomes obvious by considering that failure of a structure can result in catastrophic loss. Existing civil structures deteriorate by aging and under different loading conditions imposed from natural phenomena such as earthquakes, typhoons, flood and etc. Therefore, it is imperative to investigate the safety of continuing to use these structures, especially after occurring major loads on them from these phenomena.

With the advent of new technologies, instrumentation of structures is becoming widespread. The data acquired from the instrumented structures can provide beneficial information on their structural conditions. However, efficient techniques and methods are necessary in processing this data in order to assess the functionality of the structure.

As an example, consider a structure such as Figure 1.1, which we need to assess its current conditions (safe or unsafe). The sensors located on the structure provide data measured from the structure at any time. This data can be acquired from the undamaged and possibly damaged (current) structure and subsequently processed (compared) to evaluate if the structure is damaged or not, by using damage identification techniques.

Damage identification methods are the main component of structural health monitoring which process the data in order to detect damages in the structure. Among these methods, the statistical subspace damage identification method has a strong theoretical foundation. This technique can detect the damage in a structure by creating a subspace from measurement data in a reference (healthy) state. This subspace is based on the modeshapes of the structure but without actual computation of them. This subspace is employed in a statistical comparison along with the data measured from the possibly damaged structure in assessing the condition of the structure.

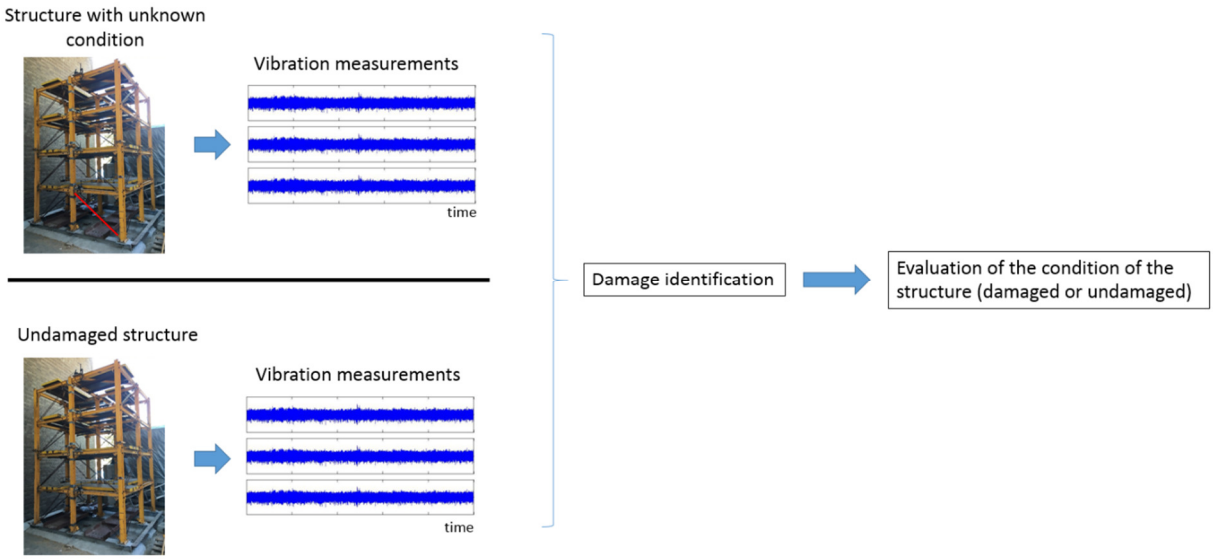

Figure 1.1 Structural condition evaluation using the damage identification techniques

The overarching goal in this thesis is to close the gap between the theory and applications, in order to have a method with strong theoretical background and great functionality under real test conditions. This goal is towards the vision behind this thesis, which is to create a platform in real-time monitoring of the conditions of any structure. Theoretical analyses of this method are carried out, and the theories and methods necessary to achieving this goal are developed. These theories and methods are verified by analytical models, and finally validated by the real data acquired from several tests on an experimental structure, i.e. the Yellow frame, at UBC.

1.1 Vision

The long-term vision behind this thesis is to create a platform to monitor the conditions of any structure or infrastructure continuously in real-time. This monitoring includes all levels of damage identification through ambient vibration testing: detecting if the structure is damaged, locating the damaged element/s, quantizing the extent of the damage and finally predicting the remaining life of the structure. This also helps in assessing the resilience of a structure. Particularly, the first three levels of damage identification in this platform are envisioned as a chart, namely a control chart,

depicting a damage index which represents the condition of the structure versus time in comparison to a threshold, namely, safety threshold. This damage index is evaluated from a statistical test using the statistical subspace damage detection and localization method ((Basseville et al. 2000); (Basseville et al. 2004)). This chart is exemplified in Figure 1.2.

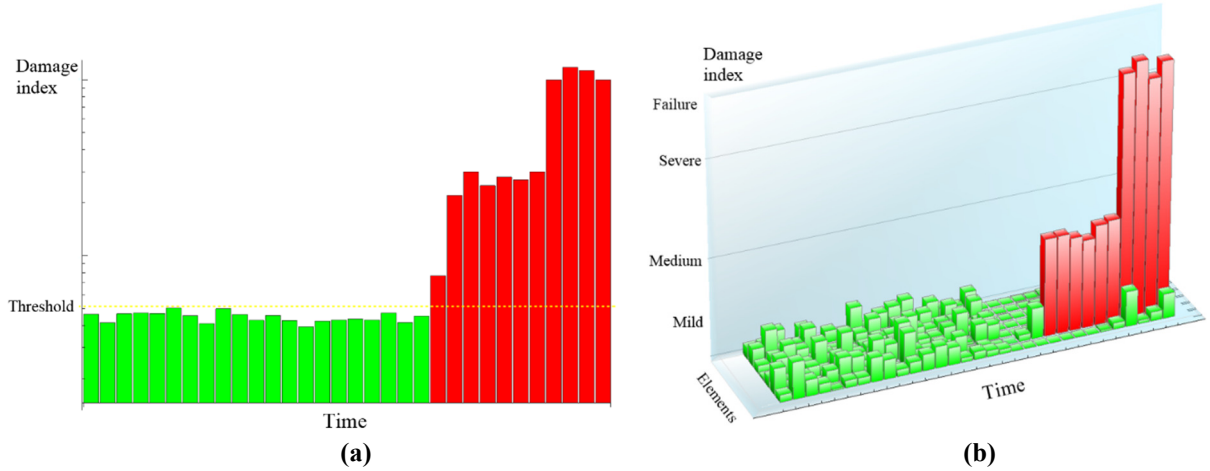

Figure 1.2 Control chart used in assessing the condition of the structure in terms of (a) existence of damage in the structure and (b) the location and extent of the detected damage

This vision entails assessing the functionality of the statistical subspace damage identification method in facing the problems occurring in real test conditions, specifically, the effect of measurement noise, limited number of samples and low number of sensors. This assessment needs to be performed both from a theoretical and experimental basis.

Aligned to this vision, in this thesis the effect of several challenges faced in real testing conditions, are studied on the statistical subspace damage identification method. Hence, the underlying theories and methods will be developed, and then they will be verified using simulated data from analytical models; finally, they will be validated by real data from experimental tests.

1.2 State-of-knowledge

There are numerous researches found in the literature dealing with damage identification of structures. These methods use different responses of structure and are reviewed in Chapter 2. One

category of these techniques include the methods employing statistical tests in identifying the damage. The statistical subspace damage identification method is categorized in this group.

Since the damage in a structure results in changes in its natural frequencies and modeshapes, monitoring these modal parameters can be used in identifying the damage. However, identification of modal parameters is not usually accurate (especially for higher modeshapes) and it needs manual processing of the data; therefore they are not appropriate for real-time health monitoring. In the SSDD method, there is no need to estimate the natural frequencies and modeshapes, making this approach capable of being used in real-time monitoring of structures. In this way, the whole eigenstructure, i.e. modeshapes and natural frequencies, of the measurements are included in the damage detection and the focus is not only on dominant frequencies. Including higher modes in this evaluation makes the damage detection approach more robust, considering that the main effect of local damages is on higher modeshapes.

In most of the statistical damage detection methods including SSDD, the noise can be treated robustly by taking the data related uncertainty into account. This will make these methods able to deal with sparsely instrumented structures, at least for the level one of damage detection, namely investigating the existence of damage. It was demonstrated in (Döhler et al. 2014b) and (Döhler and Hille 2014) that SSDD technique can perform robustly under ambient excitations with changing statistics. The SSDD method was used in (Döhler et al. 2014a) to detect the damage with the real test data acquired from S101 bridge. The effects of measurement noise and limited number of samples were not studied on this method, which are key issues in practicing a detection approach. The study of these effects is among the objectives of this thesis.

Localizing the damage is the second level of damage identification and is more challenging in practice than damage detection. Some reasons for this fact, are the low number of sensors and

the need for a link between the data and the physical properties of the structure. Many localization methods locate the damage by using the modeshapes which are in turn, highly dependent on the number and location of the sensors. The statistical subspace damage localization (SSDL) method (Balmès et al. 2008; Basseville et al. 2004) locates the damage in a structure by testing each element with a statistical test. The SSDL method was used and investigated for small-scale academic simulations in (Balmès et al. 2008) and (Döhler et al. 2014c). This method was not tested on the real data before, which is included in the objectives of this study. Furthermore, there are several challenges needed to be addressed to enable the SSDL method for real data. There are some methods proposed in (Balmès et al. 2008) and (Döhler et al. 2014c) to deal with some of these challenges which need to be investigated under real test conditions. This evaluation is one of the focuses in this study, along with proposal of new enhanced methods for dealing with these challenges.

Another challenge in damage localization of structures stems from the detectability of the location of damage. The detectability of damage increases by using more sensors and higher frequency mode shapes which are less identifiable, or by optimizing their geometrical location. This detectability using the SSDL method was not studied before and composes another objective of this thesis.

1.3 Motivation

During last decades numerous studies have been performed on the subject of damage detection and localization methods. In the literature, some of these methods are proven to be promising; however, an ideal damage identification method that can perform robustly under real testing conditions for every type of structure is not developed yet. On the other hand, although most of these methods perform well for simulated data, few of them are successful under real test

conditions. Therefore, investigating a damage identification method under real test conditions is a significant step in evaluating it as a practical and robust damage identification method. The overarching goal in this study is to smooth the path of SSDD and SSDL method towards damage identification of structures under real test conditions.

Among the main challenges faced in the health monitoring of real structures is the existence of noise in the measurements. Existence of noise in experimental data is inevitable. There are different sources of the noise in measuring a structure and processing the data, such as the unknown excitation (Döhler et al. 2014b; Döhler and Hille 2014), measurement noise and limited data length. Besides, the data quality (e.g. measurement noise ratio) can affect significantly on the damage detection output (some of the studies are reviewed in (Alvandi and Cremona 2006)). Thus, investigating the effect of this inherent characteristic of the measurements, i.e. measurement noise, on the SSDD technique is an important factor in assessing its functionality.

Another challenge in damage identification of real structures is the limited number of samples or data length. One of the focuses in this thesis is on the effect of number of samples on the SSDD technique. By having such information, these factors might be controlled while employing this method in practice.

Although the theories and functionality of the SSDL method was investigated for simulated data, still the detailed analysis and necessary improvements under real test conditions of a real or controlled experimental structure is needed. Therefore, the other focus of this study is motivated on the damage localization under real test conditions using the SSDL technique.

Detectability is not the same throughout a structure, and is different depending on the location and number of sensors, and the extracted modal parameters. Knowing which elements are less detectible is a critical information to know what damage, we are not able to observe. Moreover,

it provides valuable information in optimizing the location of the sensors to increase the detectability of all or some selected elements of the structure. Hence, the detectability of damage in each element is another topic motivated to be investigated in this thesis.

Thus, detecting the existence and the location of a damage in a structure using the statistical subspace technique along with investigating its functionality and applicability for real test conditions are the motivated goals of this study.

1.4 Objectives and tasks

In this study the objectives are multifold and can be envisioned in three main directions. Firstly, the focus is on a theoretical study on the effects of different factors faced under real testing conditions on the SSDD technique. Specifically, these factors can be named as: measurement noise and data duration (number of samples).

Secondly, the focus is shifted to the damage localization using the SSDL technique. The theories and methods needed in using the SSDL method under real test conditions will be developed. The SSDL method functionality from real test data needs to be assessed. Consequently, the developed methods and theories need to be verified and validated from the simulated data and real data. Another objective in this direction is to study and develop the underlying theories to find an index showing the detectability of damage in each element.

Lastly, as mentioned before the developed theories and proposed methods need to be first verified by using analytical methods, and then, validated by the real test experiments. For this purpose, the objective is to create several numerical simulations, simple and sophisticated (finite element models). Subsequently, these theories and methods will be validated with data measured from a real experimental structure namely, the Yellow frame, assembled during this research at

UBC in 2016. Thanks to its modular properties, different damage scenarios are created and the real data is measured. This data is used in validating the proposed theories and methods.

Therefore, these objectives are addressed with following specific tasks:

I) Theoretical investigation on the practicability of the SSDD technique:

   a- Theoretical investigation on the effect of number of samples (data length) on the SSDD method

   b- Theoretical investigation on the effect of measurement noise on the SSDD method

II) Investigation on damage localization using the SSDL technique for real test conditions

   a- Investigating the formation of the Jacobians from analytical data or combination of analytical and real data

   In the SSDL method an analytical model, e.g. finite element model, of the structure is necessary to find the location/s of damage/s. The modeshapes and natural frequencies are related to each physical parameter, e.g. stiffness of elements or dimensions of sections or elemental mass, through this analytical model. In order to connect this analytical model to the χ^2-test, a matrix of Jacobians needs to be computed. The formation of this matrix can be computed purely from analytical modal parameters or from a combination of the analytical and real modal parameters. These two formations and their differences need to be studied in practice.

   b- Creating a method in scaling the modeshapes acquired from real data (decoupling if coupled) to the ones evaluated from the analytical model

   The modeshapes from the real data might need to be scaled to the modeshapes from analytical model in composing the Jacobians with latter formation in II-a, i.e. combination of analytical and real data. Creating and investigating a scaling method is

another objective in this direction. It is seen that some modeshapes from the real data are coupled together due to their very close natural frequencies, therefore, they need to be decoupled by this scaling method as well.

c- Investigation on the functionality of the proposed new clustering approach (HFC) in comparison to *k*-means for the SSDL technique

Due to the low number of sensors in practice, the structural elements need to be clustered in the SSDL method. This clustering was performed using *k*-means (Altman et al. 1960) approach. This approach is investigated in practice and compared to another clustering method, i.e. hierarchical Fisher-information-matrix-based clustering (HFC) method, proposed in this thesis.

d- Proposing an index indicating the detectability of damage in each element

III) Verification and validation of proposed theories and methods in application

This objective encompasses the creation of several simple and sophisticated models along with an experimental test in order to verify and then validate the methods and theories.

a- Verification of the proposed theories and methods by simulated models (simple and sophisticated)

b- Assessing the functionality of SSDL method in localizing of damage from real experimental data (the Yellow frame structure)

c- Validation of proposed theories and methods by the real data

1.5 Scope

Since the statistical subspace damage identification is an output only approach, the underlying test is an ambient vibration test. Therefore, the data from ambient vibration test in the context of

operational modal analysis is considered. Accordingly, the structure is assumed to behave linear elastic, under ambient vibrations. Non-linearity or inelasticity are not in the scope of this thesis.

Moreover, the damage is considered as a linear damage. The linear damage is defined as a damage that does not change the behavior of a linear structure to nonlinear behavior (Doebling et al. 1998). The extent of the damage is considered to be from cracks up to sever damages without failure: the structure is still operational and no failure has happened.

The focus in this thesis is on using statistical tests for detecting and locating the damage in a structure. Thus, the probabilistic analysis of the damage/failure (such as (Maier et al. 2001)) is out of scope.

The considered damage identification levels, are the first two levels: damage detection and damage localization. The damage quantification and life prediction are excluded.

The environmental effects such as temperature, moisture, soil-structure interaction, and changes in the statistical characteristics of input excitations are excluded. However, the effect of output measurement noise on the SSDD method is considered in this study.

The output measurement noise is assumed to be white noise with Gaussian distribution. The change of covariance or colorful noise is not in scope of this thesis.

In SSDD and SSDL method the damage can be a change in any structural parameter that changes the dynamic behavior and modal parameters of the structure. In this thesis, the damage is modeled as a reduction of stiffness or change of the mass of one or some elements.

1.6 Exegesis

Several terms employed throughout this thesis need to be defined. The terms damage “detection” and “localization” refer to, in order, detecting the existence of damage and locating it. Besides, the term “damage identification” is referred as all the 4 levels of damage detection, localization,

quantification and remaining-life-prediction. Since in this thesis only damage detection and localization are considered, this term is also used in referring to these two levels.

The term "detectability of damage" of an element is defined as the increase of damage index from the safety threshold, per unit of damage ratio in that element. In other words, if the damage ratio in all elements are considered equal, the elements with higher detectability will result in higher damage index, and therefore, the damage is easier to be monitored in them.

While the term noise is used as its general definition, the term "measurement noise" or "output measurement noise" (defined in Chapters 3 and 4) is defined as the difference between the response of structure at one sensor location and the recorded measurement from that sensor. Furthermore, the term "additional measurement noise" is the measurement noise that will be added to the real outputs from sensors. Since every sensor in real life always contains some unknown measurement noise, the noise added to the real data is named as the additional measurement noise.

The term "eigenstructure" is referred to the combination of eigenvalues and eigenvectors of a system. Hence, it can also be used in referring to the combination of natural frequencies and modeshapes of a structure.

The term "verification" is used when the proposed theories or methods are assessed with analytical models. On the other hand, the term "validation" is used when the proposed theories or methods are assessed using the real data. These definitions are based on the book by (Oberkampf and Roy 2010).

The term "real data" refers to the data measured from testing a real or experimental structure. Therefore in this thesis, it is also used for the data obtained from testing the Yellow frame structure. The term "simulated data" is used to refer to the data which is obtained from analytical models.

1.7 Methodology

The methodology employed in addressing the tasks pointed out in 1.4 is described in this section.

I) Theoretical investigation on the practicability of the SSDD technique

a- Number of samples is already exposed in the χ^2-test theory. The effect of this parameter will be conveyed back to the final χ^2-value. Hence, the final χ^2-value is formulated in terms of number of samples, and its effect will be investigated for damaged and undamaged structures.

b- The effect of measurement noise on the χ^2-test is investigated with adding a Gaussian distributed white noise to the output measurements. Using the state-space system representation, the effect of this extra added term will be evaluated in a closed form manner on the final χ^2-value. The closed form formulation of the final χ^2-value with respect to the added noise, represents the effect of the measurement noise on the χ^2-test. This extra nuisance term is assumed to be zero mean and Gaussian distributed with standard deviation equal to a ratio of standard deviation of output measurements. The effect of the measurement noise will be investigated with different characteristics for damaged and undamaged structures in the data from the reference or testing states.

II) Investigation on damage localization using the SSDL technique for real test conditions

a- Two formations of composing the Jacobian matrix will be addressed. The practicability of these formations will be investigated. They will be assessed by using the real data from the Yellow frame structure.

b- When the Jacobian matrix is supposed to be formed from the modal parameters from both real and analytical data, the modeshapes acquired from real data need to

be scaled to the ones evaluated from the analytical model. The scaling approach will be elaborated. Moreover, some modeshapes acquired from the Yellow frame are coupled due to their very close natural frequencies, therefore, the scaling method will be extended to decouple and scale these modeshapes as well.

c- A new clustering method (HFC) will be developed to cluster the elements using the Fisher information matrix. This method will be elaborated. The advantages and disadvantages of this method compared to the *k*-means will be investigated.

d- The relation of the diagonals of the Fisher information matrix with the detectability of each element from the sensitivity based approach, is investigated theoretically. Furthermore, a robust Fisher-information-matrix-type value is investigated to indicate the detectability of damage in each element when using the MinMax test.

III) Verification and validation of proposed theories and methods in application

a- Four analytical models, including three simple structures and one sophisticated finite element model of a bridge, i.e. S101, are used in verifying the theories and methods addressed in I.a, I.b, II.c and II.d. The models are tailored to reflect purely the functionality of the proposed theories and methods.

b- The real data acquired from the Yellow frame is used in assessing the functionality of the SSDL method in damage detection and localization. Different damage configurations are created in the structure by removing its modular braces.

c- The proposed theories and methods addressed in I.a, I.b, II.a, II.b, II.c and II.d are validated by the results from this real data.

1.8 Overview of dissertation

In this section the organization of this thesis is explained and the address of objectives through this organization are given. In Chapter 2, a literature review on the methods dealing with structural damage identification is presented. These methods are categorized into several groups and from each group some researches are exemplified. At the end of that chapter, the researches on the statistical subspace damage identification method are also reviewed.

In Chapter 3, the background of the statistical subspace damage detection and localization methods is presented. The underlying basic theories of this method are elaborated, since they are used in developing of new theories, proposed in this thesis.

In Chapter 4, the SSDD is in the focus. The effects of two practical challenges in real test conditions, namely the measurement noise and length, are evaluated theoretically. In this chapter objectives I are addressed. The theories on these effects are provided in this chapter and the rest are shown in Appendix A.

In Chapter 5, the theories and methods for damage localization under real test conditions are developed and described. In this chapter objectives II are addressed.

In Chapter 6 the developed theories and methods are verified using analytical models. Subsequently, in Chapter 7 the experimental test, the Yellow frame, is introduced and the developed theories and methods are validated from the real data measured from this test. Therefore, objectives III are addressed in these two chapters. The instrumentation of this test is described in Appendix E.

Finally, the contributions, conclusions and recommended future work are presented in Chapter 8.

Chapter 2: Literature Review

2.1 Introduction

Numerous researches can be found in the literature and different approaches are proposed to detect possible damages in a structure. Some of these tests include sampling of the structure, which may affect the functionality of structure. These tests are named destructive tests. However the other type of the tests, namely non-destructive tests, do not involve with any action that can damage the structure or affect its functionality. Due to the need of continuation of the serviceability of the structure, more researchers have been focusing on the latter approach.

Nondestructive damage detection techniques can be categorized into two groups based on their requirements ((Fan and Qiao 2010), (Doebling et al. 1998)): (I) local techniques, which need access to all parts of the structure or the location of damage if known, and (II) global damage techniques which use vibration data to evaluate global dynamic characteristics of the structure. Employing the local techniques may lead to interference in the operation of the structure and is not suitable for major structures. However, in the latter techniques there is no need to know or have access to the location of damage in priori.

The global techniques can be also categorized into two groups based on their approach to the problem. In the first category, the structural properties are identified and employed to assess the condition of the structure. The structural properties identified from these approaches include stiffness, damping, mass, load paths and boundary conditions (supports, connections, etc.). In the second category, the eigenstructure of the problem is employed to evaluate the condition of the safety of the structure. In these methods, modal properties such as natural frequencies, modal damping values and modeshapes are used to identify any changes in the structure. Any change in the structural properties leads to a change in the modal parameters of the structure. However

generally, identifying the modal parameters in a structure is more practical and accurate than the structural properties.

In order to keep the structure in operation, shaking the structure artificially or using impact loads are not promising. Therefore by employing ambient vibration testing, the operation of the structure will not be interfered. In this case due to the fact that the input excitation to the structure, such as wind, traffic, earth vibration, cannot be measured practically, output-only damage detection techniques are of interest. Moreover, the process of evaluating and matching the modal parameters of a structure is also time consuming (Salawu 1997) and it usually cannot be employed in real-time monitoring of structures which are not well instrumented. In addition, local damage in a structure affects typically on higher frequency modeshapes ((Doebling et al. 1998) and (Worden et al. 2007)) which are not usually identifiable to be used in damage detection due to their high modal density and low participation factors (Farrar et al. 2001). Evaluation of these modal characteristics can be avoided by using output-only statistical approaches e.g. Kalman filter technique (Yan et al. 2004), outlier analysis method (Worden et al. 2000) or the statistical subspace damage detection technique (SSDD) ((Abdelghani and Benveniste 2000), (Basseville et al. 2004)).

2.2 An overview on damage identification methods in structural health monitoring

It is about five decades that vibration based health monitoring of structures is utilised to evaluate the conditions of the structures. At the beginning, it was basically focused over the offshore oil industries and aerospace engineering problems and now it is widespread throughout the civil and mechanical engineering communities as well. In this context, the damage can be identified as the change in: the boundary conditions of the structure, the geometrical/material properties of the composing elements and or the connectivity of these elements. Based on this definition, it should

be noted that the damage cannot be identified in a structure without comparing it in two system states (Worden et al. 2007).

Damage detection of the structures can be categorized into 4 groups based on their level of identification: I) identifying the damage existence, II) identifying the geometrical location of the damage, III) quantification of the severity of damage and IV) evaluation of the remaining service life of the structure. Most of the literature is concentrated on the level 1 to 3 of the detection on the controlled laboratory structures and some on-field tests.

Several extensive review papers can be found in literature on the topic of damage detection ((Fan and Qiao 2010), (Doebling et al. 1998), (Worden et al. 2007) and (Carden and Fanning 2004)). Also some of the damage detection methods are originating from the Control domain. Some overview studies in this topic can be named as review papers by (Willsky 1976) and (Frank 1990), and books such as (Patton et al. 1989).

The damage identification methods can be categorized based on their approach in detecting the damage, by using a model of the structure, i.e. model-based, or using only the measured data, i.e. data-driven. In data-driven methods the damage is identified with using only the recorded response of the structure. These methods are usually simpler to be used than the model-based methods, since there is no need of creating and adjusting a model to the structure. Although, independency of these methods to a model makes them simpler in use, their resolution in localizing the damage in elements and estimating its severity is not as good. In the model-based approaches the model of the structure is updated based on the response (usually modal parameters) of the system. These methods are reviewed in 2.2.5. In these methods, there is a need in processing the data and then updating the model based on it. This will delay the identification procedure and makes these methods less appealing for real-time damage detection. However, the model will

enhance the damage localization resolution and it helps in evaluating the damage severity. There is a third group of methods recently emerged in the literature (such as the SSDD and SSDL method) that are a combination of data-driven and model-based methods. In these methods the data is used in damage detection and a model of the structure is used in localization and estimating the extent of the damage from the data. In these methods there is no need to update the model continuously and it is only created in the reference state (undamaged condition) of the structure. The SSDD/SSDL method will be reviewed at the end of this section.

It can be seen in the literature that identification of the damage in a structure can be performed by employing different properties of a system. These can be named as (Rytter 1993) suggests:

1) Natural frequency based methods
2) Modeshape based methods (modeshapes, their curvature/strain)
3) Dynamic flexibility method
4) Residual force vector method
5) Matrix/model updating methods
6) Methods employing Genetic or neural network algorithms or wavelets
7) Statistical methods

2.2.1 Natural frequency based methods

There are numerous researches found on the damage detection based on the shifts in the natural frequencies of the systems ((Mirza et al. 1990), (Ågårdh 1991), (Kato and Shimada 1986), (Adams et al. 1978), (Gudmundson 1982), (Springer et al. 1988), (Hearn and Testa 1991)). Salawu reviewed some of these researches in (Salawu 1997). The fact that the change in the properties of

a structure will affect the resonant frequencies of that structure forms the basis of this category of methods.

Cawley and Adams (Cawley and Adams 1979) propose a method that can identify the damage location and extent from two frequencies of a pair of modeshapes. This study is done for a 2D plane structure. They also showed that the ratio of the changes in frequency is also a function of damage location. Kulla also used the change in the natural frequencies as a basis of identifying the existence of damage for a real bridge structure (Kullaa 2003). In (Magalhães et al. 2008) it is also shown that Magalhães used the natural frequencies obtained from Frequency Domain Decomposition (FDD) method ((Brincker et al. 2000, 2001b)), in real-time monitoring of the conditions of a long span bridge.

It should be noted that the damage identification based on the natural frequencies is not much accurate due to the low sensitivity of frequency shifts to the damage. However, the natural frequencies identified in a structure have less variance due to the noise than other modal parameters (Doebling et al. 1998). The other problem in this category of damage detection is that the damage is usually localized in a specific point of structure that affects more on the higher modeshapes and resonant frequencies of the structure. While the modal density is high on higher frequencies and the modal participation factor is less, the detection of damage is harder by using the modal parameters such as the natural frequencies.

In another study by Chen et al (Chen et al. 1995) it was shown that the critical damage in a structure could change the natural frequencies less than 10%. They also discussed that the environmental effects can change this value with magnitude of 5-10%, which can hide this shift of frequencies.

Most of the success in use of natural frequencies in damage detection was achieved for single damage in small and simple laboratory structures (Carden and Fanning 2004). In a study by Lee and Chung (Lee and Chung 2000), by using a FE model, and using a ranking system, the damage was detected in a beam structure. Then they could also locate and quantify the damage, i.e. crack in their study, by using this system. It was shown in their study that the damage in the cantilever beam, is less detectible when is close to the clamped end.

Yang et al (YANG et al. 2001) developed a model from a beam with two boundary conditions, i.e. simply supported and fixed-fixed, to locate the damage (crack) in a beam by using frequency contours. These contours are based on the location and depth of crack. They could locate the damage based on the assumption that if crack is located in a vibration node of a specific mode, the frequency of that modeshape will not be changed. In other studies such as (Chinchalkar 2001), (MORASSI 2001) and (Cerri and Vestroni 2000) the damage was identified and located in beams or rods using the shifts in natural frequencies.

2.2.2 Modeshape based methods (modeshapes, their curvature/strain)

In another category of methods for damage detection the modeshapes features are employed in order to detect the damage in a structure. In one type of these methods, the modeshapes are compared between two states of the structure to detect the damage. One of these methods is the Modal Assurance Criterion (MAC) factor (Allemang and Brown 1982). This value which varies between 0 and 1, indicates the similarity of two vectors of modeshapes. Since the modeshapes are spatial vectors, the location of damage can also be found from this comparison. However, to achieve the precision needed for such a comparison, many sensors or many locations of excitation (roving exciter) are required. Araújo dos Santos et al (Araújo Dos Santos et al. 2000) proposed a technique based on the orthogonality of the modeshapes for composite materials. The results were

more sensitive to damage than the modeshapes. Moreover, a finite element model of the structure was employed in this method. In subsequent studies by Ren and De Roeck ((Ren and De Roeck 2002a) and (Ren and De Roeck 2002b)), this method was shown to have difficulties in locating the damage from real test data because of the noise and measurement errors existing in a real test data.

In the methods using the curvatures of the modeshapes, it is assumed that the location of high curvature in a modeshape is near the damage location. The same concept is also used in modal strain energy methods.

There is a discrepancy between the usefulness of these methods in the literature. In some studies they are shown to be more sensitive than the natural frequency method, however doubts are raised for their use from real case studies. It is shown in the literature that the modal strain energy methods are promising for some case studies, e.g. Z24 bridge (Abdel Wahab and De Roeck 1999). Some methods also use modal strain energy in order to detect the damage which can be categorized in this group as well. Some of the researches using the modal strain energy in damage identification can be named as (Kim and Stubbs 1995) and (Kim and Stubbs 2002).

A seven story full-scale concrete building was tested by Moaveni et al (Moaveni et al. 2010) and several ambient vibration tests were performed on the structure after exciting it with different earthquake records. Several modal parameters were used in identifying the damage in conjunction with a model updating approach. It was shown that the modal parameters identified from the ambient vibration input match better with the linear model, compared to the ones obtained when the input to the system is white noise.

The damage considered as the delamination in composite beams was located in (Ratcliffe and Bagaria 1998) using the curvature of the modeshapes. A FE model is used instead of data from

the healthy state of the beam and then the modeshapes are evaluated from the data measured from damaged structure. A review paper on the vibration based damage detection in composite structures is (Zou et al. 2000).

Oh and Jung (Oh and Jung 1998) used the static displacement data and the modeshapes slope or curvature in detecting damage in a continuous two-span beam. Cornwell et al (Cornwell et al. 1999) used the modal strain energy in locating the damage in plate-like structures.

Hu et al (Hu et al. 2001), detected and localized the damage in a beam structure based on the modal strain energy. This method was tested for simulated data from a planar truss structure and for measured data from a fixed-fixed beam. The modal strain energy method was also employed by Peterson et al ((Peterson et al. 2001a) and (Peterson et al. 2001b)) in identifying the damage in timber beams. It was shown that due to the inherent variability of timber beams, the severity of damage needed to be high, i.e. $1/3^{rd}$ of the depth of beam.

In the research done by Brincker et al (Brincker et al. 2001a), the combination of the natural frequency changes and modeshape changes and even damping was used in detecting the damage in the Z24 highway bridge. The use of damping as a parameter in damage detection was also investigated by C. Willimas and OS. Salawu in (Williams and Salawu 1997) and Curadelli et al in (Curadelli et al. 2008).

2.2.3 Dynamic flexibility method

Another category of methods use the dynamic flexibility matrix to detect the damage. This matrix is based on the square of modeshapes and inverse of natural frequencies. In practical problems, it is only constructed from low frequency modeshapes since they can be evaluated in practice and they have higher contribution in the final constructed dynamic flexibility matrix. Although in some studies it was shown that this method is more sensitive to damage than other methods, e.g. (Zhao

and DeWolf 1999), in a study by Farrar and Doebling (Farrar and Doebling 1999) it was shown that this method could not find damage in most of the damage scenarios while the damage curvature method showed to be the most sensitive approach. In (Pandey and Biswas 1994) the flexibility matrix was used in detecting and locating the damage. This matrix was shown to be accurately built by some lower frequency mode shapes. The flexibility matrix was combined with the stiffness matrix by Yan and Golinval in (Yan and Golinval 2005) to detect and locate the damage. In their method no finite element model is needed.

Li et al in (Li et al. 1999) used the flexibility method in identifying the damage in cantilevers. They modeled tall buildings and chimneys as cantilevers. They could detect the damage by using a small number of modeshapes, i.e. 2 modeshapes.

2.2.4 Residual force vector method

In the residual force vector method, the eigenequation of the system in the healthy and damaged states are subtracted resulting in some vectors, namely residual force vector, which by applying it to the undamaged structure, it responds as a modeshape of damaged structure. If the damage occurs in the structure, the element of the residual force vector corresponding to that element will be large.

In (Sheinman 1996), this method is used in identifying the damage in three analytical models including a 3D truss structure. Kosmatka and Ricles (Kosmatka and Ricles 1999), used this method in detecting and localizing the damage in an experimental test of space truss. In this study they considered the change in mass or stiffness and the variations of modeshapes and natural frequencies.

Farhat and Hemez (Farhat and Hemez 1993) used an iterative approach in updating the model using the residual load vectors. In their study, the incomplete modeshapes were expanded. In (Castello et al. 2002), Castello et al used a modeshape projection method to make the

experimental and analytical modeshapes compatible. They tested this method in identifying the damage in a cantilever beam and a truss structure. Kahl and Sirkis (Kahl and Sirkis 1996) also used this method in localizing the damage in a cantilever beam. They concluded that they need higher frequency modeshapes in locating the damage in beams compared to the truss structures.

2.2.5 Matrix/model updating methods

Another method of damage detection is the use of physical parameters, e.g. mass, stiffness, damping and etc., from the structure and updating them in a sense that the model based on them can predict the structural dynamic behaviour (specially the modal parameters). The correlation between this model and the structure is usually achieved by an optimization algorithm using least square method. There are several obstacles which must be dealt with when using this method. The size of the model should not be large since the model must be analyzed many times. Moreover, the accuracy of the initial model should be acceptable as it affects the whole procedure of the updating. The number of parameters which can be identified is also a usual problem in model updating because the number of model parameters is always very large in civil structures compared to the measured points or identifiable modal parameters. In theory, the maximum number when only natural frequencies are considered is equal to the number of natural frequencies. If the modeshapes are also considered in the model updating then the number of measuring points times the modeshapes is an upper limit to the number of identifiable parameters based on the study in (Gola et al. 2001). Another problem in this method is the lack of uniqueness in the updated model. Unless the number of degrees of freedom of the model is not less than the actual structure, the solution is not unique (Berman 2000). They concluded since the real structure has infinite number of DOFs, always the identified model is not unique. However, any updated model of a structure is useful to show the dynamic behaviour of the structure in limited cases. For some problems such

as damage detection, the updated model might not be a good representative of the damage, since knowing the true change of parameters in the right locations is needed to identify the damage (Berman 2000). In general, in model updating technique the engineer needs to use his/her own judgment in the modelling process and in making decision between the possible solutions.

In a study by Moaveni et al (Moaveni et al. 2009), the effect of uncertainty in evaluation of the modal parameters on the damage identification from model updating was investigated for different factors. It was shown that the effect of mesh size of the model is the most significant one on the mean of identified damage, although its effect on the evaluated modal parameters is not high.

In some of these methods, the damaged model matrices are updated which are referred as optimal matrix methods ((Baruch and Bar-Itzhack 1978), (Liu 1995), (Zimmerman and Kaouk 1994) and (Kaouk and Zimmerman 1994)). A review paper on these methods is (Smith and Beattie 1991). Some other type of model updating approaches are sensitivity based approaches. In these methods the first order Taylor series is used in approximating the updated matrices. For this purpose, the first order sensitivity of the parameters with respect to variables e.g. stiffness matrix, is needed. Some of the researches in this topic can be named as (Sanayei and Onipede 2001), (Mottershead et al. 2011) and (Sanayei et al. 1992).

Jang et al (Jang et al. 2002) used a regularization in regulating the error function defined between the identified modeshapes from the analytical FE model and measured data. The damage was modeled as saw cut in the elements of a grid-type bridge laboratory experiment. It was shown that the damage could be identified and located.

In several researches ((Marwala et al. 1998) and (Cha and Tuck-Lee 2000)) the use of frequency response functions (FRF) in model updating can be observed. By converting the data

from the time domain to the frequency domain, the dimension of the problem is reduced. However, by assuming that the system is linear, Friswell and Penny (Friswell, M. I. and Penny 1997) suggest that there is no information lost due to this compression. The frequency domain compared to the modal domain is less compact, notwithstanding it is argued that since the structural response is dominated by its lower frequency modal parameters, the modal domain and frequency domain are the same (Friswell, M. I. and Penny 1997). Some researchers, e.g. (Lee and Shin 2002), differentiate these two domains further into the errors associated in identifying the modal parameters when using the modal domain. Also one more advantage of using FRFs compared to the modal parameters is that it conveys more information in a specific frequency range compared to the modal domain which includes the same information as FRF but only in one point (Lin and Ewins 1990). These methods are also compared in (Maia et al. 2003) by Maia et al for simulated data from a beam structure.

2.2.6 Methods employing Genetic or neural network algorithms or wavelets

In another category of approaches, the neural network or genetic algorithm methods are used in order to identify the damage in a system. These methods are used in diverse applications in artificial intelligence, machine learning and also vibration based damage detection ((Feng and Bahng 1999), (Zubaydi et al. 2002), (Waszczyszyn and Ziemiański 2001), (Marwalla and Hunt 1999), (Wu et al. 1992) and (González and Zapico 2008)). Neural networks are usually used in systems with large measured databases. As an example for the neural network approaches, Ramu and Johnson (Ramu and Johnson 1995) used the neural network approach in conjunction with Fuzzy logic concept and proposed a method to identify damage in composite materials. For this purpose an experimental data was used to train the neural network prior to employing it for damage

detection. Ostacowicz (Ostachowicz et al. 2002) also used genetic algorithm in order to find the change in the lumped masses in a plate structure based on its fundamental frequencies.

In a number of researches such as ((Chiang and Lai 1999) and (Moslem and Nafaspour 2002)), the residual force vector is used to locate the damage and then the genetic algorithm is employed to quantify the damage. In (Gomes and Silva 2008), the genetic algorithm is also used as an optimization tool in detection and localizing the damage using a finite element model of the structure. It was concluded that the quantification of the damage could not be achieved accurately. Hao and Xia (Hao and Xia 2002) used the genetic algorithm along with three criteria, namely frequency and modeshapes changes and their combination, to compare the measurements from a reference state with a damaged state which leads to identifying the damage.

The wavelet transformation is also used in several studies ((Rucka and Wilde 2006), (Kim and Melhem 2004), (Liew and Wang 1998) and (Hou et al. 2000)) in identifying the damage in structures. The wavelets are useful in detecting singularities and steep changes in a system, e.g. in modeshapes or time history. According to Carden et al in (Carden and Fanning 2004) the resolution of the sensors, i.e. the number of sensors, affect significantly on the functionality of using wavelets in damage detection of structures.

2.2.7 Statistical methods

Among the methods above, least researchers are investigating the statistical methods for damage detection. There were promising results obtained from proposed methods in this category and therefore the focus of this dissertation is on the statistical approaches.

Farrar and Doebling in ((Farrar and Doebling 1999) and (Doebling et al. 1998)) suggested that the damage detection with using the vibrations of a system is fundamentally a statistical pattern recognition (Schiffer et al. 2014). They also argue that since the variability of the inputs to these

methods cannot be completely eliminated, this variability must be quantified by using statistical methods.

In a study by Zaurin et al (Zaurin et al. 2016), the sensor data along with camera images was used in detecting the damage of a bascule bridge. The traffic video from the cameras was used in identifying the load on the bridge and the strain in the bridge was evaluated from the sensors. Some influence lines were then evaluated from these data and by using a statistical outlier analysis the damage was identified.

In two studies by M. Gul and F. N. Catbas ((Gul and Catbas 2011a) and (Gul and Catbas 2011b)) a time series analysis was proposed in which an auto regressive with eXogenous input (ARX) model is created from the healthy state of the structure. This model is created based on the prediction of the reference sensor by considering the outputs of other sensors in a cluster. This model then was associated to damage by two approaches and was tested successfully on a large scale experimental laboratory model.

Sohn and Farrar (Sohn and Farrar 2001) also used a combination model of ARX and AR models to locate the damage by comparing the data from the reference state to the damaged state. This difference was identified as the difference between the prediction of these models and the actual measured data.

Worden et al (Worden et al. 2000) proposes a method that by using an outlier analysis, the features of the structure which have discordance compared to the reference state of the structure would be identified. They use a Mahalanobis distance (Mahalanobis 1936) in order to quantify this discordance.

In a study by Todd et al (Todd et al. 2001) a feature, namely the average local attractor ratio, was proposed to detect and quantify the damage by using it along with an outlier analysis.

In some other studies, simple statistical features such as mean or fourth statistical moment (kurtosis) of the distribution is used as the damage sensitive feature to be monitored (Martin 1989). In this concept Fugate et al. (Fugate et al. 2000) used the outlier analysis in detecting damage from an experimental data set. In another study (Fugate et al. 2001) he uses the control charts along with the statistical methods in detecting the damage. They suggested that the environmental variations can influence on the statistical approaches significantly and therefore their effects must be studied. In some studies such as (Peeters et al. 2001; Rohrmann et al. 2000) the effects of environmental conditions like temperature or change in the loading conditions were studied. The principal component analysis (PCA) was used by Yan et al, in (Yan et al. 2005a) to take into account the effect of environmental changes. They also extended this method to nonlinear cases in (Yan et al. 2005b). The damage detection in nonlinear systems are investigated in several papers. In (Farrar et al. 2007), several nonlinear system identification methods are exemplified in damage detection of structures.

Fanning and Carden (Fanning and Carden 2001) studied the damage identification in a telecommunication mast using an autoregressive model and by defining an error term between the predicted values and the measured values. They tried to identify the damage using control charts of the mean and variance of this error term.

The statistical subspace damage detection technique (SSDD) ((Abdelghani and Benveniste 2000), (Basseville et al. 2004), (Benveniste and Basseville 1987) and (Basseville et al. 2001)) is another approach in the category of statistical methods. In this approach a residual (Basseville 1998) is constructed from the difference between two states of the system and then with the use of a χ^2-test, an index for the change is defined. This approach is also used in damage localization of the simulated models in ((Balmès et al. 2008) and (Döhler et al. 2014c)) which illustrated

promising results for analytical FE models. In this method there is no need in identifying the modal parameters of the data which makes it robust in real-time monitoring of structures.

The damage detection from this method is tested on real test data such as S101 bridge in Austria (Döhler et al. 2014a).The effect of environmental excitation variations on this technique was also investigated in ((Döhler et al. 2014b), (Döhler and Hille 2014) and (Döhler and Mevel 2013)) where a residual was proposed which was insensitive to the covariance variation of the input noise to the system. This feature is a very significant parameter in health monitoring of structures which increases the robustness of this approach. Moreover, the effect of temperature on this method was also investigated in (Balmes et al. 2008) and (Balmes et al. 2009). In the latter study the effect of the temperature was rejected by assuming it as a nuisance parameter and removing its effect with projection.

Chapter 3: Background of the Statistical Subspace Damage Detection and Localization Technique

3.1 Introduction

In this chapter, the theoretical background of the statistical subspace damage detection and localization techniques are introduced, mainly based on references (Basseville et al. 2000), (Basseville et al. 2001) and (Basseville et al. 2004). The Statistical Subspace Damage Detection (SSDD) technique evaluates the global condition of a structure by identifying changes in the eigenstructure of the system. This change can be identified by detecting the changes in the mean of a residual. This residual is built from the current measurements of the structure and a data-driven subspace (referred as mold in Figure 3.1) made in the reference state, i.e. undamaged structure. This detection is possible since the changes of the mean of this residual is related to the change in the structure occurred from damage. It should be noted that the damage in the structure results in the change in its physical parameters, e.g. stiffness, dimension reduction of sections, mass of elements, and also it results in change in modeshapes and natural frequencies of a structure. Figure 3.1 shows this procedure of damage detection and localization using the SSDD and SSDL method.

Therefore, the damage can be detected by comparing a statistical model from the possibly damaged structure to thresholds obtained from a reference state. A subspace based residual function between these states is defined and compared using a χ^2-test. The results from χ^2-test can be displayed and monitored in a chart, namely control chart (Carden and Fanning 2004). Thus, there is no need to estimate the natural frequencies and mode shapes (for the detection part), making this approach capable of being used in real-time monitoring of structures. In this way, the whole eigensystem of the measurements are included in the damage detection and the focus is not

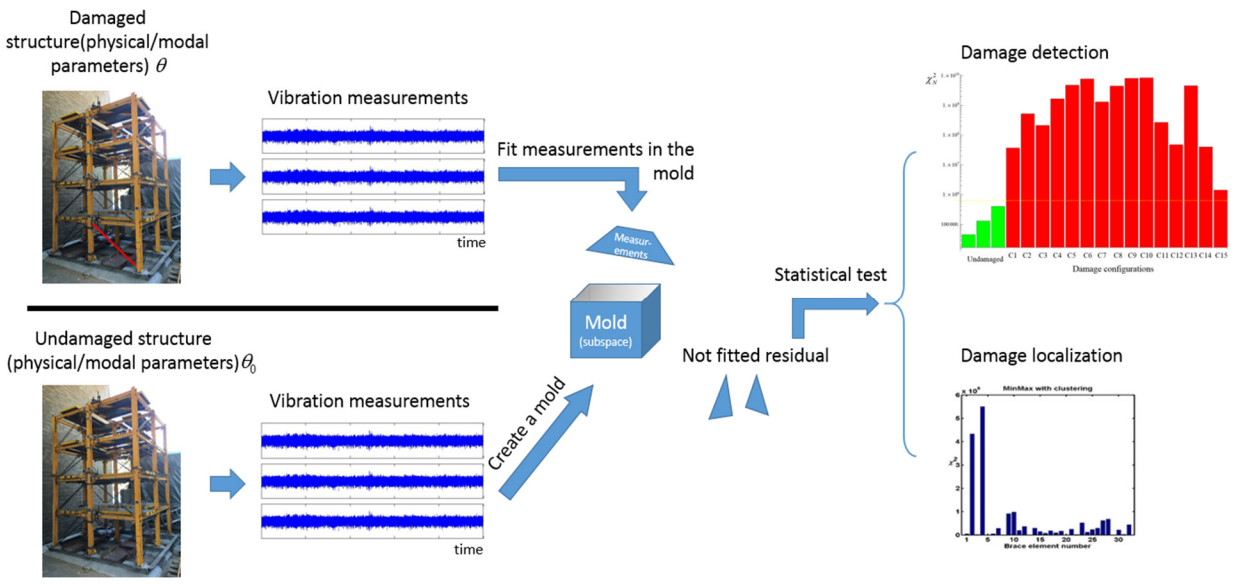

Figure 3.1 Statistical subspace damage detection and localization procedure

only on dominant frequencies. This is because there is no natural frequencies or modeshapes estimated or used in the damage detection procedure. Including higher modes in this evaluation makes the damage detection approach more robust, considering that the main effect of local damages is usually seen in higher mode shapes.

Following the detection of existence of damage in a structure, the second level of damage identification is to locate the damage. The objective of the damage localization is to find which part or parts of the structure are damaged. On one hand, the damage in a structure results in changes in its physical parameters, e.g. stiffness, mass or damping characteristics, and on the other hand, the change in the physical parameters of a structure alters the eigenstructure of the system. Identifying this alteration is the basis of damage detection and by tracing the source of this change in the physical parameters, the location of the damage can be identified.

In this chapter the SSDD technique and its theoretical basis will be described. Subsequently, the SSDL approach is described. The fundamental theoretical basis and some of the numerical implementation of this approach will be presented.

3.2 The statistical subspace damage detection method

The theories and formulations of SSDD method stem from the subspace based system identification. In this section, models, parameters and formulations needed to derive the final residual used in assessing the condition of the system along with some properties of this method is presented based on studies in (Basseville et al. 2000, 2004).

3.2.1 Dynamic equilibrium equation in discrete time domain

The state-space representation of a dynamic system is well known. Herein, the governing equation for the dynamic behavior of a structural system is presented and then it is reformed to the state-space representation. The dynamic behavior of a structure can be represented by the following continuous model:

$$\begin{cases} M\ddot{u}(t) + C\dot{u}(t) + Ku(t) = p(t) \\ y(t) = L\ddot{u}(t) + e(t) \end{cases} \quad \textbf{(3-1)}$$

where M, C and K are mass, damping and stiffness matrices, respectively, and u represents the displacement vector in all degrees of freedom of the system. Vector p is the vector of forces and t denotes continuous time. It should be noted that the external force p is unknown while it is assumed to be a non-stationary white noise. Vector y contains the measured output responses at the observed degrees of freedom of the structure. Based on the type of the sensor recording: acceleration, velocity or displacement, the second part of the equation changes; herein, the type of the sensor is assumed as accelerometers. Matrix L states the location of the sensors in relation to the geometry of the degrees of freedom, and e represents the measurement noise. As an example, the matrix L for a simple cantilever beam of 6 degrees of freedom and 3 sensors (shown in Figure 3.2) is

$$L = \begin{bmatrix} 1 & & & & & \\ & 0 & & & 0 & \\ & & 1 & & & \\ & & & 0 & & \\ & 0 & & & 1 & \\ & & & & & 0 \end{bmatrix}.$$

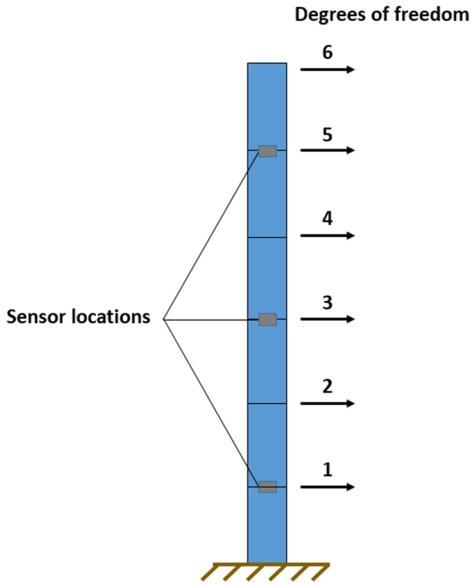

Figure 3.2 A 6 degrees of freedom structure instrumented with 3 sensors

The eigenstructure (μ , ψ) of the system can be computed from

$$(\mu_j^2 M + \mu_j C + K)\Psi_j = 0, \qquad \psi_j = L\Psi_j \qquad \text{for} \quad j = 1 \cdots n \tag{3-2}$$

where n is the system order. The discrete-time state-space representation of model (3-1) can be written by performing sampling with time step τ in step k as

$$\begin{cases} x_{k+1} = Fx_k + w_k \\ y_k = Hx_k + \varepsilon_k \end{cases} \tag{3-3}$$

in which $x \in \mathbb{R}^n$ is representing the state of the system and the measured output is represented by $y \in \mathbb{R}^r$. r is the number of sensors. $F \in \mathbb{R}^{n \times n}$ is the state transition matrix and $H \in \mathbb{R}^{r \times n}$ is the observation matrix. The state noise w_k and output measurement noise ε_k (which is a combination

of $e(t)$ and inputs to the system (3-7)) are generally assumed to be white noise for output-only system identification approaches. The state *x* and the measured output *y*, are related to the displacement vector with equation (3-4).

$$x_k = \begin{bmatrix} u(k\tau) \\ \dot{u}(k\tau) \end{bmatrix}, \quad y_k = y(k\tau). \tag{3-4}$$

Therefore, the state transition matrix is

$$F = e^{\mathcal{L}\tau} \text{ where } \mathcal{L} = \begin{bmatrix} 0 & I \\ -M^{-1}K & -M^{-1}C \end{bmatrix}, \tag{3-5}$$

and the observation matrix is

$$H = -LM^{-1}\begin{bmatrix} K & C \end{bmatrix} \tag{3-6}$$

based on the definition of the output as the acceleration. From this reformation of the system, the output measurement noise is evaluated as

$$\varepsilon_k = LM^{-1}p(k\tau) + e(k\tau) \tag{3-7}$$

which is composed from the input and measurement noise.

The eigenstructure (λ , φ) of system (3-3) can be computed similarly to (3-2) from

$$(F - \lambda_j \mathbf{I})\phi_j = 0, \qquad \varphi_j = H\phi_j \tag{3-8}$$

for $j = 1 \cdots n$. The modal parameters of the dynamic model (3-1), which are present in its eigenvalues μ_j, and modeshapes Ψ_j, are related to the eigenvalues λ_j and eigenvectors ϕ_j of the state transition matrix *F*:

$$\begin{cases} \lambda_j = e^{\mu_j \tau} \\ \varphi_j = \psi_j \end{cases} \quad \text{where} \quad \varphi_j = H\phi_j \quad \text{and} \quad \psi_j = L\Psi_j \quad \text{for } j = 1 \cdots n. \tag{3-9}$$

The natural frequencies *f*, modeshapes $\wp$ and damping coefficient ξ of the structure are related to the eigenstructure (μ,ψ) by

$$f_j = \frac{a}{2\pi}, \quad \wp_j = \psi_j \quad \text{and} \quad \xi_j = -\frac{b}{a} \tag{3-10}$$

for $j = 1\cdots n$, where $a = \left|\mu_j\right|, b = \Re(\mu_j)$. It should be noted that typically for buildings and bridges $0 < \xi < 1$. The eigenvalues μ is also related to *f* and ξ by

$$\mu_j = -2\pi f_j \xi_j + i\, 2\pi f_j \sqrt{1-\xi_j^2}\ . \tag{3-11}$$

The eigenstructure parameterization of system (3-3) is formed by pairs (λ,φ) which is referred as the system eigenstructure and can be employed as the system parameter in the vector form of

$$\begin{bmatrix} \Lambda \\ \mathrm{vec}(\Phi) \end{bmatrix} \tag{3-12}$$

in which Λ is the vector containing all the eigenvalues λ and Φ is the matrix composed of all eigenvectors φ . The function vec() is the vectorization function.

3.2.2 System parameter

Before defining hypotheses and testing them, some parameters of the system are needed to be chosen whose change represent the damage in the system. Let such as a parameter be called θ , and its value in the reference state be θ_0 where the structure is assumed to be undamaged. The system parameter includes any parameters in the system that their change shows a damage in the system. The damage in any element results in changes in the physical parameters, e.g. stiffness of element, cross section change, mass change, which leads to a change in the eigenstructure of the system, i.e. modeshapes and natural frequencies. Therefore, this parameter can be chosen as this physical parameter corresponding to each element of the structure or the continuous-time/discrete-

time eigenstructure, e.g. vector (3-12). Since in damage localization we are looking to locate the damage in physical elements, the system parameter is defined as the physical parameters of the structure when localizing the damage.

3.2.3 Output-only covariance based subspace system identification

In order to compute a residual vector between the reference and the current states of the system, the output-only covariance based subspace system identification method (Van Overschee and De Moor 1996) is employed. By defining the output covariance as $R_i = \mathbf{E}(y_k y_{k-i}^T)$ and parameters p and q such that $qr \geq (p+1)r \geq n$, the block Hankel matrix $\mathbf{H}_{p+1,q}$ is composed as

$$\mathbf{H}_{p+1,q} = \begin{bmatrix} R_1 & R_2 & \cdots & R_q \\ R_2 & R_3 & \cdots & R_{p+1} \\ \vdots & \vdots & \ddots & \vdots \\ R_{p+1} & R_{p+2} & \cdots & R_{p+q} \end{bmatrix} = \text{Hank}(R_i). \tag{3-13}$$

The output covariances satisfy $R_i = HF^{i-1}G$ (Van Overschee and De Moor 1996), where $G = \mathbf{E}(x_{k+1} y_k^T)$ is the cross covariance between the states and the outputs, which leads to the well-known factorization property of

$$\mathbf{H}_{p+1,q} = \mathrm{O}_{p+1}\mathrm{C}_q \tag{3-14}$$

where $\mathrm{C}_q \in \mathbb{C}^{n \times qr}$ and

$$\mathrm{O}_{p+1} = \begin{bmatrix} H \\ HF \\ \vdots \\ HF^p \end{bmatrix}, \qquad \mathrm{C}_q = [G \;\; FG \cdots F^{q-1}G] \tag{3-15}$$

in which we have $\mathrm{O}_{p+1} \in \mathbb{C}^{(p+1)r \times n}$. The observation matrix H, state transition matrix F, and subsequently the system parameters θ, can be computed from the defined observability matrix O_{p+1}. The observation matrix can be directly found from the first block row of the observability

matrix O_{p+1}. Moreover, by considering the shift invariance property of the observability matrix in (3-15), the observation matrix F is computed by solving

$$\mathrm{O}_p^{\uparrow} F = \mathrm{O}_p^{\downarrow} \tag{3-16}$$

in which

$$\mathrm{O}_p^{\uparrow} = \begin{bmatrix} H \\ HF \\ \vdots \\ HF^{p-1} \end{bmatrix} \quad \text{and} \quad \mathrm{O}_p^{\downarrow} = \begin{bmatrix} HF \\ HF^{2} \\ \vdots \\ HF^{p} \end{bmatrix} \tag{3-17}$$

By measuring data from the current state of the structure, an estimation of the block Hankel matrix, i.e. $\hat{\mathbf{H}}_{p+1,q}$, is computed from the covariance estimates $\hat{R}_i$ as

$$\hat{R}_i = \frac{1}{N-i} \sum_{k=1+i}^{N} y_k y_{k-i}^T, \quad \hat{\mathbf{H}}_{p+1,q} = \mathrm{Hank}(\hat{R}_i) \tag{3-18}$$

where N is the total number of samples. The factorization of the estimated Hankel matrix $\hat{\mathbf{H}}_{p+1,q}$ is also achieved by performing a Singular Value Decomposition (SVD) as

$$\hat{\mathbf{H}}_{p+1,q} = \begin{bmatrix} \hat{U}_1 & \hat{U}_2 \end{bmatrix} \begin{bmatrix} \hat{\Delta}_1 & 0 \\ 0 & \hat{\Delta}_0 \end{bmatrix} \begin{bmatrix} \hat{V}_1 \\ \hat{V}_2 \end{bmatrix}. \tag{3-19}$$

By truncating the decomposed matrices at system order n the observability matrix is estimated as $\hat{\mathrm{O}}_{p+1} = \hat{U}_1 \Delta_1^{\frac{1}{2}}$. From this observability matrix the system matrices F and H will be computed and subsequently the system parameters θ will be formed from the eigenstructure (λ, φ) calculated from these system matrices.

3.2.4 Definition of residual vector and hypotheses

By assuming that the system parameter in reference state of the structure is θ_0 and in current state is θ , a residual function is defined between these states which reacts to the changes in the system due to, for instance, damage. In order to create such a residual, the left null-space of the observability matrix O_{p+1}, namely orthonormal matrix *S*, is defined. Due to property (3-14), the Hankel matrix $\mathbf{H}_{p+1,q}$ and observability matrix O_{p+1} share the same left null space and therefore *S* can be computed directly from performing a singular value decomposition of $\mathbf{H}_{p+1,q}$. The reference state $\theta = \theta_0$ by having $S_0 \overset{\text{def}}{=} S(\theta_0)$ is then characterized by

$$S_0^T \mathrm{O}_{p+1}(\theta_0) = 0 \,. \tag{3-20}$$

Due to the factorization property (3-14), the left null-space of $\mathbf{H}_{p+1,q}$ is equal to $S(\theta_0) \in \mathbb{R}^{(p+1)r \times s}$ where $s = (p+1)r - n$. Hence (3-20) can be rewritten as

$$S_0^T \mathbf{H}_{p+1,q} = 0 \,. \tag{3-21}$$

By defining damage as a change in the system parameter θ , i.e. $\theta \neq \theta_0$, two hypotheses can be written as follows;

$$\begin{cases} H_0: & \theta = \theta_0 \;\; \therefore \text{ unchanged system} \\ H_1: & \theta \neq \theta_0 \;\; \therefore \text{ changed system (damaged)} \end{cases} . \tag{3-22}$$

$\mathbf{H}_{p+1,q}$ contains information from the dynamic properties of the system and, hence, any change in the system will be reflected in a change in $\mathbf{H}_{p+1,q}$. A simple way of monitoring those changes is to compare $\mathbf{H}_{p+1,q}$ to its value in the reference state or even simply to compare $S_0^T \mathbf{H}_{p+1,q}$ with zero.

Therefore to test these hypotheses, a residual function needs to be defined based on property (3-21) that holds if and only if $\mathbf{H}_{p+1,q}$ corresponds to the reference state. Since matrix S_0 depends implicitly on parameter θ_0 (we are treating it as a function of θ_0 (Basseville et al. 2004)), a representation of the current state parameter of the structure, i.e. θ , is needed. In view of (3-21), the empirical block Hankel matrix $\hat{\mathbf{H}}_{p+1,q}$ is used to create residual function (3-23) which corresponds to the difference between θ and θ_0 (Basseville et al. 2000, 2004).

$$\zeta = \sqrt{N}\,\mathrm{vec}(S_0^T \hat{\mathbf{H}}_{p+1,q}) . \tag{3-23}$$

In view of section 3.2.2, a change in the system parameter can be formulated based on the asymptotic local approach for change detection (Benveniste and Basseville 1987) as

$$\theta = \theta_0 + \delta\theta / \sqrt{N} . \tag{3-24}$$

where $\delta\theta$ is defined as the (unknown) parameter change vector normalized by $\sqrt{N}$.

In order to test the residual for a change, the information on the probability distribution of the residual is required, which depends on for example the noise distribution which is not available in general. However, an asymptotic analysis for $N \to \infty$ shows that the residual distribution can be approximated by a normal distribution. In fact, it will be shown that the residual satisfies the central limit theorem and is thus asymptotically normal distributed. To achieve this property, the factor $\sqrt{N}$ has been introduced in (3-23) and (3-24). Furthermore, it should be noted that definition (3-24), results in interesting properties of the detection technique: if the change in parameters θ is small, the change might be still detectable with large number of samples *N*, since $\sqrt{N}(\theta - \theta_0) = \delta\theta$.

Now, as the Central Limit Theorem (CLT) states, the average of a sequence of independent and identically distributed (any distribution) random samples is distributed normally when multiplied by $\sqrt{N}$. In view of (3-13), the Hankel matrix is composed of the covariance estimates $\hat{R}_i$ which are computed as an average as (3-18). Based on this and the fact that S_0 is evaluated only in the reference state and is constant in each test, in view of (3-23) each element of the residual vector is distributed normally as the CLT states. The mean of this distribution is zero if the system is unchanged. If the system is changed, the mean can be computed by a Taylor expansion theorem. By using a first order Taylor expansion from the reference state to the damaged state, the expectation of the residual writes as

$$\mathbf{E}_\theta\left[\zeta(\theta)\right] \approx \mathbf{E}_{\theta_0}\left[\zeta(\theta_0)\right] + \frac{\partial}{\partial \eta}\mathbf{E}_\eta\left[\zeta(\eta)\right]\Big|_{\eta=\theta_0}(\eta-\theta_0)\,. \tag{3-25}$$

Since in the reference state $\mathbf{E}_{\theta_0}\left[\zeta(\theta_0)\right]=0$, in view of definition (3-24), (3-25) can be rewritten as

$$\mathbf{E}_\theta\left[\zeta(\theta)\right] \approx \frac{1}{\sqrt{N}}\frac{\partial}{\partial \eta}\mathbf{E}_\eta\left[\zeta(\eta)\right]\Big|_{\eta=\theta_0}\delta\theta \tag{3-26}$$

which by defining $\frac{1}{\sqrt{N}}\frac{\partial}{\partial \eta}\mathbf{E}_\eta\left[\zeta(\eta)\right]\Big|_{\eta=\theta_0} \overset{def}{=} J$ is rewritten as

$$\mathbf{E}_\theta\left[\zeta(\theta)\right] \approx J\delta\theta \tag{3-27}$$

Therefore, by considering the Central Limit Theorem (CLT), for $N \to \infty$

$$\zeta \to \begin{cases} \mathcal{N}(0,\Sigma) & \text{under } H_0 \\ \mathcal{N}(J\delta\theta,\Sigma) & \text{under } H_1 \end{cases} \tag{3-28}$$

in which Σ is the asymptotic covariance computed in 3.2.6, and J is the asymptotic sensitivity of the residual computed in Chapter 5.

3.2.5 Hypothesis test

In order to test hypotheses (3-22), a generalized likelihood ratio (GLR) test is employed (Basseville et al. 2000). Based on the parameter chosen, it leads to two possible approaches: a non-parametric and a parametric χ^2-test. In damage localization, since the system parameters include the information from physical parameters of the structure, the parametric test is always employed to detect the change in these parameters. However, for the damage detection method the non-parametric test is simpler to use as there is no need to localize the damage in each parameter.

3.2.5.1 Parametric χ^2-test

Define $L(Z \mid h)$ as the likelihood function of Z under hypothesis h:

$$L(Z \mid h) = (2\pi)^{-d/2} \left(\det(\Sigma)\right)^{-1/2} \exp\left(-\frac{1}{2}(Z - \overline{Z}_h)^T (\Sigma)^{-1} (Z - \overline{Z}_h)\right) \tag{3-29}$$

where Z is a normally distributed variable with dimension d, covariance matrix Σ and mean $\overline{Z}_h = \mathbf{E}(Z \mid h)$, conditioned on hypothesis h.

The GLR test for hypothesis (3-28) is written as

$$GLR(\zeta) = -2 \log \frac{L(\zeta \mid \theta_0)}{\sup_{\theta \in H_1} L(\zeta \mid \theta)} \tag{3-30}$$

where $L(\zeta \mid \theta_0)$ and $L(\zeta \mid \theta)$ are the likelihood functions of residual under, respectively, the null hypothesis and alternative hypothesis (3-28). The GLR test will be expanded as

$$\begin{aligned} GLR(\zeta) &= \zeta^T \Sigma^{-1} \zeta + \sup_{\theta \in H_1} \left(-\left(\zeta - J\delta\theta\right)^T \Sigma^{-1} \left(\zeta - J\delta\theta\right)\right) \\ &= \sup_{\theta \in H_1} \left(2\delta\theta^T (J)^T \Sigma^{-1} \zeta - \delta\theta^T J^T \Sigma^{-1} J \delta\theta\right) \end{aligned} . \tag{3-31}$$

The gradient of the GLR is zero at $\delta\theta = \left((J)^T \Sigma^{-1} J\right)^{-1} J^T \Sigma^{-1} \zeta$ and therefore

$$GLR(\zeta) = \zeta^T \Sigma^{-1} J \left(J^T \Sigma^{-1} J\right)^{-1} J^T \Sigma^{-1} \zeta \, . \tag{3-32}$$

In view of (3-28), the GLR test is asymptotically χ^2-distributed with degrees of freedom equal to d=rank$(J) = \dim(\theta)$ and non-centrality parameter $\delta\theta^T J^T \Sigma^{-1} J \delta\theta$ under H_1 and 0 under H_0, and thus

$$\chi^2 = \zeta^T \Sigma^{-1} J \left(J^T \Sigma^{-1} J \right)^{-1} J^T \Sigma^{-1} \zeta \,. \tag{3-33}$$

The χ^2-variable is the parametric representation of a damage index and is compared with a threshold of safety. Since its distribution is shifted with the given non-centrality parameter under H_1, if its value surpasses this threshold, it shows that the condition of the structure is being changed. Hence, it indicates that a damage in the system has happened. This test is particularly used in damage localization for different parameters and will be discussed in 3.3 and Chapter 5.

3.2.5.2 Non-parametric χ^2-test

By computing a null-space from a reference data set, a non-parametric residual is created for which there is no need to evaluate any parameters. This test is very robust and hence can be used in global damage detection of structures.

The null-space S_0 is obtained by a singular value decomposition of the estimated Hankel matrix from the measurement data in the reference state as discussed in 3.2.3 and 3.2.4 based on (Balmes et al. 2008). Since no explicit system parameterization is used, we have $J = \mathbf{I}$ in the residual distribution (3-28), where $\mathbf{I}$ is the identity matrix. Therefore, (3-28) can be rewritten as

$$\zeta \rightarrow \begin{cases} \mathcal{N}(0,\ \Sigma) & \text{under } H_0 \\ \mathcal{N}(\delta,\ \Sigma) & \text{under } H_1 \end{cases} \tag{3-34}$$

where δ is now directly linked to the change in the residual vector (when normalized by $\sqrt{N}$). Subsequently, the χ^2-test variable (3-33) simplifies to

$$\chi^2 = \zeta^T \Sigma^{-1} \zeta \,. \tag{3-35}$$

Similarly to (3-33), this variable is asymptotically χ^2-distributed with $d = \dim(\zeta)$ degrees of freedom. Its non-centrality parameter is 0 under H_0 and $\delta^T \Sigma^{-1} \delta$ under H_1.

This test can be also viewed as the Mahalanobis distance (Mahalanobis 1936) of the test dataset to the reference state dataset. The covariance matrix will account for the effect of noise in the data and uncertainties in the estimation of the residual vector.

3.2.6 Covariance matrix computation

The covariance matrix of the residual vector ζ in the reference state is defined as

$$\Sigma = \lim_{N \to \infty} \mathbf{E}\left(\zeta \zeta^T\right) \tag{3-36}$$

since the expectation of the residual is zero (3-28).The covariance matrix includes the uncertainty in estimation of the residual vector and measurement noise. This effect is taken into account by including the covariance matrix (Basseville et al. 2004; Mahalanobis 1936) in the χ^2-test. The computation of the covariance matrix is performed by dividing the whole measurement data into b blocks containing N_b samples such that $N = N_b b$. Hence, the covariance matrix can be estimated in view of (3-36) as

$$\hat{\Sigma} = \frac{1}{N} \sum_{i=1}^{b} \zeta_i \, \zeta_i^T \tag{3-37}$$

where ζ_i is the residual vector computed from the *i*th block of the total *b* blocks. This estimation is affected by the excitation for finite number of samples (Basseville et al. 2004). Therefore, it is preferable to compute it for each test. However, by assuming unchanged statistical characteristics of the input noise (white noise) and the output measurement noise, the estimated covariance matrix in the reference state can be used for the test too. Moreover, because the data in the reference state is usually big enough, the estimated covariance is accurate. This will increase the efficiency of the

method computationally since evaluating the covariance matrix is computationally expensive. However, it will also affect on the χ^2-test as will be discussed in Chapter 4.

3.3 Statistical Subspace damage localization

Based on the theories developed in 3.2, the damage localization can be further developed as will be presented in this section. A concise review on the presented theories will be done in the next section and subsequently the theories will be further developed to the localization tests.

3.3.1 Hypothesis test with parametric χ^2-test

With the interpretation that if the system is damaged, the system parameter θ becomes changed, i.e. $\theta \neq \theta_0$, two hypotheses were defined in (3-22) and a generalized likelihood ratio (GLR) test was employed as stated in 3.2.5.

In order to test (3-22) the GLR test was defined in two approaches based on the parameters used, i.e. non-parametric and parametric. Because in damage localization the system parameters are physical parameters of the structure, the parametric test is employed to detect the change in these parameters through Jacobian vectors from (3-33). In the damage detection, we are interested to test if $\theta \neq \theta_0$. However, in damage localization we are interested in finding the parameter in the vector of θ that is responsible for this change, i.e. $\theta \neq \theta_0$. This parameter corresponds to the damaged element. Since a finite element model is employed to connect the residual values to each parameter, the Jacobian vectors are the components of this bridge. The computation and composition of these Jacobian vectors will be described and elaborated in Chapter 5.

The change in a physical parameter of the structure can be computed by evaluating the χ^2-test of it using the Jacobian matrix computed. This test can be performed in two ways as described in the following sections. It should be noted that in these tests, the scaling of the columns of the

Jacobian will not affect the final χ^2-value and the test only reacts to the directions of these vectors (columns).

3.3.2 Sensitivity based approach

The damage in the structure can be modelled as a change in a parameter, e.g. p_k, of the analytical model as used in (Balmès et al. 2008; Basseville et al. 2004).This change can be defined as δp_k and its effect on the residual function is shown in (3-28). For this purpose the system parameter is defined as the vector containing p_k for $k = 1 \cdots N_\rho$, where N_ρ is the total number of parameters. In this test, the χ^2-value is derived for each element *k* from (3-33) by assuming $\delta p_l = 0$ for $\forall l \neq k$. Now, define

$$\tilde{\zeta} = \hat{\Sigma}^{-\frac{1}{2}} \zeta \qquad \text{and} \qquad \tilde{J}_k = \hat{\Sigma}^{-\frac{1}{2}} \hat{J}_{p_k} \tag{3-38}$$

where $\hat{J}_{p_k}$ is the consistent estimate of $J(p_k)$ and $\hat{\Sigma}^{-\frac{1}{2}}$ is the matrix square root of the inverse of $\hat{\Sigma}$. Such decomposition of the covariance matrix to its inverse roots is possible since it is positive definite.

Based on (3-38) and in view of (3-28), the new residual is distributed as

$$\tilde{\zeta} \rightarrow \begin{cases} \mathcal{N}(0, \mathbf{I}) & \text{under } H_0 \\ \mathcal{N}(\tilde{J}\delta\theta, \mathbf{I}) & \text{under } H_1 \end{cases} \tag{3-39}$$

where $\tilde{J}$ is a matrix collecting all vectors $\tilde{J}_k$ for $k = 1 \cdots N_\rho$, as its columns. Hence, the GLR test (3-32) yields the χ^2-test for each parameter p_k as

$$\chi^2(p_k) = \frac{\tilde{\zeta}^T \tilde{J}_k \tilde{J}_k^T \tilde{\zeta}}{\tilde{J}_k^T \tilde{J}_k} \tag{3-40}$$

Therefore, the damaged (changed) element can be identified as the element *k* with higher $\chi^2(p_k)$ value (Balmès et al. 2008; Basseville et al. 2004).

The proposed test for each element k is based on the assumption of damage only in the element being tested. This assumption is not true when more than one element is damaged or when testing the undamaged elements while another element is damaged. Thus, the results from this test are approximate in these situations as the effect of other elements might be partially present in the evaluated χ^2-value. This effect is identified in following subsection and a remedy is introduced.

3.3.3 MinMax test

In this test, the effect of changes in other elements on the χ^2-test value of an element is removed. This removal is achieved in (Basseville 1997; Döhler et al. 2014c) by projecting the residual on the element being tested and removing the projections from other elements (being "blind" to other elements). Therefore, in this test the computed χ^2-value for an element conveys only the information from the change in that element while being blind to the changes in other elements. This will reduce the chance of false positive result for the undamaged elements.

In order to evaluate the projected χ^2-test for an element, e.g. k with property p_k and $k = 1 \dots N_\rho$, the corresponding Jacobians are partitioned as

$$\begin{cases} \tilde{J}_a = \hat{\Sigma}^{-\frac{1}{2}} \hat{J}_{p_k} \\ \tilde{J}_b = \hat{\Sigma}^{-\frac{1}{2}} \left[\hat{J}_{p_1} \cdots \hat{J}_{p_{k-1}} \hat{J}_{p_{k+1}} \cdots \hat{J}_{p_{N\rho}} \right] \end{cases} \tag{3-41}$$

By this definition, the Fisher information matrix can also be partitioned consistently as

$$F = \begin{bmatrix} \tilde{J}_a & \tilde{J}_b \end{bmatrix}^T \begin{bmatrix} \tilde{J}_a & \tilde{J}_b \end{bmatrix} = \begin{bmatrix} F_{aa} & F_{ab} \\ F_{ba} & F_{bb} \end{bmatrix} \tag{3-42}$$

in which

$$\begin{aligned} F_{aa} &= \tilde{J}_a^T \tilde{J}_a, \qquad F_{ab} = \tilde{J}_a^T \tilde{J}_b, \\ F_{ba} &= \tilde{J}_b^T \tilde{J}_a, \qquad F_{bb} = \tilde{J}_b^T \tilde{J}_b. \end{aligned} \tag{3-43}$$

By defining $\tilde{\zeta} = \hat{\Sigma}^{-\frac{1}{2}}\zeta$ and in view of (3-41), the partial residuals $\tilde{\zeta}_a$ and $\tilde{\zeta}_b$ corresponding to the discretization *a* and *b* can be defined as

$$\tilde{\zeta}_a = \tilde{J}_a^T \tilde{\zeta} \ , \qquad \tilde{\zeta}_b = \tilde{J}_b^T \tilde{\zeta} \tag{3-44}$$

which are normally distributed in consideration of (3-28) as

$$\begin{cases} \tilde{\zeta}_a \to \mathcal{N}(F_{aa}\delta_a + F_{ab}\delta_b, F_{aa}) \\ \tilde{\zeta}_b \to \mathcal{N}(F_{ba}\delta_a + F_{bb}\delta_b, F_{bb}) \end{cases} \tag{3-45}$$

where $\delta_a = \delta p_k$ and $\delta_b = \begin{bmatrix} \delta p_1 & \cdots & \delta p_{k-1} & \delta p_{k+1} & \cdots & \delta p_{N_p} \end{bmatrix}^T$. Therefore, the robust residual ζ_a^* defined as

$$\zeta_a^* = \tilde{\zeta}_a - F_{ab}F_{bb}^{-1}\tilde{\zeta}_b \tag{3-46}$$

is also distributed normally as

$$\zeta_a^* \to \mathcal{N}(F_a^*\delta_a, F_a^*) \tag{3-47}$$

where

$$F_a^* = F_{aa} - F_{ab}F_{bb}^{-1}F_{ba} \, . \tag{3-48}$$

The corresponding robust χ^2-test can be then defined as

$$\chi^{*2}(p_k) = \zeta_a^{*T} F_a^{*-1} \zeta_a^* \, . \tag{3-49}$$

The robust χ^2-test in δ_a is independent of δ_b as can be seen in (3-47) and (3-48).

It should be noted that the expected value of the robust χ^2-test is zero when $\delta_a = 0$ while the expected value of the test from the sensitivity based approach is not zero and equals to $F_{ab}\delta_b$. Moreover, although for a damaged element the robust χ^2-test has smaller or equal value than the

sensitivity based approach (as $F_{ab}F_{bb}^{-1}F_{ba}$ is semi positive definitive)[1], but the effect of damage in other elements is removed from this factor. This makes the damaged elements more distinguishable than the other test.

This test can be repeated for each element and the elements with higher robust χ^2-value are linked to the changed elements. It is worth mentioning that this test is also independent of the scaling of the Jacobian matrices (Basseville 1998; Döhler 2011) as will be discussed in Chapter 5.

[1] Semi definiteness comes from the occurrence that modeshapes sensitivities (*a* and *b*) be orthogonal

Chapter 4: Impact of Measurement Noise and Length on the Statistical Subspace Damage Detection Technique

4.1 Introduction

Two main challenges in health monitoring of real structures are low number of sensors and existence of noise in the measurements. Statistical damage detection methods including SSDD have a robust architecture that can deal with sparsely instrumented structures, at least for the level one of damage detection, namely investigating the existence of damage. Moreover, these methods can also deal with noisy data due to their intrinsic statistical approach to the problem. In order to assess and to predict the performance of the SSDD method in real-life SHM problems, the impact of the measurement noise and also of the measurement length on the performance of the SSDD method is of interest. While previous studies (Döhler et al. 2014b; Döhler and Mevel 2013) investigated the effect of changes in the unknown excitation properties on the SSDD technique, the impact of measurement noise and length have never been elaborated.

In this chapter both effects on the SSDD technique will be investigated in the mathematical theory of the method. Existence of noise in experimental data is inevitable. There are different sources of the noise in ambient vibration testing of a structure such as the change in the excitation sources (Döhler et al. 2014b; Döhler and Hille 2014), noise of measuring instruments and human error. Moreover, as suggested in different studies such as (Alvandi and Cremona 2006), the data quality (noise ratio) can affect significantly on the damage detection test and , therefore, investigating the effect of measurement noise on the SSDD technique is an important factor in assessing its functionality. It was demonstrated that SSDD technique can perform robustly under ambient excitations with changing statistics (Döhler et al. 2014b; Döhler and Mevel 2013).

In this chapter, the main contributions include analyzing the theory associated to the effects of the measurement noise and number of samples on the SSDD technique. This study helps in having a better understanding of the results from the SSDD approach. Moreover, these theorems help on the evaluation of system identification approaches, because the variance of the identified system parameters (in here, system parameter refers to the eigenstructure) are directly related to the noise. Although this noise does not have effect on the expected value of the parameters evaluated from system identification approaches, but they affect on the variance of these parameters which is recently of interest to operational model analysis approaches too.

4.2 Properties of χ^2-test

The residual ζ is a function of number of samples and the noise in the measured data. The dependence of this variable on the number of samples is explicit in equation (3-23). Moreover, analogous to the effect of change in the excitation properties (Döhler et al. 2014b), additional measurement noise superposed on the measured data will affect on the cross covariance between the outputs, and hence, on the estimated Hankel matrix. Thus, the evaluated residual (3-23) and its covariance Σ are a function of the superposed noise.

Since in this chapter mainly the effect of measurement noise and number of samples is investigated, the dependence of variables to these parameters are needed to be notified over their symbols. Therefore, for example, ζ_N^e, $\hat{\Sigma}^e$ and χ_N^2 will be used, respectively, instead of ζ, $\hat{\Sigma}$ and χ^2, with keeping the same properties. The indices *N* and *e* represent, in order, the number of samples and measurement noise level in the measured data.

It should be noted that the estimated covariance matrix is a function of number of samples as well, but in its asymptotic basis, the effect of number of samples is removed as *N* goes towards infinity, i.e. $\Sigma^e = \lim_{N\to\infty} \Sigma_N^e$.

Hence, both the number of samples and measurement noise can change the residual and the final evaluated χ^2-value. In this section their effect on the non-parametric χ^2-test is studied for a constant damage.

It is always assumed that the residual covariance Σ^e is estimated once on healthy data from the reference state of the structure, where usually lots of data is available allowing for a good covariance estimation (Döhler et al. 2014b). The covariance is never recalculated when testing a residual ζ_N^e for damage that is computed on new test data as discussed in subsection 3.2.6.

Before starting the analysis, we recall a basic property of the χ^2-distribution: let γ be a χ^2-distributed variable, d its number of degrees of freedom and n_c its non-centrality parameter, then we have

$$\mathbf{E}\gamma = d + n_c . \tag{4-1}$$

4.3 Effect of number of samples

The effect of number of samples can be seen in residual (3-23) both explicitly in terms of $\sqrt{N}$ and implicitly such as its variance and the change in the system parameter. The reason of pre-multiplying the square root of number of samples in the residual vector is that based on the Central Limit Theorem, the resultant product, i.e. (3-23), is distributed asymptotically normal as stated in (3-28), with its covariance being independent of the number of samples. A detailed analysis is made in this section.

4.3.1 Effect on the residual covariance

Since the asymptotic residual covariance is the same in reference and damaged states (see Eq. (3-28)), an estimate $\hat{\Sigma}^e$ of the covariance matrix Σ^e is more conveniently obtained from data in the reference state of the structure under the assumption of no changes in the noise properties of the

system (Döhler et al. 2014b). The computation of the covariance estimate is described in detail in (Döhler et al. 2014b) and in section 3.2.6. Note that the asymptotic covariance Σ^e is independent of the number of samples N, which can also be seen in (3-28) considering the CLT. Hence, the expected value of the covariance estimate $\hat{\Sigma}^e$ neither depends on the number of datasets nor their length used in the estimation. Of course, the quality of the estimation improves when using more data, and we assume that sufficient data has been used to achieve an accurate estimation.

4.3.2 Effect on the χ^2-test value

Considering CLT and (3-28), the residual is approximately Gaussian for large number of samples N, and it holds

$$\zeta_N^e \approx \begin{cases} \mathcal{N}(0,\ \Sigma^e) & \text{under } H_0 \\ \mathcal{N}(\delta,\ \Sigma^e) & \text{under } H_1 \end{cases} \tag{4-2}$$

where $\delta = \sqrt{N}\,\Upsilon^e$ with $\Upsilon^e = \mathbf{E}\left(\text{vec}(S_0^T \hat{\mathbf{H}}_{p+1})\right) = \text{vec}(S_0^T \mathbf{H}_{p+1})$.

Note that Υ^e depends on the expected value $\mathbf{H}_{p+1}$ of the Hankel matrix of the current system (which is independent of the number of samples N), and $\hat{\mathbf{H}}_{p+1}$ is a consistent estimate of matrix $\mathbf{H}_{p+1}$. Note also that $\Upsilon^e = 0$ if the system is in the reference state due to the definition of the null-space.

In the following, the influence of N on the expected value of the χ^2-test variable in (3-35) is investigated.

4.3.3 Proposed theorems on the effect of number of samples on the χ^2-test

In this section, two theorems will be proposed and proved in order to predict the behavior of the χ^2-test under the influence of number of samples when the structure is damaged or undamaged. These theorems are presented in the following.

Theorem 4.1: *Under the undamaged state of the structure, i.e. H_0 is true, increase or decrease of the number of samples does not change the mean of the χ^2 value.*

Proof: Since $\zeta_N^e \approx \mathcal{N}(0,\Sigma^e)$ under H_0 (for sufficiently large number of samples N), the non-centrality parameter of the resulting χ^2-test variable in (3-35) is 0, as stated in (3-34). From the property (4-1) of the χ^2-distribution it follows $\mathbf{E}(\chi_N^2) \approx d$ where $d = \dim(\zeta_N^e)$, and d is the number of degrees of freedom of χ^2-value and independent of N.

Theorem 4.2: *If the structure is damaged, i.e. H_1 is true, change of the number of samples will result in a change (in the same direction) in the mean of the evaluated χ^2 test variable.*

Proof: Under H_1 the non-centrality parameter of χ^2-value is $\delta^T(\Sigma^e)^{-1}\delta$. Because $\delta = \sqrt{N}\,\Upsilon^e$, the non-centrality parameter yields $N(\Upsilon^e)^T(\Sigma^e)^{-1}\Upsilon^e$, where both Υ^e and Σ^e are independent of N. From the property (4-1) of the non-central χ^2-distribution, it follows $\mathbf{E}(\chi_N^2) \approx d + N(\Upsilon^e)^T(\Sigma^e)^{-1}\Upsilon^e$ (for sufficiently large number of samples N). Thus, the mean of the test variable grows (or decreases) when the number of samples of the same damaged system grows (or decreases).

4.4 Effect of measurement noise

Effect of the amount of measurement noise is investigated in two settings. In the first one, the properties of the measurement noise are the same in the reference state and possibly damaged state, while in the second setting they are different. Each of these settings are investigated in the following two subsections.

First, some properties regarding the noise properties of the state space system (3-3) are recalled (Van Overschee and De Moor 1996). They are given by

$$\mathbf{E}\left[\begin{pmatrix} w_k \\ \varepsilon_k \end{pmatrix}\begin{pmatrix} w_k^T & \varepsilon_k^T \end{pmatrix}\right] = \begin{bmatrix} Q & S \\ S^T & R \end{bmatrix}. \tag{4-3}$$

Only matrix R depends on the variance of the measurement noise. Note that the measurement noise is denoted as e, and the output noise term ε_k is in fact a sum of the measurement noise and the excitation noise in the case of acceleration measurements (reader is referred to (3-7)). In this case matrix S only depends on the excitation noise, assuming that excitation and measurement noise are independent.

With these definitions, the expected value of the Hankel matrix does not depend on the measurement noise, since $R_i = \mathbf{E}(y_k y_{k-i}^T) = HF^{i-1}G$ for $i \geq 1$, where $G = FDH^T + S$, with D being the state covariance (assuming zero mean). None of these quantities depend on the measurement noise under the previous assumptions.

However, the residual covariance $\Sigma^e = \lim_{N\to\infty} \mathbf{E}((\zeta_N^e - \mathbf{E}\zeta_N^e)(\zeta_N^e - \mathbf{E}\zeta_N^e)^T)$ depends on the measurement noise. The mathematical analysis of the relationship between residual covariance and measurement noise is demonstrated in Appendix A. It can be seen that the residual covariances before and after addition of noise are related as

$$\Sigma^{e_2} = \Sigma^{e_1} + \Delta_\Sigma^v. \tag{4-4}$$

By assuming that a Gaussian distributed noise is applied to the measurements with the mean equal to zero and the standard deviation equal to a ratio β of the standard deviation of the measurements, Δ_Σ^v is a matrix containing fourth order polynomials of β (Appendix A). For the analysis of the effect of changes in the measurement noise, e_1 refers to the noise properties of the data before applying an additional measurement noise and e_2 refers to the data with the additional measurement noise, i.e. $e_2 = e_1 + \delta_e$. This is the case if each of the measured signals in the first

configuration have a lower signal to noise ratio than the respective signals in the second configuration (while the properties of the ambient excitation noise remain the same). A higher measurement noise leads to larger variations in the residual and thus to a bigger residual covariance as shown in Appendix A.

The effect of changes in the measurement noise is now investigated in two settings. In the first one, the noise properties in the reference state and in the possibly damaged state are the same, while in the second setting they are different.

4.4.1 Effect of noise with equal properties between the reference state and possibly damaged state

In this section, it is assumed that the measurement noise properties in data from reference state and possibly damaged state are equal. We compare different noise properties that are equal in both states. Note that the residual covariance matrices Σ^{e_1} and Σ^{e_2} for different noise properties e_1 and e_2 are assumed to be obtained from reference datasets under their respective conditions. Two theorems (for damaged and undamaged structures) are presented in here on the effect of measurement noise with equal properties in the reference state and test state.

4.4.1.1 Proposed theorems

Theorem 4.3: *If the structure is undamaged and the noise properties of both the reference state data and the current state data are equal, then an increase or decrease of the noise in both states does not change the expected* χ^2*-value. In other words,* $\mathbf{E}\left[(\zeta_N^{e_1})^T(\Sigma^{e_1})^{-1}\zeta_N^{e_1}\right] = \mathbf{E}\left[(\zeta_N^{e_2})^T(\Sigma^{e_2})^{-1}\zeta_N^{e_2}\right]$ *under* H_0.

Proof: From the property of the χ^2-distribution in (4-1) it follows that the expected value of the respective χ^2-values is $d = \dim(\zeta_N^{e_1}) = \dim(\zeta_N^{e_2})$ under H_0, as in proof of Theorem 4.1, which is independent of the noise.

Theorem 4.4: *If the structure is damaged and the noise properties of both the reference state data and the current state data are equal, then an increase or decrease of the noise in both states results in a change (in inverse direction) in the expected χ^2 value for a constant damage. In other words, if $e_2 = e_1 + \delta_e$ then $\mathbf{E}\left[(\zeta_N^{e_2})^T(\Sigma^{e_2})^{-1}\zeta_N^{e_2}\right] < \mathbf{E}\left[(\zeta_N^{e_1})^T(\Sigma^{e_1})^{-1}\zeta_N^{e_1}\right]$ under H_1.*

Proof: As shown in Section 3.1.1, the measurement noise does not influence the expected value of the respective Hankel matrices. Hence, $\delta = \mathbf{E}\zeta_N^{e_1} = \mathbf{E}\zeta_N^{e_2}$ is equal for both noise configurations (see also (3-34)), while the non-centrality parameters are $n_c^{e_1} = \delta^T(\Sigma^{e_1})^{-1}\delta$ and $n_c^{e_2} = \delta^T(\Sigma^{e_2})^{-1}\delta$, respectively. Due to assumption $\Sigma^{e_2} = \Sigma^{e_1} + \Delta_{\Sigma_\zeta}^v$ it follows $n_c^{e_2} = \delta^T(\Sigma^{e_2})^{-1}\delta = \delta^T(\Sigma^{e_1} + \Delta_{\Sigma_\zeta}^v)^{-1}\delta$. By using the matrix inverse lemma it holds $(\Sigma^{e_1} + \Delta_{\Sigma_\zeta}^v)^{-1} = (\Sigma^{e_1})^{-1} - (\Sigma^{e_1})^{-1}\left((\Delta_{\Sigma_\zeta}^v)^{-1} + (\Sigma^{e_1})^{-1}\right)^{-1}(\Sigma^{e_1})^{-1}$. Thus, $(\Sigma^{e_2})^{-1} = (\Sigma^{e_1})^{-1} - \Delta_\Sigma^{-1}$ and $n_c^{e_2} = n_c^{e_1} - \delta^T\Delta_\Sigma^{-1}\delta$ where

$$\Delta_\Sigma^{-1} = (\Sigma^{e_1})^{-1}\left((\Delta_{\Sigma_\zeta}^v)^{-1} + (\Sigma^{e_1})^{-1}\right)^{-1}(\Sigma^{e_1})^{-1}. \qquad \textbf{(4-5)}$$

Since Σ^{e_1} and $\Delta_{\Sigma_\zeta}^v$ (as shown in Appendix A) are positive definite matrices, Δ_Σ^{-1} is a positive definite matrix and therefore $\delta^T\Delta_\Sigma^{-1}\delta > 0$. Hence we have $n_c^{e_2} < n_c^{e_1}$. Then, the assertion follows from property (4-1) of the χ^2-distribution.

4.4.2 Effect of noise with different properties between the reference state and possibly damaged state

In this section it is assumed that the measurement noise will change in the test data irrespective to the noise in the reference data where the residual covariance was computed. Note that since under this condition the noise properties of the residual do not correspond to its covariance, one would need to repeat the computation of the covariance matrix to accommodate noise changes in a correct test (Döhler et al. 2014b). However as mentioned before, in practice the numerical computation of the covariance on each tested dataset is complex and impractical. Hence, the covariance is usually only computed once in the reference state assuming that the statistical characteristics of the noise are not changed. In this section we investigate the consequences of using different noise properties, which violates this assumption.

First, the effect of changes in the measurement noise of the test data are investigated, while the noise level in the residual covariance remains constant. Subsequently, the effect of different noise levels in the residual covariance are investigated, while the noise level in the test data remains constant. Two theories on these effects of the measurement noise on the χ^2-test are presented in the following section.

4.4.2.1 Proposed theorems

Theorem 4.5: *Change in the noise properties of the test data results in a change in the expected χ^2-value in the same direction, regardless to the state of the structure. In other words, if* $e_2 = e_1 + \delta_e$ *then* $\mathbf{E}\left[(\zeta_N^{e_2})^T(\Sigma^{e_1})^{-1}\zeta_N^{e_2}\right] > \mathbf{E}\left[(\zeta_N^{e_1})^T(\Sigma^{e_1})^{-1}\zeta_N^{e_1}\right]$ *both under H_0 and H_1.*

Proof: Analogous to proof of Theorem 4.4, it follows from property (4-1), that $\mathbf{E}\left[(\zeta_N^{e_2})^T(\Sigma^{e_2})^{-1}\zeta_N^{e_2}\right] = d + \delta^T(\Sigma^{e_2})^{-1}\delta$. Having $(\Sigma^{e_2})^{-1} = (\Sigma^{e_1})^{-1} - \Delta_\Sigma^{-1}$, it follows from (4-5)

$\mathbf{E}\left[(\zeta_N^{e_2})^T(\Sigma^{e_2})^{-1}\zeta_N^{e_2}\right] = \mathbf{E}\left[(\zeta_N^{e_2})^T(\Sigma^{e_1})^{-1}\zeta_N^{e_2}\right] - \mathbf{E}\left[(\zeta_N^{e_2})^T\Delta_\Sigma^{-1}\zeta_N^{e_2}\right]$. The left expectation corresponds now to a standard χ^2-distribution and hence

$$\begin{aligned}\mathbf{E}\left[(\zeta_N^{e_2})^T(\Sigma^{e_1})^{-1}\zeta_N^{e_2}\right] &= (d + \delta^T(\Sigma^{e_2})^{-1}\delta) + \mathbf{E}\left[(\zeta_N^{e_2})^T\Delta_\Sigma^{-1}\zeta_N^{e_2}\right] \\ &= (d + \delta^T((\Sigma^{e_1})^{-1} - \Delta_\Sigma^{-1})\delta) + \mathbf{E}\left[(\zeta_N^{e_2})^T\Delta_\Sigma^{-1}\zeta_N^{e_2}\right] \\ &= d + \delta^T(\Sigma^{e_1})^{-1}\delta - \delta^T\Delta_\Sigma^{-1}\delta + \mathbf{E}\left[(\zeta_N^{e_2})^T\Delta_\Sigma^{-1}\zeta_N^{e_2}\right]\end{aligned}$$

which is rewritten as

$$\mathbf{E}\left[(\zeta_N^{e_2})^T(\Sigma^{e_1})^{-1}\zeta_N^{e_2}\right] = \mathbf{E}\left[(\zeta_N^{e_1})^T(\Sigma^{e_1})^{-1}\zeta_N^{e_1}\right] - \delta^T\Delta_\Sigma^{-1}\delta + \mathbf{E}\left[(\zeta_N^{e_2})^T\Delta_\Sigma^{-1}\zeta_N^{e_2}\right]. \quad \textbf{(4-6)}$$

Define $\xi_N^{e_2} = \zeta_N^{e_2} - \delta$, then we have $\xi_N^{e_2} \to \mathcal{N}(0,\ \Sigma^e)$ by considering (3-34). By this definition (4-6) is rewritten as

$$\mathbf{E}\left[(\zeta_N^{e_2})^T\Delta_\Sigma^{-1}\zeta_N^{e_2}\right] = \mathbf{E}\left[(\xi_N^{e_2} + \delta)^T\Delta_\Sigma^{-1}(\xi_N^{e_2} + \delta)\right] = \mathbf{E}\left[\delta^T\Delta_\Sigma^{-1}\delta\right] + \mathbf{E}\left[(\xi_N^{e_2})^T\Delta_\Sigma^{-1}\xi_N^{e_2}\right] + 2\mathbf{E}\left[\delta^T\Delta_\Sigma^{-1}\xi_N^{e_2}\right]$$

in which $\mathbf{E}\left[\delta^T\Delta_\Sigma^{-1}\xi_N^{e_2}\right] = \delta^T\Delta_\Sigma^{-1}\mathbf{E}\left[\xi_N^{e_2}\right] = 0$. Therefore, in view of (4-6)

$$\mathbf{E}\left[(\zeta_N^{e_2})^T(\Sigma^{e_1})^{-1}\zeta_N^{e_2}\right] = \mathbf{E}\left[(\zeta_N^{e_1})^T(\Sigma^{e_1})^{-1}\zeta_N^{e_1}\right] + \mathbf{E}\left[(\xi_N^{e_2})^T\Delta_\Sigma^{-1}\xi_N^{e_2}\right]$$

where $\mathbf{E}\left[(\xi_N^{e_2})^T\Delta_\Sigma^{-1}\xi_N^{e_2}\right] > 0$ since Δ_Σ^{-1} is positive definite. Comparing now with $\mathbf{E}\left[(\zeta_N^{e_1})^T(\Sigma^{e_1})^{-1}\zeta_N^{e_1}\right]$, the assertion follows both for H_0 (where $\delta = 0$) and for H_1.

Theorem 4.5 may be somewhat counterintuitive as it states “less noise leads to a weaker reaction of the test”. However, this would not be the case if the appropriate covariance matrix had been used, which would be of lower magnitude and thus would normalize the residual correctly by dividing it with lower values.

Theorem 4.6: *Regardless of the state of the system, change in the noise properties of the reference data, on which the residual covariance is computed, results in a change in inverse*

direction in the expected χ^2 value. In other words, if $e_2 = e_1 + \delta_e$ then $\mathbf{E}\left[(\zeta_N^{e_1})^T(\Sigma^{e_2})^{-1}\zeta_N^{e_1}\right] < \mathbf{E}\left[(\zeta_N^{e_1})^T(\Sigma^{e_1})^{-1}\zeta_N^{e_1}\right]$ *both under H_0 and H_1.*

Proof: The proof is analogous to the proof of Theorem 4.5. We have $\mathbf{E}\left[(\zeta_N^{e_1})^T(\Sigma^{e_1})^{-1}\zeta_N^{e_1}\right] = d + \delta^T(\Sigma^{e_1})^{-1}\delta$, and since $(\Sigma^{e_2})^{-1} = (\Sigma^{e_1})^{-1} - \Delta_\Sigma^{-1}$, $\mathbf{E}\left[(\zeta_N^{e_1})^T(\Sigma^{e_2})^{-1}\zeta_N^{e_1}\right] = \mathbf{E}\left[(\zeta_N^{e_1})^T(\Sigma^{e_1})^{-1}\zeta_N^{e_1}\right] - \mathbf{E}\left[(\zeta_N^{e_1})^T\Delta_\Sigma^{-1}\zeta_N^{e_1}\right]$. Hence the assertion follows both for H_0 and for H_1, because Δ_Σ^{-1} is positive definite.

4.5 Discussion and practical conclusions

Considering Theorems 4.1 and 4.2, the expected χ^2-value is not affected by data duration in the ideal undamaged state. This will make the test insensitive to the number of samples. However, when the structure is damaged, the χ^2-value will be affected by the number of samples. In other words, if there is more data the damage state becomes more distinct and identifiable. Therefore, by having more samples, the damage detectability will be increased.

It can be inferred from Theorems 4.3 and 4.4 that if the noise in the test data is being increased, the detectability of damage will be less. Moreover, Theorem 4.4 is also intuitive in the sense that higher noise, i.e. a lower signal-to-noise ratio, decreases the quality of the data and makes it harder to detect damage, which is reflected in the lower χ^2-test value.

Considering Theorems 4.5 and 4.6, the unequal noise between the reference state and the test state results in the false alarm or not detecting the damage, when the noise level is high. Based on Theorem 4.5 if the reference state includes a very higher noise ratio than the test state, the damage cannot be identified, and if the test state has a very higher noise ratio than the reference state, then the false alarm would be the result. Hence, the noise ratio should be almost similar between these states in order to have an appropriate result from the χ^2-test.

Therefore, it can be concluded that the number of samples should be high enough in the reference state and test state. Moreover, for the safety threshold creation and testing, the number of samples should be similar and not changed. With having a higher number of samples we will be able to detect smaller damages and vice versa.

Furthermore, the measurement noise characteristics between the reference state and test state should be almost similar and not very different. The lesser the noise ratio would be, the better the quality of the detection will be.

Finally, it should be noted that in a real case study, as will be shown, the expected value of the residual in the undamaged condition is not zero as suggested in (3-34) and it is a small value, namely ε. Therefore, Theorems 4.1 and 4.3 will not be valid for the undamaged condition in practice and the χ^2-test will behave same as for the damaged conditions, i.e. Theorems 4.2 and 4.4, but with less intensity (since ε is small). This will be shown and discussed in Chapters 6 and 7.

Chapter 5: Statistical Subspace Damage Localization in Practice

5.1 Introduction

As shown in section 3.3, the SSDD framework offers the possibility to detect parameters that are responsible for the changes in the residual function. Hence, by defining the parameter set as the collection of parameters linked to a finite element model, e.g. stiffness, mass, damping etc., we can detect the parts of the model that has changed due to this damage.

While the theoretical framework for this localization approach has been set up previously, as described in section 3.3, it has never been applied to real structures in combination with realistic finite element models. Reasons for this were the missing link between the data-driven residual and the finite element model, which is made through a sensible parameter choice (and clustering) and the respective sensitivity computations. In this chapter, an applicable scheme for the required sensitivity computation is proposed for realistic applications, which makes the application of the damage localization possible in practice.

As mentioned, in this approach in addition to the data driven residual, an analytical model of the structure, e.g. finite element model, is used to localize the damage. This analytical model needs to be created for the system in the reference state only and there is no need to update the model for the damage testing. This model is used to calculate Jacobians of the data driven residual to each physical parameter of the structure. The Jacobians are a bridge in connecting the data driven domain, i.e. residual, to the analytical model domain, i.e. physical parameters. Herein, the challenges in connecting the data-driven residual from the SSDD method to the physical parameters of the structure will be addressed. Finally, some methods are proposed in dealing with these challenges.

5.2 Sensitivity analysis

In this section, the sensitivity of the residual is developed with respect to physical parameters of the structure. Let the system parameter θ be set as the vector containing all physical properties (p_k for $k = 1 : N_\rho$) of the elements of the structure (e.g. stiffness, mass, sectional area, elasticity modulus, reduction factor, etc). Therefore, we have $\theta = \left[p_1 \cdots p_{N_\rho} \right]^T$, where N_ρ is the total number of parameters considered for damage localization. By this definition and by assuming damage as change in one or some of the system parameters θ, in view of (3-28) the expected value of the residual ζ under the hypothesis of small deviation is computed as

$$\mathrm{E}(\zeta) \simeq J \delta\theta \tag{5-1}$$

where J is the sensitivity of the residual function with respect to all of the parameters θ, i.e. all physical properties p_k.

In order to compute Jacobian J, each of its columns are the sensitivities of the residual vector with respect to each physical parameter p_k for $k = 1 : N_\rho$, i.e. $J = \left[J_{p_1} \quad J_{p_2} \quad \cdots \quad J_{p_{N_\rho}} \right]$. The methodology is in finding the dependencies in a consequential manner as shown in next figure.

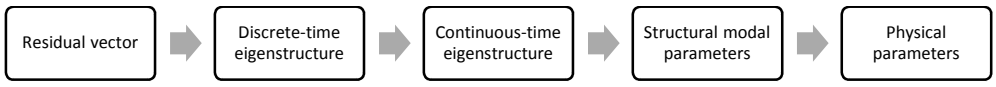

Figure 5.1 Connecting the data-driven residual to the analytical model

As shown in Figure 5.1, the residual vector is firstly related to the discrete-time eigenstructure. The reason is that the observability matrix (from which the residual is evaluated) can be directly related to the discrete-time eigenstructure in its modal basis (see Appendix B.1). In the next stage this eigenstructure is related directly to the continuous-time eigenstructure as shown in (3-9). Subsequently, the continuous-time eigenstructure is related to the modal parameters

through equations (3-10) and (3-11), and finally, the modal parameters are depending on the physical parameters of the structure. This dependency is evaluated using an analytical model, e.g. finite element model, of the structure. Accordingly, the Chain rule is employed in connecting the residual function (3-23) to the physical parameters p_k based on Figure 5.1 as

$$J(p_k) = J(\lambda,\varphi) J^{(\lambda,\varphi)}_{(\mu,\psi)} J^{(\mu,\psi)}_{(f,\xi,\varphi)} J^{(f,\xi,\varphi)}_{p_k} \tag{5-2}$$

in which, $J(p_k)$ is one column of the Jacobian matrix J, i.e. $[J]_k = J(p_k)$, and J is consisting of vectors corresponding to all elements considered in damage localization test; $J(\lambda,\varphi)$ is the sensitivity of the residual to the eigenstructure (λ,φ) and $J^{\bullet}_{\circ}$ is the consistent Jacobian of parameters $\bullet$ with respect to $\circ$. Computation of the Jacobians in (5-2) is described in the next subsection.

5.2.1 Calculating the sensitivities

Since the modal parameters of the discrete-time and continuous-time systems are complex conjugate values, computation of Jacobian matrices in (5-2) is performed in two ways based on the arrangement of these modal parameters: complex-valued and real-valued approaches. The difference between the real-valued approach and the complex-valued approach is in the numerical computation procedure; in the real-valued approach the complex valued eigenstructure is replaced by its real and imaginary parts consistently which will make the computational procedure more efficient and practical. Therefore, the eigenstructures of the discrete-time and continuous-time systems can be represented either in their complex-valued format, i.e. $(\tilde{\lambda},\tilde{\varphi})$ and $(\tilde{\mu},\tilde{\psi})$ or real-valued format, i.e. (λ,φ) and (μ,ψ). Because the computation of these Jacobians is more efficient and practical in real-valued format, these eigenstructures are used as real-valued parameters.

It should be noted that both the real-valued and complex-valued Jacobians result in the same final Jacobian in (5-2) and only their procedure is different in the organization of the parameters. These approaches will be discussed in the following subsections.

5.2.1.1 Computation of Jacobian $J(\lambda,\varphi)$

The Jacobian matrix $J(\lambda,\varphi)$ contains the sensitivities of the residual vector with respect to the real-valued modal parameters of the discrete-time system, i.e. (λ,φ). The computation of this Jacobian is performed by composing the observability matrix from the eigenstructure (λ,φ) and subsequently derivating the residual computed from this matrix with respect to (λ,φ).

5.2.1.1.1 Complex valued Jacobian computation

The defined parameters in (5-3) contain the eigenstructure $(\tilde{\lambda},\tilde{\varphi})$ which are pairs of conjugated complex eigenvalues and modeshapes. Therefore, computation of complex-valued Jacobian $J(\tilde{\lambda},\tilde{\varphi})$ involves calculation of Jacobian with respect to the complex numbers which can be done directly as discussed in this section.

In order to calculate the first part of (5-2) in complex-valued format, i.e. $J(\tilde{\lambda},\tilde{\varphi})$, some definitions are necessary which are elaborated as follows. Let the model parameter $\tilde{\eta}$ be defined as the eigenstructure $(\tilde{\lambda},\tilde{\varphi})$ with model order *n*, i.e.

$$\tilde{\eta}=\begin{bmatrix}\Lambda\\ \mathrm{vec}(\Phi)\end{bmatrix} \quad \text{and} \quad \Lambda=\begin{bmatrix}\lambda_1\\ \lambda_2\\ \vdots\\ \lambda_n\end{bmatrix}, \tag{5-3}$$

in which, Φ represents a matrix containing all the vectors of the modeshapes φ_i and vec() is the vectorization function of a matrix. By factorizing the block Hankel matrix $\mathbf{H}_{p+1,q}$ as

$$\mathbf{H}_{p+1,q} = \tilde{\mathrm{O}}_{p+1}\tilde{\mathrm{C}}_q\,, \tag{5-4}$$

the complex-valued observability matrix $\tilde{\mathrm{O}}_{p+1}$ is written in modal basis (look at Appendix B.1) as

$$\tilde{\mathrm{O}}_{p+1} = \begin{bmatrix} \Phi \\ \Phi\Delta \\ \vdots \\ \Phi\Delta^p \end{bmatrix} \tag{5-5}$$

where Δ is a diagonal matrix containing the eigenvalues λ, i.e. $\Delta = \mathrm{diag}(\Lambda)$. It should be noted that, as mentioned in Chapter 3, $\mathbf{H}_{p+1,q}$ and $\tilde{\mathrm{O}}_{p+1}$ share the same complex-valued left null space $\tilde{S}_0$. Therefore, the left null space can be calculated from a Singular Value Decomposition (SVD) of $\tilde{\mathrm{O}}_{p+1}$ or $\mathbf{H}_{p+1,q}$ and hence

$$\tilde{S}_0^T\tilde{\mathrm{O}}_{p+1} = 0\,. \tag{5-6}$$

The derivative of the observability matrix (5-5) is introduced from (Basseville et al. 2000, 2004) and writes as

$$\tilde{\mathrm{O}}'_{p+1} = \frac{\partial \mathrm{vec}\tilde{\mathrm{O}}_{p+1}}{\partial\tilde{\eta}} = \left[\begin{array}{ccc|ccc} \Lambda_1'^{(p)}\otimes\varphi_1 & \cdots & 0 & \Lambda_1^{(p)}\otimes\mathbf{I}_r & \cdots & 0 \\ \vdots & \ddots & \vdots & \vdots & \ddots & \vdots \\ 0 & \cdots & \Lambda_n'^{(p)}\otimes\varphi_n & 0 & \cdots & \Lambda_n^{(p)}\otimes\mathbf{I}_r \end{array}\right] \in \mathbb{C}^{nr(p+1)\times n(r+1)} \tag{5-7}$$

where,

$$\Lambda_j^{(p)} \overset{\text{def}}{=} [1 \quad \lambda_j \quad \lambda_j^2 \quad \cdots \quad \lambda_j^p]^T, \quad \Lambda_j'^{(p)} \overset{\text{def}}{=} [0 \quad 1 \quad 2\lambda_j \quad \cdots \quad p\lambda_j^{p-1}]^T \text{ for } 1 \le j \le n\,. \tag{5-8}$$

Now, in view of (3-23) and defining the parameter as (5-3),

$$J(\tilde{\lambda},\tilde{\varphi}) = \frac{\partial}{\partial\tilde{\eta}}\mathrm{vec}(\tilde{S}_0^T\mathbf{H}_{p+1,q}) \tag{5-9}$$

which based on (5-4) and vectorization property $\mathrm{vec}(ABC) = (C^T\otimes A)\mathrm{vec}(B)$, can be rewritten as

$$J(\tilde{\lambda},\tilde{\varphi}) = (\tilde{C}_q^T \otimes \tilde{S}_0^T)\tilde{\mathrm{O}}'_{p+1}. \tag{5-10}$$

Finally, since from (5-4) it follows $\tilde{C}_q = \tilde{O}_{p+1}^{\dagger}\mathbf{H}_{p+1,q}$ ($\dagger$ represents pseudo inverse function), (5-10) writes

$$J(\tilde{\lambda},\tilde{\varphi}) = (\tilde{\mathrm{O}}_{p+1}^{\dagger}\mathbf{H}_{p+1,q} \otimes \tilde{S}_0)^T \tilde{\mathrm{O}}'_{p+1}. \tag{5-11}$$

5.2.1.1.2 Real valued Jacobian computation

In structural vibration analysis, typically the parameter $\tilde{\eta}$ defined in (5-3) consists of m pairs of conjugate complex values ($n = 2m$). Therefore, the computation of real-valued Jacobian $J(\lambda,\varphi)$ can be performed in an alternative approach dealing with only real values, based on (Basseville et al. 2004).

Based on definition (5-3), Λ and Φ can be reorganized based on their consisting conjugate value pairs of (Λ_c, Φ_c) as

$$\Lambda = \begin{bmatrix} \Lambda_c \\ \overline{\Lambda_c} \end{bmatrix}, \qquad \Phi = \begin{bmatrix} \Phi_c & \overline{\Phi_c} \end{bmatrix}. \tag{5-12}$$

The parameter $\tilde{\eta}$ can also be analogously defined as pairs of conjugate parameters $(\eta_c, \overline{\eta_c})$ such that

$$\eta_c = \begin{bmatrix} \Lambda_c \\ \mathrm{vec}(\Phi_c) \end{bmatrix} \tag{5-13}$$

from which, the observability matrix is reorganized as

$$\tilde{\mathrm{O}}_{p+1} = \begin{bmatrix} \Phi_c & \overline{\Phi_c} \\ \Phi_c\Delta_c & \overline{\Phi_c\Delta_c} \\ \vdots & \vdots \\ \Phi_c\Delta_c^p & \overline{\Phi_c\Delta_c^p} \end{bmatrix}, \qquad \Delta_c = \mathrm{diag}(\Lambda_c). \tag{5-14}$$

Now by defining the real valued parameter as

$$\eta = \begin{bmatrix} \Re(\eta_c) \\ \Im(\eta_c) \end{bmatrix} = \begin{bmatrix} \Re(\Lambda_c) \\ \mathrm{vec}(\Re(\Phi_c)) \\ \Im(\Lambda_c) \\ \mathrm{vec}(\Im(\Phi_c)) \end{bmatrix}, \tag{5-15}$$

the real valued observability matrix can be computed by

$$\mathrm{O}_{p+1} = \begin{bmatrix} \Re(\Phi_c) & \Im(\Phi_c) \\ \Re(\Phi_c\Delta_c) & \Im(\Phi_c\Delta_c) \\ \vdots & \vdots \\ \Re(\Phi_c\Delta_c^p) & \Im(\Phi_c\Delta_c^p) \end{bmatrix} = \begin{bmatrix} \Re(\tilde{\mathrm{O}}_{p+1}) & \Im(\tilde{\mathrm{O}}_{p+1}) \end{bmatrix} \tag{5-16}$$

where,

$$\mathrm{O}_{p+1} = \tilde{\mathrm{O}}_{p+1} T, \qquad T = \frac{1}{2}\begin{bmatrix} \mathbf{I}_m & -i\,\mathbf{I}_m \\ \mathbf{I}_m & i\,\mathbf{I}_m \end{bmatrix}. \tag{5-17}$$

Based on the relation between the real valued and complex valued observability matrix, i.e. (5-17), and that the conversion matrix T is unitary, the left null space of O_{p+1}, i.e. S_0, is the same as the left null space of $\tilde{\mathrm{O}}_{p+1}$, i.e. $\tilde{S}_0$. Therefore, the left null space of the real valued observation matrix can be used in computation of the residual function with the real valued parameter η.

In the next step, by considering (5-15) and (5-16) the Jacobian of the real valued observability matrix writes as

$$\mathrm{O}'_{p+1} = \frac{\partial\,\mathrm{vec}(\mathrm{O}_{p+1})}{\partial\eta} = \begin{bmatrix} \dfrac{\partial\,\mathrm{vec}(\Re(\tilde{\mathrm{O}}_{p+1}))}{\partial\,\Re(\eta_c)} & \dfrac{\partial\,\mathrm{vec}(\Re(\tilde{\mathrm{O}}_{p+1}))}{\partial\,\Im(\eta_c)} \\ \dfrac{\partial\,\mathrm{vec}(\Im(\tilde{\mathrm{O}}_{p+1}))}{\partial\,\Re(\eta_c)} & \dfrac{\partial\,\mathrm{vec}(\Im(\tilde{\mathrm{O}}_{p+1}))}{\partial\,\Im(\eta_c)} \end{bmatrix}. \tag{5-18}$$

In order to compute the Jacobian matrix O'_{p+1} expanded in (5-18), its parameters will be related to the complex valued observability matrix $\tilde{\mathrm{O}}'_{p+1}$ computed in (5-7). Thus, each complex value of $\tilde{\mathrm{O}}'_{p+1}$ is expanded and then simplified using the Wirtinger derivatives operators as follows.

$$\begin{aligned}\tilde{\mathrm{O}}'_{p+1} &= \frac{\partial \operatorname{vec}(\Re(\tilde{\mathrm{O}}_{p+1}))}{\partial \eta_c} + i\frac{\partial \operatorname{vec}(\Im(\tilde{\mathrm{O}}_{p+1}))}{\partial \eta_c} \\ &= \frac{1}{2}\left(\frac{\partial \operatorname{vec}(\Re(\tilde{\mathrm{O}}_{p+1}))}{\partial \Re(\eta_c)} - i\frac{\partial \operatorname{vec}(\Re(\tilde{\mathrm{O}}_{p+1}))}{\partial \Im(\eta_c)}\right) + \frac{i}{2}\left(\frac{\partial \operatorname{vec}(\Im(\tilde{\mathrm{O}}_{p+1}))}{\partial \Re(\eta_c)} - i\frac{\partial \operatorname{vec}(\Im(\tilde{\mathrm{O}}_{p+1}))}{\partial \Im(\eta_c)}\right)\end{aligned} \tag{5-19}$$

whose elements satisfy the Cauchy-Riemann equations ($\tilde{\mathrm{O}}_{p+1}$ is a polynomial function and hence complex differentiable) as

$$\begin{cases} \dfrac{\partial \operatorname{vec}(\Re(\tilde{\mathrm{O}}_{p+1}))}{\partial \Re(\eta_c)} = \dfrac{\partial \operatorname{vec}(\Im(\tilde{\mathrm{O}}_{p+1}))}{\partial \Im(\eta_c)} \\ \dfrac{\partial \operatorname{vec}(\Re(\tilde{\mathrm{O}}_{p+1}))}{\partial \Im(\eta_c)} = -\dfrac{\partial \operatorname{vec}(\Im(\tilde{\mathrm{O}}_{p+1}))}{\partial \Re(\eta_c)} \end{cases}. \tag{5-20}$$

Now by substituting (5-20) into (5-19)

$$\tilde{\mathrm{O}}'_{p+1} = \frac{\partial \operatorname{vec}(\Re(\tilde{\mathrm{O}}_{p+1}))}{\partial \Re(\eta_c)} - i\frac{\partial \operatorname{vec}(\Re(\tilde{\mathrm{O}}_{p+1}))}{\partial \Im(\eta_c)},$$

$$\begin{cases} \Re(\tilde{\mathrm{O}}'_{p+1}) = \dfrac{\partial \operatorname{vec}(\Re(\tilde{\mathrm{O}}_{p+1}))}{\partial \Re(\eta_c)} = \dfrac{\partial \operatorname{vec}(\Im(\tilde{\mathrm{O}}_{p+1}))}{\partial \Im(\eta_c)} \\ \Im(\tilde{\mathrm{O}}'_{p+1}) = -\dfrac{\partial \operatorname{vec}(\Re(\tilde{\mathrm{O}}_{p+1}))}{\partial \Im(\eta_c)} = \dfrac{\partial \operatorname{vec}(\Im(\tilde{\mathrm{O}}_{p+1}))}{\partial \Re(\eta_c)} \end{cases} \tag{5-21}$$

from which, (5-18) is rewritten as

$$\mathrm{O}'_{p+1} = \begin{bmatrix} \Re(\tilde{\mathrm{O}}'_{p+1}) & -\Im(\tilde{\mathrm{O}}'_{p+1}) \\ \Im(\tilde{\mathrm{O}}'_{p+1}) & \Re(\tilde{\mathrm{O}}'_{p+1}) \end{bmatrix}. \tag{5-22}$$

Finally, the real-valued Jacobian $J(\lambda, \varphi)$ similar to (5-11) and (5-9) is computed as

$$J(\lambda,\varphi) = (\mathrm{O}_{p+1}^{\dagger}\mathbf{H}_{p+1,q} \otimes S_0)^T \mathrm{O}_{p+1}{}' . \tag{5-23}$$

5.2.1.2 Computation of Jacobians $J_{(\mu,\psi)}^{(\lambda,\varphi)}$ and $J_{(f,\xi,\wp)}^{(\mu,\psi)}$

The Jacobian of the eigenstructure of the discrete-time system, i.e. (λ,φ) to the one from continuous system, i.e. (μ,ψ), is represented by $J_{(\mu,\psi)}^{(\lambda,\varphi)}$. By considering equation (3-9), the eigenvectors of both systems are equal and hence their corresponding Jacobian for each part, i.e real and imaginary parts, are identity matrix of size *mr* (*r* is the number of sensors).

In order to calculate the derivation of the eigenvalue λ_j with respect to μ_j, we should consider them in two real and imaginary parts based on the definition of real-valued parameterization (5-15). Hence, the Jacobian needs to be computed for real and imaginary part of eigenvalue λ_j with respect to real and imaginary parts of eigenvalue μ_j. In view of (3-9),

$$\lambda_j = e^{\tau\left(\Re(\mu_j)+i\Im(\mu_j)\right)} = e^{\tau\Re(\mu_j)}\left(\cos(\tau\Im(\mu_j)) + i\sin(\tau\Im(\mu_j))\right)$$

which yields

$$\Re(\lambda_j) = e^{\tau\Re(\mu_j)}\cos(\tau\Im(\mu_j)), \qquad \Im(\lambda_j) = e^{\tau\Re(\mu_j)}\sin(\tau\Im(\mu_j)) .$$

Therefore, the derivations are evaluated as

$$\begin{aligned} \frac{\partial\Re(\lambda_j)}{\partial\Re(\mu_j)} &= \tau\Re(\lambda_j), \qquad & \frac{\partial\Re(\lambda_j)}{\partial\Im(\mu_j)} &= -\tau\Im(\lambda_j) \\ \frac{\partial\Im(\lambda_j)}{\partial\Re(\mu_j)} &= \tau\Im(\lambda_j), \qquad & \frac{\partial\Im(\lambda_j)}{\partial\Im(\mu_j)} &= \tau\Re(\lambda_j) \end{aligned} . \tag{5-24}$$

Thus, considering that eigenvalues of a system are independent $J_{(\mu,\psi)}^{(\lambda,\varphi)}$ can be defined based on (Basseville et al. 2004) as

$$J_{(\mu,\psi)}^{(\lambda,\varphi)} = \left[\begin{array}{ccc|ccc} \mathcal{I}_1 & & & -\mathfrak{I}_1 & & \\ & \ddots & & & \ddots & \\ & & \mathcal{I}_m & & & -\mathfrak{I}_m \\ & & \mathbf{I}_{mr} & & & 0 \\ \hline \mathfrak{I}_1 & & & \mathcal{I}_1 & & \\ & \ddots & & & \ddots & \\ & & \mathfrak{I}_m & & & \mathcal{I}_m \\ & & 0 & & & \mathbf{I}_{mr} \end{array}\right]. \qquad \textbf{(5-25)}$$

where $\mathcal{I}_j = \tau\Re(\lambda_j)$ $\quad ,\mathfrak{I}_j = \tau\mathfrak{I}(\lambda_j)$. The discretization of (5-25) is based on definition of parameter η in (5-15).

Jacobian matrix $J_{(f,\xi,\varphi)}^{(\mu,\psi)}$ represents the Jacobian of the eigenstructure (μ,ψ) to the frequencies, damping ratios and modeshapes of the structure. The modeshapes of the structure are not changed in these systems similar to the eigenvectors of the continuous and discrete systems and therefore by positioning them all together, for each part the Jacobian will be equal to unitary matrix with dimension *mr*. Based on (3-11), the other derivatives are calculated as

$$\begin{aligned} &\frac{\partial\Re(\mu_j)}{\partial f_j} = -2\pi\xi_j, \qquad \frac{\partial\Re(\mu_j)}{\partial \xi_j} = -2\pi f_j \\ &\frac{\partial\mathfrak{I}(\mu_j)}{\partial f_j} = 2\pi\sqrt{1-\xi_j^2}, \quad \frac{\partial\mathfrak{I}(\mu_j)}{\partial \xi_j} = \frac{-2\pi f_j\xi_j}{\sqrt{1-\xi_j^2}} \end{aligned} \qquad \textbf{(5-26)}$$

By defining row vectors

$$\mathcal{I}_j^M = \left[\frac{\partial\Re(\mu_j)}{\partial f_j} \quad \frac{\partial\Re(\mu_j)}{\partial \xi_j}\right] \text{ and } \mathfrak{I}_j^M = \left[\frac{\partial\mathfrak{I}(\mu_j)}{\partial f_j} \quad \frac{\partial\mathfrak{I}(\mu_j)}{\partial \xi_j}\right],$$

the Jacobian matrix is evaluated as

$$J_{(f,\xi,\wp)}^{(\mu,\psi)} = \left[\begin{array}{ccccc} \mathcal{I}_1^M & & & & \\ & \ddots & & & \\ & & \mathcal{I}_m^M & & \\ & & & \mathbf{I}_{mr} & 0 \\ \hline \mathcal{J}_1^M & & & & \\ & \ddots & & & \\ & & \mathcal{J}_m^M & & \\ & & & 0 & \mathbf{I}_{mr} \end{array}\right] \qquad \textbf{(5-27)}$$

in which, the parameters $(f,\xi,\wp)$ are organized as pairs of frequency and damping ratios, followed by the modeshapes.

It should be noted that the computed damping ratio is one of the high variance variables in operational modal analysis. Moreover, in modal analysis of finite element models usually the damping is ignored. Therefore, the identified modeshapes will be also all real. In this case, all the columns related to the imaginary part of modeshapes (the most right columns) and the damping ratio can be removed from $J_{p_k}^{(f,\xi,\wp)}$ in (5-27), consistently.

5.2.1.3 Linear model sensitivity analysis with respect to physical parameters, $J_{p_k}^{(f,\xi,\wp)}$

The computation of the sensitivities of eigenstructure of a model to all its physical parameters is usually time consuming, since usually the model of structures consists of large number of parameters. This computation can be performed directly or by using mathematical differential approximation methods such as finite difference approach. In the following these two approaches are described.

5.2.1.3.1 Direct sensitivity approach

In this approach the last two Jacobians of (5-2), i.e. $J_{p_k}^{(\mu,\psi)} = J_{(f,\xi,\wp)}^{(\mu,\psi)} J_{p_k}^{(f,\xi,\wp)}$ can be evaluated directly for each parameter without the need of evaluating $J_{(f,\xi,\wp)}^{(\mu,\psi)}$.

Based on derivation of eigenequation (3-2) for a linear model

$$\frac{\partial \mu_j}{\partial p_k}(2\mu_j M + C)\Psi_j + (\mu_j^2 \frac{\partial M}{\partial p_k} + \mu_j \frac{\partial C}{\partial p_k} + \frac{\partial K}{\partial p_k})\Psi_j + (\mu_j^2 M + \mu_j C + K)\frac{\partial \Psi_j}{\partial p_k} = 0 . \quad \textbf{(5-28)}$$

Premultiplying (5-28) by Ψ_j^T results in

$$\frac{\partial \mu_j}{\partial p_k}\Psi_j^T(2\mu_j M + C)\Psi_j + \Psi_j^T(\mu_j^2 \frac{\partial M}{\partial p_k} + \mu_j \frac{\partial C}{\partial p_k} + \frac{\partial K}{\partial p_k})\Psi_j + \Psi_j^T(\mu_j^2 M + \mu_j C + K)\frac{\partial \Psi_j}{\partial p_k} = 0 \quad \textbf{(5-29)}$$

which in view of (3-2) yields

$$\frac{\partial \mu_j}{\partial p_k} = -\frac{\Psi_j^T(\mu_j^2 \frac{\partial M}{\partial p_k} + \mu_j \frac{\partial C}{\partial p_k} + \frac{\partial K}{\partial p_k})\Psi_j}{\Psi_j^T(2\mu_j M + C)\Psi_j} . \quad \textbf{(5-30)}$$

By assuming of negligible damping and mass normalized modeshapes $\bar{\Psi}_j$, i.e. $\bar{\Psi}_j^T M \bar{\Psi}_j = \mathbf{I}$, (5-30) will be simplified to

$$\frac{\partial \mu_j}{\partial p_k} = -\frac{1}{2\mu_j}\bar{\Psi}_j^T(\mu_j^2 \frac{\partial M}{\partial p_k} + \frac{\partial K}{\partial p_k})\bar{\Psi}_j . \quad \textbf{(5-31)}$$

The sensitivity of modeshapes to the parameter p_k can also be computed by rewriting (5-28) as

$$(\mu_j^2 M + \mu_j C + K)\frac{\partial \Psi_j}{\partial p_k} = -\frac{\partial \mu_j}{\partial p_k}(2\mu_j M + C)\Psi_j - (\mu_j^2 \frac{\partial M}{\partial p_k} + \mu_j \frac{\partial C}{\partial p_k} + \frac{\partial K}{\partial p_k})\Psi_j . \quad \textbf{(5-32)}$$

and substituting (5-30) into it.

It should be noted that (5-32) does not have a unique solution, since if $\frac{\partial \Psi_j}{\partial p_k} = J_k$ is a solution then $\frac{\partial \Psi_j}{\partial p_k} = J_k + \alpha\Psi_j$ for $\alpha \in \mathbb{R}$ is also a solution for (5-32). This can be seen by writing the solution for (5-32) as

$$J_k = (\mu_j^2 M + \mu_j C + K)^{\dagger}\left(-\frac{\partial \mu_j}{\partial p_k}(2\mu_j M + C)\Psi_j - (\mu_j^2 \frac{\partial M}{\partial p_k} + \mu_j \frac{\partial C}{\partial p_k} + \frac{\partial K}{\partial p_k})\Psi_j \right). \quad \textbf{(5-33)}$$

Now another solution is computed by adding eigenequation (3-2) to (5-32) as

$$(\mu_j^2 M + \mu_j C + K)\left(\frac{\partial \Psi_j}{\partial p_k} - \alpha\Psi_j \right) = -\frac{\partial \mu_j}{\partial p_k}(2\mu_j M + C)\Psi_j - (\mu_j^2 \frac{\partial M}{\partial p_k} + \mu_j \frac{\partial C}{\partial p_k} + \frac{\partial K}{\partial p_k})\Psi_j \ .$$

whose solution is

$$\begin{aligned} \mathcal{J}_k &= (\mu_j^2 M + \mu_j C + K)^{\dagger}\left(-\frac{\partial \mu_j}{\partial p_k}(2\mu_j M + C)\Psi_j - (\mu_j^2 \frac{\partial M}{\partial p_k} + \mu_j \frac{\partial C}{\partial p_k} + \frac{\partial K}{\partial p_k})\Psi_j \right) + \alpha\Psi_j \\ &= J_k + \alpha\Psi_j \ . \end{aligned} \quad \textbf{(5-34)}$$

Therefore, any solution as $\frac{\partial \Psi_j}{\partial p_k} = J_k + \alpha\Psi_j$ for $\alpha \in \mathbb{R}$ is a solution for the eigenvector Jacobian. It should be noted that in section 5.2.1.4 it will be shown that the final Jacobian is independent of the particular solution of $\frac{\partial \Psi_j}{\partial p_k}$. However, in the damage localization of a structure for the sake of consistency, the basis of $\frac{\partial \Psi_j}{\partial p_k}$ can be made unique by imposing a constraint, e.g. $\Psi_j^T \frac{\partial \Psi_j}{\partial p_k} = 0$, on the solution.

Again it should be emphasized that after choosing the solution, it needs to be pre-multiplied by matrix *L* to calculate the sensitivities of modeshapes ψ, as seen in (3-2).

In evaluating the sensitivities directly, the stiffness, mass and damping matrices of the structure are needed to be evaluated and then their sensitivities to the parameters be calculated. This might be a problem in using commercial software in modelling big structures or complex FE models. Moreover, in case of using these software, there might be no access granted to the full stiffness and mass matrices.

5.2.1.3.2 Finite difference method

One of the simplest methods of indirect sensitivity analysis is the finite difference method. This method is computational more expensive than the direct method, however due to its simplicity and the increase of computational power of computers it is still widely used. The reason for being simple is that there is no extra analysis other than the evaluation of the function needed in computing the Jacobian.

The basis of the theory in finite difference is based on the following equation:

$$\frac{\partial F}{\partial p_k} = \lim_{\delta p_k \to 0} \frac{F(p_k + \delta p_k) - F(p_k)}{\delta p_k} \tag{5-35}$$

where F is a function of physical variables p_k. In calculating the sensitivity to each variable the other variables are kept constant and therefore the evaluation of function F needs to be repeated to the number of variables. Since (5-35) is exact if $\delta p_k \to 0$, in practice only an approximation of the sensitivity can be computed by choosing δp_k small enough. It should be noted that the value chosen for δp_k cannot be chosen too small considering machine precision and computational error. Furthermore, it cannot be chosen large due to the high approximation of (5-35). Hence, the optimal value of this parameter can be evaluated by running a series of tests of different small δp_k and choosing the smallest value which does not change the sensitivity values unreasonably. By decreasing δp_k the change rate of the sensitivities should be decreased. Moreover, there are some other researches on choosing the optimal perturbation value δp_k for dynamic models such as (De Pauw and Vanrolleghem 2003).

5.2.1.4 Independence of the residual Jacobian to non-uniqueness of modeshapes sensitivities

It was shown in (5-32), that the solution for $\frac{\partial \Psi_j}{\partial p_k} = J_k$ is not unique and it can be any combination of $\frac{\partial \Psi_j}{\partial p_k} = J_k + \alpha_j \Psi_j$ for $\alpha_j \in \mathbb{R}$. However, the final Jacobian is independent of $\alpha_j \Psi_j$. In other words, in any basis that the solution for $\frac{\partial \Psi_j}{\partial p_k} = J_k$ is gained, the final Jacobian of residual $J(p_k)$ calculated from it yields similar unique result. This will be proved in the following lemma. This is important because it will help us in understanding why the evaluated Jacobian from different sensitivity analysis methods might be different, while the final Jacobian computed from these must be still identical.

Lemma 5.1: The final Jacobian of residual $J(p_k)$ is unique, although the solution for $\frac{\partial \Psi_j}{\partial p_k} = J_k$ is not unique.

Proof: For simplification, this proof will be demonstrated in complex format of the eigenstructure. As mentioned before, the calculation of Jacobians can be performed in either real-valued or complex-valued format and the final results are similar.

After premultiplication by matrix *L* as suggested in section 5.2.1.3.1 (reader is referred to equation (3-2)) the effect of $\alpha_j \psi_j$ will be investigated as a multiplier to all parameters of (5-2) preceding $J^{(\mu,\psi)}_{(f,\xi)}$. Since this part is only added on the modeshapes part of parameters, (5-2) with $J^{(\tilde{\mu},\tilde{\psi})}_{p_k} = J^{(\tilde{\mu},\tilde{\psi})}_{(f,\xi,\varphi)} J^{(f,\xi,\varphi)}_{p_k}$ is rewritten as

$$J(p_k) = J(\tilde{\lambda},\tilde{\varphi}) J^{(\tilde{\lambda},\tilde{\varphi})}_{(\tilde{\mu},\tilde{\psi})} J^{(\tilde{\mu},\tilde{\psi})}_{p_k}, \quad J^{(\tilde{\mu},\tilde{\psi})}_{p_k} = J^{(\tilde{\mu},\tilde{\psi})}_{p_k} + l_{\alpha\psi} \tag{5-36}$$

where

$$l_{\alpha\psi} = \begin{bmatrix} 0 \\ \alpha_1\psi_1 \\ \vdots \\ \alpha_n\psi_n \end{bmatrix} \tag{5-37}$$

Therefore, the evaluated Jacobian is written as

$$J(p_k) = J(\tilde{\lambda},\tilde{\varphi})J^{(\tilde{\lambda},\tilde{\varphi})}_{(\tilde{\mu},\tilde{\psi})}J^{(\tilde{\mu},\tilde{\psi})}_{p_k} + J(\tilde{\lambda},\tilde{\varphi})J^{(\tilde{\lambda},\tilde{\varphi})}_{(\tilde{\mu},\tilde{\psi})}l_{\alpha\psi} \tag{5-38}$$

whose second part needs to be equated to zero so that the proof is achieved.

As shown in 5.2.1.2, the modeshapes are constant in the discrete and continuous systems and therefore $J^{(\tilde{\lambda},\tilde{\varphi})}_{(\tilde{\mu},\tilde{\psi})}$ will not affect this vector, i.e. $J^{(\tilde{\lambda},\tilde{\varphi})}_{(\tilde{\mu},\tilde{\psi})}l_{\alpha\psi} = l_{\alpha\psi}$. Moreover, since $\psi_j = \varphi_j$ as per (3-9), we have

$$l_{\alpha\psi} = \begin{bmatrix} 0 \\ \alpha_1\varphi_1 \\ \vdots \\ \alpha_n\varphi_n \end{bmatrix}. \tag{5-39}$$

Now by multiplying $J(\tilde{\lambda},\tilde{\varphi})$ to $l_{\alpha\psi}$ in view of (5-10) it yields

$$J(\tilde{\lambda},\tilde{\varphi})J^{(\tilde{\lambda},\tilde{\varphi})}_{(\tilde{\mu},\tilde{\psi})}l_{\alpha\psi} = J(\tilde{\lambda},\tilde{\varphi})l_{\alpha\psi} = (\tilde{C}^T_{p+1}\otimes\tilde{S}^T_0)\tilde{\mathrm{O}}_{p+1}{}'l_{\alpha\psi} = (\tilde{C}^T_{p+1}\otimes\tilde{S}^T_0)\begin{bmatrix} (\Lambda^{(p)}_1\otimes\mathbf{I}_r)\alpha_1\varphi_1 \\ \vdots \\ (\Lambda^{(p)}_n\otimes\mathbf{I}_r)\alpha_n\varphi_n \end{bmatrix}. \tag{5-40}$$

From the mixed-product property of Kronecker product for $j = 1\cdots n$

$$(\Lambda^{(p)}_j\otimes\mathbf{I}_r)\alpha_j\varphi_j = \alpha_j(\Lambda^{(p)}_j\otimes(\mathbf{I}_r\varphi_j)) = \alpha_j(\Lambda^{(p)}_j\otimes\varphi_j)$$

which by comparing to the composition of $\tilde{\mathrm{O}}_{p+1}$ in (5-5) it can be seen that each nonzero element of (5-40) equals to a vector of $\tilde{\mathrm{O}}_{p+1}$, i.e. $(\Lambda^{(p)}_j\otimes\varphi_j) = [\tilde{\mathrm{O}}_{p+1}]_j$. Hence,

$$\begin{bmatrix} (\Lambda_1^{(p)} \otimes \mathbf{I}_r)\alpha_1\varphi_1 \\ \vdots \\ (\Lambda_n^{(p)} \otimes \mathbf{I}_r)\alpha_n\varphi_n \end{bmatrix} = \mathrm{vec}(\tilde{\mathrm{O}}_{p+1}\mathrm{A})$$

where A is a diagonal matrix with α_j on its diagonals. Hence, (5-40) is rewritten as

$$J(\tilde{\lambda},\tilde{\varphi})J^{(\tilde{\lambda},\tilde{\varphi})}_{(\tilde{\mu},\tilde{\psi})}l_{\alpha\psi} = (\tilde{C}_q^T \otimes \tilde{S}_0^T)\mathrm{vec}(\tilde{\mathrm{O}}_{p+1}\mathrm{A}) \tag{5-41}$$

which by employing the vectorization property of Kronecker product yields

$$J(\tilde{\lambda},\tilde{\varphi})J^{(\tilde{\lambda},\tilde{\varphi})}_{(\tilde{\mu},\tilde{\psi})}l_{\alpha\psi} = (\tilde{C}_q^T \otimes \tilde{S}_0^T)\mathrm{vec}(\tilde{\mathrm{O}}_{p+1}\mathrm{A}) = \mathrm{vec}(\tilde{S}_0^T\tilde{\mathrm{O}}_{p+1}\mathrm{A}\tilde{C}_q)\,. \tag{5-42}$$

Since $\tilde{S}_0^T\tilde{\mathrm{O}}_{p+1} = 0$ in view of (5-6),

$$J(\tilde{\lambda},\tilde{\varphi})J^{(\tilde{\lambda},\tilde{\varphi})}_{(\tilde{\mu},\tilde{\psi})}l_{\alpha\psi} = \mathrm{vec}(\tilde{S}_0^T\tilde{\mathrm{O}}_{p+1}\mathrm{A}\tilde{C}_q) = 0 \tag{5-43}$$

and hence, the second part of (5-38) is zero from which the assertion follows.

5.2.1.5 Independence of the residual Jacobian to modeshapes scaling

The scaling type of the modeshapes acquired from the analytical model of structure or the measured data will not emerge in the final χ^2-value because it will not be affecting the Jacobian *J*, as will be demonstrated in here. Therefore, the scaling of the modeshapes can be any type such as mass-normalized or unit maximum value. However, they need to be scaled with the same procedure throughout the whole procedure of calculating (5-2). In other words, the scaling of the modeshapes used in building the observability matrix and all other parameters in (5-2) need to be identical. In here, the independence of Jacobian *J* to the modeshape scaling is proved in the following lemma.

Lemma 5.2: The modeshapes scaling type, e.g. mass normalized or unit maximum value, does not affect the final Jacobian *J*.

Proof: This can be proved by looking into the constituting parts of J in (5-2). $J(\lambda,\varphi)$ is computed from (5-23) in which O_{p+1} is composed from the modeshapes. Since the scalar scaling of the modeshapes only affects on $\mathrm{O}^{\dagger}_{p+1}$ inversely and on $J^{(f,\xi,\varphi)}_{p_k}$ directly, this scalar factor will be removed by the multiplication of $\mathrm{O}^{\dagger}_{p+1}$ and $J^{(f,\xi,\varphi)}_{p_k}$ in (5-2). It should be noted that the Jacobians related to the modeshapes in the other parameters, i.e. $J^{(\lambda,\varphi)}_{(\mu,\psi)}$ and $J^{(\mu,\psi)}_{(f,\xi,\varphi)}$, are unit and therefore do not affect the scalar factor. Hence, the final Jacobian will be independent of the scaling of the modeshapes used in $\mathrm{O}^{\dagger}_{p+1}$ and $J^{(f,\xi,\varphi)}_{p_k}$ as long as they are identical.

5.2.1.6 Invariance of the sensitivity and MinMax tests to the scaling of final Jacobians

The scaling of the columns of Jacobian matrix J does not affect the χ^2-test in both the sensitivity based test and MinMax test (Döhler 2011), as will be proved in here. Therefore, this Jacobian is only projecting the residual based on its direction for each parameter on the χ^2-value. This directionality and its implications will be used and discussed in clustering of elements later in this chapter. In this section, this invariance is demonstrated.

Lemma 5.3: The χ^2-test from both the sensitivity based and MinMax approaches is invariant to the scaling of the columns of the Jacobian matrix *J*.

Proof: For the sensitivity based approach by keeping the same notation and using $\alpha\tilde{J}_k$ instead of $\tilde{J}_k$, where α is a scalar variable, the test (3-40) is written as

$$\chi^2(p_k) = \frac{\tilde{\zeta}^T(\alpha\tilde{J}_k)(\alpha\tilde{J}_k^T)\tilde{\zeta}}{(\alpha\tilde{J}_k^T)(\alpha\tilde{J}_k)} = \frac{\tilde{\zeta}^T\tilde{J}_k\tilde{J}_k^T\tilde{\zeta}}{\tilde{J}_k^T\tilde{J}_k} \qquad \textbf{(5-44)}$$

which shows the invariance property of the test to the scaling factor α.

In order to show the invariance property in the MinMax test, by using the same notation and substituting the Jacobians $\tilde{J}_a$ and $\tilde{J}_b$, with $\tilde{J}_a T_a$ and $\tilde{J}_b T_b$, respectively, where T_a and T_a are invertible matrices, the new scaled Fisher information matrix $\tilde{F}$ is computed as

$$\tilde{F} = \begin{bmatrix} \tilde{F}_{aa} & \tilde{F}_{ab} \\ \tilde{F}_{ba} & \tilde{F}_{bb} \end{bmatrix} = \begin{bmatrix} T_a^T F_{aa} T_a & T_a^T F_{ab} T_b \\ T_b^T F_{ba} T_a & T_b^T F_{bb} T_b \end{bmatrix}. \quad \textbf{(5-45)}$$

Moreover, in view of (3-44) and (3-46), the scaled robust residual $\tilde{\zeta}_a^*$ and writes as

$$\tilde{\zeta}_a^* = T_a^T \zeta_a^* \quad \textbf{(5-46)}$$

and (3-48) is rewritten as

$$\tilde{F}_a^* = T_a^T F_{aa} T - (T_a^T F_{ab} T_b)(T_b^T F_{bb} T_b)^{-1}(T_b^T F_{ba} T_a) = T_a^T F_a^* T_a . \quad \textbf{(5-47)}$$

Therefore, the χ^2-test (3-49) is rewritten as

$$\tilde{\chi}^{*2}(p_k) = \tilde{\zeta}_a^{*T} \tilde{F}_a^{*-1} \tilde{\zeta}_a^* = \zeta_a^{*T} T_a (T_a^T F_a^* T_a)^{-1} T_a^T \zeta_a^* = \zeta_a^{*T} F_a^{*-1} \zeta_a^* \quad \textbf{(5-48)}$$

and hence

$$\tilde{\chi}^{*2}(p_k) = \chi^{*2}(p_k) \quad \textbf{(5-49)}$$

which implies that the χ^2-test is independent of the Jacobian matrix scaling. By having this invariance of the MinMax test and sensitivity based approach the assertion follows.

5.2.2 Formation of the parameters of the Jacobian in the chain rule

In the previous section it was described how to evaluate the Chain derivatives of (5-2) from the eigenstructure of the system. However, in the SSDD damage localization technique these parameters can be evaluated from an analytical model, e.g. finite element model, and or from the measured data from ambient vibration test. Thus, there are two sets of eigenstructures available for each part in the Jacobian Chain.

It is emphasized that the fundamental idea behind the SSDL method is to use the information from an analytical model of the structure along with the data measured. This model is the analytical relation between the eigenstructure and the physical parameters. The use of the analytical model is mainly in the Jacobian and it makes a connection between the data driven residual and the physical system parameters.

5.2.2.1 Measured data eigenstructure versus analytical model modal parameters

The residual defined in the SSDL method is derived from the mathematical operations on the measured data and has a mathematical notion while the finite element model is directly connected to the physical behaviour of the structure. In order to be able to use this model, a bridge connecting the mathematical notion to the physical model is needed. The derivative Chain in (5-2) is the bridge connecting these two domains. This will let us to benefit from a physical model of the structure along with the measured data to identify the damage.

For the formation of this bridge, there should be a decision made on the use of the measured data eigenstructure versus the modal parameters from the analytical model, on each part of the Jacobians. The reason is that, the modal parameters identified from these two sources are generally not exactly the same even if a model updating has been performed. The parameters from the measured data are assumed more precise conditional to a good identification procedure. In general, the model updating on the analytical model is not necessary and not needed in the subspace damage localization procedure unless the modal parameters are very different than the identified ones and the model is not a good representative of the dynamic behaviour of the structure. The important accuracy needed for the damage localization is in the sensitivity values of modal parameters with respect to physical parameters. The scaling of these sensitivities is not affecting on the final χ^2-value as shown in 5.2.1.6.

Herein, two options are described and their performance will be investigated in Chapter 7.

Since $J_{(\mu,\psi)}^{(\lambda,\varphi)}$ and $J_{(f,\xi,\wp)}^{(\mu,\psi)}$ in the Jacobian formation, have closed-form evaluations and are related to transition from different systems, i.e. continuous and discrete systems, they can be both chosen from the same parameters from either the measured data or analytical model. Therefore, only based on the choice of the first and last Jacobians the two formations are defined:

***Formation 1*:** The first combination is simply chosen by evaluating all parts of (5-2) from the analytical model. In this way, all the parameters are consistent and the Jacobian is purely computed from the analytical model. Like so, the modal parameters of the analytical model are used in forming the observability matrix O_{p+1}, and only the Hankel matrix $\mathbf{H}_{p+1}$ and S_0 are from the measured data.

***Formation 2*:** Using this formation, the first, second and third parts of the Jacobian are evaluated from the measured data eigenstructure and the last part is evaluated from the modal parameters of the analytical model. It should be noted that the modal parameters of the analytical model and the eigenstructure of the measured data need to be identified and adjusted in terms of scaling and order. Hence, one system identification is needed in the reference state prior to the localization of damage.

The scaling of the modeshapes from the analytical model and the measured data need to be identical and therefore this scaling is described in the following subsection.

5.2.2.2 Scaling of modeshapes from two sources

By using the second formation described in previous subsection, there is a need in scaling the modeshapes obtained from the analytical model, i.e. $\wp$, and measured data, i.e. φ or ψ since, $\varphi = \psi$. This scaling can be performed in typical ways such as modal mass scaling or unit maximum member. However, usually the mass matrix of the analytical model is complicated to truncate and

the modeshapes are obtained from limited number of degrees of freedoms on which a sensor is located. Therefore, the general scaling of these vectors is performed as follows.

Since the scaling of the modeshapes are not matching, we have

$$\alpha \wp_j = \varphi_j \tag{5-50}$$

where α is a constant scalar. Thus, the adjusted modeshapes $\tilde{\wp}$ where $\tilde{\wp}_j = \alpha \wp_j$, can be evaluated as

$$\tilde{\wp}_j = \frac{\wp_j^H \varphi_j}{\wp_j^H \wp_j} \wp_j . \tag{5-51}$$

5.2.2.3 Coupled modeshapes scaling/decoupling

Coupled modeshapes happen mostly in symmetric or nearly symmetric structures which have sets of two close eigenvalues. In these cases, the identified modeshapes are coupled and result in a linear combination of the analytical modeshapes. In order to solve this issue, the scaling needs to be done by solving a double linear equation. Let $\wp_1$ and $\wp_2$ be the two coupled modeshapes corresponding to the analytical modeshapes φ_1 and φ_2, respectively. The linear combination is written as

$$C\,\Gamma_{1,2} = \Phi_{1,2} \text{ where } C = \begin{bmatrix} c_1 & c_2 \\ c_3 & c_4 \end{bmatrix},\ \Gamma_{1,2} = \begin{bmatrix} \wp_1^T \\ \wp_2^T \end{bmatrix} \text{ and } \Phi_{1,2} = \begin{bmatrix} \varphi_1^T \\ \varphi_2^T \end{bmatrix}. \tag{5-52}$$

Therefore, we have $C = \Phi_{1,2}\Gamma_{1,2}^{\dagger}$ and then the scaled modeshapes $\tilde{\Gamma}_{1,2} = \begin{bmatrix} \tilde{\wp}_1^T \\ \tilde{\wp}_2^T \end{bmatrix}$ can be evaluated as

$$\tilde{\Gamma}_{1,2} = \Phi_{1,2}\Gamma_{1,2}^{\dagger}\Gamma_{1,2} . \tag{5-53}$$

5.3 Clustering

The number of physical parameters in a structure is usually higher than the identified modal parameters and hence, the Jacobian matrix J is usually a "wide" matrix. Since the number of sensors is considerably less than the number of DOFs of the structure, the resolution of the identification in terms of elements is not high and the columns of the Jacobian corresponding to *close elements* are pointing to the same direction. This causes the χ^2-test of the *close* elements to react the same way. This *closeness* stems from the modal behaviour of the elements which in turn is related to their geometrical and physical closeness and modal direction in the considered modeshapes.

Furthermore, the *close* elements cannot be directly treated in the MinMax test, because the Jacobian matrix is required to be full column rank. The reason is that the MinMax test insures of seeing purely the change in the tested element by removing the other elements effect. However, if two elements are *close* and one of them is damaged, when testing the damaged element the effect of damage is removed from the test by its *close* element. This will reduce drastically the χ^2-test reaction to damage for the damaged element and therefore generates false negative results. In order to remove this effect, clustering of elements is necessary.

The closeness of the elements can be identified from the directions of their corresponding Jacobian vectors which will be used in the clustering procedure. Figure 5.2 illustrates how the vectors of Jacobians of *close* elements look like.

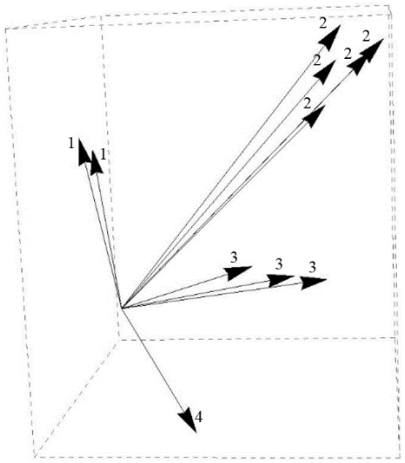

Figure 5.2 Schematic illustration of closeness of Jacobian vectors

In clustering the columns of Jacobian matrix, the normalized Jacobians are used because in both the sensitivity approach and MinMax test, $\tilde{J}$ (reader is referred to (3-38) for the definition) is the basis of χ^2-test. This will assure that the Jacobian vectors are clustered consistent to the χ^2-test in (3-40) and (3-49) as the directions of columns in $\tilde{J}$ are not necessarily the same as J.

Since the scaling of the columns of Jacobian will not affect the test value (as demonstrated in 5.2.1.6), the angles of them in the vector space is the only parameter for measuring *closeness* and their sizes are used in section 5.4 in assessing the detectability of the elements in terms of damage. Therefore, the Columns of Jacobian should be normalized to unit vector prior to clustering, to remove any effect of their scaling on the clustering approach. This normalization can be performed as

$$\overline{J}_k = \frac{\tilde{J}_k}{\left\|\tilde{J}_k\right\|} \qquad \textbf{(5-54)}$$

where $\overline{J}_i$ is the normalized Jacobian column corresponding to element *k* with unit length.

It should be noted that the final χ^2-value of all the tests proposed herein, is not affected by the scale (size) of Jacobians. Therefore, one way in dealing with the elements with small size of

Jacobian columns $\tilde{J}_k$ is to remove them before the testing. The reason of this removal is the fact that, with similar variances, the columns of Jacobian matrix with small scaling will pose higher error on the test than the larger ones. However, the decision of removal or keeping these vectors are based on the engineering judgment of the tester.

Two approaches of clustering *close elements* are described in the following.

5.3.1 *k*-means clustering

The *k*-means clustering, is a vector quantization approach frequently used in signal processing, image processing and machine learning fields. In this algorithm, firstly *k* number of groups is assumed and then randomly *k* points (vectors) in the space are selected from the total N_ρ points as the centroids for these groups. Subsequently, the other points in the space are categorized to each of these points based on their minimum distance to the centroids. Iteratively, the mean of each group is calculated and each point in the space is re-associated to the group with closest centroid. This iteration converges when no point is re-associated to other groups. The clusters and their centroids are illustrated schematically in the following figure:

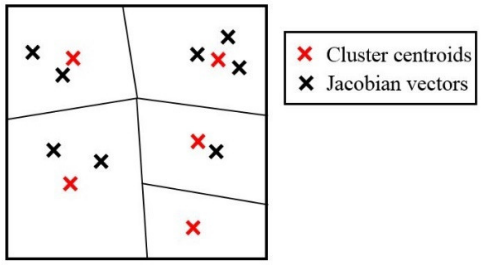

Figure 5.3 Schematic illustration of *k*-means clustering

Although this algorithm is frequently used in clustering approaches in literature, there are some important shortcomings of it which will be described in here.

This algorithm is highly dependent on the number of groups, i.e. *k*, and the starting random points. It is not guaranteed to converge while it only can converge to local minima. Therefore,

different starting points can result in different classifications. Moreover, the number of groups of the structural elements are unknown and the resultant χ^2-test is highly depending on that. Furthermore, even after convergence of this algorithm *close* elements are not necessarily categorized into the same group and hence the results are not promising from the Min-Max test. This algorithm is also computationally not efficient since the running time of it is given as $O(N_p ki)$, where *i* represents the number of iterations to convergence.

Due to these disadvantages of this approach, the Fisher information matrix is used in clustering of the elements as proposed in the following subsection.

5.3.2 Hierarchical Fisher-information-matrix-based clustering (HFC)

The *closeness* of the elements of the Jacobian matrix $\overline{J}$ can be assessed by the correlation between the vectors. This correlation is calculated as the normalized Fisher information matrix f,

$$f = \overline{J}^T \overline{J} . \tag{5-55}$$

Each element f_{ij} of this matrix corresponds to the *closeness* of vectors *i* and *j* of the normalized Jacobians and is computed as

$$f_{ii} = 1, \quad f_{ij} = \frac{\tilde{J}_i^T \tilde{J}_j}{\left\| \tilde{J}_i \right\| \left\| \tilde{J}_j \right\|} . \tag{5-56}$$

The normalized Fisher information matrix (NFIM) is positive definite and symmetric due to its composition in (5-55). An element of this matrix with value near 1 corresponds to the *close* vectors of the Jacobians and a small value near 0 shows the opposite. Therefore, the clustering can be done by grouping the elements corresponding to high values in the normalized Fisher information matrix (NFIM). For this purpose, a hierarchical clustering approach is used to group the elements based on upper triangle of NFIM. Figure 5.4 is a dendrogram depicting the hierarchical clustering of 32 elements based on their corresponding values in *f*. In this picture, as

the height of the connections are increased, their *closeness* is decreased; the height of the connections is an inverse ratio of their corresponding value in the NFIM.

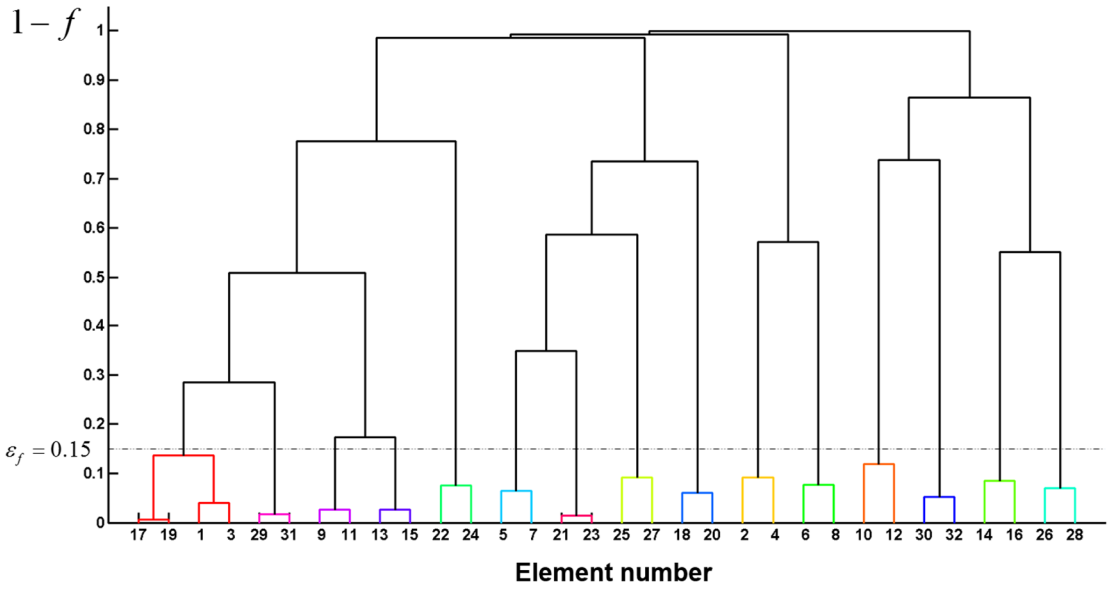

Figure 5.4 Hierarchical clustering of 32 elements

The elements clustered at the lowest level, two by two in Figure 5.4 are not distinguishable in terms of damage from each other and hence they become clustered in the first step. This happens when two elements are very *close*.

After having the classification shown in Figure 5.4, a threshold ε_f needs to be selected on the difference of f_{ij} from 1. This threshold defines the amount of *closeness* of vectors needed in order to classify them as one vector. The dashed line in Figure 5.4 shows the threshold $\varepsilon_f = 0.15$ from which the elements are clustered into 15 clusters.

By increasing this value, the number of clusters will decrease, the resolution of the damage localization is decreased and the uniqueness (perpendicularity) of the clusters will increase. Therefore, there is a compromise between the resolution of damage localization and uniqueness of clusters which can be adjusted by ε_f. The optimal ε_f can be chosen by minimizing it while having

the constraint of sufficient perpendicularity of the clusters. This is achieved by looking at the dendrogram of the clustering and the resultant NFIM in an iterative manner, only in the reference state.

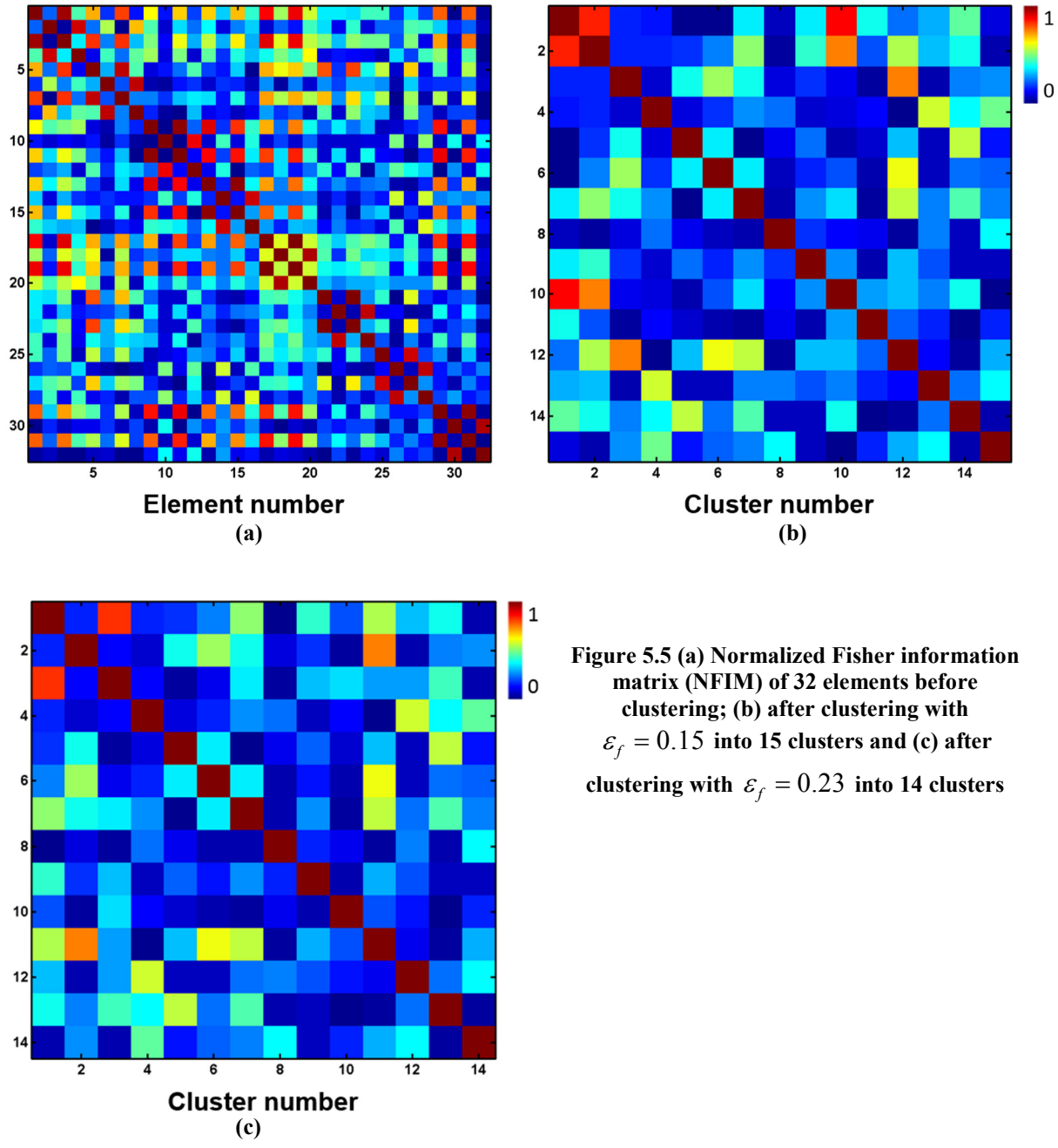

Figure 5.5 (a) Normalized Fisher information matrix (NFIM) of 32 elements before clustering; (b) after clustering with $\varepsilon_f = 0.15$ into 15 clusters and (c) after clustering with $\varepsilon_f = 0.23$ into 14 clusters

After having this clustering, the mean of the vectors associated to each cluster is used as the centroid of that cluster. The NFIM of the 32 elements before and after clustering are compared in Figure 5.5.

It can be seen from this figure that the number of elements with high values (warm colors) of f_{ij} are reduced after clustering. To further reduce the remaining orange spots, we need to increase ε_f which as discussed will reduce the resolution of the damage localization.

5.3.3 Application of clusters in tests

After clustering the Jacobians matrices, the clusters need to be applied in the sensitivity based and MinMax test. This application can be done in different ways for each test, which will be described in here.

5.3.3.1 Clusters in Sensitivity approach test

By clustering the normalized Jacobian matrix $\overline{J}$, into N_c clusters, the sensitivity test (3-40) can be performed on the centroids of the clusters from *k*-means or HFC approach as

$$\chi^2(p_k) = \frac{\tilde{\zeta}^T C_j C_j^T \tilde{\zeta}}{C_j^T C_j}, \quad \text{for} \quad \forall k \in \mathbf{C}_j,\ j = 1 \cdots N_c . \tag{5-57}$$

In (5-57), $\mathbf{C}_j$ is the *j*th cluster with centroid C_j. In view of (5-57), all the elements inside a cluster will be identified as damaged or undamaged based on the χ^2-value of their corresponding cluster centroid.

5.3.3.2 Clusters in MinMax test

The use of clusters in the MinMax test can be performed in two approaches based on the definition of $\tilde{J}_a$ in (3-41).

First approach: In this approach, $\tilde{J}_a$ is chosen as the centroid of one cluster to be tested and $\tilde{J}_b$ is formed consistently to (3-41) from the centroids of other clusters. Therefore, (3-41) is rewritten as

$$\begin{cases} C_a = C_j \\ C_b = \left[C_1 \cdots C_{j-1} C_{j+1} \cdots C_{N_c} \right] \end{cases}, \quad j = 1 \cdots N_c . \tag{5-58}$$

Thus, all the elements in the cluster are treated similarly as damaged or not damaged.

***Second approach*:** In this approach each of the elements in a cluster can be tested which results in a higher resolution than the first approach. To achieve that, the Jacobian is discretized as

$$\begin{cases} C_a = \overline{J}_k \\ C_b = \left[C_1 \cdots C_{j-1} C_{j+1} \cdots C_{N_c} \right] \end{cases}, \quad k \in \mathbf{C}_j,\ j = 1 \cdots N_c . \tag{5-59}$$

Therefore, each element in a cluster is tested while removing the effects of other clusters. Since, the other clusters do not include the elements *close* to the element being tested, the damage effect will not be removed from the resulting χ^2-test.

After partitioning the Jacobians from either approach the normalized Fisher information matrix F_c can be defined consistently from the cluster centroids as $F_C = \left[C_a \quad C_b \right]^T \left[C_a \quad C_b \right]$ and partitioned similar to (3-43) as

$$F_C = \begin{bmatrix} F_{C_{aa}} & F_{C_{ab}} \\ F_{C_{ba}} & F_{C_{bb}} \end{bmatrix}. \tag{5-60}$$

By defining the residuals as $\tilde{\zeta}_{C_a} = C_a^T \tilde{\zeta}$ and $\tilde{\zeta}_{C_b} = C_b^T \tilde{\zeta}$ the robust residual will be $\zeta_{C_a}^* = \tilde{\zeta}_{C_a} - F_{C_{ab}} F_{C_{bb}}^{-1} \tilde{\zeta}_{C_b}$. Hence, the robust χ^2-test writes as

$$\chi^{*2} = \zeta_{C_a}^{*T} F_{C_a}^* \zeta_{C_a}^* \tag{5-61}$$

where $F^*_{C_a} = F_{C_{aa}} - F_{C_{ab}} F^{-1}_{C_{bb}} F_{C_{ba}}$.

Based on the definition of C_a from the two approaches, the χ^2-test (5-61) identifies the location of the damage in each cluster or element. It should be noted that although in the second approach the test is performed on each element, but the resolution of damage localization is highly depending on the number and location of sensors. Therefore, the resolution of the test is higher in the second approach while limited by the available information from data.

Based on the characteristics of the MinMax test and HFC clustering, the combination of these two with the second approach should be a very robust approach. From such combination, the detection resolution is element basis and the effect of each element is investigated without the interruption of condition of other elements.

The other alternative is the sensitivity based approach with/out clustering. There is no need to cluster this method. From this approach the resolution is element based if no clustering is used. However, the condition of other elements will affect the result of testing a specific element which may lead to possible false positive results.

5.4 Detectability of damage in each physical element

Due to the high number of elements, low number of sensors and comparably low number of identifiable modal parameters from the measured data, the detectability of all elements is not identical. This detectability is affected by the comparative location of sensors to the element, number of sensors, comparative noise in relation to the location of element and sensitivity of the identifiable modal parameters to the physical properties of element. By looking closer to the un-normalized Fisher information matrix (the "real" Fisher information matrix) built from un-normalized Jacobians $\tilde{J}$, it can be seen that it includes all the mentioned factors. The fisher information matrix measures the amount and quality of information that a random variable carries.

This information is a function of size of Jacobian of the element normalized by its variance. While the Jacobian includes information from the sensitivity of the modal parameters to the element and the location and number of sensors, the variance will reduce the value of FIM for elements with comparatively higher noise ratios. Therefore, the diagonals of the Fisher information matrix with original (un-normalized) columns $\tilde{J}_k$ of Jacobian, can be a potential index in assessing the detectability of damage in each element.

It should be noted that, the location and number of sensors can be adjusted to increase the detectability of damage in a certain element. The modeshapes that are highly dependent on an element in terms of deflection (or curvature) will contribute the most in identification of damage in that element. Consequently, organizing the sensors to capture those modeshapes and including them in the Jacobian formation will increase their detectability.

5.4.1 Theoretical investigation of detectability of damage

The relation between the detectability of an element and its corresponding element on the diagonal of the FIM can also be demonstrated in the mathematical way: the χ^2-value from parametric test (3-33) has *d* degrees of freedom with non-centrality parameter $\delta\theta^T J^T \Sigma^{-1} J \delta\theta$ under H_1, when the structure is damaged. Hence, in view of (4-1), the expectation of the χ^2-value under H_1 is

$$\mathbf{E}(\chi^2) = d + \delta\theta^T J^T \Sigma^{-1} J \delta\theta \,. \tag{5-62}$$

This expectation can be rewritten as

$$\mathbf{E}(\chi^2) = d + \delta\theta^T F \delta\theta \tag{5-63}$$

where *F* is the Fisher information matrix and $F = \tilde{J}^T \tilde{J}$. By assuming damage only in one element, for example element *k*, the corresponding value in $\delta\theta$, i.e. δp_k, will be nonzero, while the rest will be zero. Therefore, for this damage condition, (5-63) will be boiled down to

$$\mathbf{E}(\chi^2(p_k)) = d + \delta p_k^2 F_{kk} \tag{5-64}$$

in which F_{kk} is the diagonal of the FIM corresponding to element *k*. Hence, for a constant damage in each element, the expected χ^2-value is dependent on the diagonal of FIM corresponding to that element. A higher diagonal value of the FIM leads thus to a stronger reaction of the test for the respective element when the damage is constant.

If there are more than one element damaged, the detectability of them is depending on a combination of their FIM diagonals and some non-diagonal members of FIM matrix. Thus, this detectability theorem is only valid for one damaged element.

5.4.2 Detectability of damage from MinMax test

In the MinMax test (3-49) or (5-61), the detectability of elements can be further investigated as the values of F^* instead of the diagonals of Fisher information matrix. This is seen by comparing the definition of the robust residual in (3-47) and the χ^2-value defined in (3-49). The expectation of this χ^2-value for damage δp_k when testing element *k* writes as

$$\mathbf{E}(\chi^{*2}(p_k)) = d^* + \delta p_k^2 F_k^* \tag{5-65}$$

Thus, the value of F^* evaluated for each element is a good representative for detectability of damage in that element for the MinMax test.

5.5 Step-by-step procedure of the SSDD and SSDL methods

In this section the procedures of performing the SSDD and SSDL techniques along with the methods presented in this chapter are described. The flowchart of the algorithm is shown in Appendix G.

After measuring the structure in undamaged conditions, the correlations of the measurements between different sensors are calculated considering a shift in time. Based on this

shift, several correlation matrices can be created which are used in composing a Hankel matrix based on the procedure shown in Chapter 3. In the next step, this Hankel matrix is decomposed using the SVD method. The reference subspace S_0 is then created from the left singular vectors acquired from the results of this SVD. The reference subspace S_0 is used as the basis of comparison between the conditions of the undamaged and possibly damaged structures.

Subsequently, similar to the procedure explained for the reference state, another Hankel matrix is built from the measurements acquired from the possibly damaged structure. By multiplication of this Hankel matrix and the reference subspace, a residual is shaped which reflects the change (damage) in the structure compared to the reference state conditions.

This residual is then statistically tested using a χ^2-test method. The result is a χ^2-distributed parameter, namely χ^2-value, that represents a norm of the residual as shown in Chapter 3.

When the structure is undamaged, several measurements are acquired and similar to the reference state, their corresponding Hankel matrices are computed. By computing the residual for each measurement, a safety threshold can be created as a percentile of the probability of exccedance. Therefore, for each χ^2-value computed from the possibly damaged structure, if the value is higher than this threshold the structure has a high probability of being damaged.

After detecting the existence of damage, we need to localize it in the structure. For this purpose, a FE model of the structure is needed to be created which is a good representative of the dynamic behaviour of the structure.

Consequently, a sensitivity analysis is needed in computing the derivation of the modal parameters with respect to each element's physical properties such as stiffness or cross sectional dimensions. The sensitivity of the residual vector to each physical parameter can then be computed from the results of this sensitivity analysis and the formulations described in this chapter. These

sensitivities can be computed from two alternative formations proposed in this thesis. If the modal parameters from the real-data and FE model are used in this formation, the modeshapes need to be scaled and decoupled (if needed) from the proposed methods in this chapter, in order to match to each other.

All of these sensitivity vectors will compose a matrix, namely Jacobian matrix. In the next step, using the vectors of the Jacobian matrix corresponding to each element, the elements of the FE model are clustered by a clustering approach such as HFC method (proposed in this chapter). In the next step, these clusters are used in the MinMax and or sensitivity based approach in calculating a χ^2-value associated to each element. By comparing these values, the elements with a higher χ^2-value are identified as being damaged. Finally, using the indexes proposed in this chapter, the detectability of damage can also be computed from a Fisher information matrix computed from the Jacobian matrix to better understand the severity of damage detectible in each element.

5.6 Conclusions

In this chapter the underlying theories in evaluating the Jacobian matrix from a Chain rule was presented. This Jacobian matrix is used directly in localizing the damage in the structure using the SSDL method. Several important independencies of the final χ^2-test to the scale of Jacobians or modeshapes and to the non-uniqueness of Jacobians were also presented. These theories need to be considered in practice for composing the Jacobian matrix as they comfort the procedure.

Two formations of the Jacobian matrix were elaborated. In one formation only the modal parameters evaluated from the analytical model is used in composing the Jacobian matrix. This formation enjoys the consistency of the parameters in the Chain rule. The other formation uses the modal parameters evaluated from both real and analytical data. In order to compose the Jacobians

from these modeshapes coming from different sources, they need to be matched and scaled to each other. Therefore, a scaling approach was also proposed. Since in some structures, such as the Yellow frame, the modeshapes are coupled, the scaling method was extended to decouple these coupled modeshapes.

A new clustering approach (HFC) was proposed in this chapter. Based on its stability and consistency with the SSDL method, it is expected to have a better performance in comparison to the *k*-means approach.

Finally, two indices were presented in assessing the detectability of each element. It was theoretically proved that these indices are in a direct relationship with the detectability of each element. These indices were created for both the sensitivity based and MinMax methods.

Chapter 6: Application through Analytical Models

6.1 Introduction

The ideal test that can be used to evaluate a damage detection technique is to damage a real structure progressively and measure its response continuously. Having a clear understanding of the condition of the structure before damaging it and the type of damage play a critical role in the test results. Furthermore, in addition to the cost of the procedure, damaging a structure and restoring it to its undamaged condition for the next test, is not practical; it even becomes more complicated when different elements of the structure are needed to be damaged in separate tests to various extents.

In addition to experimental tests, simulating the damage in a structure and subsequently generating data that represents the ambient vibration test measurement can be a useful preliminary approach to evaluate damage detection techniques. Since this data can be an acceptable benchmark to evaluate the functionality of these techniques by allowing control on the test conditions, e.g. structural properties and damage effects, in this chapter some analytical models will be elaborated. In these models, different damage scenarios are simulated and various measurement noise ratios are imposed on the simulated measured data to study the effect of noise on the SSDD technique. The results from the damage detection and localization of these models will be demonstrated in this chapter.

6.2 Analytical models: introduction

In order to evaluate the functionality of the subspace-based damage identification technique, the ambient vibration test data can be simulated from analytical models for different damage types and amounts. In order to simulate this data, a finite element model is created from the structure and then it might be calibrated to the real structure. It should be mentioned that calibration of the

structure does not have a direct effect on the damage detection technique. In other words, the damage detection technique should be able to detect the damage in any structural model including the uncalibrated one, as long as the base of comparison is identical (the same model is damaged). In the Statistical Subspace Damage Localization (SSDL) method, the analytical model does not need to be calibrated as well. However, it should be a good representative of the dynamic behavior of the real structure. Herein, in one of the models, calibration to a real structure is performed to obtain a realistic model and simulate the damage in it.

6.2.1 Ambient vibration simulation

Although in the theoretical development of output-only approaches used in ambient vibration testing the input to the system is assumed as a white noise excitation, in reality the input is never purely white and is colored noise or their combinations. However, the output-only approaches usually result in outcomes with acceptable precision. In this dissertation, for simulating the ambient vibration data, the input to the system is assumed to be white noise excitation.

6.2.1.1 Data simulation

In a real structure the excitation is imposed from different sources, such as wind, ambient vibration of base, excitations from users and close structures or trees and etc, in different locations of the structure. Therefore, the simulation of the ambient vibration should be performed in different locations of the structure with different random excitations to excite more modeshapes of the model.

For this purpose, several points of the structure are excited using white noise excitation in all dimensions. Different excitations are imposed on the structure in order to excite the structure as randomly as possible. This excitation can be done by acceleration or load forces in different points of the structure. It should be noted that these load forces will excite different modeshapes of the

structure based on their location. In order to excite all the modeshapes of a finite element model, every degree of freedom needs to be excited with a unique random excitation (not identical to other excitations). Since for a large finite element model it is practically expensive to impose separate excitations to each degree of freedom, the location of the excitation forces can be chosen to excite the dominant modeshapes of the structure based on the prior knowledge to the structural modal behavior and engineering judgment.

The simulated data can be obtained by measuring acceleration time histories of all the degrees of freedom or the sensor locations. Subsequently, the simulated data will be analyzed in order to compute the natural frequencies and their corresponding modeshapes. These can be used to check which modeshapes can be captured by the simulated white noise excitation. Based on the positioning of the sensors and or insufficient excitation of the structure, some modeshapes may not be captured. For the latter, the excitation must be modified to impose an excitation close to the white noise in different points of the structure and in different directions. For this purpose, in a loop, the location of these vectors based on the detectable modes from the simulated data will be adjusted.

6.2.1.2 Damage simulation

As discussed in Chapter 1, the damage in a structure can be defined based on its effect on the structure: the structure is not functional for what it is designed for, but it is still operational (as defined in (Worden et al. 2007)). With this definition damage in terms of severity is in the middle of defect, e.g. existing defects found in materials, and fault, i.e. failure of the structure in being operational. Therefore, the goal in structural health monitoring of a structure can be viewed as monitoring the condition of the structure, i.e. the damage conditions, in order to alleviate damages and prohibit their transformation into faults.

The damage in a structure is differentiated based on **I)** the type of damage, e.g. corrosion, blast, outside forces (hitting of car to peer) **II)** the damaged element type, e.g. girders, columns, slab, **III)** the extent of damage, i.e. from a crack to total failure of an element and **IV)** the linearity or nonlinearity of damage (Doebling et al. 1998). The linear damage does not change the linear-elastic behavior of the structure while the nonlinear damage will change it to nonlinear behavior. Most of the literature is focused on linear damages, since the initiation of damage is usually linear. Furthermore, the damage can be related to the change in stiffness with constant mass or change in the mass of a structure with constant stiffness. The latter can happen when the non-structural elements or the structural elements with low contribution on stiffness, e.g. some parts of slabs, detach from the structure. Detecting this change in the structure is of importance in structural heath monitoring and plenty of the damage detection techniques cannot detect it.

Herein, the damage is modeled as a linear damage with various extents. The damage in different elements of the model is simulated by reducing the dimensions or modulus of elasticity of one or some of the elements in the intended location of damage. The damage in mass is modeled simply by changing the mass value in the location of damage. The amount of the damage is defined in terms of the ratio of this reduction. The type of the damage is not investigated in here, however, the damage in different element types is considered for a sophisticated finite element model, namely, model of S101 bridge, which will be presented in 6.2.3.3.

6.2.1.3 Measurement noise simulation

The imposed measurement noise $e(t)$ on the data is created using a random generation algorithm. The simulated test data in each point and each direction is defined as a measurement channel. The probability distribution of the random generator is normally distributed and its standard deviation is chosen as a ratio, i.e. noise ratio, of the standard deviation of each channel. Therefore, the

standard deviation σ_i in each measurement channel *i* is evaluated and then by multiplying it to the noise ratio N_r, the standard deviation of the random numbers is defined. The random vector e_i is evaluated from

$$e_i = \text{random}_{\text{Gaussian}}(0, N_r\sigma_i)\,. \tag{6-1}$$

In the next step, the random vector e_i is added to the measured data d_i for the corresponding channel, i.e. *i*. Hence, the modified measured data d_i^e can be evaluated as

$$d_i^e = d_i + e_i \tag{6-2}$$

It should be noted that the mean of the generated noise vector, e_i, is zero. As an example, in Figure 1.2, a Gaussian wave packet function is modified with 10% of noise ratio. The original data and the generated Gaussian noise, with standard deviation of 10% of the standard deviation of the data, are added together to create the modified data with noise.

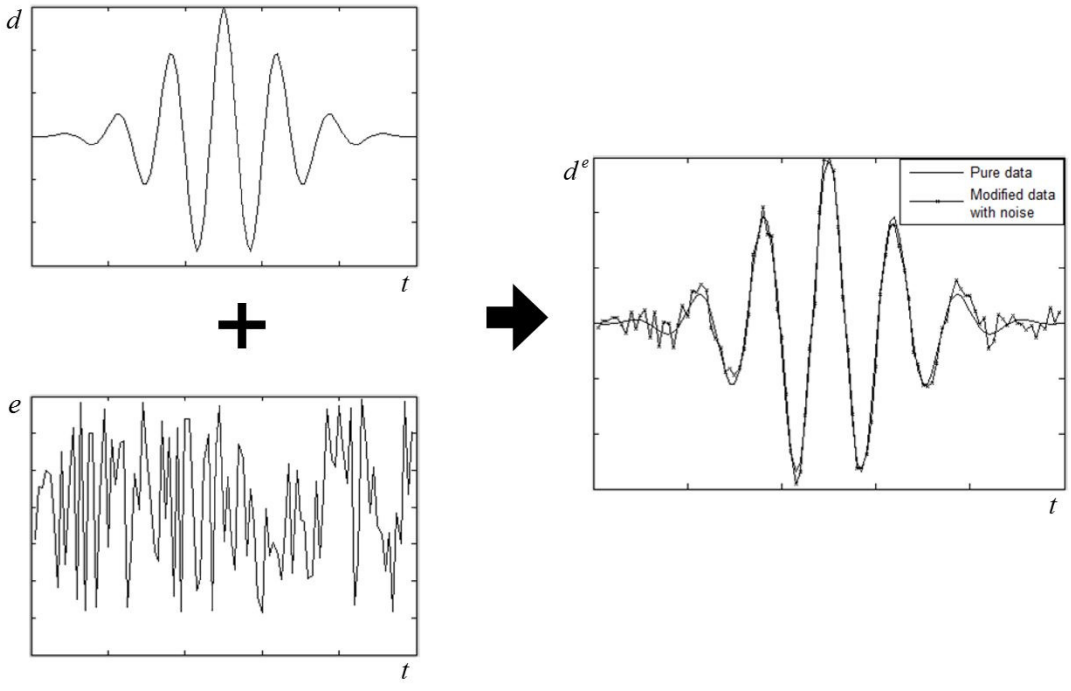

Figure 6.1 The original and modified data with noise ratio of 10%; the noise signal is a Gaussian white noise (at bottom left) and the data is a Gaussian wave packet function (at top left)

It can be inferred from Figure 1.2 that the imposed noise affects the low amplitude parts of the measurement more than the higher amplitude parts of the excitation. This is due to the constant distribution of the noise during the time.

It is worthwhile to illustrate how noise may affect on the eigenstructure of the measurements, especially that the SSDD technique is sensible to the changes in the eigenstructure of the problem.

In Figure 6.2, the simulated data in a sensor (from S101 bridge FE model 6.2.3.3) is shown in frequency domain. In this figure the Fourier transformation of the data without noise and with 30% noise ratio are compared. It can be seen that the lower amplitude frequencies of the data are *drowning* in the noise. The higher the noise ratio becomes, higher amplitudes will be *drown*. It should be expected that the higher measurement noise ratio makes the modeshapes and natural frequencies with lower amplitudes unidentifiable.

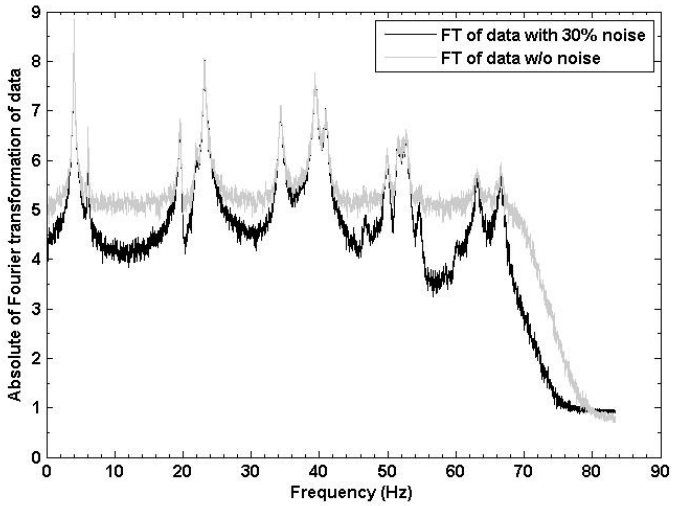

Figure 6.2 The frequency domain of original and modified data with noise ratio of 30%; the noise signal is a Gaussian white noise

6.2.2 Sensitivity analysis

The sensitivity analysis of the models used in damage localization approach is performed from the methods described in Chapter 5. The sensitivity analysis of simple models is performed from the direct sensitivity analysis and for complicated models, the finite difference approach is employed. In case of using the finite difference approach, the perturbation ratio is confirmed by computing the sensitivities with different perturbation factors and checking the convergence of the resultant sensitivities.

Since the modeshapes are evaluated in sensor locations, the sensitivities of the modeshapes are also evaluated in the degrees of freedoms corresponding to these sensor locations in the simulated models. The sensitivity analysis is used only in the statistical subspace damage localization approach for the analytical simple models and the finite element model of the experiment.

The computation of other components of the Jacobian matrix is performed as suggested in Chapter 5. Because the model is analytical, all these components are computed from the modal parameters of the analytical model, i.e. *Formation 1* in Chapter 5.

6.2.3 The models

There are several analytical models employed in demonstrating the theoretical properties described in Chapters 4 and 5. These models range from simple, such as mass-spring model, to complicated models such as finite element model of a bridge. These models are solved using programming codes or modeled in commercial software.

6.2.3.1 Mass-spring model

A mass-spring chain model is one of the simplest models usually used in simulating the ambient vibration test. The schematic shape of this model for 6 degrees of freedom is shown in Figure 6.3.

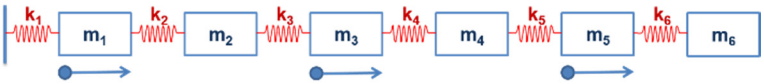

Figure 6.3 The schematic model of a mass-spring chain model and sensor locations

The model is directly built from the stiffness and mass matrices of this system in closed-form solution. The number of the masses and therefore degrees of freedom can be different. In here, the number of masses is assumed to be 6 and the number of sensors is 3 which are located at the mass numbers 1, 3 and 5 shown in Figure 6.3. It should be noted that for simplicity, the stiffness and mass values are equivalent in the system. There is a 2% damping associated to all modeshapes.

The sensitivity analysis is performed by the direct sensitivity analysis method. The calculation of other components of the Jacobian vector is done as suggested in Chapter 5. All these components are computed from the analytical modal parameters, i.e. *Formation 1* of Jacobian.

The data is simulated from Gaussian white noise excitations as explained in section 6.2.1. All the degrees of freedom are excited and the acceleration of the masses are recorded in the location of sensors.

Two types of damage is considered based on the change in the mass or stiffness of the system. Firstly, the value of one or some of the stiffness of springs or mass values are changed. Then this change is detected and subsequently located using the SSDD and SSDL method. Since this model is small, there is no need to cluster the elements.

The output measurement noise is assumed to be 5% in damage localization. This ratio is varied in damage detection when studying the effect of measurement noise on the test to investigate the proposed theories. The damping ratio is also chosen as 2%.

6.2.3.2 Shear wall model

The shear wall model is considered in two configurations composed from 7 or 12 elements. These configurations are designed to demonstrate the functionality of clustering approaches in the

damage localization. The damage detection and localization of each configuration is performed to detect the damage effect as a change in stiffness or mass of the one or some elements. The schematic shapes of the structure are shown in Figure 6.4 for both configurations.

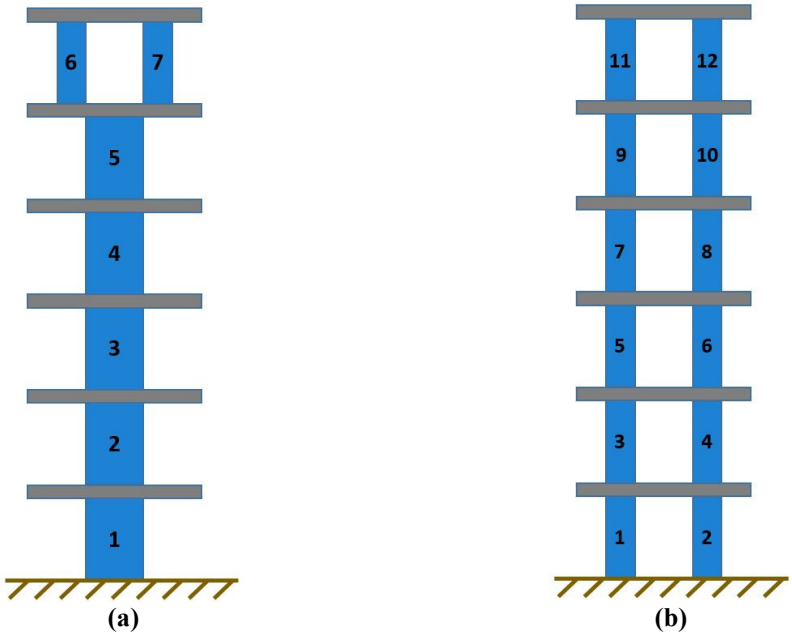

Figure 6.4 The schematic model of a shear wall model for two configurations

The stiffness and the mass are equal for all levels. The stiffness of a double small wall, e.g. elements 6 and 7 in configuration Figure 6.4.a, is equal to the stiffness of a single big wall, e.g. element 1 in the same configuration. These configurations are made with the purpose of studying the clustering methods.

The sensitivity analysis is performed with the direct approach. After the computation of Jacobians for configuration Figure 6.4.b, the Jacobian columns corresponding to each right element of each level, i.e. 2, 4, 6, 8, 10, 12, is slightly changed randomly for the demonstration purposes as will be discussed.

The data is simulated by exciting the structure in all story levels. The sensor locations are in all levels, however the employed number of modeshapes might be different than the number of sensors for the demonstration purposes.

The damage is simulated in one or some of the columns or in masses of each story. The measurement noise is constantly chosen as 5% in all case studies of this structure. The damping ratio used is also 2% for all modeshapes.

6.2.3.3 S101 bridge model

In the damage detection, a realistic model from a finite element of a bridge, namely S101, located in Reibersdorf, Austria, is investigated. This structure was progressively damaged in different locations and elements while it was instrumented and the ambient vibration test data was recorded continuously (as reported in (Wenzel et al. 2012)). In (Döhler et al. 2014a) the SSDD method was used in evaluating the damage condition of the structure on the real data which was shown to be robust.

In this study, the finite element model of the structure which is calibrated to the real data is used in investigating the proposed theorems on the effect of measurement noise and number of samples. The effect of element type and damage ratio is also studied for this model. As mentioned before, the purpose of this calibration is to have a realistic model of a bridge and it does not affect on the assessment of the functionality of the damage detection technique. This model is only used in the damage detection and not in the damage localization.

The bridge structure and its finite element model are shown in Figure 6.5. The natural frequencies of the analytical model and the bridge structure are also compared at Table 6-1.

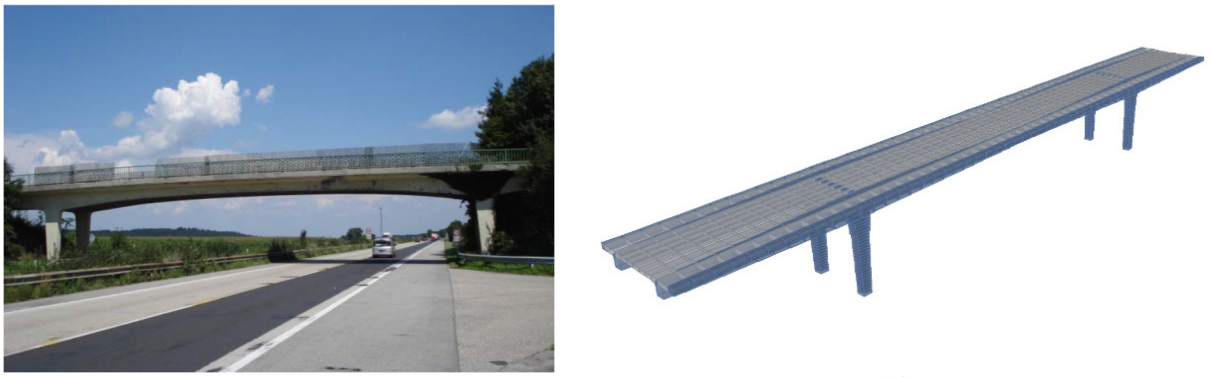

(a) (b)

Figure 6.5 (a) S101 bridge structure, Austria, (Wenzel et al. 2012) and (b) its calibrated finite element model

Table 6-1 Natural frequencies of the bridge structure in undamaged condition obtained from the measured data (Wenzel et al. 2012) and finite element model

	Measured data (Hz)	Finite element model (Hz)
First bending mode	4.05	4.04
First torsional mode	6.30	6.08
Second bending mode	9.69	10.72
Second torsional mode	13.29	12.85
Third bending mode	15.93	19.58

The modeshapes of the structure from the real data and the finite element model are illustrated and compared at Appendix D.

The effect of bearings when simulating the damage in other elements of the bridge is neglected. However, for simulating the damage in bearings the reference structure is equipped by bearings at the supports. Therefore the reference state of the structure with bearings is used to create the threshold of the χ^2-value and then the damaged-bearing models are compared with that reference state.

6.2.3.3.1 Damage simulation

The damaged element types include girders, columns, deck and bearings. Furthermore, since this bridge is composed of three spans, the damage for the girder and deck is modeled in two locations, i.e. in central span and about side span. Girders and columns are modeled by a number of finite

elements. The damage is simulated only in one of these finite elements by reducing a ratio, namely damage ratio, of its section dimension around the strong axis. This damage ratio varies among 20% (minor damage), 40% (intermediate damage) and 80% (severe damage). Damage is simulated in the deck by removing some portions of it (for two damage extents) and in the bearings by reducing their stiffness. It should be noted that, the dynamic mass is only computed from the element mass and removal of an element changes the corresponding elements in mass and stiffness matrices. Removal of deck elements affect more on the mass change than the stiffness change due to their geometry in the model. These damage scenarios are shown in Figure 6.6.

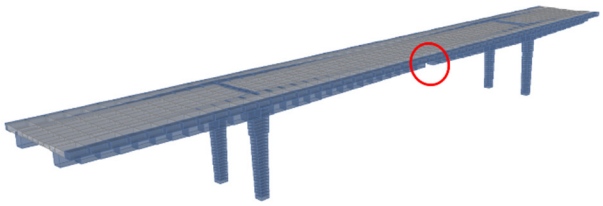

Damage in center of girder (severe)

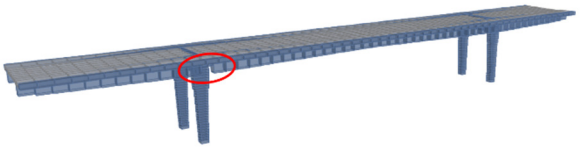

Damage in side of girder

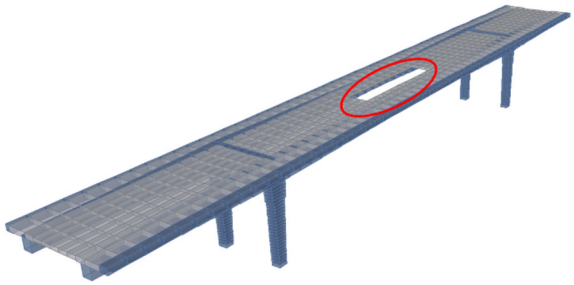

Damage in slab at central span (high)

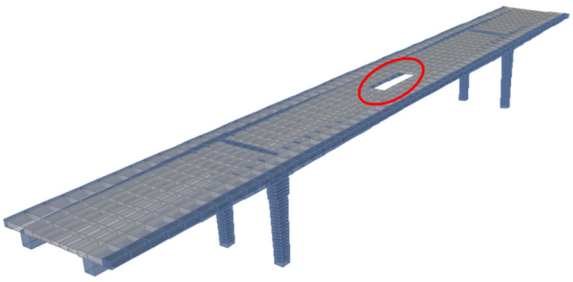

Damage in slab at central span (low)

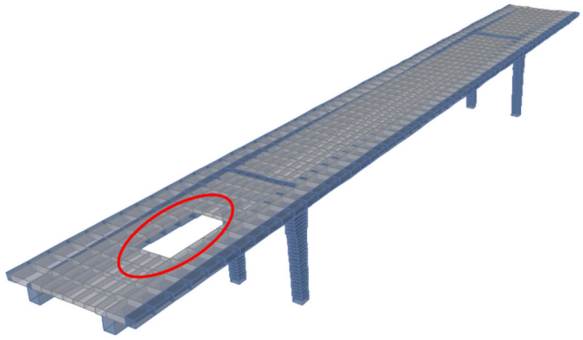

Damage in slab at side span (high)

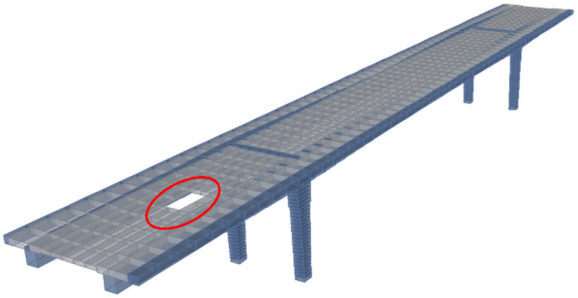

Damage in slab at side span (low)

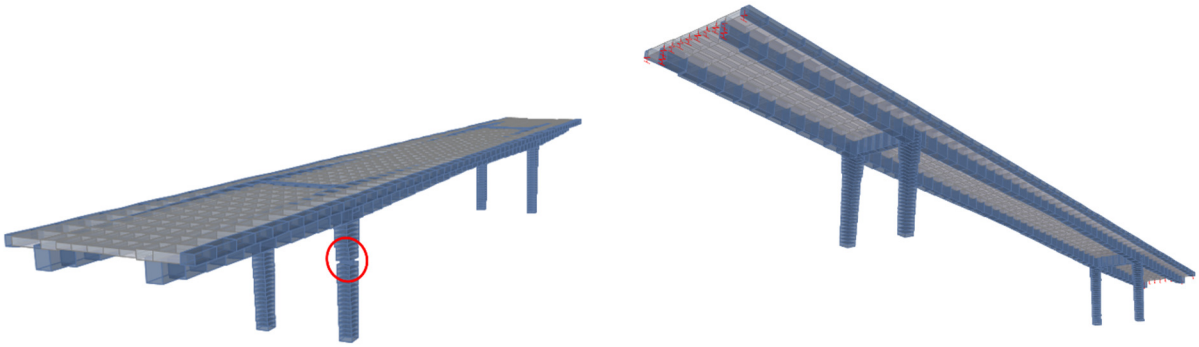

Damage in column (severe) **Damaged bearings (for model with bearings)**

Figure 6.6 Damage scenarios considered in the S101 bridge model

6.2.3.3.2 Data simulation

The finite element model of the structure is excited with a white noise excitation (as acceleration) in three directions. In addition, the structure is vibrated by different white noise loads in various locations. The measured points to record acceleration time histories are illustrated in Figure 6.7.a. Spectral densities of the simulated data with 500Hz sampling rate is obtained from undamaged reference case as shown in Figure 6.7.b.

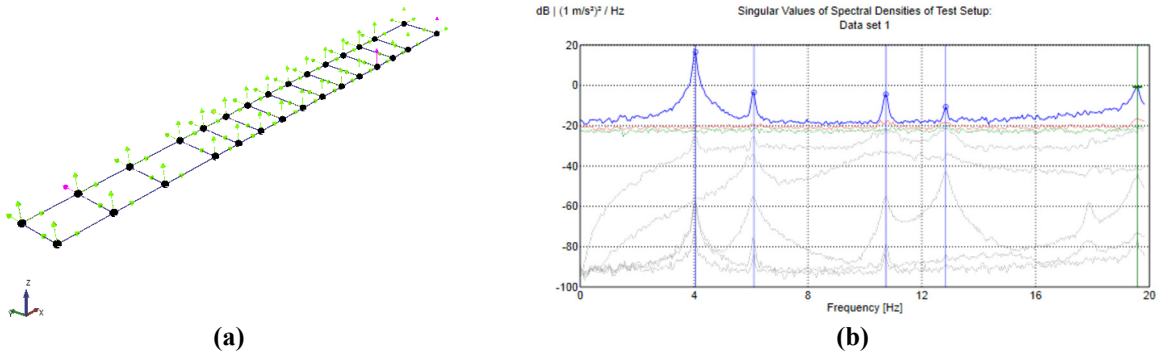

(a) **(b)**

Figure 6.7 (a) measuring-points corresponding to sensor locations; (b) Frequency domain decomposition of the simulated measurement data in undamaged structure

It is seen in Figure 6.7.b that the natural frequencies of the analytical model can be obtained from processing the simulated data accurately. Although, the structure is properly excited by white noise excitation, but some modeshapes cannot be captured. This is related to the location of the sensors and their number. As an example, some modeshapes associated to the longitudinal edges

(sidewalks) of the bridge cannot be captured by the sensors (located on the girders) due to their small accelerations occurring in the sensor locations.

6.2.3.3.3 Measurement noise addition

The measurement noise applied on the data in all the cases is 5% except when studying the effect of measurement noise on the χ^2-test. There are 90 sensors (channels) modeled for this bridge and the measurement noise for each channel is applied based on the characteristics (standard deviation) of that channel. Therefore, for each noise ratio, 90 vectors of records of measurement noise is created and applied to the data.

6.3 Damage detection in analytical models

In this section, the analytical models, i.e. mass-spring and S101 bridge model, will be employed in validating the proposed theorems regarding the effect of measurement noise and number of samples on the statistical subspace damage detection technique. In here, only the global condition of the structure, i.e. damaged or not damaged, is assessed and there is no identification of the location of damage. This study is presented in two subsections: the mass-spring model and the S101 bridge structure model. For this purpose, the ambient vibration test is simulated and the measurement noise is imposed on it, as described in 6.2.1.

6.3.1 Mass-spring model

The mass-spring model introduced in 6.2.3.1 is employed with 6 degrees of freedom and three sensor locations, i.e. masses 1, 3 and 5. The sampling rate is 50 Hz. Both the stiffness and mass parameters are changed in order to demonstrate the detection of the damage by the SSDD method. Following that, the effect of number of samples and the measurement noise will be presented in two subsequent sections.

6.3.1.1 Detecting the damage effect in stiffness or mass

In this study, the number of samples and measurement noise are constant. In the first case, the stiffness of each spring is decreased 5% (as damage), the ambient vibration is simulated and then the χ^2-value is computed for each damaged spring. In the second test, instead of stiffness of springs the mass inertia is changed and then the χ^2-value is computed for each ambient vibration test simulated for this damage in each mass-element. In order to be able to create a threshold, the undamaged mass-spring is tested 5 times and from them the threshold is assessed as the 99% quantile. The resultant χ^2-values in log-scale are demonstrated in Figure 6.8. The red colour bars show that the χ^2-value of the test (in which an element is damaged) is above the threshold, indicating that the structure is damaged.

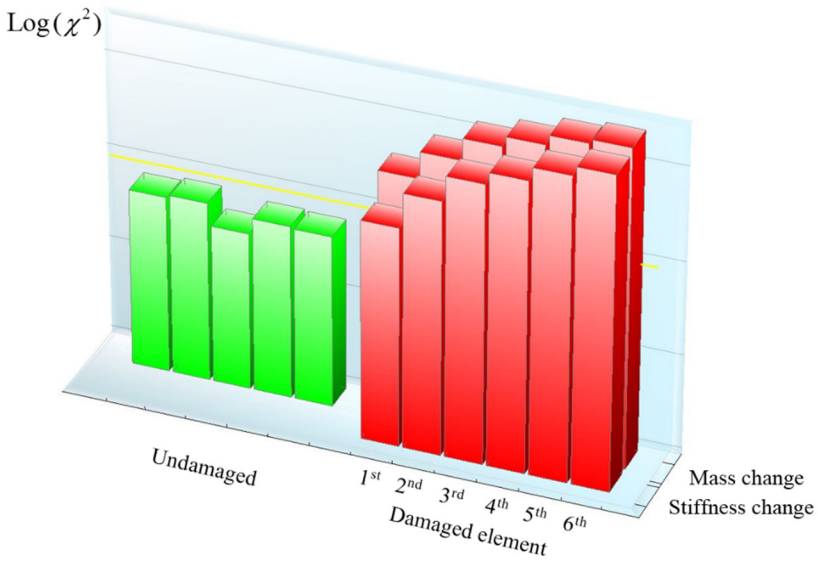

Figure 6.8 Damage detection of the mass-spring model for damage in mass or stiffness of each element

It can be seen that the damage in the stiffness or mass of all the elements is detectible using the SSDD technique. The threshold is shown as a yellow line in Figure 6.8. It should be noted that this figure only demonstrates that the global condition of the structure in case of happening damage in any element is identified to be damaged or not. This does not indicate where the damage is located.

6.3.1.2 Effect of number of samples

For this case, the number of samples is changed from 1000 to 10000 in 10 steps of equal size (1000) for both undamaged and damaged cases. In each step, 100 repetitions are made to calculate the mean, representing the expected value of the χ^2-value. The measurement noise ratio in all cases is 5%. It is observed from the results in Figure 6.9, that as stated in Theorem 4.1, when the model is not damaged, the expected χ^2-value is not changed. However, when the model is damaged (5% damage in spring 2), this value grows linearly with the number of samples, which confirms the *linear* factor N in the non-centrality parameter as shown in the proof of Theorem 4.2. In Figure 6.9, the expectation of the χ^2-value is normalized as $\left\|\mathbf{E}(\chi_N^2)\right\| = \dfrac{\mathbf{E}(\chi_N^2)}{\mathbf{E}(\overline{\chi^2})}$, where $\mathbf{E}(\overline{\chi^2})$ is the average of the χ^2-values computed from the undamaged models.

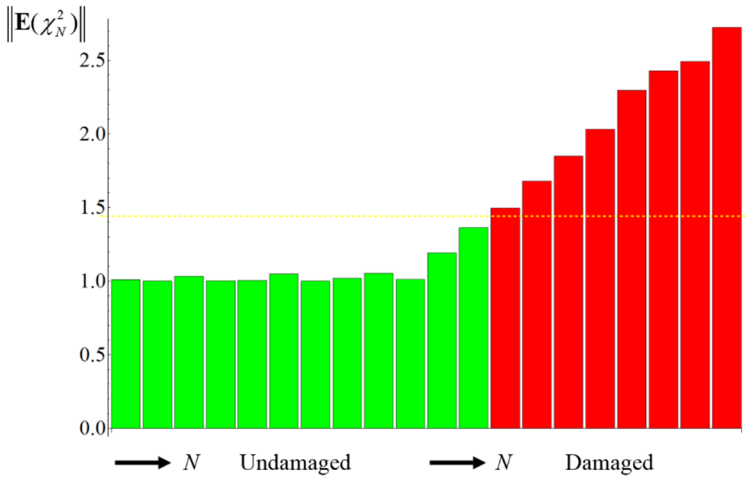

Figure 6.9 Change of the expected χ^2-value (normalized by the least value) evaluated for different number of samples in damaged and undamaged conditions (yellow line represents the 99% percentile threshold and N is changed from 1000 to 10000 in 10 equal steps of (1000))

It can be inferred from Figure 6.9 that the number of samples need to be big enough, so that the damage could be detected. Moreover, this framework allows for a trade-off between the number of samples and damage size: the χ^2-test variable may have the same value either using a

longer dataset with a smaller damage, or using a shorter dataset with a bigger damage. This also means that for constant (non-zero) damage the test variable grows with the number of samples.

6.3.1.3 Effect of measurement noise: equal properties between reference and test data

In here, the number of samples is kept constant at 10000. However, the measurement noise, which has equal properties in reference and testing state, is changed. This noise ratio is changed from 5% to 125% in 25 equal steps for damaged and undamaged conditions. Again in each step the repetition is 100 times. The results are presented in Figure 6.10. The test values in the undamaged state are constant and independent of the noise ratio, confirming Theorem 4.3. The test values in the damaged state decrease when the noise ratio increases, as shown in Theorem 4.4.

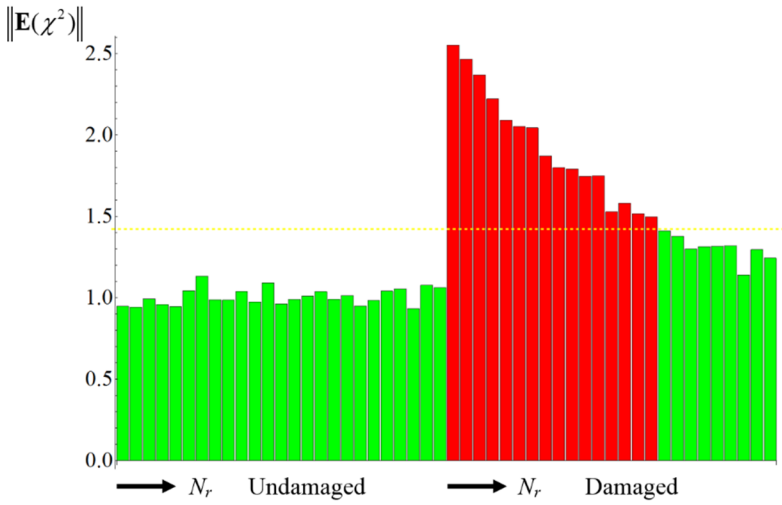

Figure 6.10 Change of the expected χ^2-value evaluated for different noise ratios with equal properties in reference and test states in damaged and undamaged conditions (yellow line represents the 99% percentile threshold and N_r is changed from 5% to 125% in 25 equal steps)

It can be seen that the increase of measurement noise reduces the detectability of damage in the structure, although it does not affect on the tests from undamaged structure.

6.3.1.4 Effect of measurement noise: unequal properties between reference and test data

In this case study, the measurement noise properties are not equal in the reference and test states. For this purpose, same as previous case study, the number of samples is constantly equal to 10000. The measurement noise is being increased in 25 equal steps from 5% to 125% with 100 repetitions

in each step. This is also investigated for damaged and undamaged conditions. In Figure 6.11 the results are shown when the measurement noise is changed only in the testing state (both in undamaged and damaged conditions, respectively). The measurement noise in the reference state that was used to set up the residual covariance is constant at 5%. It is observed that both in undamaged and damaged states the test value increases by the increase in noise level, confirming Theorem 4.5.

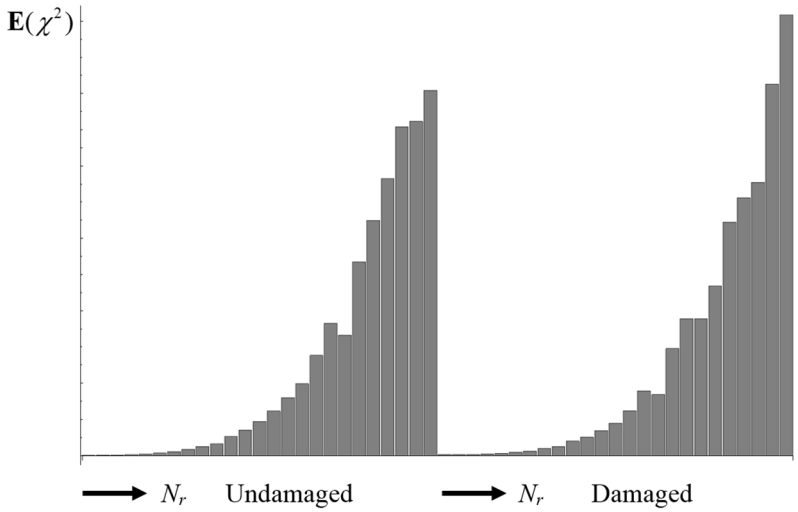

Figure 6.11 Change of the expected χ^2-value evaluated for different noise ratios only in the test data for damaged and undamaged conditions (N_r is changed from 5% to 125% in 25 equal steps)

In Figure 6.12, the study is done for the changing of measurement noise in the residual covariance computed in the reference state while the measurement noise in the test data is kept constant at 5%. It can be seen that by increasing the measurement noise in the reference data, the expected χ^2-value is being decreased for both undamaged and damaged conditions, as stated in Theorem 4.6.

The case studies in here are matching the theorems proposed in Chapter 4. In the next section the model of the S101 bridge is employed in studying these theorems.

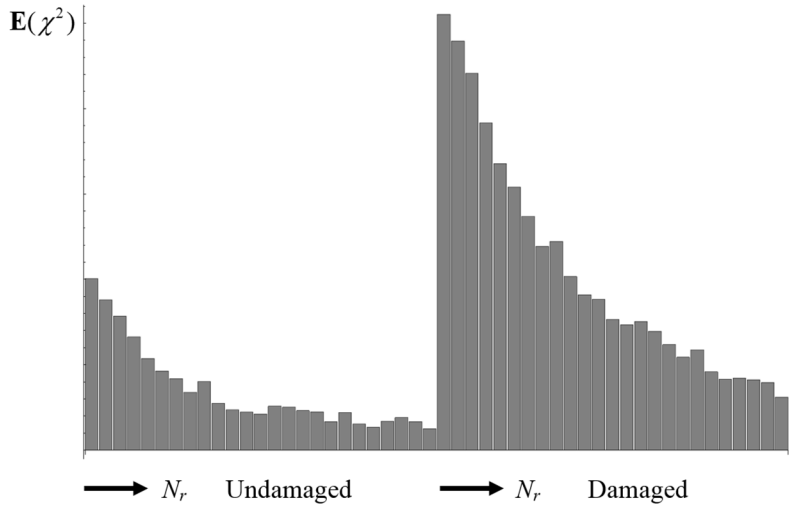

Figure 6.12 Change of the expected χ^2-value evaluated for different noise ratios only in the reference data for damaged and undamaged conditions (N_r is changed from 5% to 125% in 25 equal steps)

6.3.2 S101 bridge structure

The S101 bridge finite element model is used to study the effect of number of samples and noise ratio on the SSDD technique. The ambient vibration on the undamaged structure is simulated for a reference state and two cases. From these two cases, a safety threshold is computed.

First, different element types are damaged with different damage ratios, i.e. mild (20%), intermediate (40%) and severe (80%), as discussed in 6.2.3.3. The noise ratio for these cases is kept constantly 5%. Subsequently, only for the damage scenario related to the center of main girder, for each damage ratio, in two sections the simulated data is created with different length and measurement noise ratios to evaluate the χ^2-value. Finally, this value is compared to the computed threshold from the undamaged cases, checking the proposed theorems.

6.3.2.1 Detecting the damage effect in different element types

In this section, different element types of the finite element (FE) model of S101 bridge is damaged for three mentioned damage ratios and then the SSDD technique is employed in detecting the damage in each element type. As mentioned, the damage is applied on girders, column, deck and bearings. The results are shown in Figure 6.13.

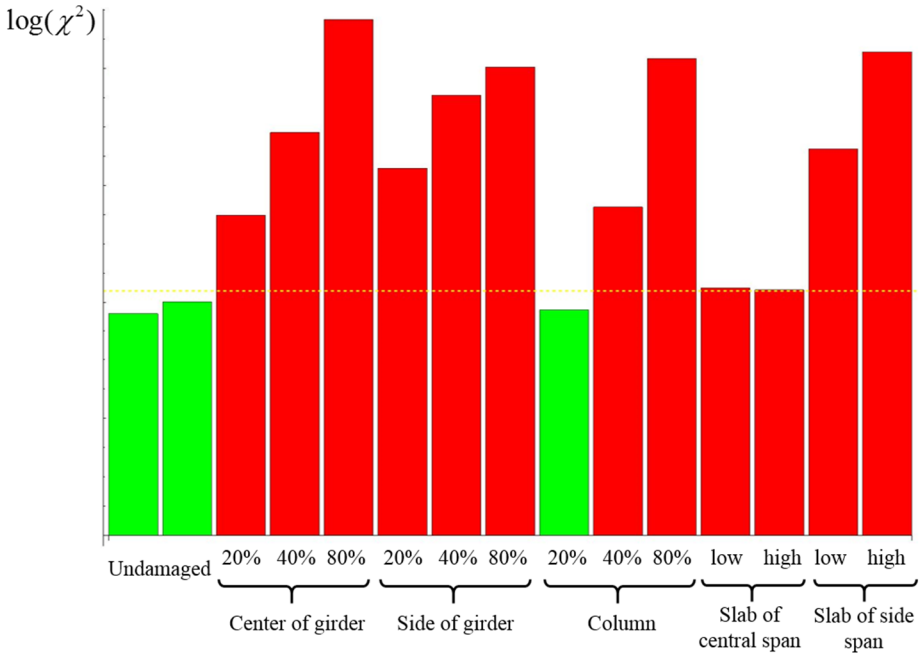

Figure 6.13 χ^2-value evaluated for the damage in different element types with different damage ratios (yellow line represents the 99% percentile threshold)

It is observed that the minor damage in the column is not detected. This is related to the high axial stiffness of the columns even when they are damaged. This stiffness plays a critical role in the formation of the vertical modeshapes of the bridge. Therefore, with this change in the column the eigenstructure of the system is not changed enough to reflect in the χ^2-test.

The effect of damage in the bearings is evaluated from the reference state acquired from the undamaged model with bearings. The stiffness of the bearings are reduced with the mentioned damage ratios and the results of the SSDD technique are illustrated in Figure 6.14.

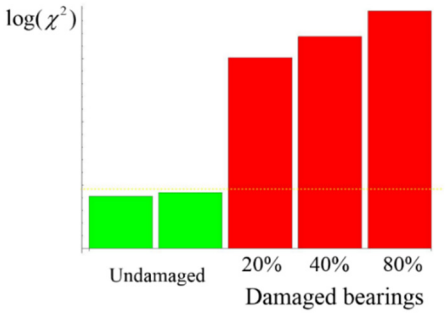

Figure 6.14 χ^2-value evaluated for the damage in bearings with different damage ratios (yellow line represents the 99% percentile threshold)

All the damage cases in the bearings are identified distinctly as can be seen in Figure 6.14.

6.3.2.2 Effect of number of samples

As a demonstrative example, the damage is considered only in the center of the main girder of the bridge. The reason of choosing this damage scenario is because of the significant effect of the main girders on the functionality of the bridge. The data length is varying among 5 min, 7.5 min, 10 min, 12.5 min, 15 min, 17.5 min and 20 min. The analysis is only performed once for each case, although the theorems proposed in Chapter 4 consider the mean of this value. However, since the input excitation is completely white noise and the structure is an analytical model without any change in time, the resultant χ^2-value is expected to be a good approximation of the mean. The results of the damage detection for different damage ratios are shown in Figure 6.15.

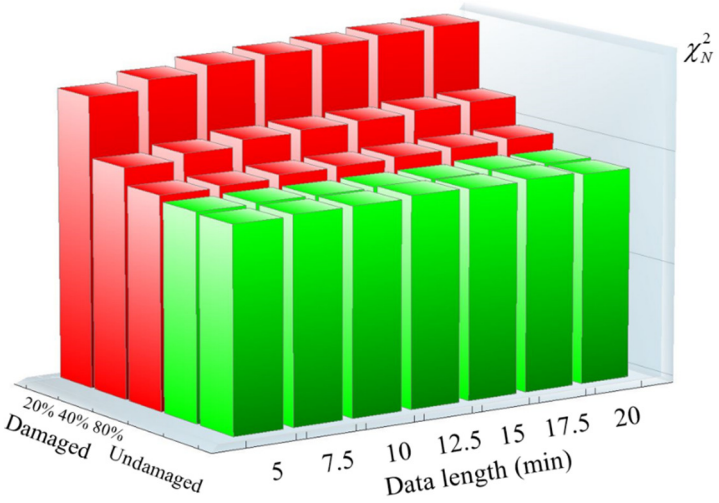

Figure 6.15 χ^2-value evaluated for different data length with different damage ratios

It is observed in this figure that the resultant χ^2-value of the damaged cases are increased linearly by the increase in the number of samples as stated in Theorem 4.2. However, the χ^2-values of the undamaged cases are almost unchanged and unaffected by the number of samples as per Theorem 4.1. It should be noted that since for each data length and damage scenario, the ambient test data (input excitation and measurement noise) are simulated independently, Υ^e is not

exactly zero and results in a slight change in the χ^2-values when changing the number of samples. The rate of this change is dependent on Υ^e value which will be elaborated in 7.2.2.

6.3.2.3 Effect of measurement noise: equal properties between reference and test data

To investigate the effect of measurement noise, the number of samples is kept constant and the measurement noise is applied on the reference and test data with the same characteristics. The noise ratio varies among 1%, 2%, 5%, 10%, 30%, 50%, 70%, 80% and 90%. The analysis is, again, performed only once in each case. The resultant χ^2-values are illustrated in Figure 6.16.

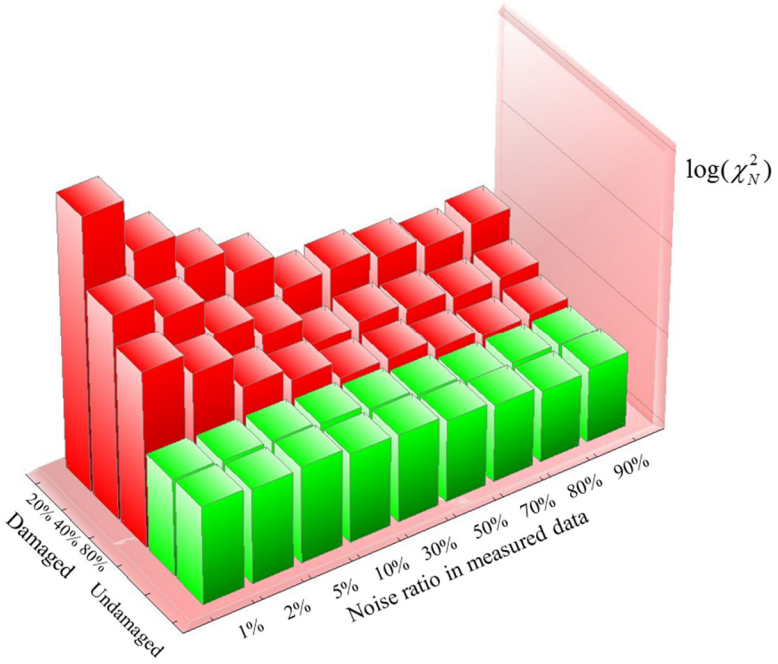

Figure 6.16 χ^2-value evaluated for different noise ratio in the reference and test data for undamaged and damaged structure with different damage ratios

Same as the mass-spring example, the χ^2-values are decreasing by the increase of measurement noise when the structure is damaged as stated in Theorem 4.4. When the structure is not damaged the resultant χ^2-values are almost unchanged as suggested by Theorem 4.3. Same as previous section, this slight change stems from the fact that Υ^e is not exactly zero. Again the rate of this change depends on Υ^e.

6.3.2.4 Effect of measurement noise: unequal properties between reference and test data

For this case, the measurement noise is changed only in the test data while the measurement noise in the reference data is kept constantly 5%. The effect of this change is investigated on this model same as the mass-spring system. The results are shown in the following figure.

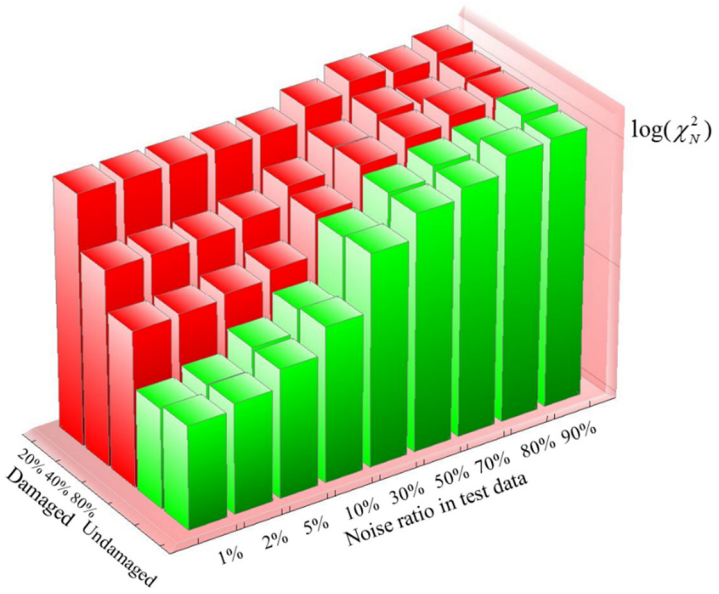

Figure 6.17 Change of the χ^2-value evaluated for different noise ratios only in test data for undamaged and damaged conditions with different damage ratios

It can be seen in Figure 6.17, that the χ^2-value is increasing by the increase in the noise ratio of the test data, confirming Theorem 4.5.

As the next study, the measurement noise is being increased only in the reference state and the χ^2-test is performed for each damage scenario. The results are shown in Figure 6.18. It is observed that as Theorem 4.6 suggests, the χ^2-value is decreasing for the undamaged and damaged cases.

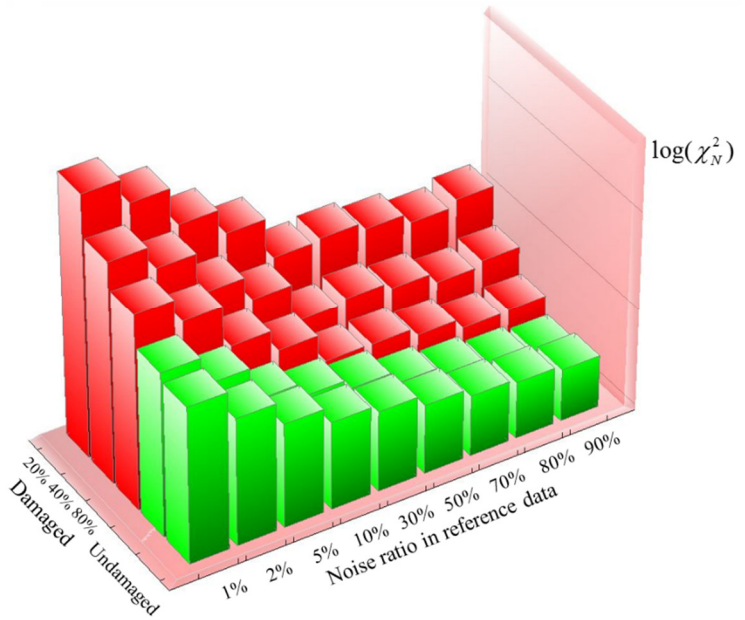

Figure 6.18 Change of the χ^2-value evaluated for different noise ratios only in reference data for undamaged and damaged conditions with different damage ratios

6.4 Damage localization

In this section the statistical subspace damage localization method is investigated in localizing the damage in two analytical models, i.e. mass-spring model and the shear wall model. The damage in stiffness or mass is to be localized and the sensitivity based and MinMax methods are used in localizing the damage. The two clustering methods are also investigated. Finally, the detectability of damage is also elaborated for each element. It should be noted that based on the results from the effect of noise and number of samples acquired from the previous section, the number of samples and measurement noise are kept constant in this section for each model to avoid their effects on the results.

6.4.1 Mass-spring model

Herein, the mass-spring model presented in 6.2.3.1 is employed with 6 degrees of freedom and three sensors at the masses 1, 3 and 5. However, in composing the Jacobian matrix, all the 6 modeshapes are used with values corresponding to the sensor locations. Again the sampling rate is 50 Hz and the stiffness and mass are damaged factors in one or two elements. Since the number

of elements is low and the Jacobians showed to be not *close*, there is no clustering needed as will be demonstrated in next subsection. Moreover, the damaged detection of this system was done in the previous section and therefore, we can continue to localize the detected damage.

6.4.1.1 MinMax and sensitivity based damage localization

In order to locate the damage in the system, four damage configurations are considered: two for damage in stiffness and two for damage in mass. For each case the Jacobian is computed with respect to each mass value or spring stiffness. The Normalized Fisher information matrix (NFIM) is then computed from the resultant Jacobian matrix. The resultant dendrogram chart for each case based on their NFIM using HFC method is shown in Figure 6.19, which shows that the elements are not *close* enough to be clustered, i.e. $1 - f \gg 0$.

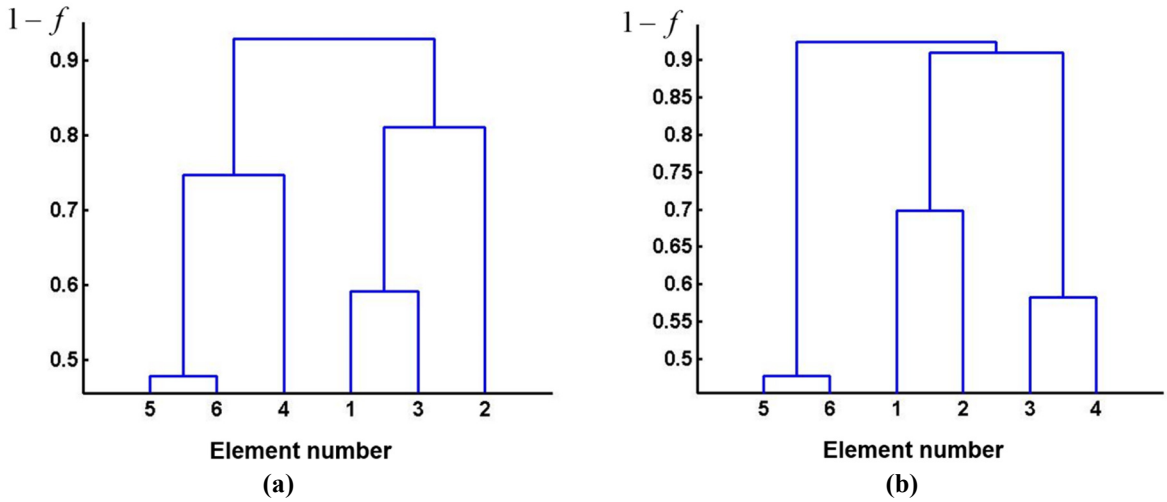

Figure 6.19 Hierarchical Fisher-information-matrix-based Clustering (HFC) of elements from Jacobians with respect to (a) stiffness and (b) mass

The damage in stiffness is applied in two configurations: damage only in element 3 and damage in elements 3 and 6. For mass, the damage is modeled in element 4 in one configuration and in another configuration it is modeled in elements 4 and 6. The damage is applied by decreasing the corresponding value of stiffness or mass by 5%. The resultant χ^2-values from the sensitivity based and MinMax approaches are shown in Figure 6.20.

(a)

(b)

(c)

(d)

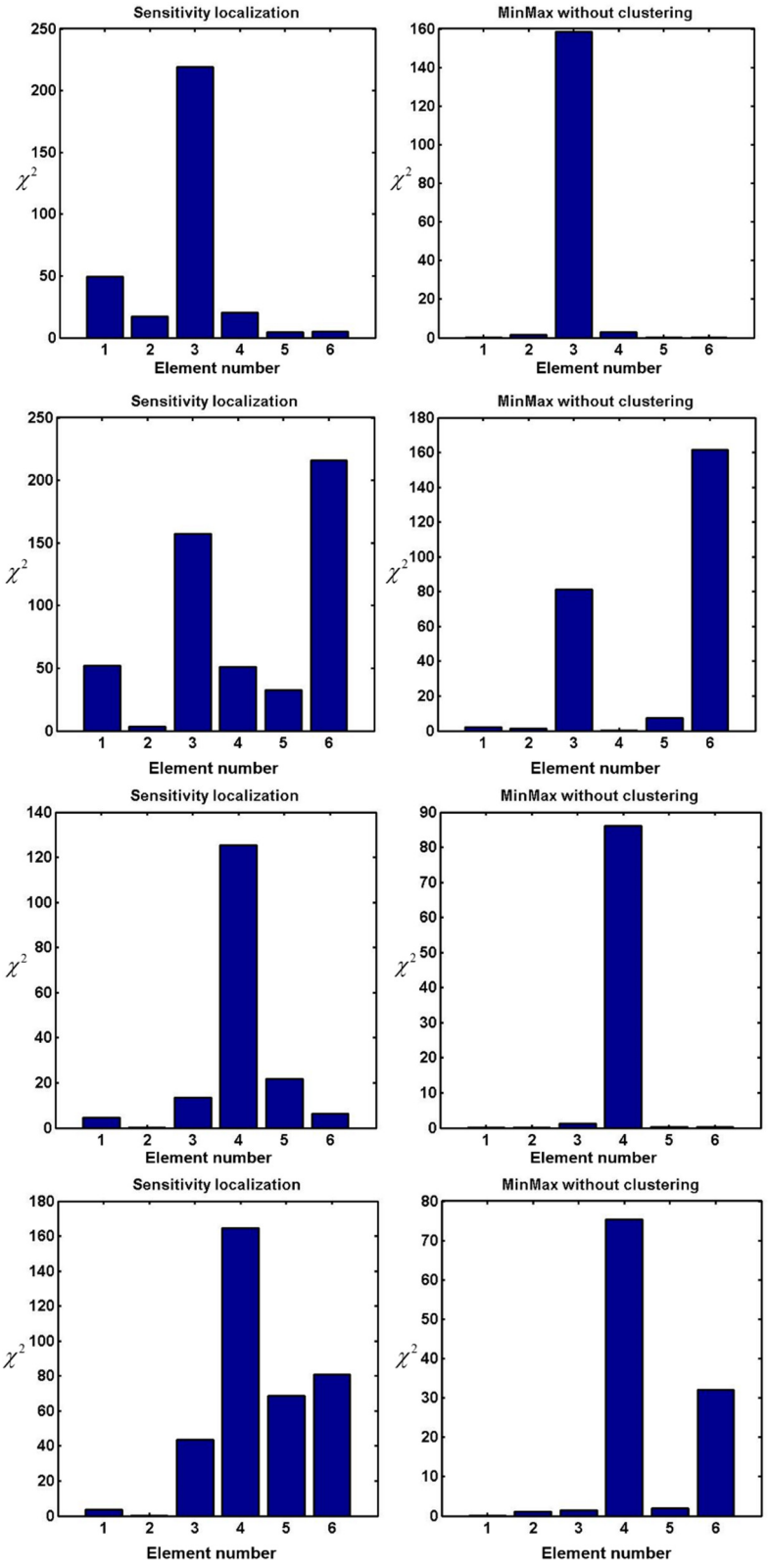

Figure 6.20 Damage localization of the mass-spring system with the sensitivity based and MinMax approach; damage in (a) spring 3, (b) spring 3 &6, (c) mass 4 and (d) mass 4 & 6

It can be seen in Figure 6.20 that damaged elements (one or two) are identified from both methods. However, the results from the MinMax approach are more distinctive than the sensitivity based approach. This is expected as explained in Chapter 5: in the sensitivity based approach the effect of damage in one element is observed in all other elements while in the MinMax approach this effect is removed.

6.4.1.2 Detectability of damage in each element

In order to be able to assess the detectability of damage in each element, in Chapter 5 the diagonal elements of the Fisher information matrix and the F^* values were proposed. These values are computed and shown in Figure 6.21. Moreover, to check the proposed detectability approach, the system is damaged in each element to an equal ratio, i.e. 5% damage ratio, and the resultant χ^2-value corresponding to the damaged element is computed from both the sensitivity based and MinMax approaches. The expectation of these values are calculated by computing these values for 100 times with different random inputs to the system and taking their average. These values are also illustrated in Figure 6.21 to be compared with the diagonal of FIM and F^* values. When an element has a higher χ^2-value with the 5% damage, it shows that the damage is more detectible in it; in other words, for smaller damage ratios the reaction of the test is still visible in terms of χ^2-value.

It can be seen that the format of the expected χ^2-value from the sensitivity based approach is the same as the diagonals of FIM, and the χ^2-value from the MinMax test is following the same format as F^* values.

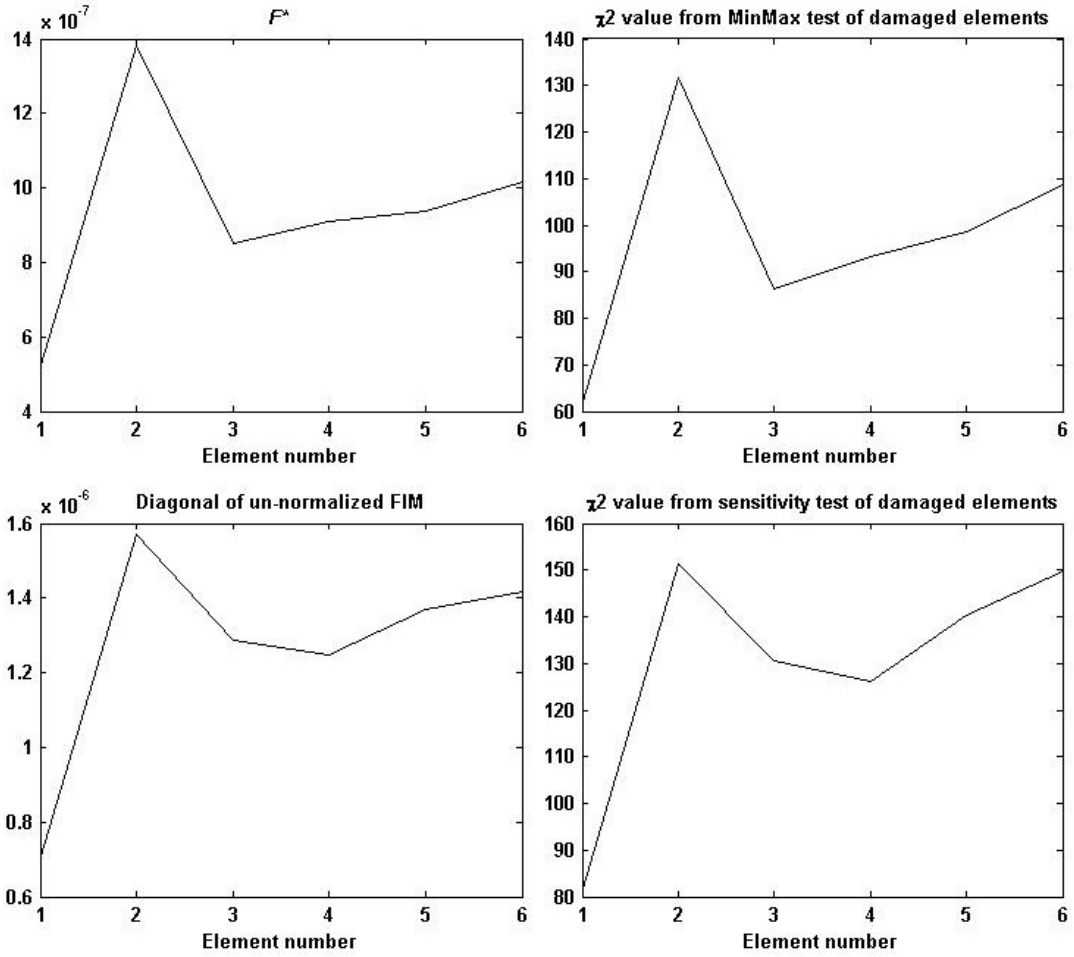

Figure 6.21 Detectability of damage in each element from the diagonals of Fisher information matrix and *F values**

6.4.2 Shear wall model

In this section, the shear wall model introduced in 6.2.3.2 is employed in investigating the damage localization and clustering approaches. There are two configurations, i.e. 7 element and 12 element, of this structure and both of them will be investigated. It should be noted that the sensors are located in every level and the number of modeshapes used in composing the Jacobian matrix is chosen to be 4 for localizing the damage in stiffness and is 6 for localizing the damage in mass.

6.4.2.1 Detecting the damage effect in stiffness or mass

The damage is modeled in both 7 and 12 elements shear walls, by decreasing the stiffness or mass of each level for 5%. Since the stiffness of both structural configurations is identical in each story,

when localizing the damage in mass, both structures will be identical. However, when the damage is occurring in the stiffness of each element, these configurations are not identical.

The damage in mass is applied for three cases: I) damage in levels 4, II) damage in level 6 and III) damage in levels 4 and 6. Additionally, the damage in stiffness is applied as one configuration for both 7 element and 12 element shear walls. For the 7 element shear wall the damage is in elements 3 and 6, and for the 12 element shear wall, the damage is in elements 5 and 11. These configurations are presented in Figure 6.22.

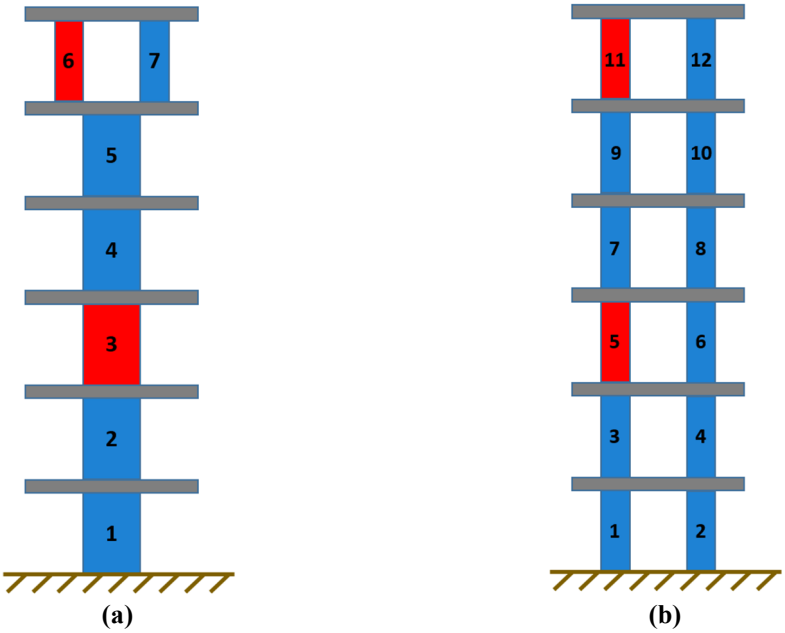

Figure 6.22 Damage configurations for the shear wall model with (a) 7 elements and (b) 12 elements

Similar to a practical approach, before localizing the damage in these structures, the damage detection should be done and if the structure is detected to be damaged, then the damage localization is sensible to be performed. Therefore, the damage detection of these damage scenarios are performed firstly; the results are shown in the following figure.

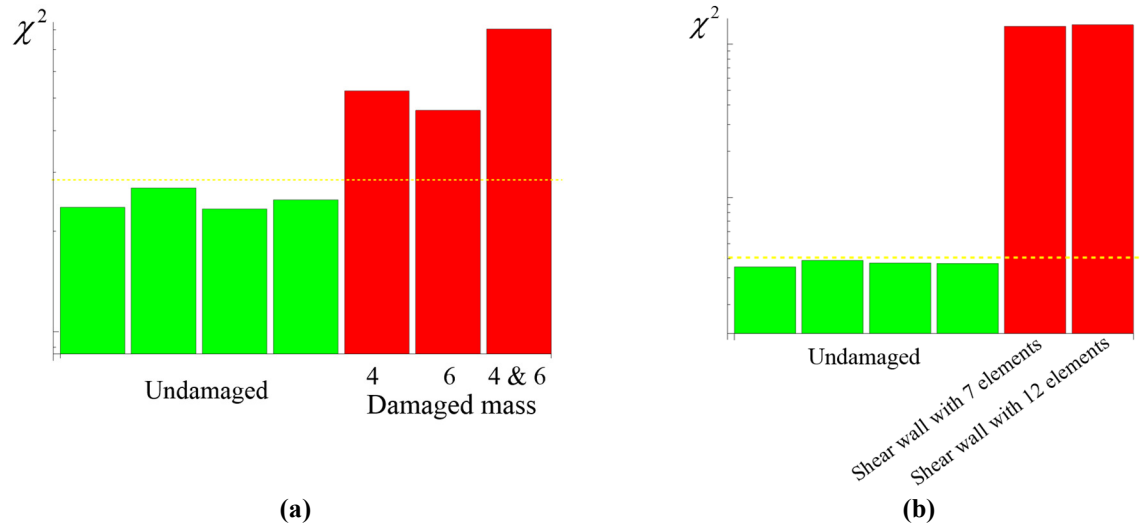

Figure 6.23 Damage detection of the shear wall for damage in (a) mass and (b) stiffness of walls

6.4.2.2 Clustering

In order to cluster the elements, the clustering approaches, i.e. *k*-means and HFC, introduced in Chapter 5 are employed. By considering the formation of the 7 and 12 element shear walls, it can be expected that the elements located in the same story level are *close* and therefore they should be clustered in the same group. Since the number of masses are only 6, same as the mass-spring example in 6.4.1, they do not need to be clustered. This is demonstrated in the following dendrogram in Figure 6.24. As noted before, both 7 and 12 element structures are practically the same when they are undamaged and hence, their FIMs composed from the Jacobians with respect to mass elements are identical.

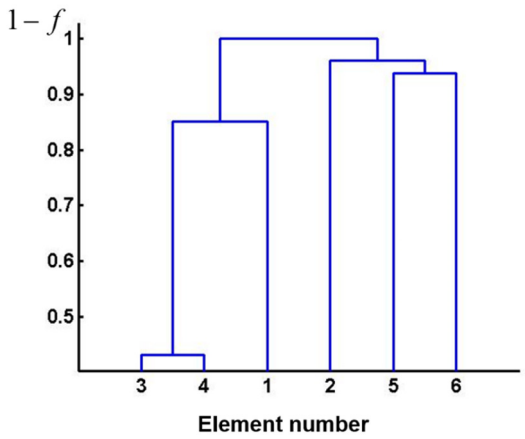

Figure 6.24 Hierarchical Fisher-information-matrix-based clustering (HFC) of mass elements for 7 and 12 element shear wall

It should be noted that the elements in the same story level are playing the role of one element in an analytical view to the structure. This means that the damage in either of the two elements results in the identical output from the same input excitation. Therefore, for this structure these two elements are almost not distinguishable in terms of damage. However, these elements are modeled and formed in this way to clarify the clustering concept and its effect on the results.

Since the Jacobian columns corresponding to the stiffness of elements located in the same story level is exactly equal (which does not happen in a typical real structure), for the demonstration purposes, in the 12 element shear wall the Jacobian columns of the right elements in each story are changed by adding a random noise vector to them. This noise vector is having a minor magnitude and is applied to the Jacobians in order to demonstrate the functionality of the clustering approaches. In this way, the corresponding elements of the normalized FIM deviate from 1.0. In order to cluster these elements, the HFC and *k*-means approach are employed. The threshold for the HFC method is chosen as $\varepsilon_f = 0.15$. The number of clusters for the *k*-means approach is chosen as 6, because the number of independent clusters/elements is 6 in both shear walls (7 and 12 element). It should be noted, as was mentioned in Chapter 5, although the threshold for the HFC method can be identical for most of the structures, the number of clusters needed as

input to the *k*-means algorithm is usually unknown and needs to be guessed. Herein, this number is chosen based on our complete knowledge on the structural behavior of this shear wall.

The hierarchical clustering of the elements using the HFC approach, for the 7 and 12 element shear walls are depicted in Figure 6.25. It is seen in this figure that all the elements in the same story level are correctly clustered in the same cluster using the HFC approach.

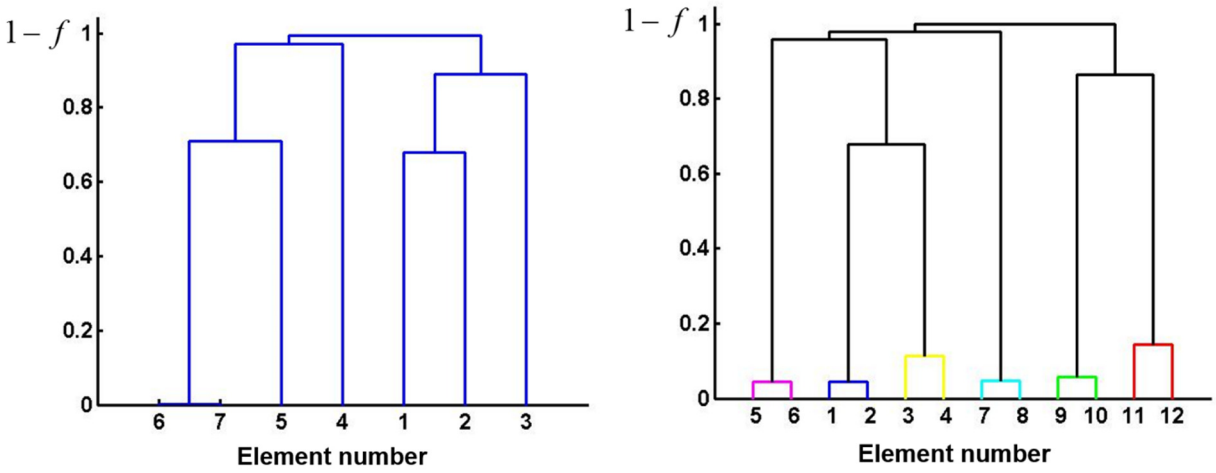

Figure 6.25 Dendrograms depicting the Hierarchical Fisher-information-matrix-based clustering (HFC) of the shear wall with (a) 7 elements and (b) 12 elements

The Normalized Fisher Information Matrix (NFIM) for the 7 and 12 element shear walls are compared with the HFC clustered NFIM in Figure 6.26. It is observed in Figure 6.26, that the elements with higher value (*close* elements) are moved into clusters and therefore the final clusters are almost perpendicular to each other.

Now, the same Jacobians are clustered with the *k*-means approach. It was observed that different clustering schemes were achieved by the *k*-means in each execution of program with the same inputs. For the 7 element shear wall, these clusters were almost unique, although in most of the cases *k*-means did not converge. One reason is that the Jacobian vectors for this structure corresponding to the 6 and 7 elements are completely identical. When *k*-means converges for the

7 element shear wall, the resultant clustering is same as the HFC approach as shown in Figure 6.25.a.

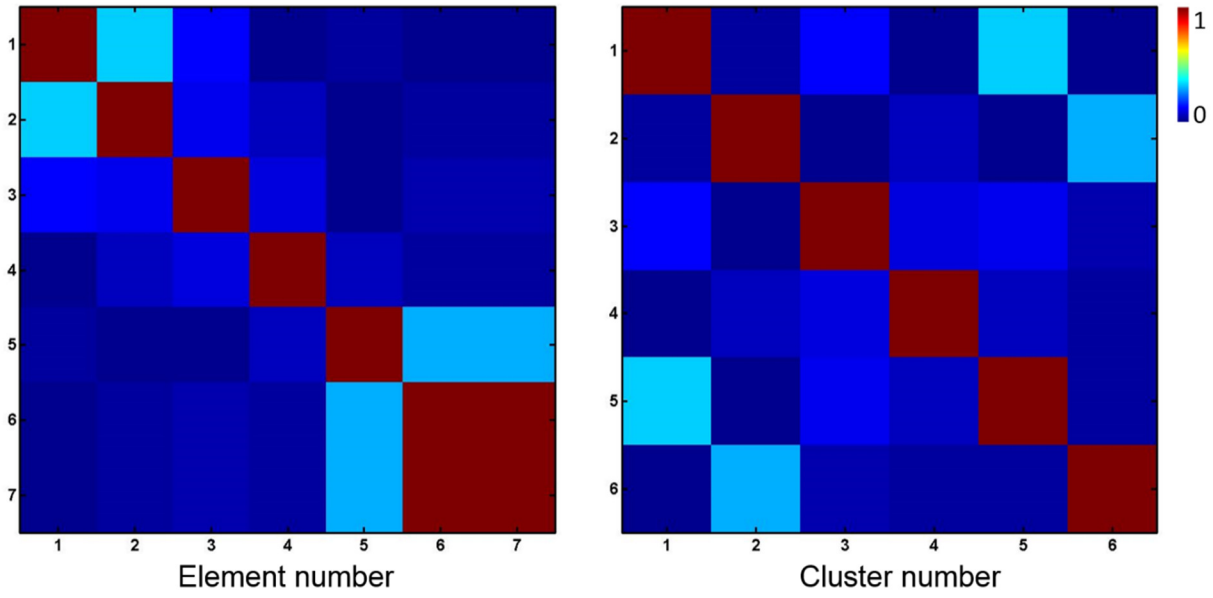

NFIM of 7 element shear wall

NFIM of centroids of clusters for 7 element shear wall

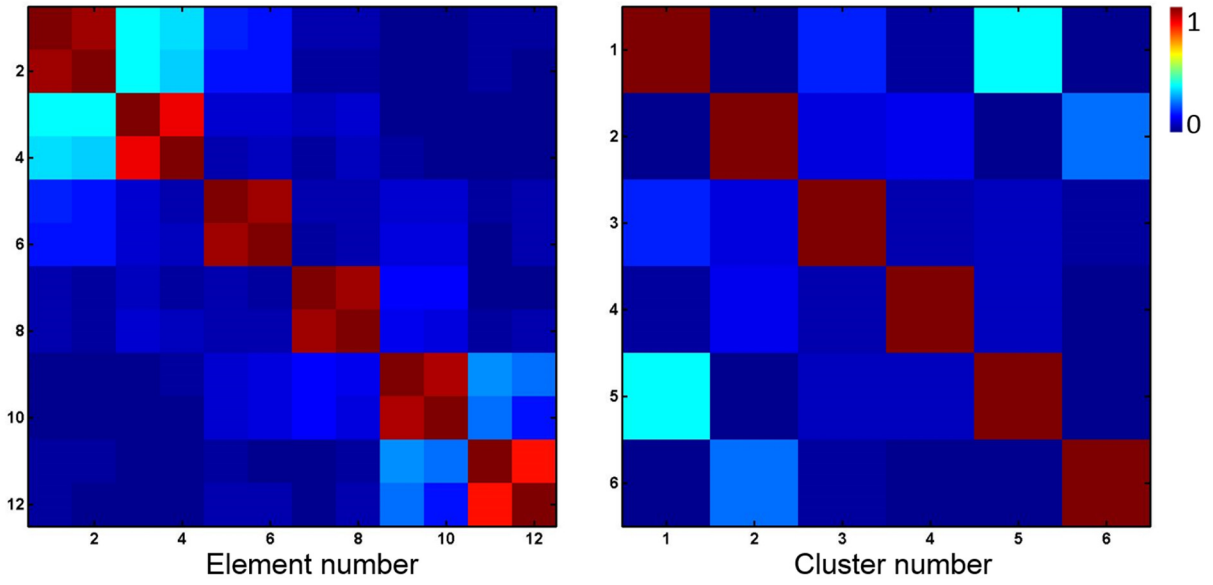

NFIM of 12 element shear wall

NFIM of centroids of clusters for 12 element shear wall

Figure 6.26 Normalized Fisher information matrix (NFIM) for the HFC clustered and uncluttered Jacobians for the shear walls with 7 and 12 elements

For the 12 element structure, *k*-means resulted in different clustering schemes for each repetition of the algorithm. In some repetitions it did not converge too. As mentioned before, the reason of this instability is that in the *k*-means method, the starting point of its clustering approach is with random selection of vectors. Since the starting point changes and each column vector has big dimension (equal to the dimension of residual vector), the resultant cluster changes regularly for this problem. It should be noted that the objective function for *k*-means in clustering is chosen as cosine between input vectors. It was observed that the results are almost the same when choosing correlation between the vectors as the objective function. Two clustering schemes achieved by the *k*-means for the 12 element shear wall are illustrated in Figure 6.27.

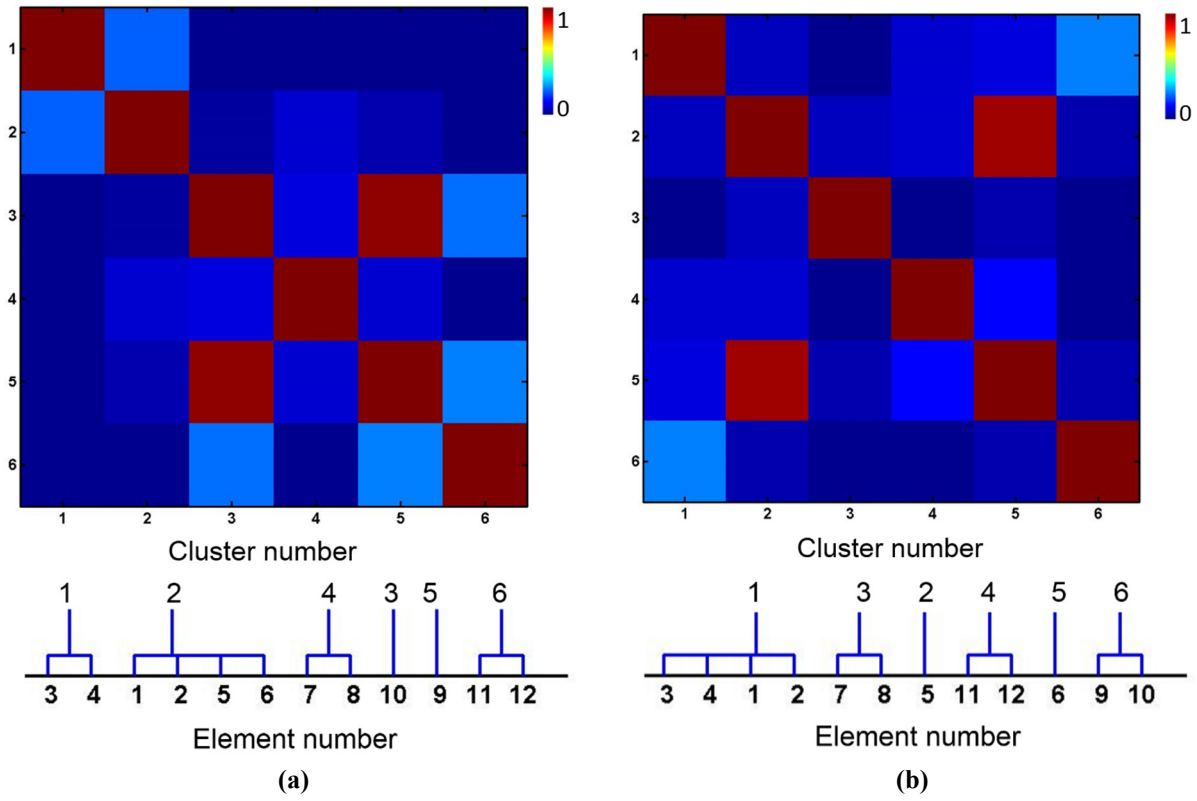

Figure 6.27 Two clustering schemes acquired for the 12 element shear wall with *k*-means approach

It can be seen in Figure 6.27 that *k*-means could not achieve in clustering the *close* elements, i.e. the elements in the same story level, into the same cluster. The warm colors are still

existing on non-diagonal elements of the clustered NFIM. It is expected that if the damage happens in elements 9 or 10, the first clustering scheme (Figure 6.27.a) would not work for the MinMax approach. Similarly, if the damage is occurring in elements 5 or 6, the damage will not be identified using the MinMax approach from the second clustering scheme (Figure 6.27.b) as will be shown in the next section.

6.4.2.3 MinMax and sensitivity based damage localization

The simulated data from the shear wall structure with different damage configurations presented before, will be localized in this section. The damage was detected from each of these configurations in 6.4.2.1 and therefore now the damage will be localized as the next step of damage identification.

In the first step the damage in the mass is localized using the MinMax and sensitivity based approaches. As mentioned before with having masses as the parameters, there is no need to cluster them. Hence, the MinMax method is performed without clustering. The results are shown in Figure 6.28.

(a)

(b)

(c)

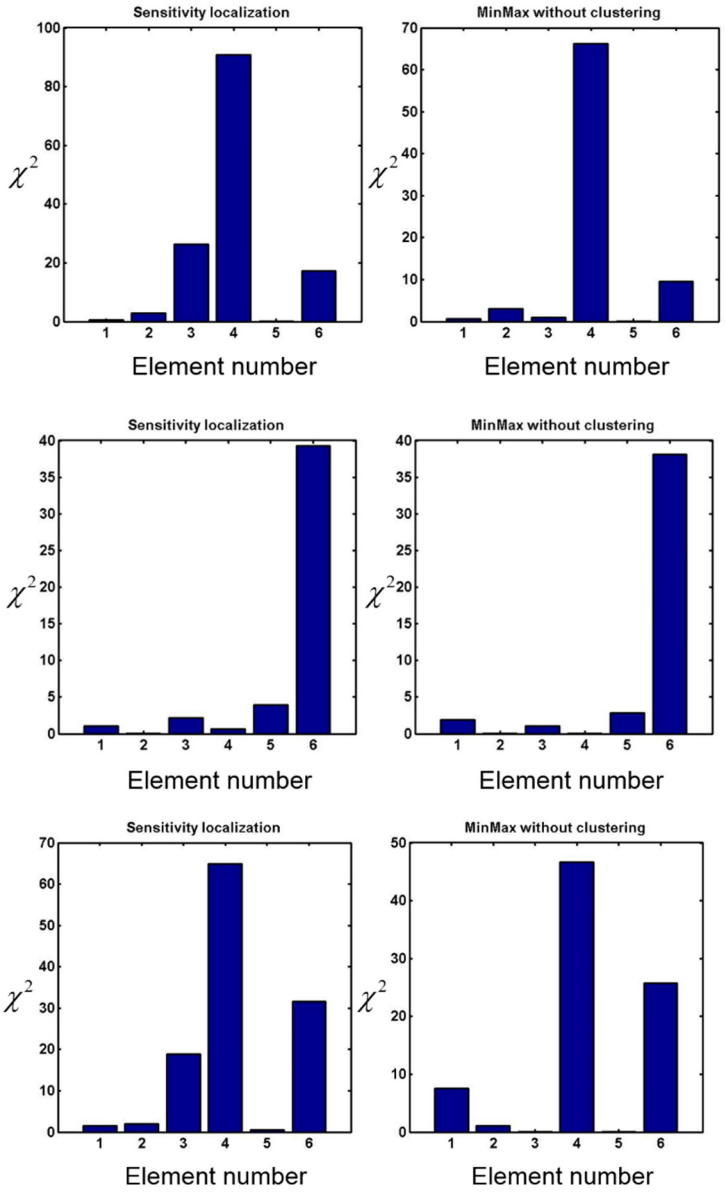

Figure 6.28 Damage localization of the shear wall with the sensitivity based and MinMax approach; damage in (a) mass 4, (b) mass 6 and (c) masses 4 & 6

In the next step, the damage in the stiffness of elements of 7 and 12 element shear walls will be localized by using the sensitivity based and MinMax approaches. For this purpose the clustering is performed using the HFC method as Figure 6.25. The results with clustering and without clustering are shown in Figure 6.29.

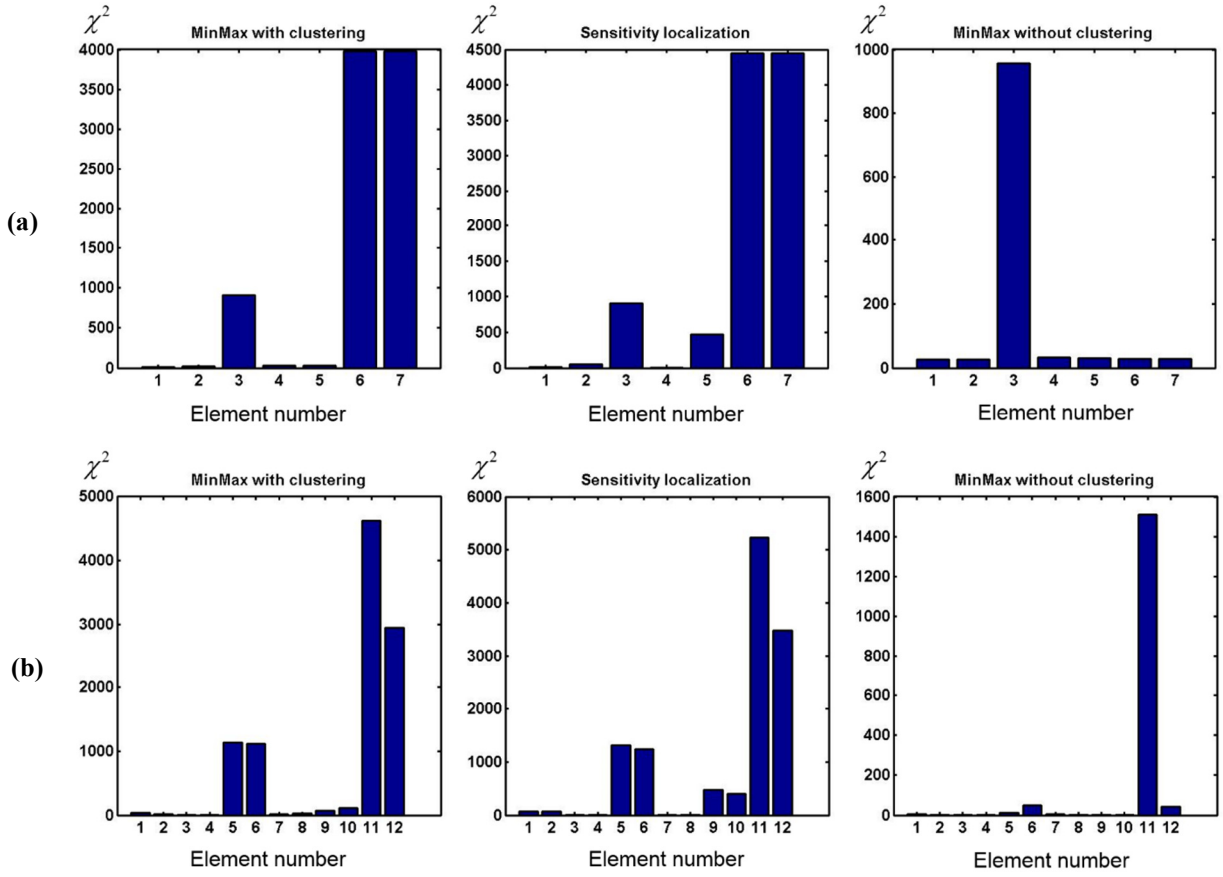

Figure 6.29 Damage localization of the (a) 7 element shear wall with damage in elements 3 and 6; (b) 12 element shear wall with damage in elements 5 and 11; the clustering method is HFC

It can be seen that the damage in the shear wall elements are correctly identified. Moreover, because the elements in the same level are *close* to each other and they are clustered by HFC method in the same cluster, the damage in one element will be reflected in other element in its cluster, in both sensitivity based and MinMax methods. It should be noted that the MinMax approach only removes the effect of the damage from the elements outside the cluster of the tested element.

Moreover, since the *close* elements were correctly clustered, the damage is distinctly identified for the cluster containing the damaged elements. As shown in Figure 6.29, without clustering the *close* elements the effect of damage is not seen on the χ^2-test.

Now, to check the *k*-means clustering approach, the clustering schemes presented in Figure 6.27 will be used in localizing the damage in the 12 element shear wall. The results are illustrated in Figure 6.30. It can be seen that as expected when the damage is occurring in the *close* elements not clustered correctly in the same cluster, the damage cannot be seen in the MinMax test (Figure 6.30.b). Therefore, these clusters suggested by the *k*-means are not appropriate in removing the effect of *closeness*.

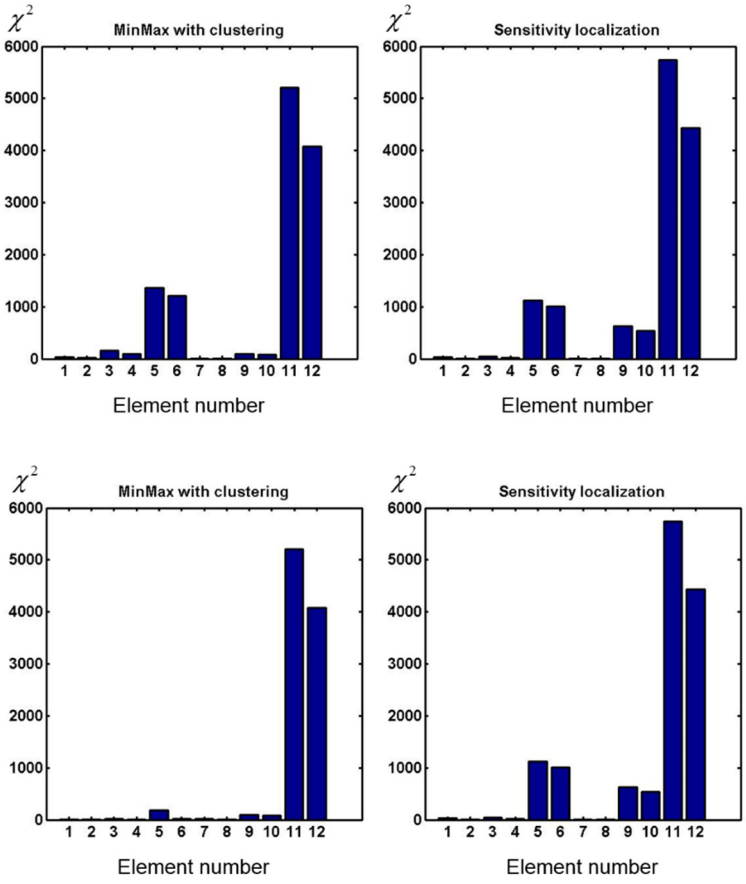

Figure 6.30 Damage localization of the 12 element shear wall with damage in elements 5 and 11 using the *k*-means clustering scheme (a) Figure 6.27.a, and (b) Figure 6.27.b

6.4.2.4 Detectability of damage in each element

Similarly to the mass-spring case-study, in here, the relation between the detectability of damage for each element and the diagonals of the un-normalized FIM are investigated by considering the trend of the evaluated expected χ^2-value of each element (when damaged with 5% ratio) and the

diagonals of FIM. Additionally, the values of expected χ^2-value from MinMax test are compared to the F^* values. Therefore, the χ^2-value of each element from the sensitivity based method and MinMax method are calculated when only that element is damaged, and then they are compared to the corresponding value in the diagonals of the FIM and F^* values. The results for the 7 element shear wall are illustrated in Figure 6.31.

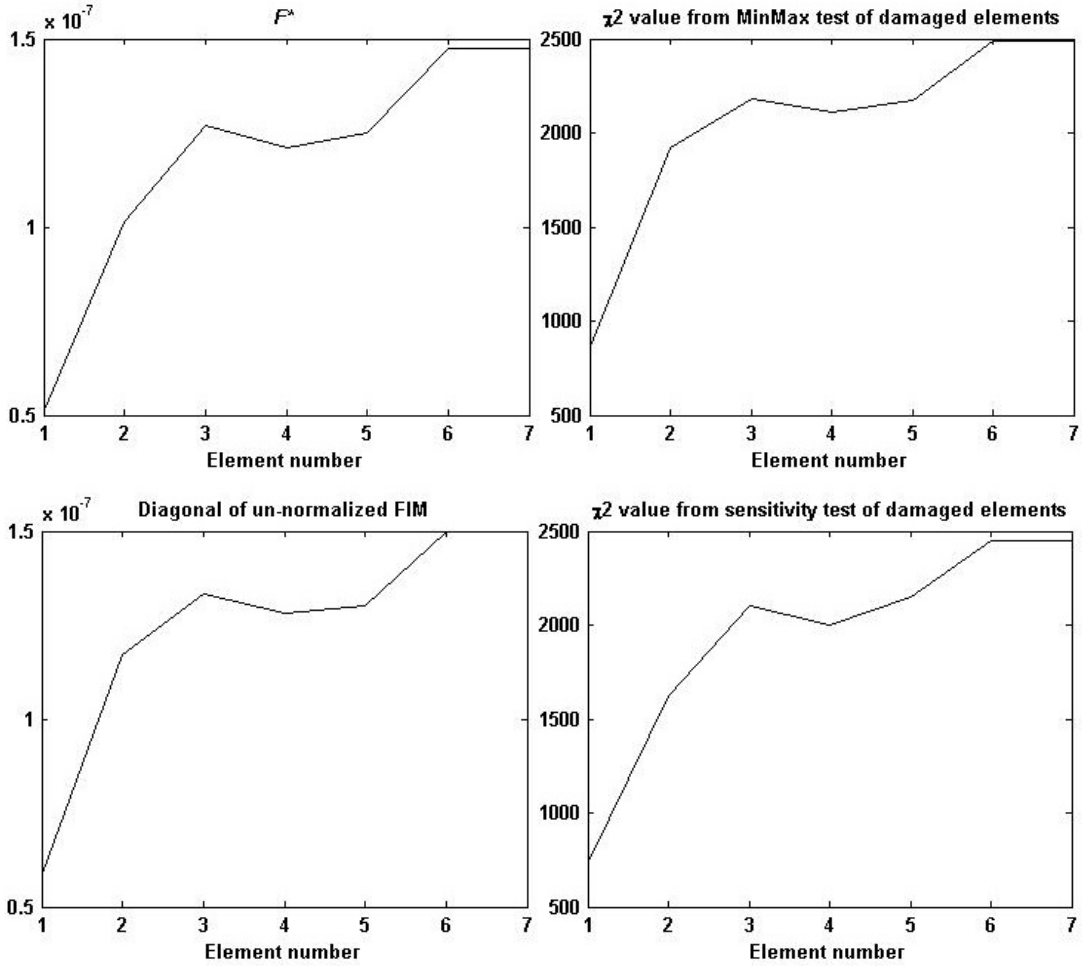

Figure 6.31 Detectability of damage in each element of 7 element shear wall from the diagonals of Fisher information matrix and *F values**

It is observed that the elements with higher values are the same in both corresponding graphs which confirms that the diagonals of FIM and F^* values are a good representative of the detectability of elements from, respectively, sensitivity based and MinMax approaches. It should

be noted that, these values are calculated with all modeshapes used in composing the Jacobian matrix. The number of repetitions to compute the expectation is 100.

6.5 Conclusions

In this chapter three analytical models were used in verifying the theories and methods introduced in Chapters 4 and 5. The effect of number of samples and noise ratio on these models could be predicted by the theories developed in Chapter 4.

The *k*-means and HFC clustering methods were used in clustering the *close* elements of the shear wall model. It was demonstrated that the HFC method could identify and cluster the *close* elements correctly, while *k*-means was not promising. The *k*-means approach could not cluster the close elements properly. The instability of this approach was shown.

Moreover, the damage was localized in two of these models using the sensitivity based and MinMax tests. It was seen that the results from the MinMax test with the HFC clustering can identify the damage distinctly. While both MinMax and sensitivity based approaches could identify the damage, the MinMax results were clearer as expected.

The two indices indicating the damage detectability were tested for two of the models. It was verified that these indices have a direct relationship with the detectability of damage in each element.

Chapter 7: Experimental Test: the Yellow Frame

Experiments on large scaled structures are one of the best ways in measuring a structure in a controlled environment with different damage scenarios to different extents. The measured data from these experiment can be used in assessing different damage detection techniques. In this chapter, the experimental measurement of a steel frame, namely the Yellow frame, is elaborated.

In order to study the effect of measurement noise and number of samples on the SSDD test, the noise is simulated and added to the measured data. Moreover, the data is cut to the length required in studying the effect of number of samples.

In case of localizing the damage in experiments using the subspace damage localization approach, an analytical model of the structure is also needed in computing the Jacobians of the modal parameters of the structure with respect to each physical parameter. Therefore, this analytical model will be presented in this chapter.

The damage localization using the SSDL technique will be elaborated and validated step by step from calculating of the Jacobians, clustering them, to the testing of each element. The results of these studies will be presented in this chapter.

7.1 Introducing the Yellow Frame

The Yellow frame is a modular 4 story, scaled (1/3) steel frame restablished during this research in 2016 at the University of British Columbia (UBC). Several damage scenarios (configurations) are designed and tested by removal of braces of the structure. These damage configurations are used in assessing the statistical subspace damage detection and localization methods.

7.1.1 Frame description

This structure is 3.6 m high and is composed of 2 spans in each direction with the total length of 2.5 m. Each floor of the structure is carrying dead loads applied to the structure by using 4 steel

plates distributed on each level. The dimensions of the steel plates are 1.5 m × 0.65 m. The weight of the steel plates for the first three floors is 17.8 kN per floor and for the fourth floor the weight is 13.34 kN. The frame is constructed from hot rolled 300W steel members. The beams are S75×11 sections and the columns are B100×9 sections. Four 50 mm square steel tubes are used to provide in-plane stability to the diaphragm of each floor. For the lateral stability, four pairs of threaded steel rods (with diameter of 12 mm) are used as braces on each side of the structure in each floor. These braces are all pretensioned by using a torque wrench. The torque moment is equal for all the braces in order to assure the same pretensioned force consistently throughout the structure. The photo of the Yellow Frame structure and its schematic plan are shown in Figure 7.1.

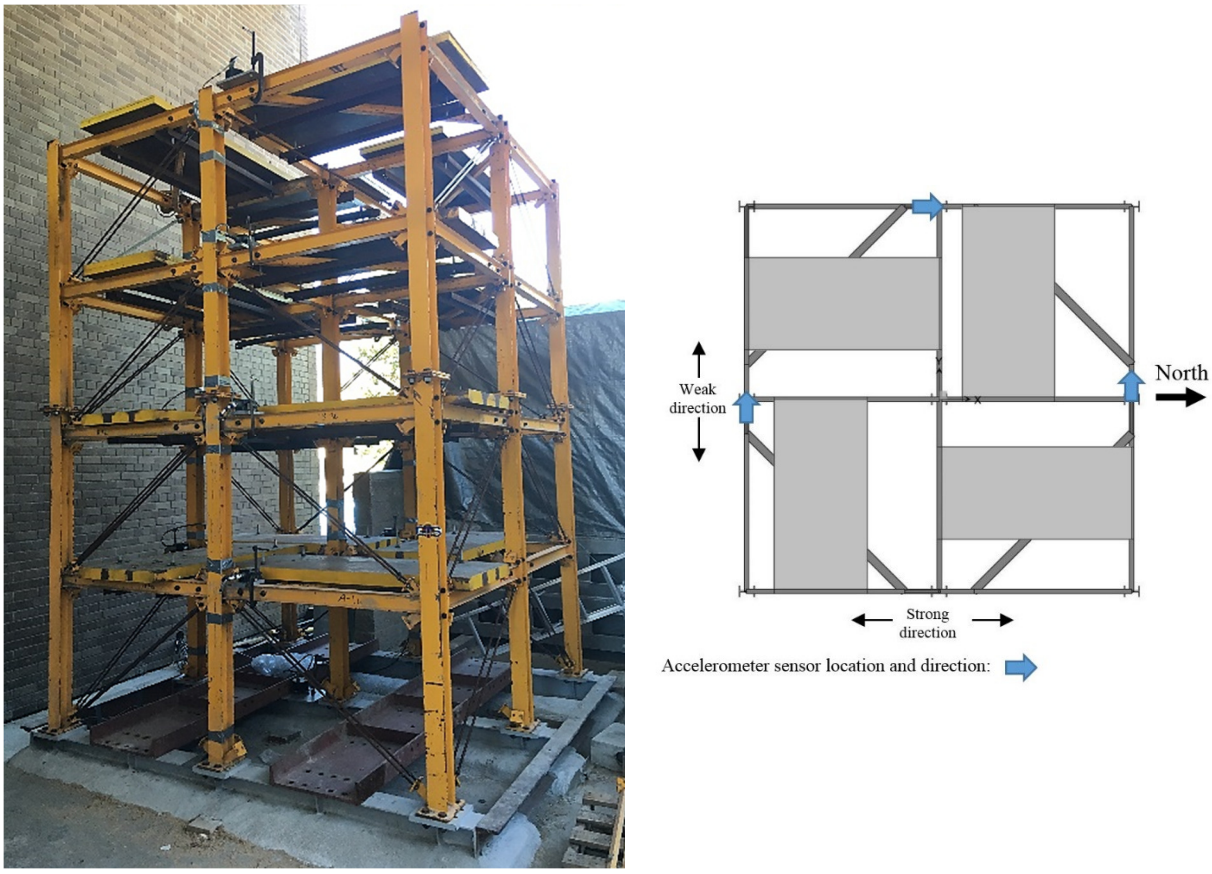

(a) **(b)**

Figure 7.1 (a) Photo of the Yellow Frame structure (south-east corner), (b) scaled plan of each level, mass plates, and location of sensors

It can be seen that the strong and weak directions of the structure are defined based on the orientation of the columns. In each level, two of the mass plates are moved towards south on the structure to increase the eccentricity and, therefore, magnify the effects of torsional modeshapes. These plates are fixed to the structure by using two channels fastening them to the beams using pretensioned screws.

There are three base beams (gray color in the photo) designed and built for this structure in order to increase the rigidity of base connections of columns. These beams are balanced and then stabilized with concrete mixture covering half of their depth. Moreover, two heavy channels are located on top of them to assure that the structure will not have relative displacement to the ground in ambient vibration testing.

7.1.2 Background on benchmark structure

This structure was previously established on a shaking table at UBC in 1999 and on the ground in 2002 as the IASC/ASCE benchmark structure. Some of the base beams are redesigned and built in order to restablish the structure. Moreover, sensor locations, the damage configurations, sensor types and location of masses are differentiated in this test. Other than that, the structure is instrumented with temperature and moisture sensors in addition to the accelerometers.

7.1.3 Instrumentation

This structure is instrumented by 15 accelerometer sensors of which three are located on the base of the structure. In each floor, three sensors are located at the north, south and west side of the structure as depicted in Figure 7.1.b. In addition, one temperature and one moisture sensor are also located on the structure for future study of the effects of these environmental factors on the damage detection method. All these sensors are connected through wires to a data acquisition system located inside the lab. The details of the instrumentation is explained in Appendix E.

The data measured from the structure is not filtered using a hardware filter and therefore, it is detrended, decimated and low-pass filtered by using developed software codes. The sampling rate is 1000 Hz which is decimated with a factor of 4 to 250 Hz. The reason is that the frequency content of the data is negligible after 125 Hz as shown in Figure 7.2.

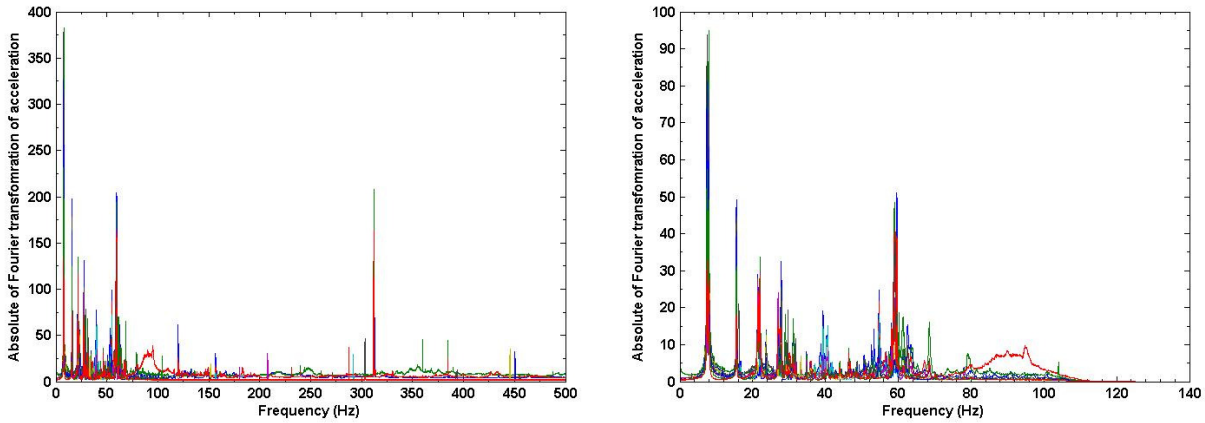

(a) **(b)**

Figure 7.2 Fourier transformation of (a) the unfiltered real data from the Yellow Frame with 1000 Hz sampling rate and (b) the decimated data with 250 Hz sampling rate

7.1.4 Eigenstructure identification

The natural frequencies and modeshapes of the structure can be identified from the measured data in the healthy state of the system. These modeshapes and natural frequencies are not needed in the damage detection or localization of the structure unless the real data eigen-parameters are chosen to be used (instead of analytical ones) in forming the Jacobian matrix (*Formation 2*) as was described in Chapter 5. Even in the latter case the system identification needs to be performed only once in the reference state of the structure and is not needed in the testing phase.

It should be noted that the analytical model does not need to be calibrated to the structure, however, the model should be a good representative of the dynamic behavior of the structure and the first (dominant) modal parameters should not have different order than the real data. Therefore, identifying the modal parameters of the system in the reference state is recommended in validating the model used in the sensitivity analysis.

The first ten modeshapes and natural frequencies of the structure from the real data are evaluated. The natural frequencies are illustrated in Figure 7.3 and their corresponding modeshapes are shown in Figure 7.4.

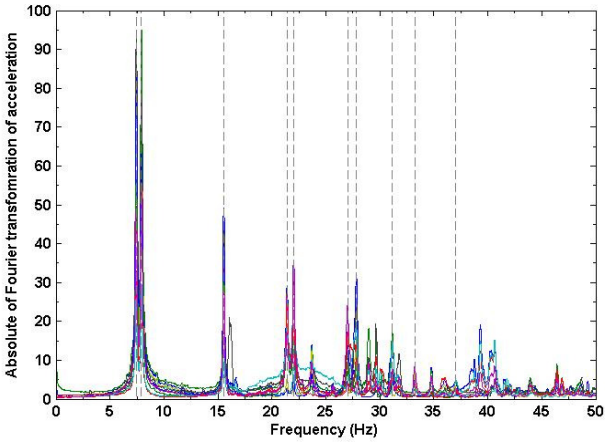

Figure 7.3 Identified 10 natural frequencies from the real data for Yellow frame structure

As illustrated in Figure 7.4, the transitional modeshapes are not in the direction of strong or weak axes and they are diagonally coupled in the direction of the combination of these axes. Each mixed couple of modeshapes are presented by symbols ⊥ and ⊢, i.e. (XY-n⊥ and XY-n⊢) represents the n'th pair of coupled transitional modeshapes. The reason for this combination is that the corresponding natural frequencies of these modeshapes are very close to each other which stems from the closeness of the stiffness of the structure in each direction. In other words, the stiffness of the structure in the strong and weak axes are very close. The onliest difference between the stiffness in each direction is in the orientation of columns as shown in Figure 7.1. Moreover, the stiffness in each direction is the sum of stiffness of the frames and the braces, and because the braces create the major part of the total stiffness in each direction, the difference of the total stiffness in each direction is comparably very small.

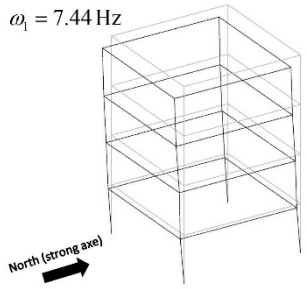

1st modeshape (transitional, coupled XY-1 ├)

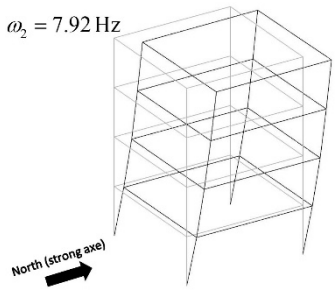

2nd modeshape (transitional, coupled XY-1⊥)

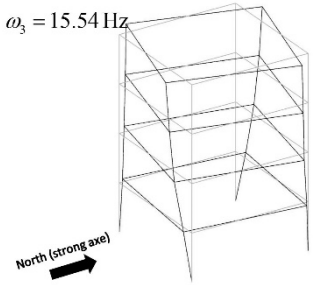

3rd modeshape (torsional, T-1)

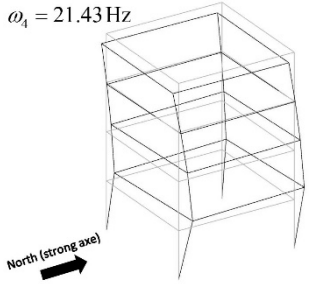

4th modeshape (transitional, coupled XY-2 ├)

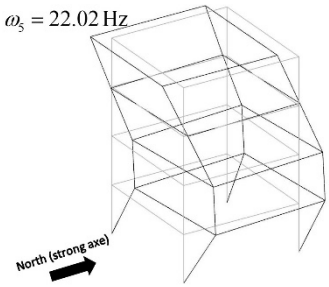

5th modeshape (transitional, coupled XY-2⊥)

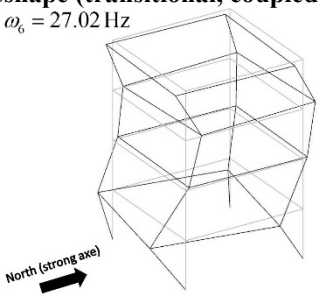

6th modeshape (transitional, coupled XY-3 ├)

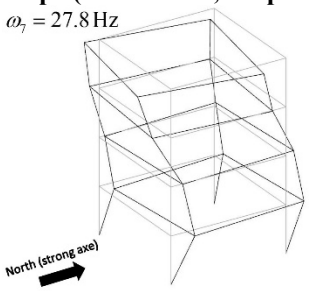

7th modeshape (transitional, coupled XY-3⊥)

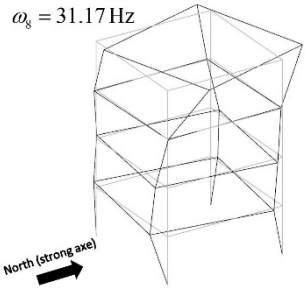

8th modeshape (torsional, T-2)

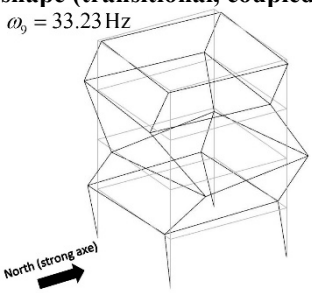

9th modeshape (transitional, coupled XY-4)

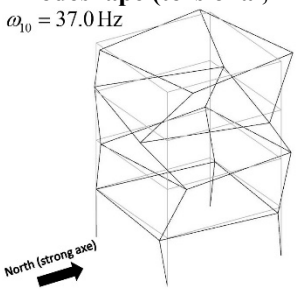

10th modeshape (torsional, T-3)

Figure 7.4 First 10 modeshapes identified from the real data measured from the Yellow frame

It should be noted that this complexity of modeshapes happens in the numerical computation of the eigenstructure of the real data. The modeshapes acquired from the analytical model will not be coupled unless the stiffness is exactly the same in each direction as will be discussed in 7.1.6.1. In other words, if the two modeshapes (in two directions) are exactly identical, any combination of them, e.g. diagonal modeshapes, can be a modeshape too.

Since the modeshapes from the analytical model are not coupled unlike to the modeshapes from the real data, the coupled modeshapes should be decoupled and scaled prior to the use in the Jacobian computation as described in Chapter 5. The reason for this decoupling and scaling is to make them consistent with the analytical modeshapes in composing the final Jacobians.

7.1.5 Damage creation

In order to evaluate the SSDD and SSDL methods, several damage scenarios need to be created on the structure. The damage is created by removal of one or both of the braces in each span at each story. The ratio of damage by removing one brace is half of the ratio for removal of both braces. Based on the number of braces, the location of removal and the combination of the removal of one or more braces, 15 damage configurations are created and investigated. It should be noted that the testing of these damage configurations was performed during 4 inconsecutive days.

Moreover, having a single damage location in the structure is the typical case investigated in damage detection methods and localizing the damage for multiple damage cases is more complicated. However in here, different multiple-damage cases are also created along with single-damage cases.

7.1.5.1 Damage configurations

The damage configurations investigated in this study are 15 configurations which are organized based on the damage ratio and their locations. Based on the numbering of the braces shown in Figure 7.5, the damage configurations are demonstrated in Table 7-1.

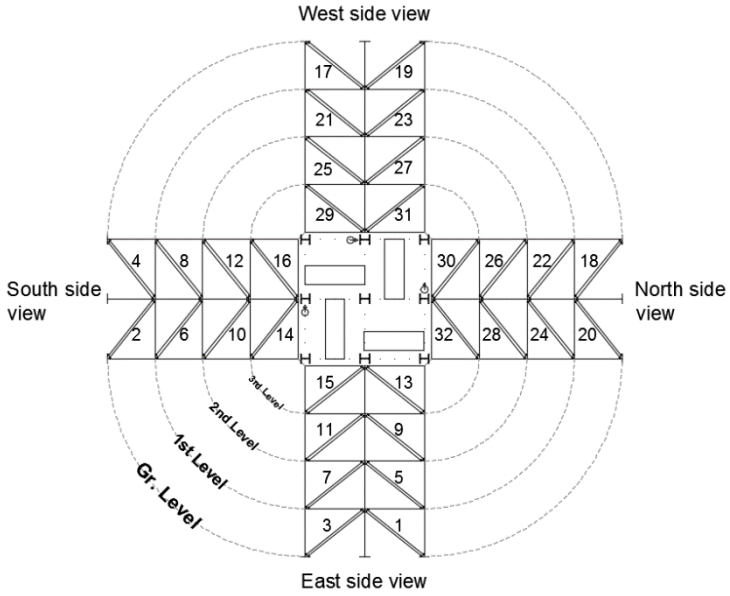

Figure 7.5 Numbering of the braces in each outside frame of the Yellow frame structure

Table 7-1 Damage configurations of the Yellow frame: the location of damage and number of removed braces

Configuration number	Removed braces (number of braces removed)
C1	2 (I)
C2	2 (II)
C3	2 (I), 4 (I)
C4	2 (II), 4 (II)
C5	2 (II), 4 (II), 18 (I), 20 (I)
C6	2 (II), 4 (II), 18 (II), 20 (II)
C7	2 (II), 4 (II), 17 (II), 19 (II)
C8	1 (I), 2 (I), 3 (I), 4 (I), 17 (I), 18 (I), 19 (I), 20 (I)
C9	1 (II), 2 (II), 3 (II), 4 (II), 17 (II), 18 (II), 19 (II), 20 (II)
C10	25 (I), 27 (I)
C11	10 (II), 12 (II)
C12	21 (II), 23 (II)
C13	10 (II), 12 (II), 21 (II), 23 (II)
C14	6 (I), 8 (I), 29 (I), 31 (I)
C15	7 (I), 8 (I), 21 (I), 22 (I)

Each configuration is depicted in Appendix F.

7.1.6 The finite element model

In order to calculate the sensitivities of the eigenstructure to the physical parameters (chosen in here as stiffness of each brace), a finite element model of the Yellow frame is created using Abaqus® software (Hibbett et al. 1998). In this model, the section properties of the elements of the Yellow frame are used in modeling the beams, braces and columns. The model of the structure is depicted in Figure 7.6.

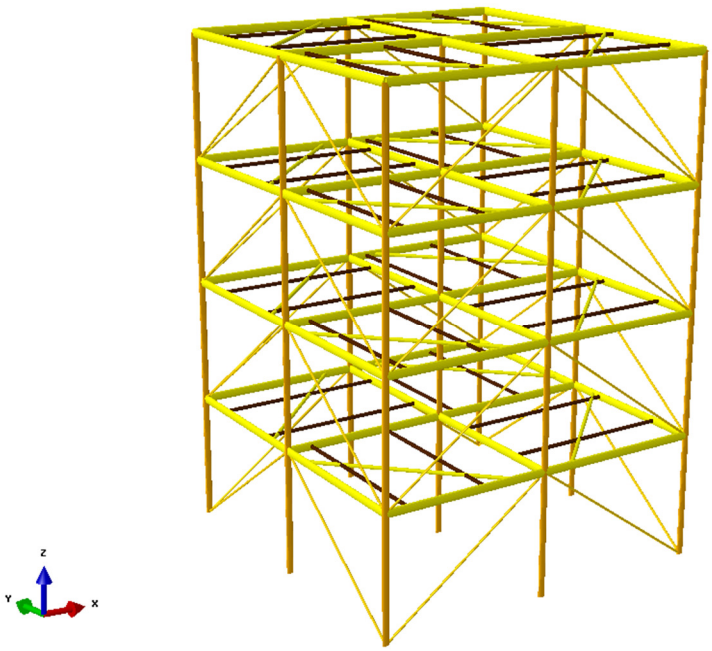

Figure 7.6 Finite element model of the Yellow frame structure (x represents North/strong axe direction)

The plates with mass are modeled as lumped mass in the four corners of each plate on the structure. Since these plates are bolted and connected with pretensioned rods to their surrounding beams (in friction), their contribution to the stiffness of structure for ambient vibration is not negligible. Therefore these plates are also modeled as two parallel beams.

The base of the structure is modeled as fixed connection to the ground. The connections of beams and columns are also modeled as fixed connection and the braces are connected as moment free hinge connections to the structure. Because each group of two braces in each floor at each span is only under axial force, they are modeled as one element with cross section area equal to the total area of both braces. Localizing damage in one brace element indicates the possibility of damage in both of these parallel braces. This structure is not updated based on the real data, and will be used in the sensitivity analysis of modeshapes and natural frequencies without calibration.

7.1.6.1 Eigenstructure evaluation

A modal analysis is performed on the finite element model and the natural frequencies and modeshapes are evaluated. The first 10 modeshapes are shown in Figure 7.7.

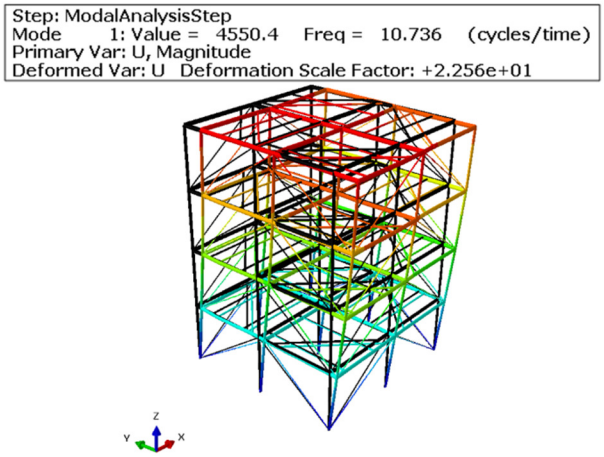

1st modeshape (transitional Y-1)

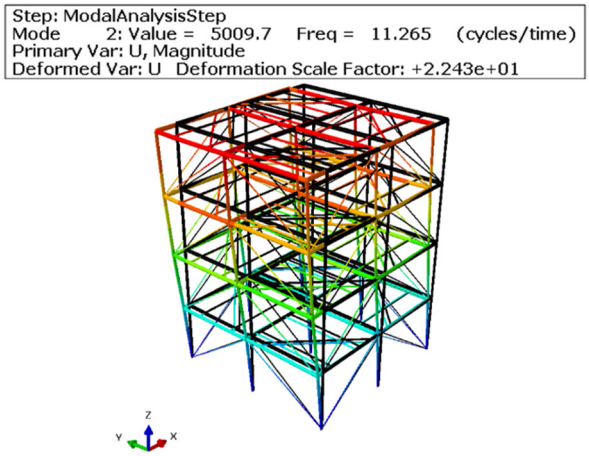

2nd modeshape (transitional X-1)

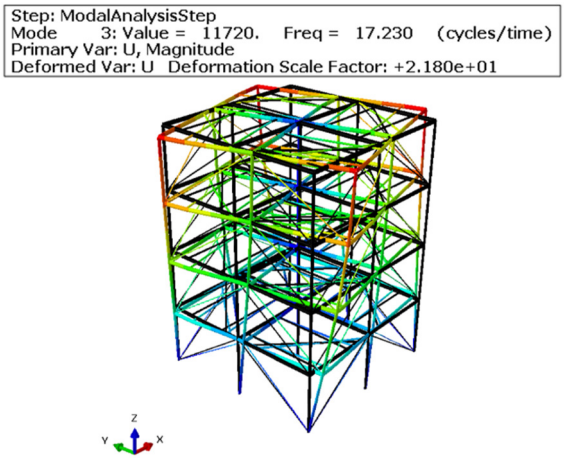

3rd modeshape (torsional, T-1)

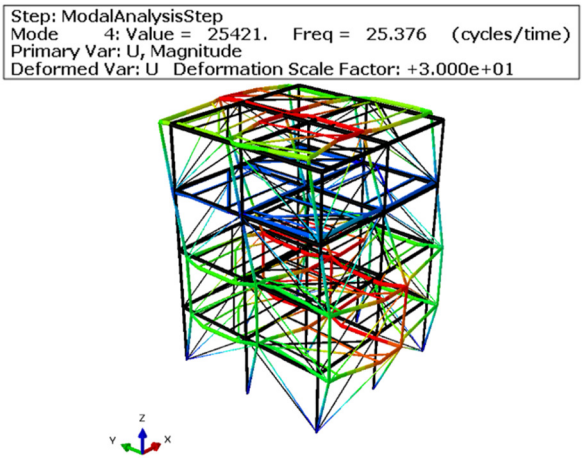

4th modeshape (transitional Y-2)

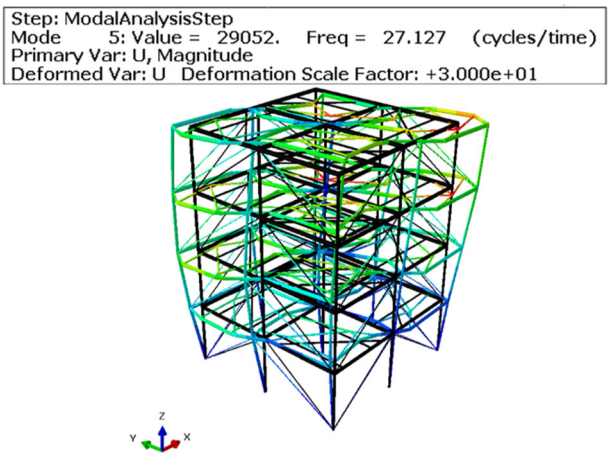

5th modeshape (Flexible diagram D-1)

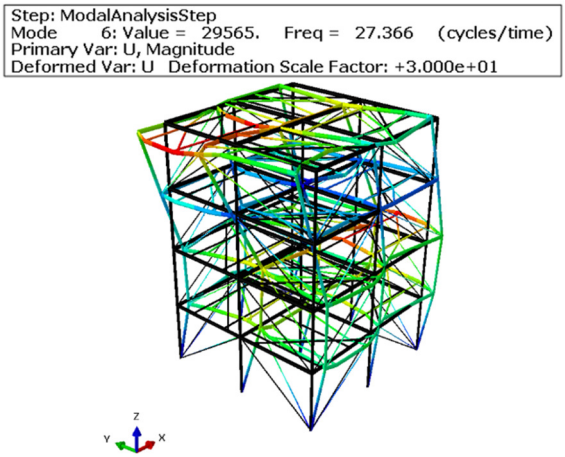

6th modeshape (transitional X-2)

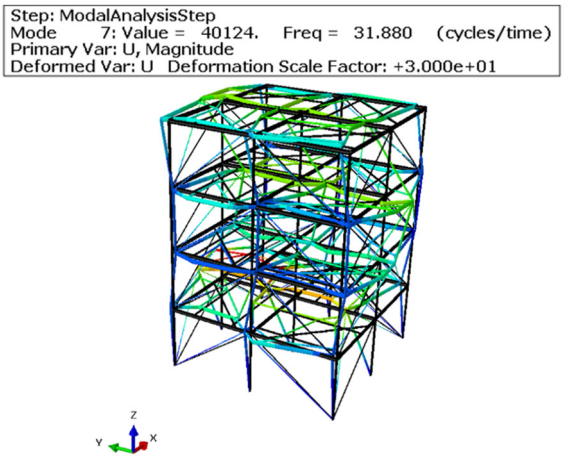

7th modeshape (transitional Y-3)

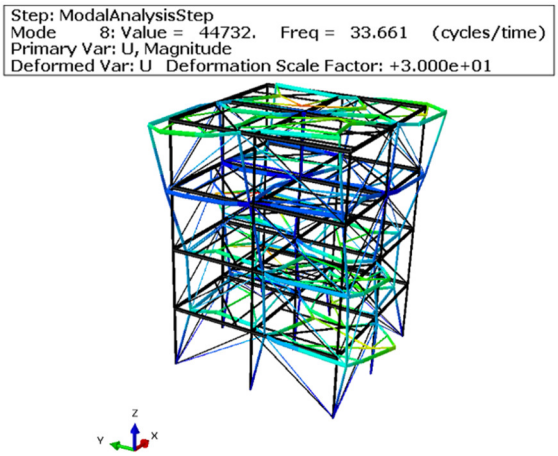

8th modeshape (Flexible diagram D-2)

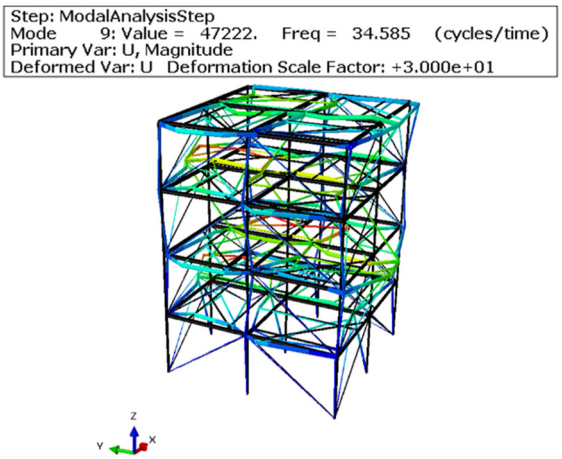

9th modeshape (transitional Y-4)

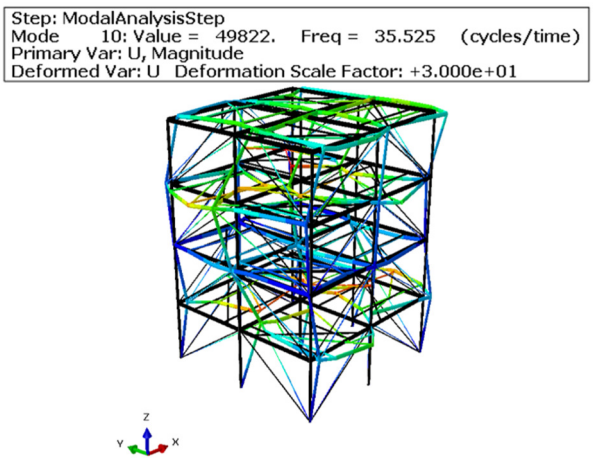

10th modeshape (transitional X-3)

Figure 7.7 First 10 modeshapes evaluated from the finite element model of the Yellow frame

It can be seen by comparing Figure 7.7 and Figure 7.4 that the order of the modeshapes identified from the real data and from the finite element model are the same from the 1st to 6th modeshape, without considering the flexible diaphragm modeshapes. Therefore, the finite element model is a good representative of the real structure. This model is not updated to match the natural frequencies to the real data, and only it is used in evaluating the sensitivities without the importance of their scaling factor. The order of the modeshapes play a more critical role than the values of their corresponding natural frequencies, since the sensitivities will be scaled in the SSDL method. The reason that the natural frequencies evaluated from the FE model and measured data are different is that the connections in joints are modeled as solid, while they need to be modeled

flexible to some ratio. Moreover, the connection of the structure to the basis is also not rigid as is modeled. These are in addition to the aleatoric uncertainties of the material and section properties present in the model.

Although in each floor, four square steel tubes are connecting the corner beams together to increase the rigidity of diaphragms, from the finite element model of the structure, it is observed that these beams do not provide enough rigidity to the diaphragm to completely remove the flexible diagram modeshapes. It should be noted that since the sensors are not located in the corners of the structure (where maximum movement occurs in flexible-diaphragm modeshapes), these modeshapes were not identified from the real data. Nevertheless, because they are present on the real structure, they will be used in its damage localization when using only the sensitivities from the FE model, i.e. *Formation 1*. However, when the sensitivities are calculated from both the FE model and real data (*Formation 2*), they need to be matched as will be shown in 7.3.

7.1.6.2 Sensitivity analysis

The computation of the sensitivities of the modal parameters of the structure to the stiffness of each brace is computed using the finite difference approach. The employed perturbation factor is 0.1% which proved to be optimal. The sensitivity analysis was performed using a Python script executed on Abaqus® software. There are 32 braces modeled in the finite element model that each of them represents two steel rods. The sensitivities of the first 10 natural frequencies and modeshapes are calculated with respect to the stiffness of each of these 32 braces.

7.1.7 Measurement noise simulation and data length

In order to study the effect of measurement noise in the data, the noise is created as white noise from the procedure mentioned in 6.2.1.3. The reason is that the measurement noise cannot be evaluated nor changed naturally with the sensors. Therefore, the measurement noise is simulated

and used as an additional measurement noise to the data (which already contains some unknown measurement noise). This simulated noise is added to each measurement channel. As mentioned before, the noise ratio is a percentage of the standard deviation of the measurement of each channel. This percentage of the standard deviation is used as the standard deviation of the Gaussian noise imposed on the measurements.

The length of data is changed by cutting the data from the beginning to the needed length. This change is performed for each case on the same measured data and only the number of samples are changed in evaluating the effect of data length on the damage detection method.

In damage localization there is no additional measurement noise imposed on the data. Moreover, the length of the data is kept constant for different damage configurations.

7.2 Damage detection in the Yellow Frame

Herein, the results from the damage detection of the experimental model introduced in 7.1 are presented. The data measured from the structure is also used in investigating the effect of number of samples by cutting the data in different lengths. Subsequently, several noise vectors are created based on output of each sensor and they are added to the data to study the effect of the additional measurement noise as stated in 7.1.7.

7.2.1 Detecting the damage for different damage configurations

The damage configurations defined in Table 7-1, are tested using the SSDD method. The data length is constant and there is no additional measurement noise added to the data. In three tests, the structure is not damaged and therefore they are used in evaluating a safety threshold based on the 99th percentile of their distribution. The resultant χ^2-values in log-scale are illustrated in Figure 7.8 from testing all the damage configurations.

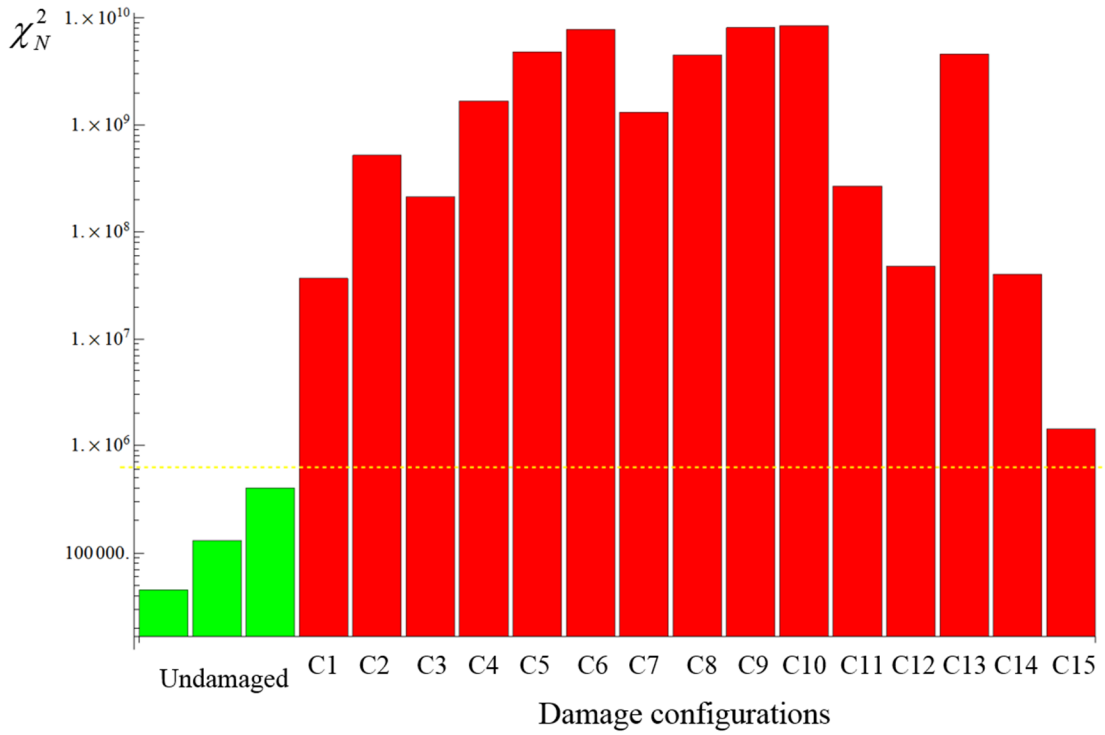

Figure 7.8 Damage detection of the damage configurations of the Yellow frame (the yellow line represents the 99% percentile threshold)

It can be seen in Figure 7.8 that all the damage configurations are detectible. It should be noted that the scale of the χ^2-value is not a representative of the amount of damage. The damage quantification using the SSDD technique is not considered in this dissertation. Since all the configurations are detectible, they are used in the damage localization as the next step of damage identification.

In the next subsection, the effect of number of samples and additional measurement noise is investigated.

7.2.2 Effect of number of samples

In order to investigate the effect of number of samples, the data from the undamaged structure and damage configuration C15 are cut to several lengths corresponding to 5 min, 7.5 min, 10 min, 12.5 min, 15 min and 18.33 min. Configuration C15 is depicted in Figure 7.9.

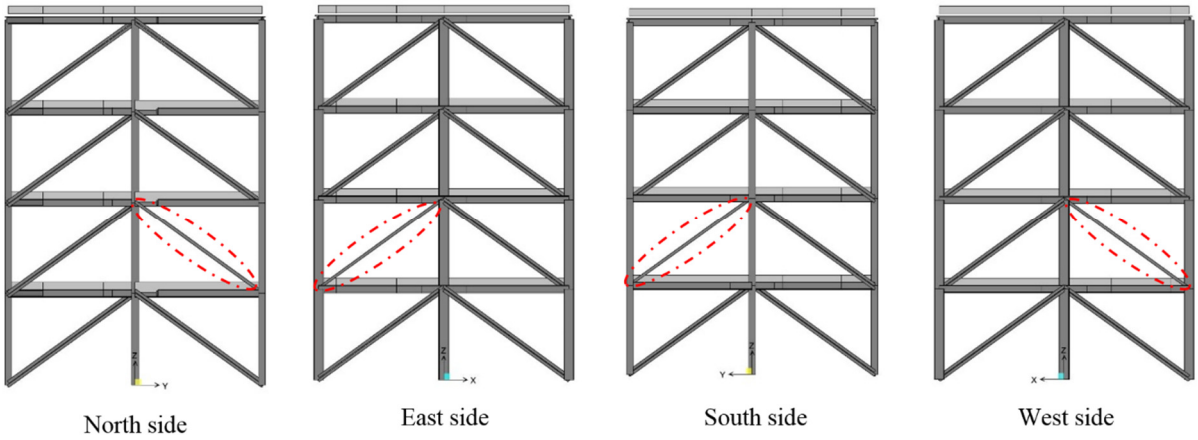

Figure 7.9 Damage configuration C15 used in studying the effect of noise and number of samples

The results for the undamaged and damaged states of the structure for no additional noise and 80% additional noise are shown in Figure 7.10. In order to calculate the expected χ^2-value, when noise is present, the analysis is performed for 30 times at each case and the average is computed. It should be noted that this expectation value is only affected by the measurement noise and not the input excitation, while in the proposed theories, the expectation is assumed on the input excitation as well as the output measurements. Therefore, the results should be assumed as an approximate of the final expectation value.

It can be seen from Figure 7.10 that there is a linear trend for the undamaged and damaged states of the structure. This linearity confirms Theorem 4.2 for the damaged state. However, for the undamaged state, because we are using real data, Υ^e is not exactly zero and equals to a small value, namely ε. This yields $\delta = \sqrt{N}\varepsilon$. Therefore, the non-centrality parameter of the resulting test variable χ^2_N is $N\varepsilon^T(\Sigma^e)^{-1}\varepsilon$, where ε is independent of N. Hence, by considering equation (4-1) we have $\mathbf{E}(\chi^2_N) = d + N(\varepsilon)^T(\Sigma^e)^{-1}\varepsilon$. Consequently, the mean of the test variable increases when the number of samples grows similar to Theorem 4.2. The growth rate is depending on the value of ε. Since ε is a small value for an undamaged structure, $\mathbf{E}(\chi^2_N)$ increases with a lower

rate compared to the damage state, as demonstrated in Figure 7.10. The value of $\mathbf{E}(\chi_N^2)$ is normalized as $\left\|\mathbf{E}(\chi_N^2)\right\| = \dfrac{\mathbf{E}(\chi_N^2)}{\mathbf{E}_0(\chi_{18.33}^2)}$ where $\mathbf{E}_0(\chi_{18.33}^2)$ represents the expected χ_N^2 value for the 18.33 min long data from undamaged structure with no additional noise.

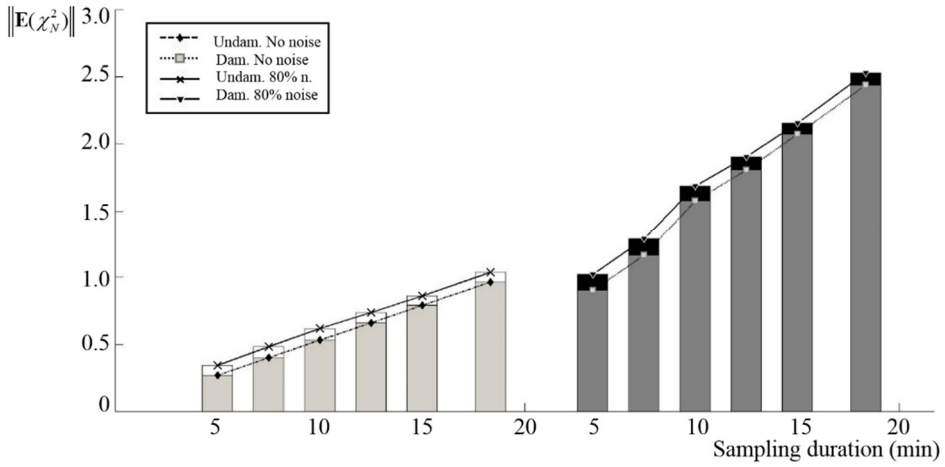

Figure 7.10 Expected χ^2-value evaluated for different number of samples in damaged and undamaged conditions of the Yellow frame

7.2.3 Effect of measurement noise

Same as previous study on number of samples, the undamaged structure and damaged structure (of configuration C15) are employed in here for investigating the effect of additional measurement noise on the data. Again in each case, to calculate the expected χ^2-value the analysis is performed for 30 times and the average is computed. As mentioned in previous section, the results should be assumed as an approximate of the real expectation value as the input is not changing. In the following two sections, this effect is studied for the equal and unequal additional measurement noise properties in the reference and test data.

7.2.3.1 Equal properties between reference and test data

In order to investigate the effect of the measurement noise on the expected χ^2-value, noise vectors with equal ratios are added to the reference and test data as an additional measurement noise. The noise ratio varies among 0%, 5%, 10%, 20%, 35%, 50%, 65% and 80%. The length of the data is

kept constant and equal to 18.3 min. The resultant expected χ^2_N is illustrated versus N_r in Figure 7.11.

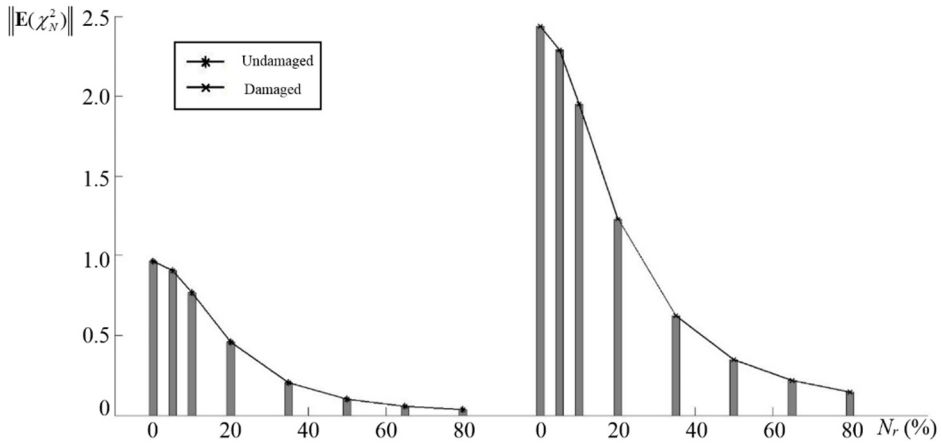

Figure 7.11 Expected χ^2-value evaluated for different noise ratios with equal properties in reference and test data for damaged and undamaged conditions of the Yellow frame

It is observed in Figure 7.11 that the expected χ^2_N value decreases by the increase of N_r for both damaged and undamaged states. Herein, same as previous case study on number of samples, since we are using real data, Υ^e is not exactly zero. Therefore the second part of equation (4-1) is not zero and will be decreased by the growth of the noise in the data based on Theorem 4.4.

7.2.3.2 Unequal properties between reference and test data

In this case study, the applied noise to the measurements of the reference and test states are different and unequal. In order to investigate the measurement noise effect on the reference and test states independently, in two studies, the noise will be applied only to one of the two states.

In the first study, the additional noise is applied with different ratios to the data from undamaged and damaged structure in the test state. There is no additional noise applied to the reference state data. The test is performed for two lengths of data: 5 min and 18.3 min. The results are illustrated in Figure 7.12. It is observed that for both damaged and undamaged structures, the expected χ^2-value increases as stated in Theorem 4.5.

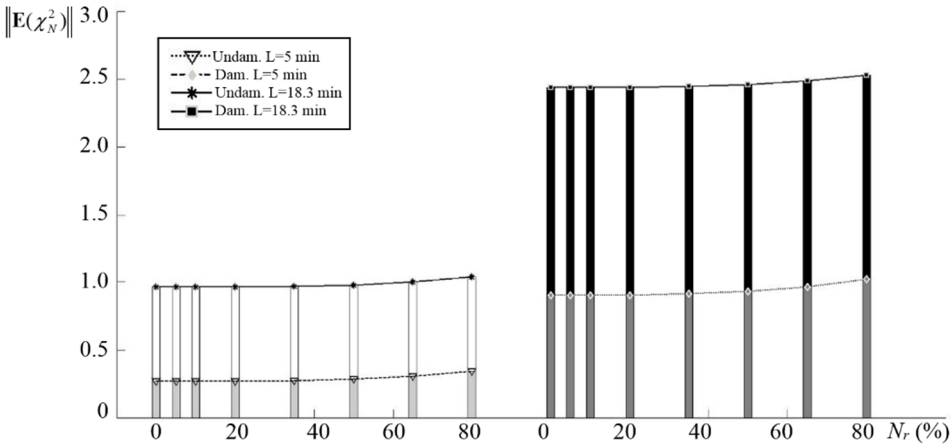

Figure 7.12 Expected χ^2-value evaluated for different noise ratios only in test data for damaged and undamaged conditions of the Yellow frame

For the second study, the noise is only applied to the reference state data. The length of the data is kept constant and equals to 18.3 min. The results of the expected χ^2-value for the undamaged and damaged structures are illustrated in Figure 7.13. It can be seen that the expected χ^2-value decreases by the increase of noise, confirming Theorem 4.6.

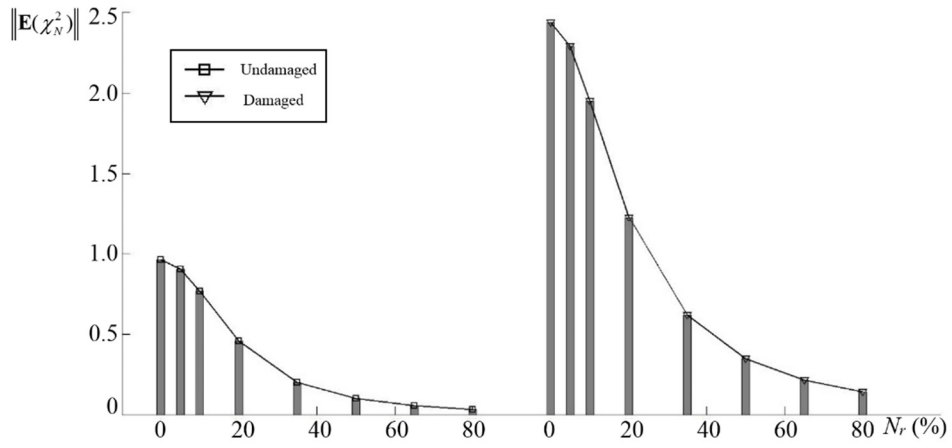

Figure 7.13 Expected χ^2-value evaluated for different noise ratios only in reference data for damaged and undamaged conditions of the Yellow frame

7.3 Damage localization in the Yellow Frame

In this section the damage localization is investigated on the real measured data acquired from the Yellow frame structure. Different damage configurations were introduced in 7.1.5.1 and they were detected in 7.2.1. As the next step of damage identification the damage is localized in the brace elements using the SSDL technique for different configurations. In this chapter, the damage will

be localized using the sensitivity based and MinMax tests. The proposed clustering approach, i.e. HFC, and the *k*-means will be used and the results will be compared. Furthermore, The Jacobians constructed from different formations introduced in Chapter 5 will be compared. Finally, the detectability of each element will be investigated.

As investigated in the damage detection of this structure, to avoid the effect of number of samples, the data length in the damage localization is not changed and it is constant among all the tests. Moreover, there is no additional measurement noise applied to the data and it contains only the original measurement noise from the test.

In the following section the two formations of Jacobians, described in Chapter 5 are constructed and compared.

7.3.1 Jacobian formation

Composing the Jacobian matrix from *Formation 1* in 5.2.2, can be achieved by using only the analytical modeshapes and natural frequencies computed from the analytical model, i.e. FE model, of the structure shown in Figure 7.7. These modeshapes are used in forming all parts of the Jacobian in (5-2). In this formation all the parts of the Jacobian are consistent, and therefore, all the evaluated modeshapes and natural frequencies will be used. However, when using *Formation 2* in 5.2.2, the modeshapes and natural frequencies from both the FE model and measured data are needed. Therefore, they need to be consistent in terms of I) number, location and order of sensors, II) number and order of natural frequencies, and III) number and order of modeshapes. For this purpose, the modeshapes acquired from the FE model and the measured data are matched in Figure 7.14.

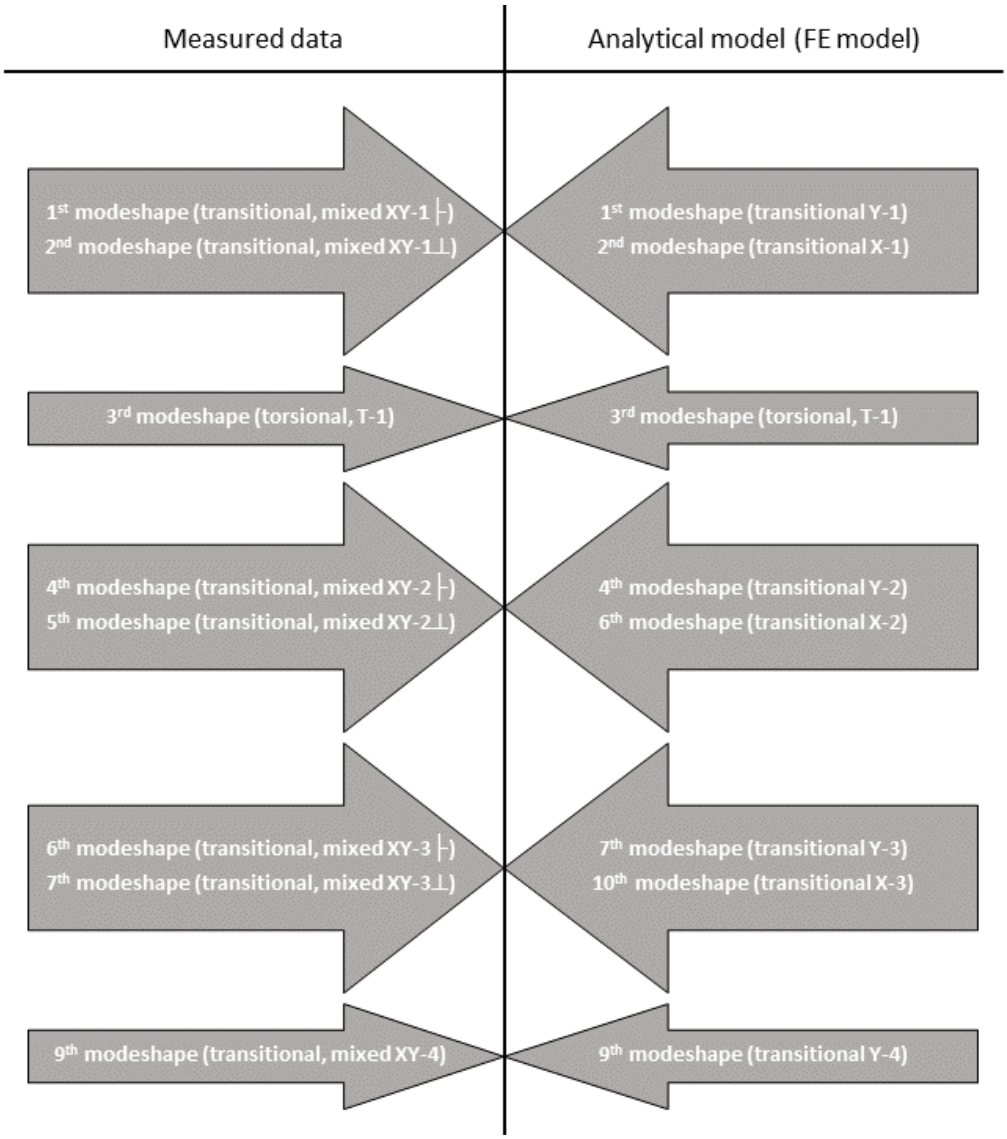

Figure 7.14 Matching the modeshapes and natural frequencies evaluated from the measured data and analytical FE model

It can be seen that the coupled modeshapes need to be scaled and decoupled using the scaling approach proposed in Chapter 5. As described before, they will be matched by the modeshapes in the analytical model. Moreover, the order of the modeshapes from the analytical model is changed in order to match the order of the modeshapes from the measured data. This will make the sensitivity analysis from the analytical modeshapes consistent with the real data. The first three modeshapes before and after the scaling are illustrated and compared in Figure 7.15. It should be noted that the values are corresponding to the sensor number in their direction.

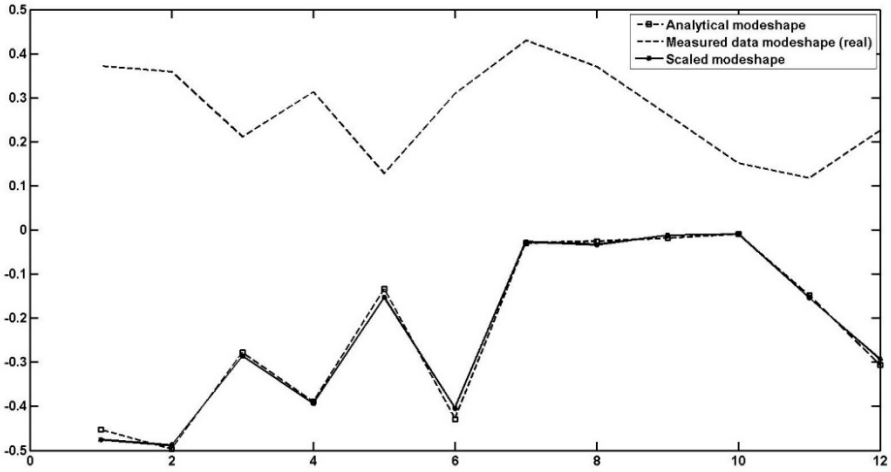

1st modeshape

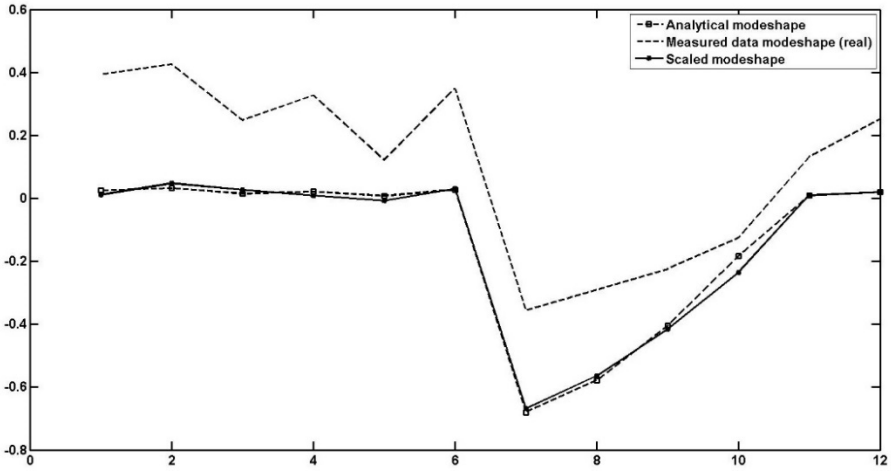

2nd modeshape

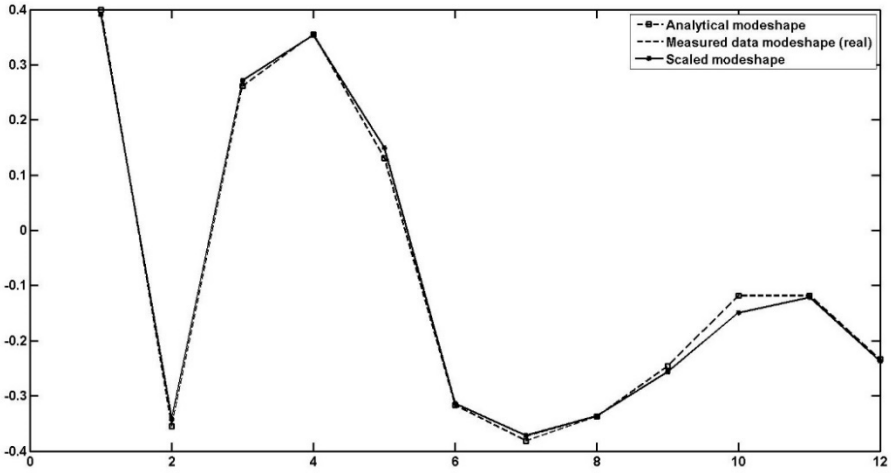

3rd modeshape

Figure 7.15 Scaling the modeshapes evaluated from the measured data to the ones from analytical FE model (the horizontal axe is sensor number)

The first and second modeshapes are coupled and therefore they are more different than the analytical modeshape. The third modeshape is not coupled and it is matching very closely to the real data, before and after scaling.

It should be noted that from this matching only 8 modeshapes can be matched and used while for *Formation 1* all the 10 modeshapes can be used. Furthermore, because in *Formation 1* all the parts of the Jacobian are made from the analytical modeshapes consistently, the order of these modeshapes needs not to be identical to the real measured data.

7.3.2 Clustering

The elements of the Yellow frame need to be clustered before damage localization. Based on the formation of the Jacobians, the clustering is different. It should be noted that the braces located in the same story level and in the same side of the structure are *close* as can be seen in Figure 7.1. Therefore, ideally the clustering methods should consider them in the same group. Since there are 16 pairs of these close braces present in the structure, the number of the resultant clusters should be less than 16. This can be used in checking the output of the clustering approaches.

7.3.2.1 Hierarchical Fisher-information-matrix-based clustering

The clustering for the structure by HFC method with using threshold of $\varepsilon_f = 0.15$ for both Jacobian formations are shown in Figure 7.16.

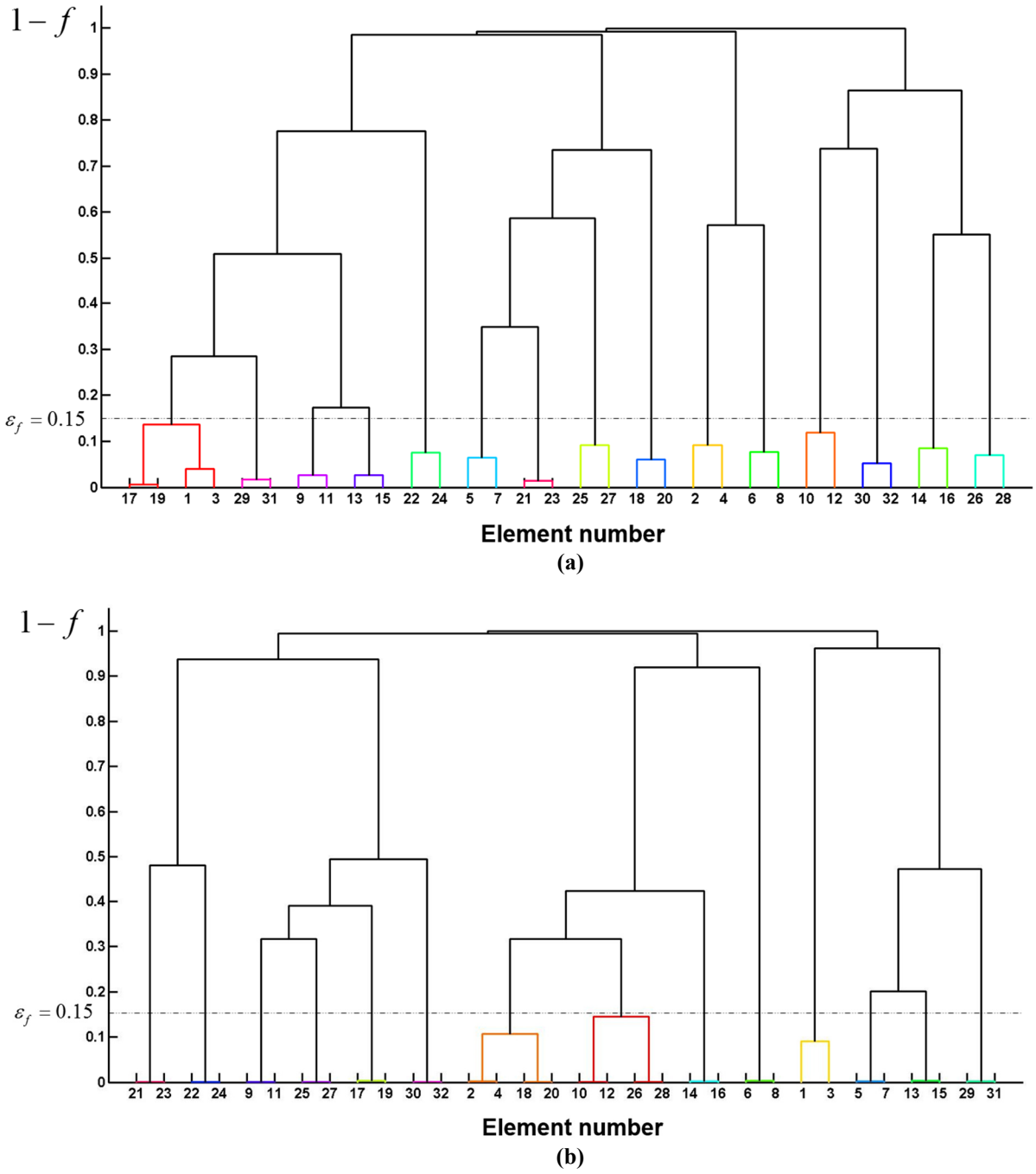

Figure 7.16 Dendrograms depicting the Hierarchical Fisher-information-matrix-based clustering (HFC) of the Yellow frame from Jacobians with (a) *Formation 1* and (b) *Formation 2*

It is observed in Figure 7.16, both formation of the Jacobians resulted in clustering schemes with 15 and 14 clusters which are less than 16 clusters. Furthermore, all the braces expected to be

close, are in the same group. Using this clustering scheme, the NFIM is evaluated and shown in Figure 7.17 for both formations of Jacobian.

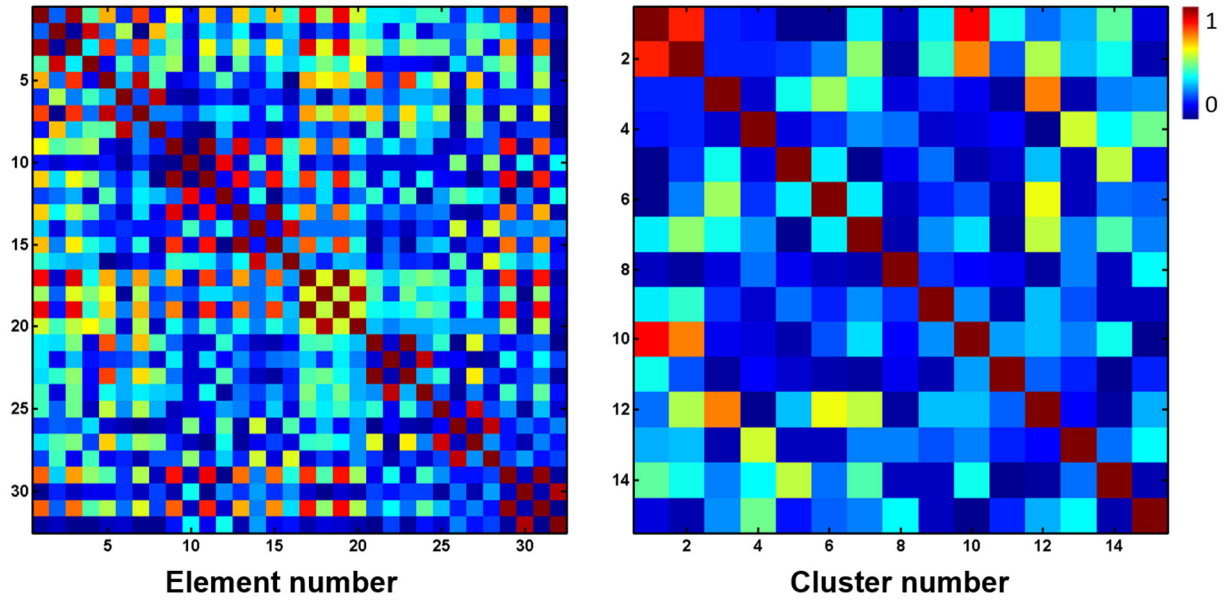

NFIM of Yellow frame for *Formation 1*

NFIM of centroids of clusters for *Formation 1*

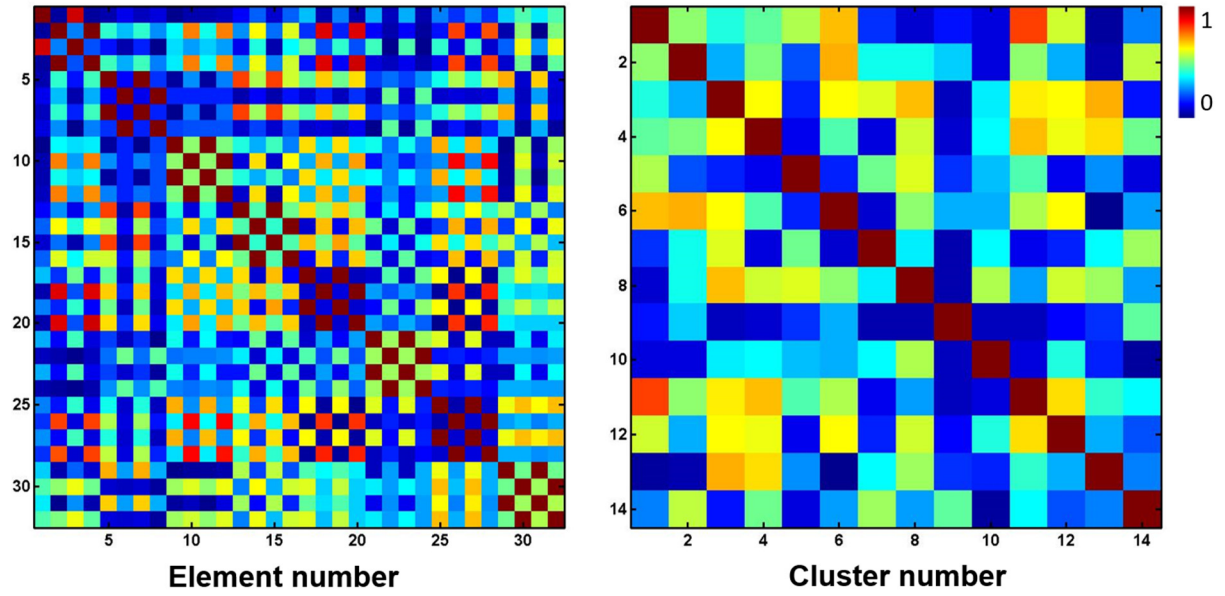

NFIM of Yellow frame for *Formation 2*

NFIM of centroids of clusters for *Formation 2*

Figure 7.17 Normalized Fisher information matrix (NFIM) for the HFC clustered and unclustered Jacobians *(Formation 1* and *Formation 2*) from the Yellow frame structure

In the next section the clustering is performed with *k*-means approach.

7.3.2.2 *k*-means clustering

In order to show the performance of *k*-means in clustering the elements, the *k*-means approach is used in clustering the Jacobians obtained from *Formation 1*. As mentioned before, the results are not unique and therefore in here, two clustering schemes are presented in Figure 7.18. The number of clusters is chosen as 15 to be comparable to the results from HFC approach. Again it should be noted that the objective function of *k*-means is chosen as cosine between input vectors, i.e. columns of Jacobian. The results was also observed to be the same when choosing the correlation between vectors as the objective function.

It can be seen in Figure 7.18, that some of the *close* braces are not in the same cluster. Therefore, in the NFIMs corresponding to these clustering schemes, several red color spots are existing which are related to these close elements. Based on these clustering schemes, it is expected that if the damage happens in close elements that are not in the same cluster, e.g. elements 18 and 20 in clustering scheme 1 or elements 2 and 4 in clustering scheme 2, the damage would not be identified.

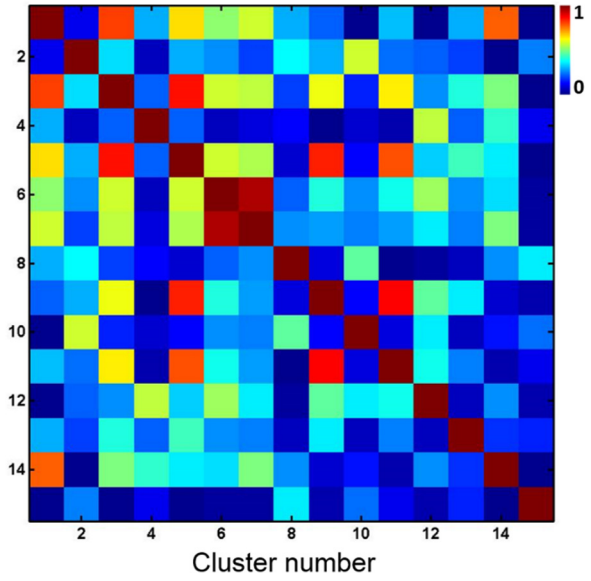

NFIM with clustering scheme 1

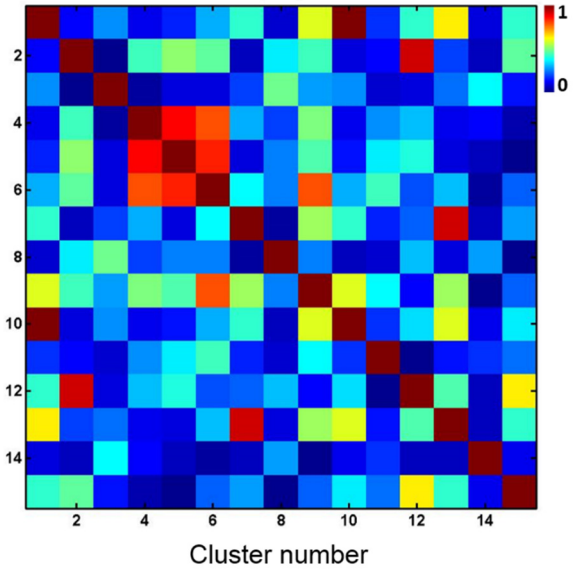

NFIM with clustering scheme 2

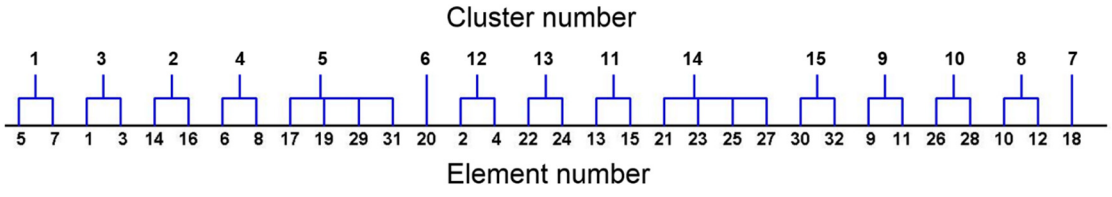

Clustering scheme 1

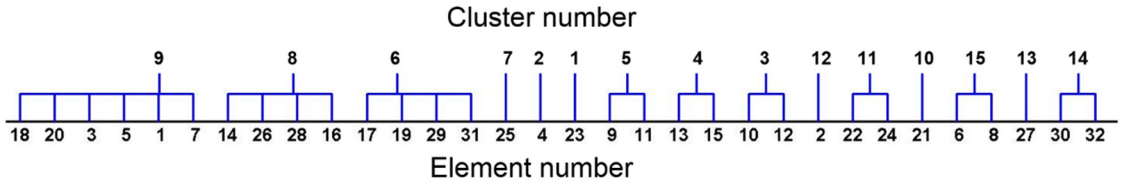

Clustering scheme 2

Figure 7.18 Two clustering schemes acquired for the Yellow frame with *k*-means approach

7.3.3 MinMax and sensitivity based damage localization

In this section, the measured data from the structure is used with the clustering schemes presented in previous section to localize the damage for different damage configurations defined in 7.1.5.1. All the damage configurations will be localized using the HFC based clustering and with Jacobians composed from *Formation 1*, i.e. Figure 7.16.a. The results are presented in Figure 7.19.

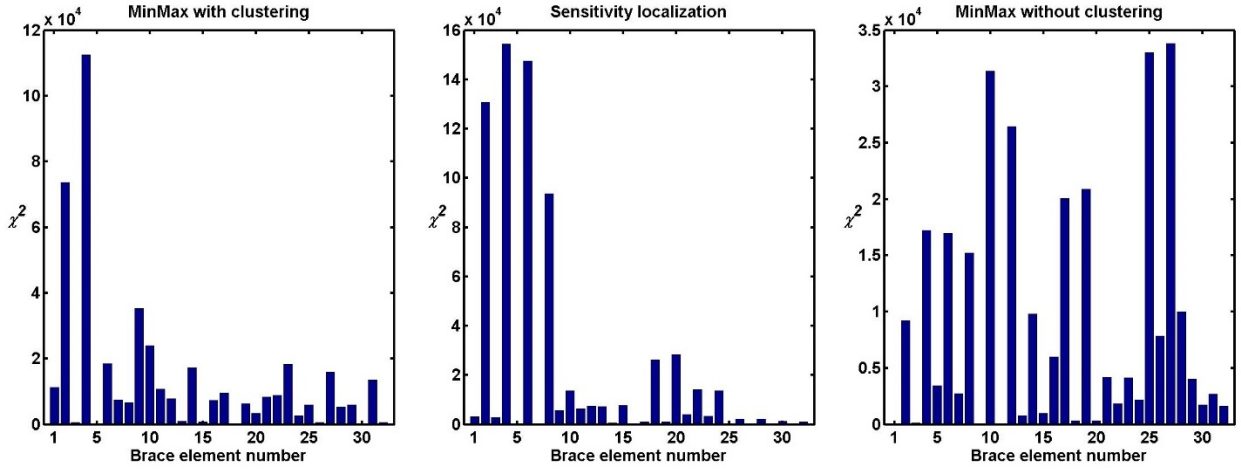

Configuration 1 (2 (I))

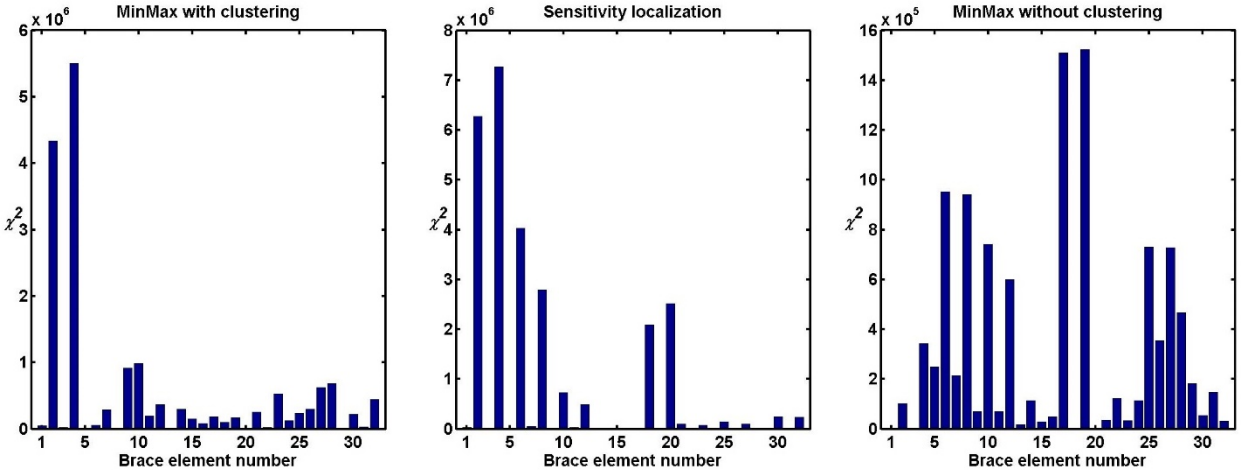

Configuration 2 (2 (II))

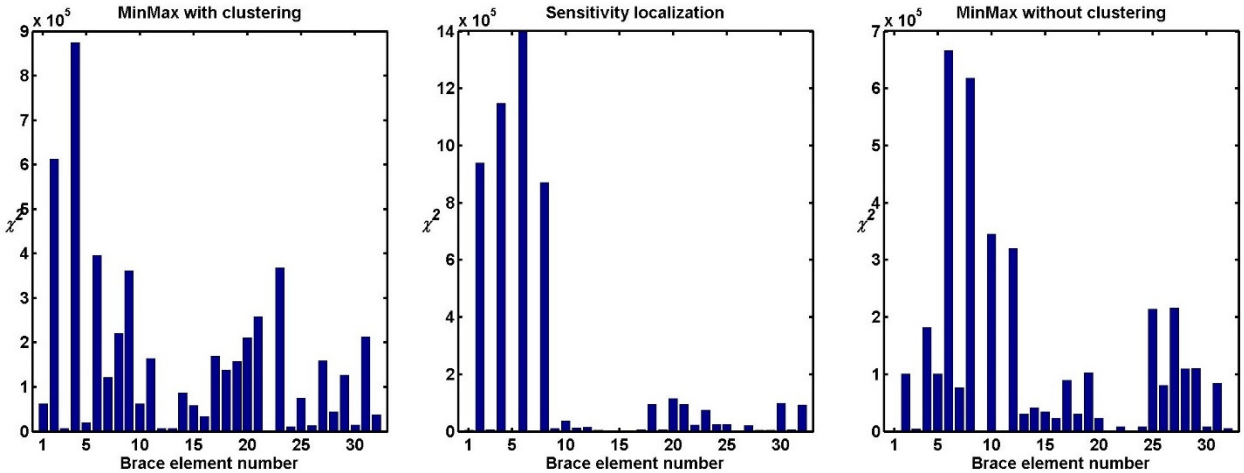

Configuration 3 (2 (I), 4 (I))

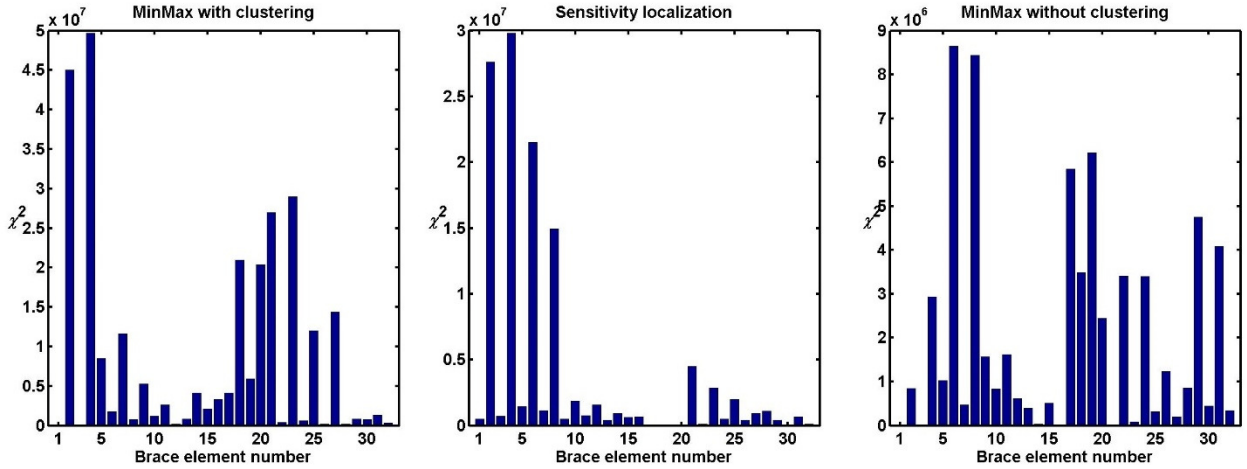

Configuration 4 (2 (II), 4 (II))

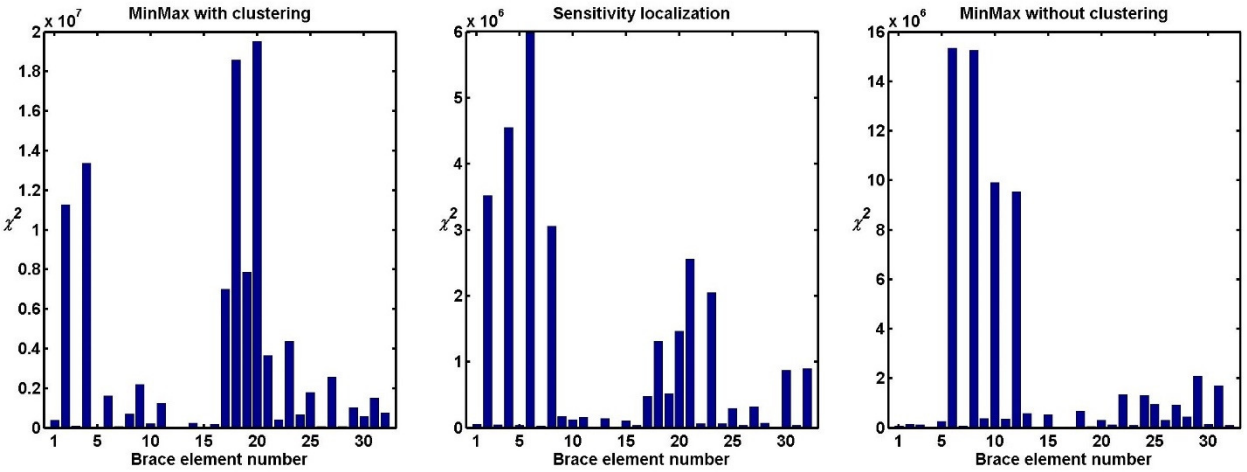

Configuration 5 (2 (II), 4 (II), 18 (I), 20 (I))

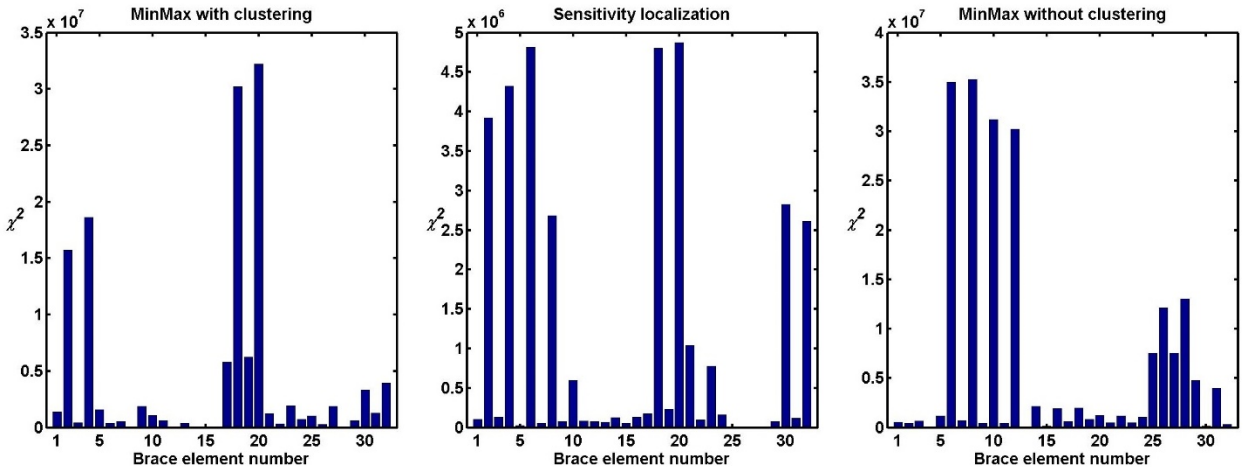

Configuration 6 (2 (II), 4 (II), 18 (II), 20 (II))

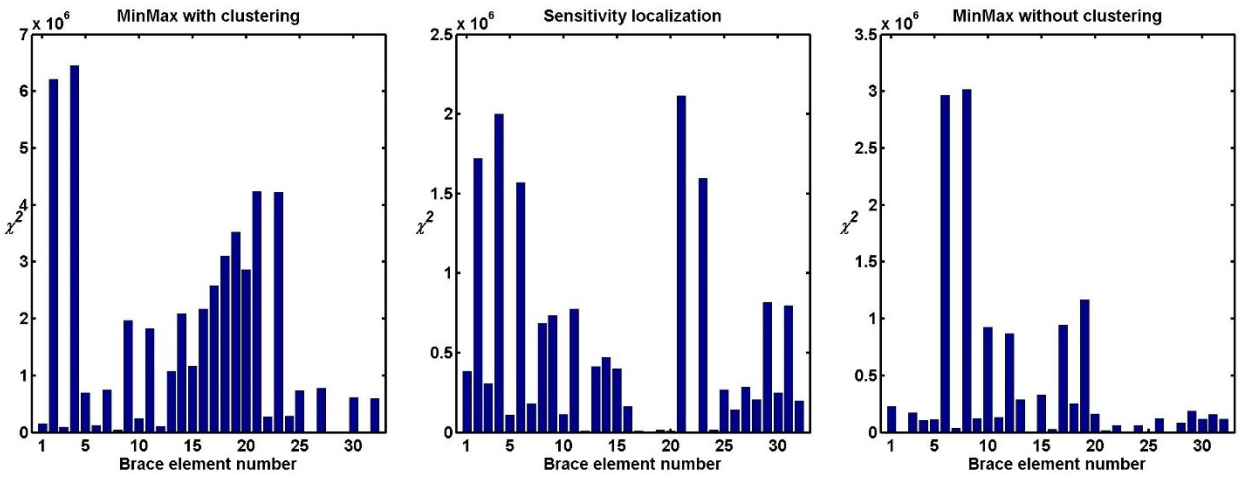

Configuration 7 (2 (II), 4 (II), 17 (II), 19 (II))

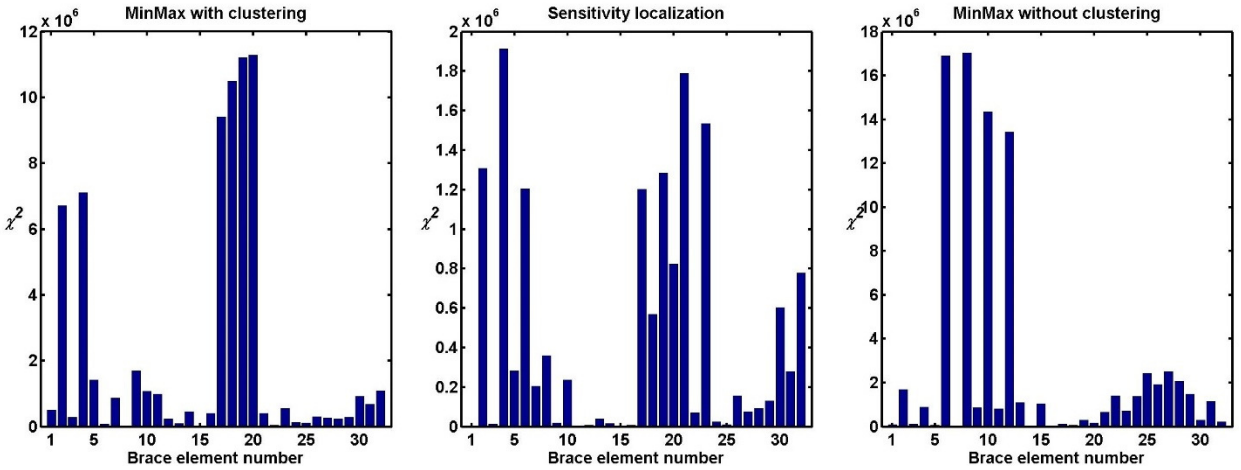

Configuration 8 (1 (I), 2 (I), 3 (I), 4 (I), 17 (I), 18 (I), 19 (I), 20 (I))

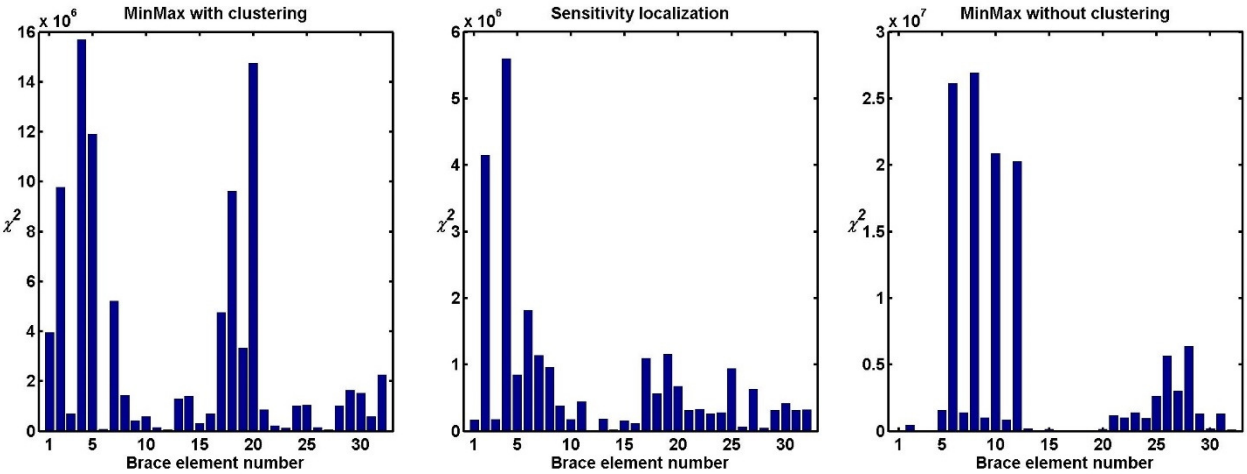

Configuration 9 (1 (II), 2 (II), 3 (II), 4 (II), 17 (II), 18 (II), 19 (II), 20 (II))

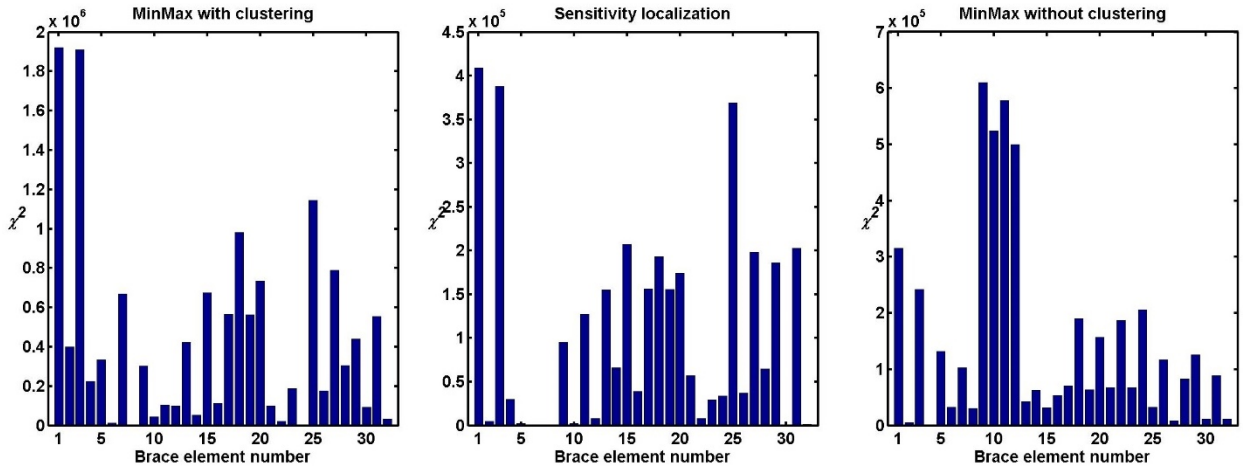

Configuration 10 (25 (I), 27 (I))

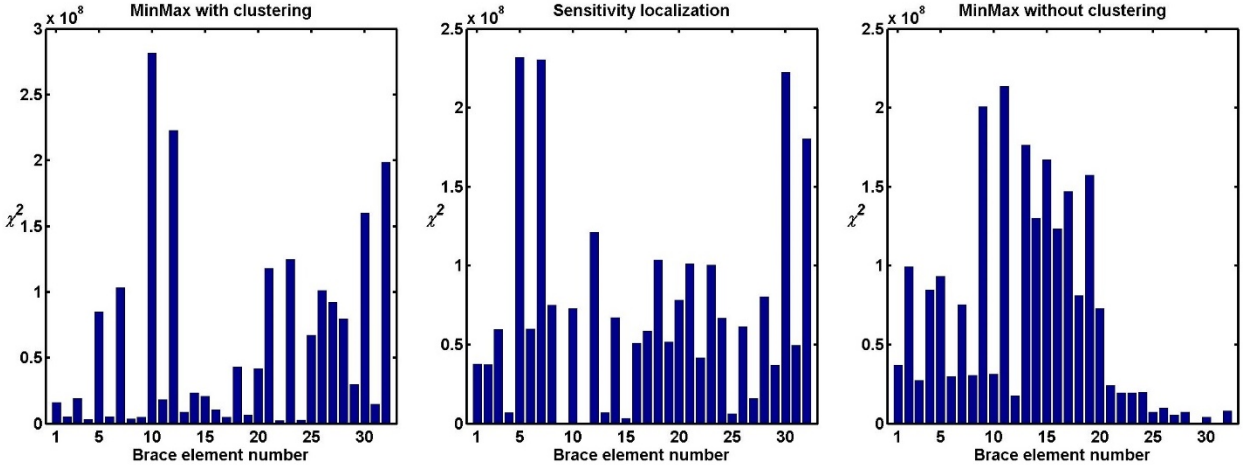

Configuration 11 (10 (II), 12 (II))

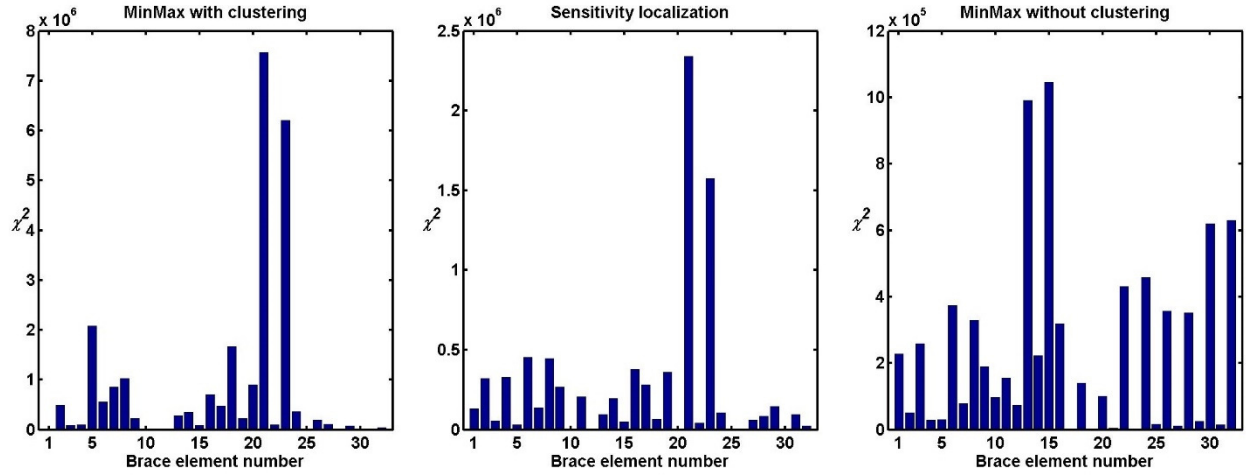

Configuration 12 (21 (II), 23 (II))

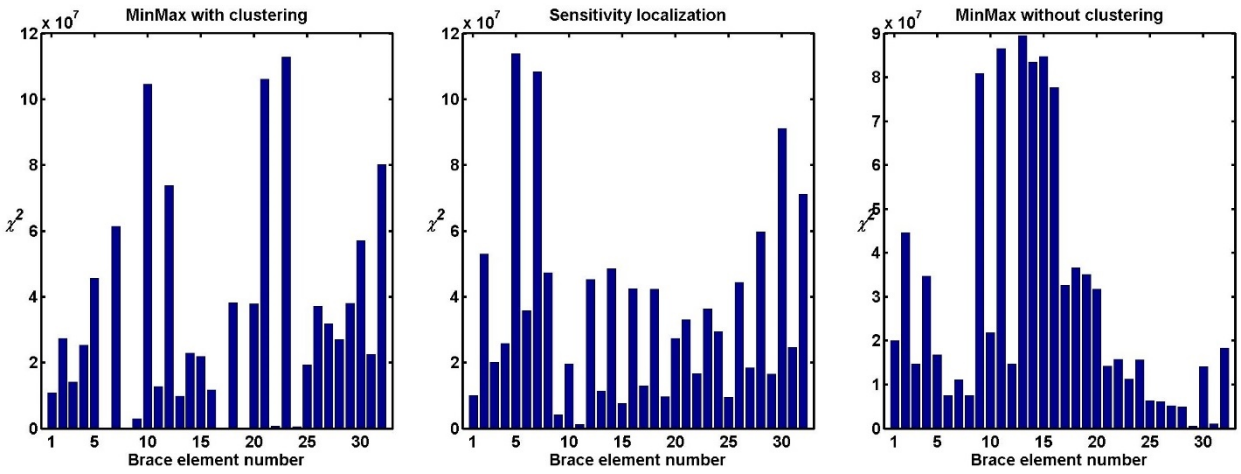

Configuration 13 (10 (II), 12 (II), 21 (II), 23 (II))

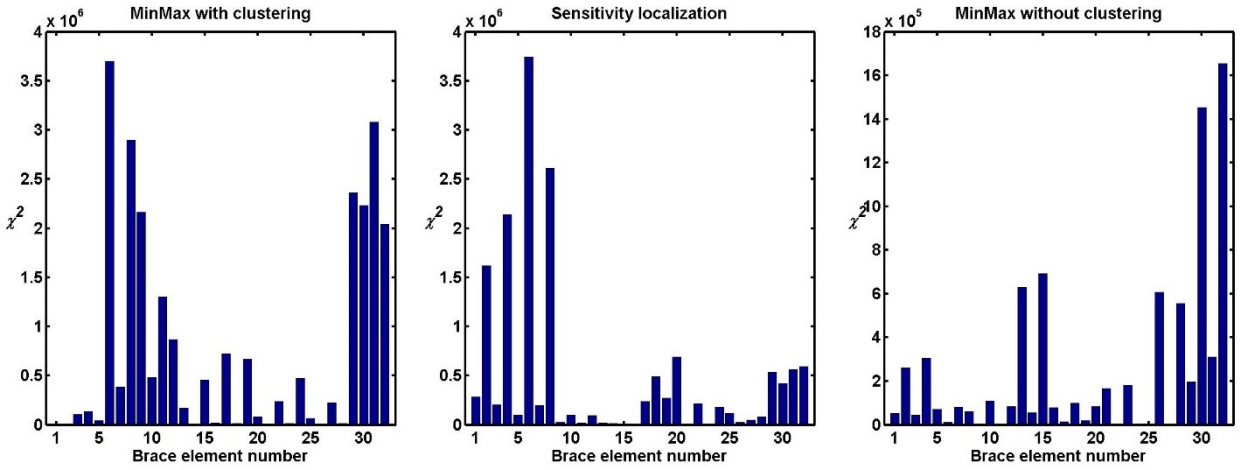

Configuration 14 (6 (I), 8 (I), 29 (I), 31 (I))

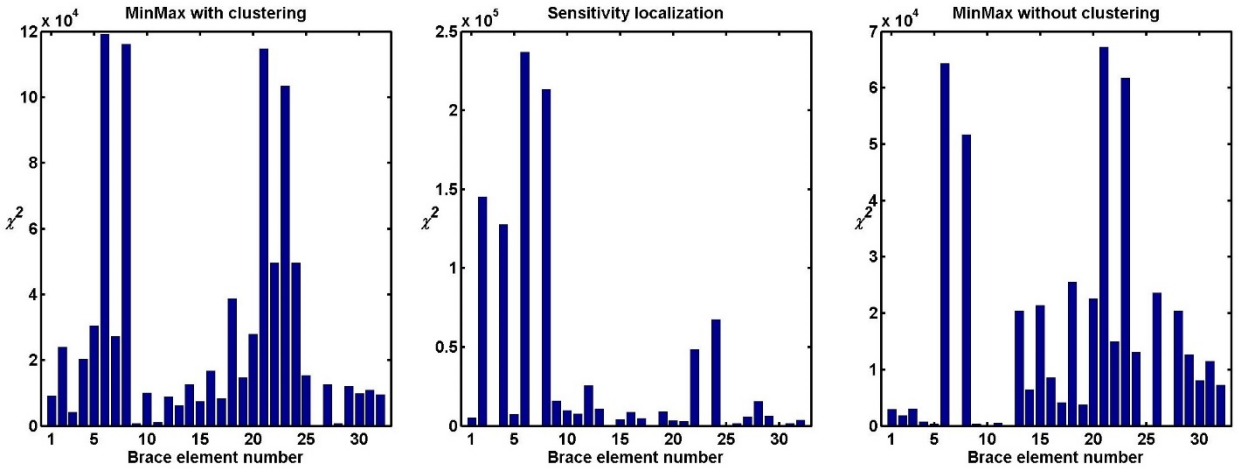

Configuration 15 (7 (I), 8 (I), 21 (I), 22 (I))

Figure 7.19 Damage localization of the Yellow frame with HFC clustered Jacobians (from *Formation 1*)

It is seen that almost in all of the damage configurations, the damaged brace/s can be identified with acceptable accuracy. It is observed that identifying the damage for multiple damage cases is possible, although the accuracy and clarity of the result will be compromised. The damage is localized more distinctly for the damage configurations of single or double damaged braces. It should be noted that the *close* braces, i.e. every couple of braces in each level at each side, cannot be distinguished in terms of being or not being damaged from each other. In other words, if one of the braces is damaged, the other *close* brace also reacts in the test as to be damaged.

The MinMax method with the HFC clustering, can clarify the damage in most of the cases compared to the sensitivity based damage localization. Furthermore, the MinMax method without clustering is always incapable of localizing the damage as predicted.

7.3.3.1 Assessing the functionality of Jacobian matrix computed from *Formation 2*

In here, some of the damage configurations, i.e. C1, C6 and C12, will be localized using the HFC based clustering Figure 7.16.b and *Formation 2* of the Jacobian. The results are illustrated in Figure 7.20.

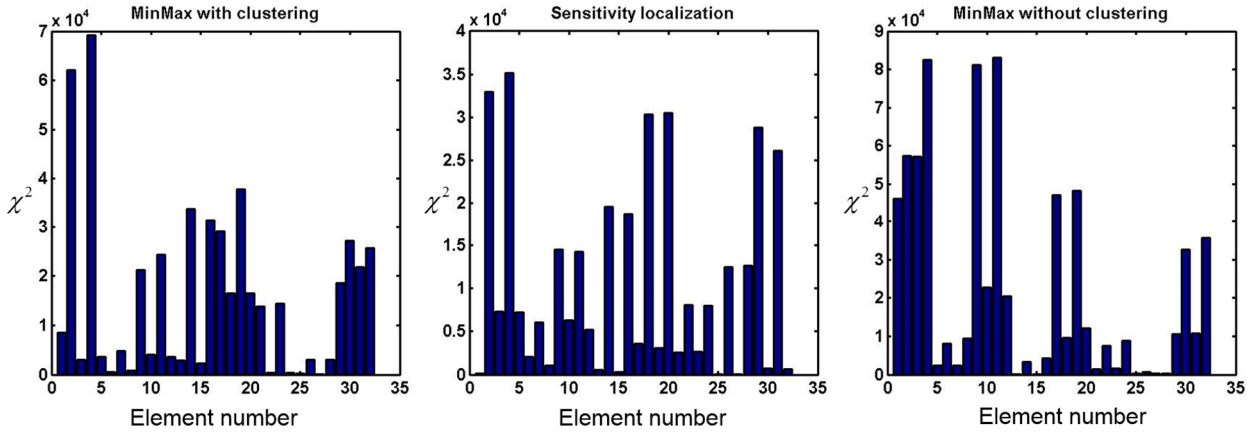

Configuration 1 (2 (I))

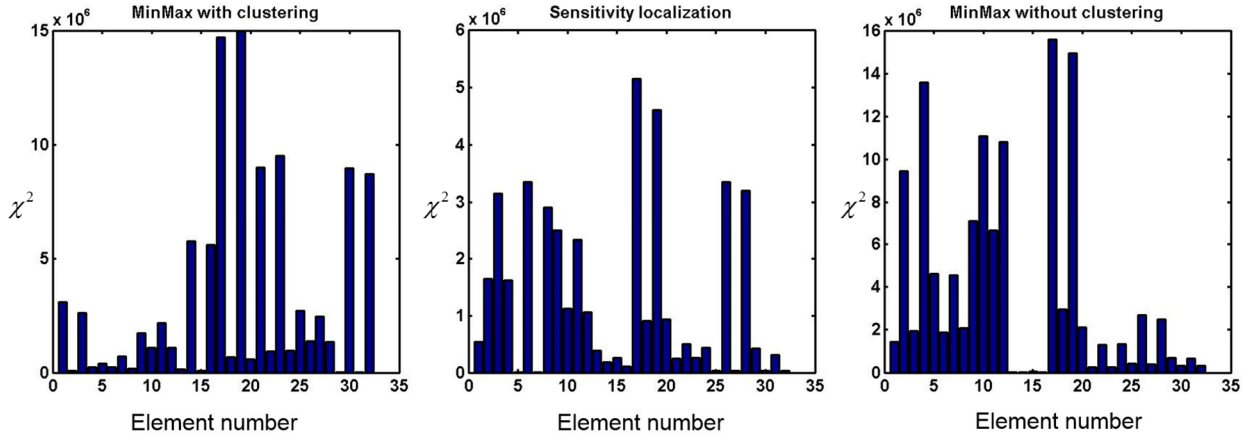

Configuration 6 (2 (II), 4 (II), 18 (II), 20 (II))

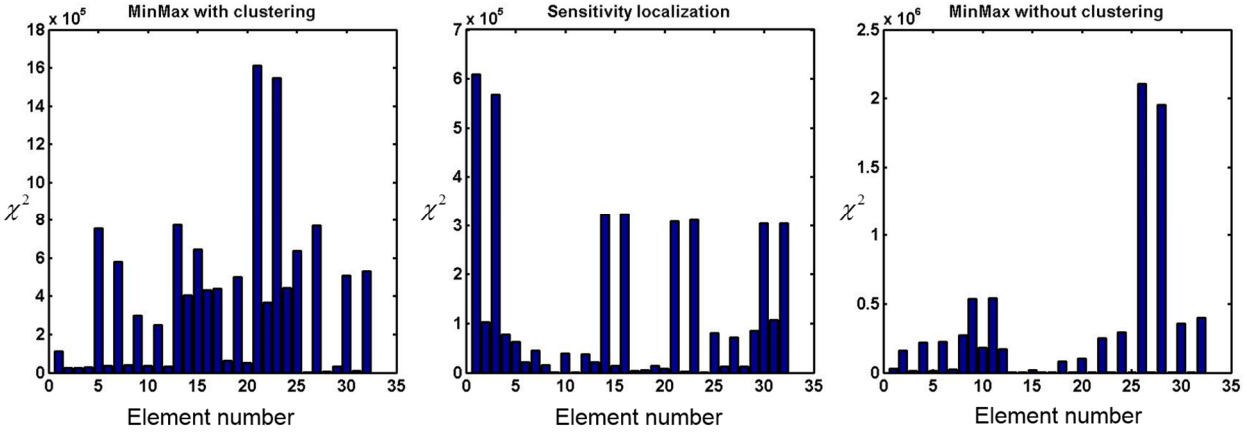

Configuration 12 (21 (II), 23 (II))

Figure 7.20 Damage localization of the Yellow frame with HFC clustered Jacobians from *Formation 2*

It can be seen from Figure 7.20, that the damage is localized in two configurations. Nonetheless, the results are not as clear as when the Jacobians are computed from *Formation 1*.

Moreover, even in some cases, e.g. configuration 6, the damage cannot be localized from the MinMax or sensitivity based approaches. The reason of this problem is that the number of modeshapes and natural frequencies being matched and used is only 8, while for *Formation 1* this number is 10. This stems from the difficulties in finding the local modeshapes and modeshapes blind to the sensor locations (in here, flexible diaphragm) from the real data, compared to the FE model. The other reason is in the slight difference and inconsistency between the modeshapes from the real measured data and the analytical model. For the latter reason, this difference showed to be very minor in this problem after the scaling is performed.

7.3.3.2 Assessing the functionality of *k*-means clustering

In order to assess the clustering schemes in Figure 7.18, computed by *k*-means approach, in here, two damage configurations, i.e. C5 and C12, are chosen to demonstrate the effect of *close* elements that are not clustered properly on the MinMax method. In damage configuration 5, elements 2 and 4 (which are close elements) and 18 and 20 (which are also close elements), are damaged. Elements 2 and 4 are not in the same cluster in clustering scheme 2 in Figure 7.18 while elements 18 and 20 are not in the same cluster in clustering scheme 1. Therefore, as can be seen in Figure 7.21, the damage in *close* elements not clustered properly is not detected. In other words, the damage in elements 2 and 4 is not detected when using clustering scheme 2 and the damage in elements 18 and 20 is not identified when clustering scheme 1 is used.

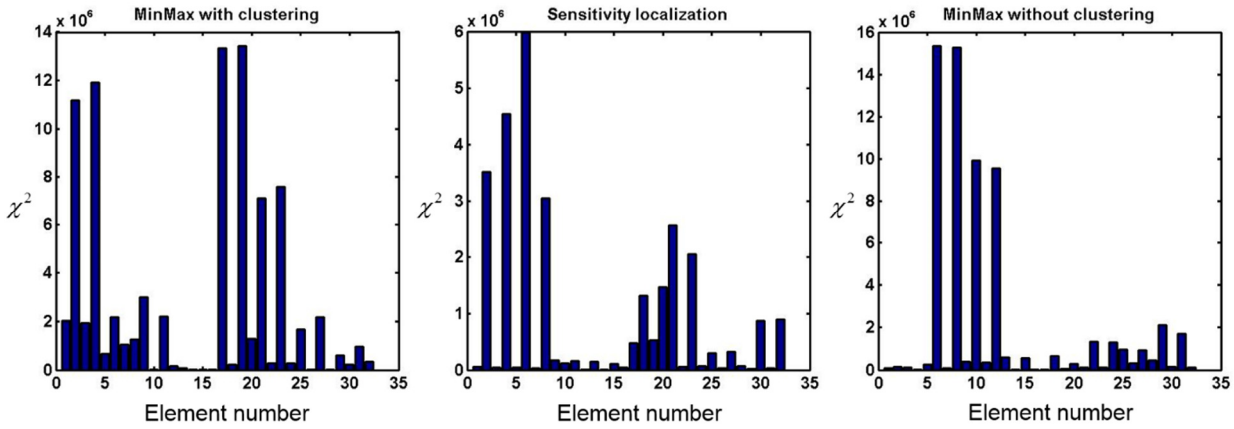

Configuration 5 (2 (II), 4 (II), 18 (I), 20 (I)) with *k*-means clustering scheme 1 (Figure 7.18)

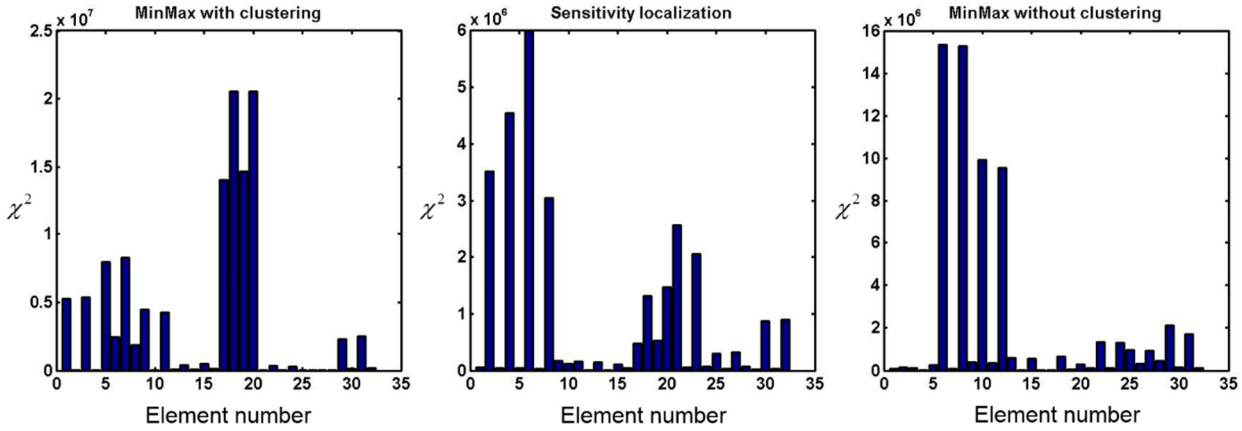

Configuration 5 (2 (II), 4 (II), 18 (I), 20 (I)) with *k*-means clustering scheme 2 (Figure 7.18)

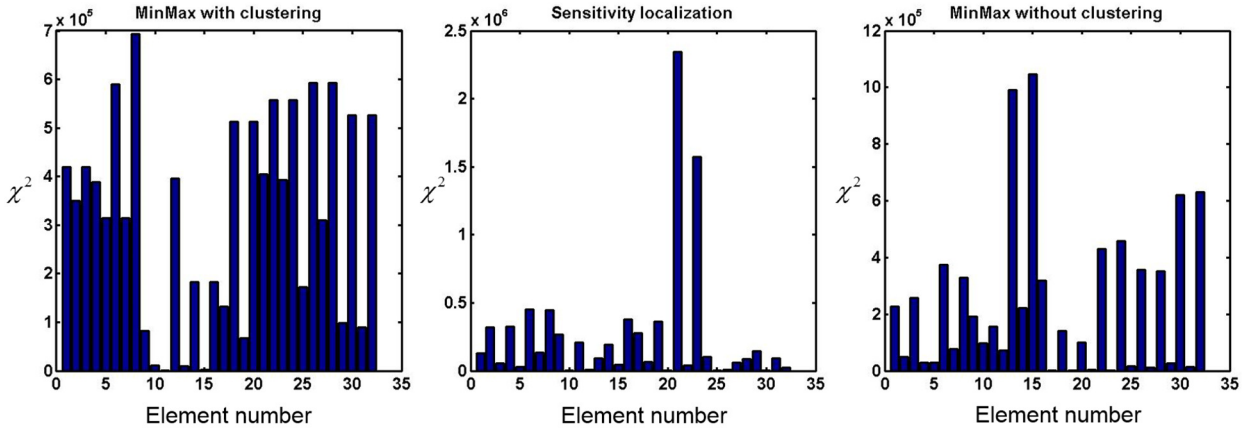

Configuration 12 (21 (II), 23 (II)) with *k*-means clustering scheme 2 (Figure 7.18)

Figure 7.21 Damage localization of the Yellow frame with *k*-means clustered Jacobians from *Formation 1*

As another example, because elements 21 and 23 are not in the same cluster in clustering scheme 2, for damage configuration 12 the damaged elements, i.e. elements 21 and 23, cannot be

identified using MinMax approach, as shown in Figure 7.21. Therefore, the clustering schemes acquired from the *k*-means approach are not appropriate in damage localization of these configurations. Subsequently, since there is no prior knowledge of the location of damage and closeness of elements in practice to check the *k*-means output and considering the unstable inherent of the *k*-means approach, it is not an appropriate clustering method to be used in SSDL method.

7.3.4 Detectability of damage in each element

The diagonals of un-normalized Fisher information matrix and F^* values computed by Jacobians acquired from *Formation 1* are shown in Figure 7.22. It can be seen that almost all the elements are equally detectible in Figure 7.22.a while from F^* values the elements located in the east frame, where no sensor is located, are in general less detectible than other elements.

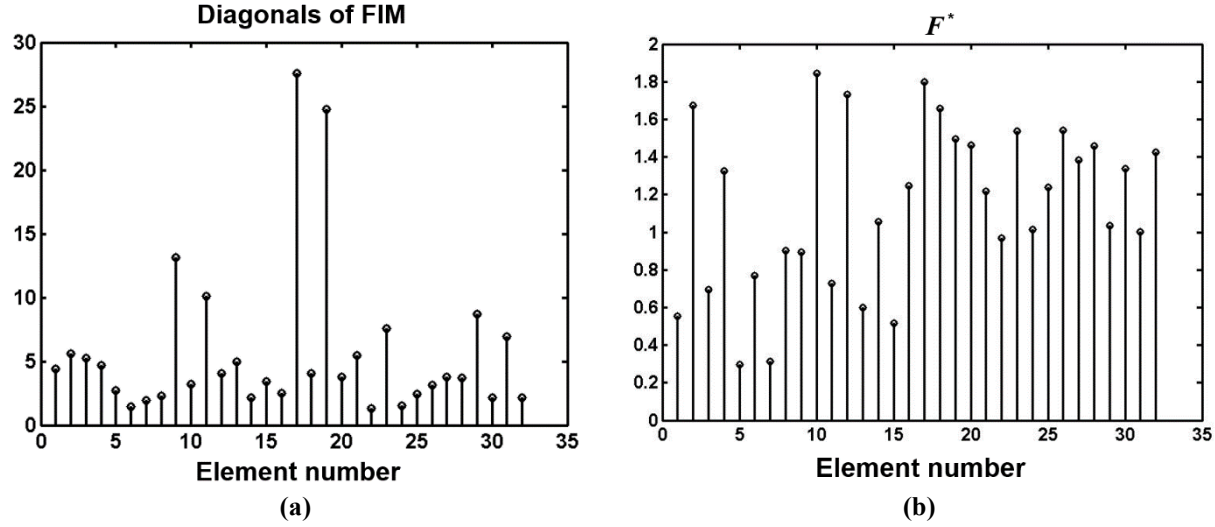

Figure 7.22 Detectability of damage in the Yellow frame from (a) the diagonals of Fisher information matrix and (b) F^*; Jacobians are computed from *Formation 1*

In order to demonstrate the relation of the diagonals of FIM and values of F^* to the detectability of each element, the 3 sensors located in the first level are removed. Since elements 17 and 19 are located in the first level and they have a very high value in Figure 7.22.a, it is expected that their corresponding value would be decreased when removing the sensors in the first

level. The Jacobians are computed from the remaining sensors using *Formation 1* and the resultant diagonals of FIM and F^* values are illustrated in Figure 7.23. It can be seen that the values corresponding to the elements 17 and 19 are decreased from both diagrams. Moreover, in the diagram from F^* values, the elements located in the first level are generally decreased to a higher percentage than the elements located in other levels. While this change is distinctly visible in F^* values of elements located in the first level compared to other elements, the diagonals of FIM are not showing this behaviour.

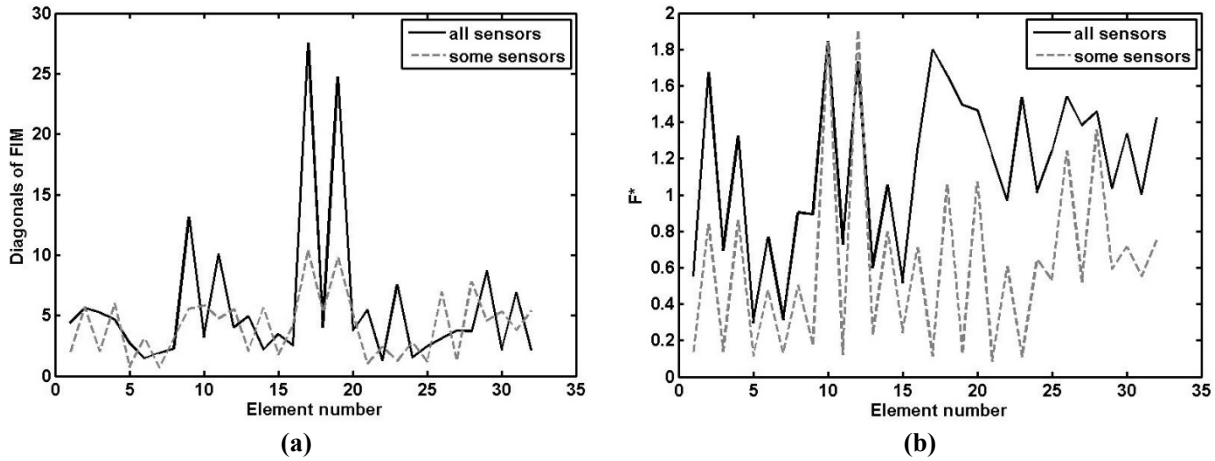

Figure 7.23 Detectability of damage in the Yellow frame from (a) the diagonals of Fisher information matrix and (b) F^*, from Jacobians computed from *Formation 1* with removal of sensors in the first level

To check the effect of the sensor removal on the detectability of damage in each element, 3 damage configurations, i.e. C2, C11 and C13, are tested. The first configuration is related to the damages in the elements in first story level and the other two are related to the damage in elements in higher story levels. The damage localization results are illustrated in Figure 7.24. It can be seen that the damage (from configuration C2) is still detectible in element 2, whose corresponding value in Figure 7.23 is still high after removal of the sensors. Moreover, in configurations C11 and C13, damage in elements 10 and 12 is detectible (more from MinMax method) while the damage in

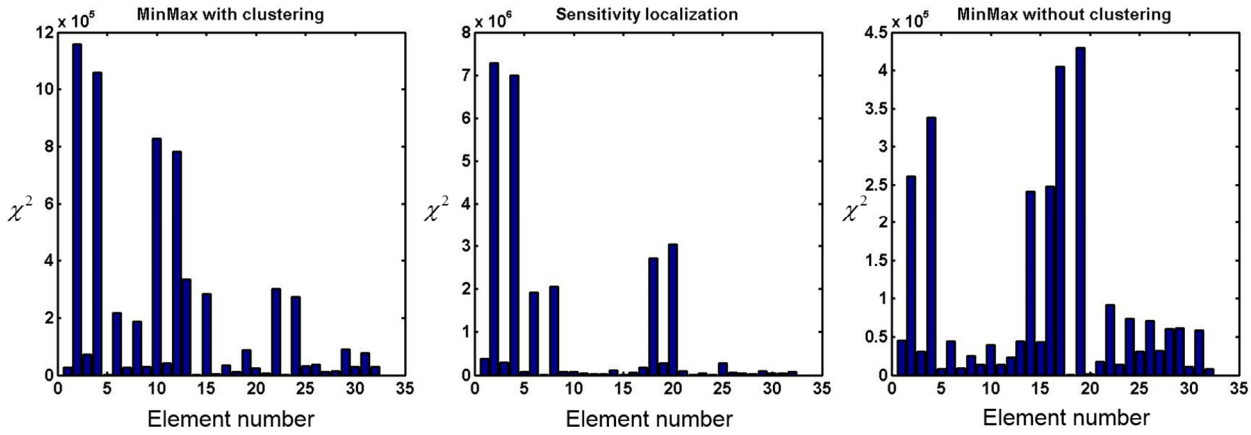

Configuration 2 (2 (II))

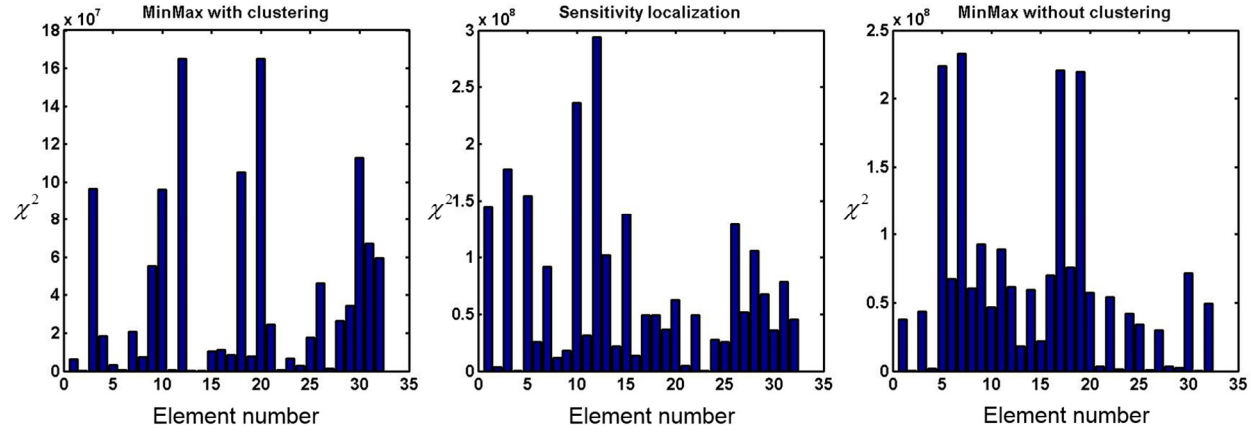

Configuration 11 (10 (II), 12 (II))

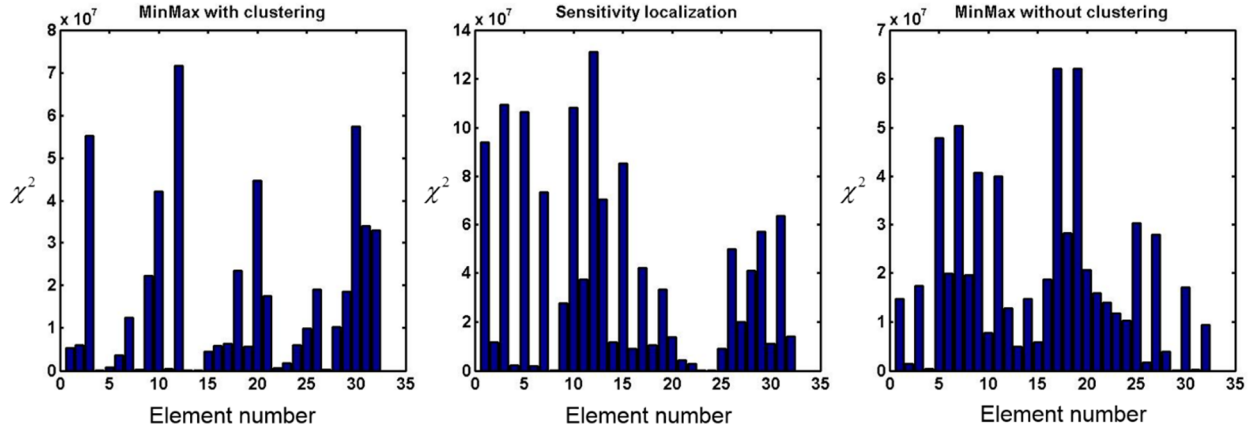

Configuration 13 (10 (II), 12 (II), 21 (II), 23 (II))

Figure 7.24 Damage localization of the Yellow frame without sensors on the first level, with HFC clustered Jacobians from *Formation 1*

elements 21 and 23 is not found. It is inferred from Figure 7.23 that in both graphs, the values corresponding to elements 10 and 12 are still high, especially for F^* values.

Furthermore, elements 21 and 23 did not have high FIM values before removal of sensors while they had high F^* values. Therefore, in Figure 7.19 (C13), they could be detected only from the MinMax approach. After removal of sensors, they have small values of both FIM and F^*, and hence, they are not detected from MinMax or sensitivity based approaches as shown in Figure 7.24.

It should be noted that these tests are performed only once and therefore the evaluated χ^2-values are one instance of the random variable and not the expected values. Therefore, these results can be viewed as an approximation to the expected value.

7.4 Comparative elemental safety threshold

In this thesis, unlike the SSDD technique there is no safety threshold used in localizing the damage; therefore, only the elements with higher χ^2-values compared to other elements, are presumed to be damaged. Hence, if the χ^2-value of one or more elements is distinctly higher than other elements, that/those elements are considered to be damaged. Investigation on a robust safety threshold tailored for the SSDL technique is also needed and recommended in Chapter 8 as the future work.

7.5 Conclusions

In this chapter, the Yellow frame structure and its testing were introduced. The data measured from this test was employed in validating the theories and methods proposed in Chapters 4 and 5. In this structure, 15 damage configurations were tested and all of them could be detected using the SSDD method. By adding additional measurement noise to the data, the theories on the effect of measurement noise and number of samples were validated. It was concluded that when the structure is undamaged, under real test conditions some assumptions made for Theories 4.1 and 4.3 were not held anymore, and instead, the effect of measurement noise and number of samples

for the undamaged structure can be evaluated same as the damaged structure from Theories 4.2 and 4.4.

Subsequently, the SSDL method was used in localizing the damage in this structure for each damage configuration. The two formations of the Jacobian matrix were investigated. It was demonstrated that using only the modeshapes from the analytical model in composing the Jacobian matrix results in more robust results. An important reason for this is that in order to compose the Jacobians from analytical and real data modal parameters, they need to be detectible in both sources. Therefore, the number of matched parameters came out to be less than the analytical modal parameters, which resulted in less precision in the test. Furthermore, the modeshapes and coupled modeshapes from the real data were decoupled and scaled to the analytical modeshapes successfully.

The HFC and *k*-means clustering were tested on the Yellow frame data. It was observed that HFC could cluster the *close* elements properly. The *k*-means approach was shown to be unstable and it could not cluster properly some *close* elements.

The MinMax and sensitivity based approach were used in localizing the damage. It was seen that the clustering scheme obtained from HFC is appropriate in localizing the damage with the MinMax test. Subsequently, all the configurations were tested from the MinMax and sensitivity based approach with *Formation 1* Jacobians clustered by HFC method. It was observed that the MinMax test with HFC can localize the damage in most of the cases, including single and multiple damage cases. Furthermore, it was observed that the damage in single damage scenarios is more distinct than multiple damage scenarios.

Finally, the detectability of damage from the proposed indices was investigated in this chapter. By removal of some sensors, the detectability was compared to the original structure. It

was seen that the damaged elements which still have a high detectability index after the removal of sensors, are still detectible. Conversely, the damaged elements which their detectability index was reduced after the removal of sensors, could not be detected.

Chapter 8: Conclusions, Contributions and Future Work

In this chapter, the contributions of this thesis will be elaborated. Subsequently, the conclusive remarks from this research on the practicability of the SSDD and SSDL methods are provided. Finally, the recommendations for the future work on this topic are suggested.

8.1 Contributions

In this section the contributions are listed, and their corresponding methodologies and objectives are addressed. The contributions can be stated, in a nut shell, as:

I) Predicting the effect of measurement length and measurement noise on the SSDD technique;

II) Enabling the SSDL method to perform on the real data under real test conditions;

III) Developing indexes which represent the detectability of damage in each element.

The contributions are listed and elaborated in the following subsections.

8.1.1 Significant contributions

8.1.1.1 Developed and validated theories to predict the effect of number of samples on the SSDD method

By the use of the developed theories we are now able to predict and recognize the effects of different measurement lengths in the SSDD result. This will help us in the correct use of the method and also in treating the results when the measurement length cannot be changed e.g. availability to only short measurements.

These theories were expanded for the effect of number of samples on damaged and undamaged structures. Based on these theories, the number of samples will affect significantly on the χ^2-test results, and hence, it needs to be taken into account while employing this technique for different data lengths. The behavior of this effect could be predicted from these theories. Accordingly,

objective I.a was addressed in Chapter 4.Using the methodology I.a, two theories reflecting the effect of number of samples on the χ^2-test were developed and described in Chapter 4 (and Appendix A).

These theories were verified using the analytical models in Chapter 6, and the results were obtained as predicated by them. Subsequently, they were validated with real data from the Yellow frame in Chapter 7. It was demonstrated that under real test conditions, the behavior of the χ^2-test for undamaged structure is the same as the ones for damaged structure. Therefore for real test conditions, the behavior of the test can be predicted for both damaged and undamaged structures using the theory related to the damaged structure.

8.1.1.2 Developed and validated theories on the effect of measurement noise on the SSDD method

Thanks to the developed theories in this thesis, the effect of measurement noise can be predicted and analyzed. This will significantly help in the practical use of the SSDD method and in predicting and understanding the results from this method. In Chapter 4 (and Appendix A), the SSDD formulations were expanded to include the effect of measurement noise in the data. The noise characteristics are assumed to be different or equal between the reference and testing states. For each case, this effect was also investigated for damaged and undamaged structures. Thus, four theories were developed to reflect each combination of noise characteristic and damage-state of the structure. It was shown that the measurement noise affects the χ^2-test results significantly. This effect can be predicted from the proposed theories. Thus, they need to be considered when using the SSDD method in practice. Objective I.b was also addressed in this chapter.

Similar to 8.1.1.1, the proposed theories were verified using analytical models in Chapter 6. In Chapter 7, the real data from the Yellow frame was employed in validating these proposed

theories. It was shown that for real data under real test conditions, similar to 8.1.1.1, when the measurement noise characteristics are the same between the reference and testing states, if the structure is damaged or not, it can be predicted from the same theory for damaged structure. The other theories were also validated in predicting the behavior of the test under real test conditions.

8.1.1.3 Proposed and validated a decoupling method for coupled modeshapes

In order to use the modeshapes from real data in conjunction with the ones from analytical model in *Formation 2*, they needed to be scaled and matched to each other. With the proposed decoupling method, these modeshapes can be decoupled fully and be used in the SSDL method. Coupled modeshapes can happen in many structures. Furthermore, some modeshapes acquired from the real data in the Yellow frame are coupled, since their natural frequencies are very close. Therefore, the scaling method needed to be extended to decouple these coupled modeshapes. The formulations of these scaling methods were derived and presented in Chapter 5. Subsequently, they were used in scaling the modeshapes from the real data of Yellow frame to its analytical ones in Chapter 7. Objective II.b was addressed in this part.

8.1.1.4 Developed and validated a new clustering approach (HFC), robust in dealing with real data

The elements of the structure need to be clustered prior to the use in the SSDL method. This clustering was previously performed by known methods such as *k*-means, which was not promising in dealing with the practical problems. In Chapter 5, a new clustering approach was proposed based on the Fisher information matrix. This method is tailored to the SSDL method and therefore it is robustly able to cluster the elements under real testing conditions. The advantages of this method in comparison to the *k*-means approach are listed in here:

1- There is no iterative algorithm in HFC and therefore, there is no convergence issues. However, *k*-means does not converge in some executions of the algorithm.

2- The results from HFC are unique and stable for the same measurements. In *k*-means due to its random starting points, the results are not unique and are unstable.

3- In HFC method a statistical value is defined which represents the amount of similarity of elements to be clustered in the same group. This value reflects the resolution of the clusters and can be defined practically without the need of in-depth information about the structure. However, in *k*-means approach, this value is the number of groups, i.e. *k* (in *k*-means), for which the user needs to gain sufficient prior knowledge about the structure, sensor locations and noise in the data (which is often not possible under real test conditions). Hence, the practicability of using the *k*-means in SSDL method is low.

4- With the HFC method, we can be assured from a theoretical point of view that the elements with similar Jacobians are clustered in the same group, while from *k*-means this is not necessarily valid. Since the MinMax test, in SSDL approach is sensitive to the similarity of Jacobians, their proper clustering is critical. Therefore, the HFC method is tailored to be used with the MinMax method, while the *k*-means approach might result in false negative results. The HFC and *k*-means clustering approaches were compared using the analytical models in Chapter 6 and using the real data in Chapter 7. The functionality of the HFC approach was verified and validated in these chapters. Objective II.c was, hence, addressed in there.

8.1.1.5 Proposed and validated indexes indicating the detectability of damage in each element

Two indexes were defined and investigated in representing the detectability of damage in each element from the sensitivity based and MinMax approaches in SSDL method. These indexes provide important information on the sensitivity of the SSDL method in detecting the damage in different elements. This will help in understanding the limits of the detection approach and in designing optimized and efficient sensor layouts. The relation of these indexes to the detectability was elaborated in Chapter 5. The proposed indexes were verified in Chapter 6 for analytical models and were used in assessing the detectability of the elements of the Yellow frame with real data in Chapter 7. Objective II.d was addressed in here.

8.1.2 Other contributions

8.1.2.1 Proposed two formations for the Jacobian formulation

In Chapter 5, two formations for calculating the Jacobian formulation used in the SSDL method were proposed and studied. It was demonstrated that one of these formations is more robust than the other one.

Since, the SSDL method was previously used only for simulated data acquired from analytical models, these formations were identical in definition. However in this research, in order to use the SSDL method in practice for real data, the formation of the Jacobians can be defined from two approaches. In one approach, referred as *Formation 1*, the Jacobians are computed from only the analytical modal parameters. In *Formation* 2 they are computed from modal parameters acquired from both analytical and real data. The difference and applicability of these formations in practice were discussed in Chapter 5, and they were investigated and validated with real data from the Yellow frame in Chapter 7. Objective II.a was addressed in here.

8.1.2.2 Assessing the functionality of SSDL method under real test conditions

The SSDL method was not tested on real data before. In this research, the SSDL technique was adjusted and smoothed to be used in localizing the damage from the data obtained from the Yellow frame. It was demonstrated in Chapter 7 that the results are promising in localizing the single and multiple damage cases. Objective III.b was addressed in here.

8.2 Concluding remarks

In this thesis several challenges in damage identification of structures using the SSDD and SSDL methods were addressed. As a general conclusion, by considering the proposed theories, the SSDD method can be used in practice and is able to detect the damage under real testing conditions. Moreover, the SSDL method could perform robustly under real test conditions by using the methods and theories developed in this thesis.

The detailed concluding remarks from this investigation are as follows:

I) The SSDD method can robustly detect the damage in the real structure (the Yellow frame)

II) It was demonstrated from a theoretical and practical point of view how measurement length will affect the SSDD method. The proposed theories were, subsequently, verified with analytical models and validated using the real data from the Yellow frame. Based on these theories, the number of samples need to be high: the higher the number of samples is, the smaller the damage that can be detected. Moreover, it was concluded that the number of samples used for the test on undamaged structure (to create a safety threshold) needs to be almost equal to the number of samples of the test data.

III) The effect of the measurement noise on the SSDD method in the reference and test data was formulated. There were 4 theories proposed in predicting this effect. These theories

were verified by the analytical models and then validated by the real data. It was shown that higher measurement noise will reduce the chance of detecting the damage or increase the chance of false alarm. It was concluded that the measurement noise should be the same when creating the safety threshold and when the test is being performed. If this measurement noise is higher or lower compared to the test data, the damage might not be detected or false alarm might happen. Furthermore, it is concluded that the data used in the reference state and the data used in the testing state should have the same amount of measurement noise. Otherwise, for each test the covariance matrix needs to be revaluated from the test data which might be computationally not efficient.

IV) The SSDL method could robustly locate the damage in real structures from MinMax test and sensitivity based approaches. The results from the MinMax test are clearer than the sensitivity based approach.

V) It was concluded that the Jacobian matrix formed from analytical modal parameters can be used robustly in the SSDL method. The Jacobian matrix formed from both analytical and real modal parameters might not be as robust due to the difference of the analytical model with the real structure and lower detectability (low number of sensors) of the modeshapes from the real data compared to the ones from the analytical model.

VI) The scaling methods proposed for the modeshapes can perfectly scale and decouple real modeshapes in order to be matched to the analytical ones.

VII) The HFC clustering approach proved to be a stable and consistent method to cluster the elements robustly for the SSDL method. The *k*-means approach is not a suitable method in clustering the elements for the SSDL method.

VIII) It was demonstrated theoretically that the proposed damage detectability indices are a good representative of detectability of damage in each element. Using the analytical models, this proposition was also verified. These indices were used and tested in the Yellow frame to show how the removal of sensors, decrease the detectability of each element.

8.3 Recommendation for future work

Several recommendations for the future research topics and tasks were identified in the course of this research. These recommendations are aligned to the vision behind this thesis and are considered the next steps towards the goals presented in the Introduction.

The effect of temperature, moisture and other environmental conditions on the SSDD and SSDL methods need to be investigated. These factors are important and need to be taken into account for real test conditions. Therefore, one of the next steps in advancing these techniques under real test conditions is to study and remove these effects on them.

After studying the environmental factors, damage quantization using the statistical subspace damage identification method should be investigated by analytical and experimental data. This will be the next level of damage identification and the theories were developed for this purpose. However, similar to this thesis, the theories and methods needed in achieving the performance under real test conditions, need to be developed and validated. Additionally, investigation on the effect of damage type and element type on the SSDD and SSDL method with real data, gives critical information on these methods especially for higher levels of damage identification.

The relation between the Hankel matrix and modal parameters, i.e. natural frequencies and modeshapes, can be defined from (3-13) using modal basis of $R_i = HF^{i-1}G$ or from analytical

solution shown in (Brincker 2017). Further investigation of this relationship is suggested in connecting the modal domain to the data-driven residual in SSDD method. This relationship can provide valuable insight on the SSDD technique in terms of number of present modeshapes in measured data and accuracy of the subspace created from the reference state and used in forming the residual.

In view of the damage localization results of the Yellow frame, it is observed that similar to the SSDD method, a safety threshold needs to be created for each element in testing if the element is damaged or not. This safety threshold was created in the SSDD technique by testing several measurements of the undamaged structure and fitting a normal distribution on them. Next, a value based on a probability of exceedance was chosen as a safety threshold. This technique can be performed in the same manner in SSDL method too, with the difference that it needs to be evaluated for each element. The practicability of this method needs to be investigated and is recommended as a future research.

Further study on the SSDD and SSDL method for various types of laboratory structures will assure its applicability in practice on different types of structures. Moreover, investigation of these methods on the real data from an existing structure (damaged and undamaged) is perfect in showing its robustness for non-laboratory structures. In this way, the effect of different input excitations on the SSDD and SSDL techniques can also be identified.

The damage detectability indexes need to be also investigated on complete tests with the real data under real test conditions. Their relation to detectability of damages, needs to be validated by the real data by tailored tests.

The necessity and needed amount of calibration of the FE model to the real data should be investigated deeper to understand its limitations and conditions. It should be noted that even if the model is calibrated to the real data it needs to be only done once in the reference state.

The other complementary studies are suggested as following: studying the effect of nonlinear damage and nonlinear structures on the SSDD method; investigation on the use of the statistical subspace identification method along with the probabilistic and reliability based methods; further work on life prediction of the elements based on the damage quantization results from this method; and creation of a platform to automatically pull the data, analyze it, identify the damage with this method and finally trigger the alarm if needed.

Bibliography

Abdel Wahab, M. M., and De Roeck, G. (1999). "Damage Detection in Bridges Using Modal Curvatures: Application To a Real Damage Scenario." *Journal of Sound and Vibration*, 226(2), 217–235.

Abdelghani, M., and Benveniste, A. (2000). "Subspace-based fault detection algorithms for vibration monitoring ☙." 36, 101–109.

Adams, R. D., Cawley, P., Pye, C. J., and Stone, B. J. (1978). "A vibration technique for non-destructively assessing the integrity of structures." *ARCHIVE: Journal of Mechanical Engineering Science 1959-1982 (vols 1-23)*, SAGE PublicationsSage UK: London, England, 20(2), 93–100.

Ågårdh, L. (1991). "Modal Analyses of Two Concrete Bridges in Sweden." *Structural Engineering International*, 1(4), 35–39.

Allemang, R., and Brown, D. (1982). "A correlation coefficient for modal vector analysis." *Proceedings of the 1st international modal*.

Altman, M., Infeld, L., Słowikowski, W., Mycielski, J., and Mrowka, S. (1960). *(In French) Bulletin de l'Académie polonaise des sciences. Série des sciences chimiques.* [Państwowe Wydawn. Naukowe].

Alvandi, A., and Cremona, C. (2006). "Assessment of vibration-based damage identification techniques." *Journal of Sound and Vibration*, 292(1), 179–202.

Araújo Dos Santos, J. V., Soares, C. M. M., Mota Soares, C. A., and Pina, H. L. G. (2000). "Damage identification numerical model based on the sensitivity of orthogonality conditions and least squares techniques." *Computers and Structures*, 78(1), 283–291.

Balmes, E., Basseville, M., Bourquin, F., Mevel, L., Nasser, H., and Treyssede, F. (2008).

"Merging Sensor Data from Multiple Temperature Scenarios for Vibration Monitoring of Civil Structures." *Structural Health Monitoring*, 7(2), 129–142.

Balmes, E., Basseville, M., Mevel, L., and Nasser, H. (2009). "Handling the temperature effect in vibration monitoring of civil structures: A combined subspace-based and nuisance rejection approach." *Control Engineering Practice*.

Balmès, E., Basseville, M., Mevel, L., Nasser, H., and Zhou, W. (2008). "Statistical model-based damage localization: A combined subspace-based and substructuring approach." *Structural Control and Health Monitoring*, 15(6), 857–875.

Baruch, M., and Bar-Itzhack, I. Y. (1978). "Optimal weighted orthogonalization of measured modes." *AIAA Journal*, 16, 346–351.

Basseville, M. (1997). "Information criteria for residual generation and fault detection and isolation." *Automatica*, 33(5), 783–803.

Basseville, M. (1998). "On-board Component Fault Detection and Isolation Using the Statistical Local Approach." *Automatica*, 34(11), 1391–1415.

Basseville, M., Abdelghani, M., and Benveniste, A. (2000). "Subspace-based fault detection algorithms for vibration monitoring." *Automatica*, 36(1), 101–109.

Basseville, M., Benveniste, A., Goursat, M., Hermans, L., Mevel, L., and Van der Auweraer, H. (2001). "Output-Only Subspace-Based Structural Identification: From Theory to Industrial Testing Practice." *Journal of Dynamic Systems, Measurement, and Control*, 123(4), 668.

Basseville, M., Mevel, L., and Goursat, M. (2004). "Statistical model-based damage detection and localization: Subspace-based residuals and damage-to-noise sensitivity ratios." *Journal of Sound and Vibration*, 275(3–5), 769–794.

Benveniste, A., and Basseville, M. (1987). "The asymptotic local approach to change detection

and model validation." *IEEE Transactions on*.

Berman, A. (2000). "Inherently incomplete finite element model and its effects on model updating." *AIAA journal*.

Brincker, R. (2017). "On the application of correlation function matrices in OMA." *Mechanical Systems and Signal Processing*, 87, 17–22.

Brincker, R., Andersen, P., and Cantieni, R. (2001a). "Identification and Level 1 Damage Detection of the Z24 Highway Bridge by Frequency Domain Decomposition." *Experimental techniques*, 25(6), 51–57.

Brincker, R., Zhang, L., and Andersen, P. (2000). "Modal identification from ambient responses using frequency domain decomposition." *Proceedings of SPIE - The International Society for Optical Engineering*.

Brincker, R., Zhang, L., and Andersen, P. (2001b). "Modal identification of output-only systems using frequency domain decomposition." *Smart Materials and Structures*, 10(3), 441–445.

Carden, E. P., and Fanning, P. (2004). "Vibration Based Condition Monitoring: A Review." *Structural Health Monitoring*, 3(4), 355–377.

Castello, D. A., Stutz, L. T., and Rochinha, F. A. (2002). "A structural defect identification approach based on a continuum damage model." *Computers & Structures*, 80(5), 417–436.

Cawley, P., and Adams, R. D. (1979). "The location of defects in structures from measurements of natural frequencies." *The Journal of Strain Analysis for Engineering Design*, 14(2), 49–57.

Cerri, M. N., and Vestroni, F. (2000). "Detection of Damage in Beams Subjected to Diffused Cracking." *Journal of Sound and Vibration*, 234(2), 259–276.

Cha, P. D., and Tuck-Lee, J. P. (2000). "Updating Structural System Parameters Using Frequency

Response Data." *Journal of Engineering Mechanics*.

Chen, H. L., Spyrakos, C. C., and Venkatesh, G. (1995). "Evaluating Structural Deterioration by Dynamic Response." *Journal of Structural Engineering*, 121(8), 1197–1204.

Chiang, D.-Y., and Lai, W.-Y. (1999). "Structural Damage Detection Using the Simulated Evolution Method." *AIAA Journal*, 37(10), 1331–1333.

Chinchalkar, S. (2001). "Determination of Crack Location in Beams Using Natural Frequencies." *Journal of Sound and Vibration*, 247(3), 417–429.

Cornwell, P., Doebling, S. W., and Farrar, C. R. (1999). "Application of the Strain Energy Damage Detection Method To Plate-Like Structures." *Journal of Sound and Vibration*, 224(2), 359–374.

Curadelli, R. O., Riera, J. D., Ambrosini, D., and Amani, M. G. (2008). "Damage detection by means of structural damping identification." *Engineering Structures*, 30(12), 3497–3504.

Doebling, S. W., Farrar, C. R., and Prime, M. B. (1998). "A Summary Review of Vibration-Based Damage Identification Methods." *The Shock and Vibration Digest*, 30(2), 91–105.

Döhler, M. (2011). "Subspace-based system identification and fault detection: Algorithms for large systems and application to structural vibration analysis." Université Rennes 1.

Döhler, M., and Hille, F. (2014). "Subspace-based damage detection on steel frame structure under changing excitation." *Structural Health Monitoring, Volume 5*.

Döhler, M., Hille, F., Mevel, L., and Rücker, W. (2014a). "Structural health monitoring with statistical methods during progressive damage test of S101 Bridge." *Engineering Structures*, 69, 183–193.

Döhler, M., and Mevel, L. (2013). "Subspace-based fault detection robust to changes in the noise covariances." *Automatica*, 49(9), 2734–2743.

Döhler, M., Mevel, L., and Hille, F. (2014b). "Subspace-based damage detection under changes in the ambient excitation statistics." *Mechanical Systems and Signal Processing*, 207–224.

Döhler, M., Mevel, L., and Hille, F. (2014c). "Efficient computation of minmax tests for fault isolation and their application to structural damage localization." *IFAC Proceedings Volumes*.

Fan, W., and Qiao, P. (2010). "Vibration-based Damage Identification Methods: A Review and Comparative Study." *Structural Health Monitoring*, 10(1), 83–111.

Fanning, P., and Carden, E. (2001). "Auto-regression and statistical process control techniques applied to damage indication in telecommunication masts." *Key Engineering Materials*.

Farhat, C., and Hemez, F. M. (1993). "Updating finite element dynamic models using an element-by-element sensitivity methodology." *AIAA Journal*, 31(9), 1702–1711.

Farrar, C. R., and Doebling, S. W. (1999). "Damage Detection and Evaluation II: field applications to large structures." *Modal Analysis and Testing NATO Science Series*, 363, pp 345-378.

Farrar, C. R., Doebling, S. W., and Nix, D. a. (2001). "Vibration-based structural damage identification." *Philosophical Transactions of the Royal Society A: Mathematical, Physical and Engineering Sciences*, 359(1778), 131–149.

Farrar, C. R., Worden, K., Todd, M. D., Park, G., Nichols, J., Adams, D. E., Bement, M. T., and Farinholt, K. (2007). *Nonlinear System Identification for Damage Detection*. Los Alamos, NM (United States).

Feng, M. Q., and Bahng, E. Y. (1999). "Damage Assessment of Jacketed RC Columns Using Vibration Tests." *Journal of Structural Engineering*, 125(3), 265–271.

Frank, P. M. (1990). "Fault diagnosis in dynamic systems using analytical and knowledge-based redundancy. A survey and some new results." *Automatica*.

Friswell, M. I., and Penny, J. E. T. (1997). "Is Damage Location Using Vibration Measurements

Practical?" *EUROMECH 365 International Workshop: DAMAS 97, Structural Damage Assessment using Advanced Signal Processing Procedures*, (July 1997), 1–7.

Fugate, M. L., Sohn, H., and Farrar, C. R. (2000). "Unsupervised learning methods for vibration-based damage detection." *Proceedings of the International Modal Analysis Conference - IMAC*, 1, 652–659.

Fugate, M. L., Sohn, H., and Farrar, C. R. (2001). "Vibration-Based Damage Detection Using Statistical Process Control." *Mechanical Systems and Signal Processing*, 15(4), 707–721.

Gola, M. M., Som, A., and Botto, D. (2001). "ON THEORETICAL LIMITS OF DYNAMIC MODEL UPDATING USING A SENSITIVITY-BASED APPROACH." *Journal of Sound and Vibration*, 244(4), 583–595.

Gomes, H. M., and Silva, N. R. S. (2008). "Some comparisons for damage detection on structures using genetic algorithms and modal sensitivity method." *Applied Mathematical Modelling*, 32(11), 2216–2232.

González, M. P., and Zapico, J. L. (2008). "Seismic damage identification in buildings using neural networks and modal data." *Computers & Structures*, 86(3–5), 416–426.

Gudmundson, P. (1982). "Eigenfrequency changes of structures due to cracks, notches or other geometrical changes." *Journal of the Mechanics and Physics of Solids*, 30(5), 339–353.

Gul, M., and Catbas, F. N. (2011a). "Structural health monitoring and damage assessment using a novel time series analysis methodology with sensor clustering." *Journal of Sound and Vibration*, 330(6), 1196–1210.

Gul, M., and Catbas, F. N. (2011b). "Damage Assessment with Ambient Vibration Data Using a Novel Time Series Analysis Methodology." *Journal of Structural Engineering*, 137(12), 1518–1526.

Hao, H., and Xia, Y. (2002). "Vibration-based Damage Detection of Structures by Genetic Algorithm." *Journal of Computing in Civil Engineering*, 16(3), 222–229.

Hearn, G., and Testa, R. B. (1991). "Modal Analysis for Damage Detection in Structures." *Journal of Structural Engineering*, 117(10), 3042–3063.

Hibbett, Karlsson, and Sorensen. (1998). "ABAQUS/standard: User's Manual."

Hou, Z., Noori, M., and Amand, R. S. (2000). "Wavelet-based approach for structural damage detection." *Journal of Engineering Mechanics*, 126(7), 677–683.

Hu, N., Wang, X., Fukunaga, H., Yao, Z. H., Zhang, H. X., and Wu, Z. S. (2001). "Damage assessment of structures using modal test data." *International Journal of Solids and Structures*, 38(18), 3111–3126.

Jang, J.-H., Yeo, I., Shin, S., and Chang, S.-P. (2002). "Experimental investigation of system-identification-based damage assessment on structures." *Journal of Structural Engineering*, 128(5), 673–682.

Kahl, K., and Sirkis, J. S. (1996). "Damage detection in beam structures using subspace rotation algorithm with strain data." *AIAA Journal*, 34(12), 2609–2614.

Kaouk, M., and Zimmerman, D. C. (1994). "Structural damage assessment using a generalized minimum rank perturbation theory." *AIAA Journal*, 32(4), 836–842.

Kato, M., and Shimada, S. (1986). "Vibration of PC Bridge during Failure Process." *Journal of Structural Engineering*, 112(7), 1692–1703.

Kim, H., and Melhem, H. (2004). "Damage detection of structures by wavelet analysis." *Engineering Structures*, 26(3), 347–362.

Kim, J.-T., and Stubbs, N. (1995). "Model-Uncertainty Impact and Damage-Detection Accuracy in Plate Girder." *Journal of Structural Engineering*, 121(10), 1409–1417.

Kim, J. T., and Stubbs, N. (2002). "Improved Damage Identification Method Based on Modal Information." *Journal of Sound and Vibration*, 252(2), 223–238.

Kosmatka, J. B., and Ricles, J. M. (1999). "Damage Detection in Structures by Modal Vibration Characterization." *Journal of Structural Engineering*, 125(12), 1384–1392.

Kullaa, J. (2003). "Damage detection of the Z24 bridge using control charts." *Mechanical Systems and Signal Processing*, 17(1), 163–170.

Lee, U., and Shin, J. (2002). "A frequency response function-based structural damage identification method." *Computers & Structures*, 80(2), 117–132.

Lee, Y.-S., and Chung, M.-J. (2000). "A study on crack detection using eigenfrequency test data." *Computers & Structures*, 77(3), 327–342.

Li, G.-Q., Hao, K.-C., Lu, Y., and Chen, S.-W. (1999). "A flexibility approach for damage identification of cantilever-type structures with bending and shear deformation." *Computers & Structures*, 73(6), 565–572.

Liew, K. M., and Wang, Q. (1998). "Application of the wavelet theory for crack identification in structures." *Journal of Engineering Mechanics*, 124(2), 152–157.

Lin, R. M., and Ewins, D. J. (1990). "Model updating using FRF data." *15th International Seminar on Modal Analysis*, 141–163.

Liu, P. (1995). "Identification and Damage Detection of Trusses Using Modal Data." *Journal of Structural Engineering*, 121(4), 599–608.

Magalhães, F., Cunha, Á., and Caetano, E. (2008). "Dynamic monitoring of a long span arch bridge." *Engineering Structures*, 30(11), 3034–3044.

Mahalanobis, P. C. (1936). "On the generalized distance in statistics." *Proceedings of the National Institute of Sciences (Calcutta)*, 2, 49–55.

Maia, N. M. M., Silva, J. M. M., Almas, E. A. M., Sampaio, R. P. C., ! A Autica, E. N., and Henrique, I. D. (2003). "Damage Detection in Structures: From Mode Shape To Frequency Response Function Methods." *Mechanical Systems and Signal Processing*, 17(3), 489–498.

Maier, H. R., Lence, B. J., Tolson, B. A., and Foschi, R. O. (2001). "First-order reliability method for estimating reliability, vulnerability, and resilience." *Water Resources Research*, 37(3), 779–790.

Martin, H. (1989). "Statistical moment analysis as a means of surface damage detection." *Proceedings of the 7th International*.

Marwala, T., Heyns, P. S., Marwala T., Heyns, P. S., Marwala, T., and Heyns, P. S. (1998). "Multiple-criterion method for determining structural damage." *AIAA Journal*, 1682–1687.

Marwalla, T., and Hunt, H. E. M. (1999). "Fault Identification Using Finite Element Models and Neural Networks." *Mechanical Systems and Signal Processing*, 13(3), 475–490.

Mirza, M. S., Ferdjani, O., Hadj-Arab, A., Joucdar, K., Khaled, A., and Razaqpur, A. G. (1990). "An experimental study of static and dynamic responses of prestressed concrete box irder bridges." *Canadian Journal of Civil Engineering*, NRC Research Press Ottawa, Canada , 17(3), 481–493.

Moaveni, B., Conte, J. P., and Hemez, F. M. (2009). "Uncertainty and sensitivity analysis of damage identification results obtained using finite element model updating." *Computer-Aided Civil and Infrastructure Engineering*, 24(5), 320–334.

Moaveni, B., He, X., Conte, J. P., and Restrepo, J. I. (2010). "Damage identification study of a seven-story full-scale building slice tested on the UCSD-NEES shake table." *Structural Safety*, 32(5), 347–356.

Morassi, A. (2001). "Identification of a Crack in a Rod Based on Changes in a Pair of Natural

Frequencies." *Journal of Sound and Vibration*, 242(4), 577–596.

Moslem, K., and Nafaspour, R. (2002). "Structural Damage Detection by Genetic Algorithms." *AIAA Journal*, 40(7), 1395–1401.

Mottershead, J. E., Link, M., and Friswell, M. I. (2011). "The sensitivity method in finite element model updating: A tutorial." *Mechanical Systems and Signal Processing*, 25(7), 2275–2296.

Oberkampf, W. L., and Roy, C. J. (2010). *Verification and Validation in Scientific Computing*. Cambridge University Press, New York, NY, USA.

Oh, B. H., and Jung, B. S. (1998). "Structural Damage Assessment with Combined Data of Static and Modal Tests." *Journal of Structural Engineering*, 124(8), 956–965.

Ostachowicz, W., Krawczuk, M., and Cartmell, M. (2002). "The location of a concentrated mass on rectangular plates from measurements of natural vibrations." *Computers and Structures*, 80(16–17), 1419–1428.

Van Overschee, P., and De Moor, B. (1996). *Subspace Identification for Linear Systems*. Springer US, Boston, MA.

Pandey, A. K., and Biswas, M. (1994). "Damage Detection in Structures Using Changes in Flexibility." *Journal of Sound and Vibration*, 169(1), 3–17.

Patton, R., Frank, P., and Clarke, R. (1989). "Fault diagnosis in dynamic systems: theory and application."

De Pauw, D., and Vanrolleghem, P. A. (2003). "Practical aspects of sensitivity analysis for dynamic models." *IMACS 4th MATHMOD Conference*.

Peeters, B., Maeck, J., and Roeck, G. De. (2001). "Vibration-based damage detection in civil engineering: excitation sources and temperature effects." *Smart Materials and Structures*, 10(3), 518–527.

Peterson, S. T., McLean, D. I., Symans, M. D., Pollock, D. G., Cofer, W. F., Emerson, R. N., and Fridley, K. J. (2001a). "Application of Dynamic System Identification to Timber Beams. I." *Journal of Structural Engineering*, 127(4), 418–425.

Peterson, S. T., McLean, D. I., Symans, M. D., Pollock, D. G., Cofer, W. F., Emerson, R. N., and Fridley, K. J. (2001b). "Application of Dynamic System Identification to Timber Beams. II." *Journal of Structural Engineering*, 127(4), 426–432.

Ramu, S. A., and Johnson, V. T. (1995). "Damage assessment of composite structures-A fuzzy logic integrated neural network approach." *Computers and Structures*, 57(3), 491–502.

Ratcliffe, C. P., and Bagaria, W. J. (1998). "Vibration technique for locating delamination in a composite beam." *AIAA Journal*, 36(6), 1074–1077.

Ren, W.-X., and De Roeck, G. (2002a). "Structural damage identification using modal data. I: Simulation verification." *Journal of Structural Engineering*, 128(1), 87–95.

Ren, W.-X., and De Roeck, G. (2002b). "Structural Damage Identification using Modal Data. II: Test Verification." *Journal of Structural Engineering*, 128(1), 96–104.

Rohrmann, R. G., Baessler, M., Said, S., Schmid, W., and Ruecker, W. F. (2000). "Structural causes of temperature affected modal data of civil structures obtained by long time monitoring." *Proceedings of IMAC-XVIII: A Conference on Structural Dynamics*.

Rucka, M., and Wilde, K. (2006). "Application of continuous wavelet transform in vibration based damage detection method for beams and plates." *Journal of Sound and Vibration*, 297(3–5), 536–550.

Rytter, A. (1993). "Vibrational Based Inspection of Civil Engineering Structures." *Fracture and Dynamics*.

Salawu, O. S. (1997). "Detection of structural damage through changes in frequency: a review."

Engineering Structures, 19(9), 718–723.

Sanayei, M., and Onipede, O. (2001). "Damage assessment of structures using static test data." *International Journal of Solids and Structures*, 38(18), 3111–3126.

Sanayei, M., Onipede, O., and Babu, S. (1992). "Selection of noisy measurement locations for error reduction in static parameter identification." *AIAA journal*.

Schiffer, S., Rothe, S., Baccar, D., and Dirk, S. (2014). "Classification of Systems ' Health Condition Using the New Adaptive Fuzzy-Based Feature Classification Approach Affca in Comparison To a Macro-Data-Based Approach." *EWSHM - 7th European Workshop on Structural Health Monitoring*.

Sheinman, I. (1996). "Damage detection and updating of stiffness and mass matrices using mode data." *Computers and Structures*, 59(1), 149–156.

Smith, S. W., and Beattie, C. A. (1991). *Model correlation and damage location for large space truss structures: secant method development and evaluation*.

Sohn, H., and Farrar, C. R. (2001). "Damage diagnosis using time series analysis of vibration signals." *Smart Materials and Structures*, 10, 446–451.

Springer, W. T., Lawrence, K. L., and Lawley, T. J. (1988). "Damage assessment based on the structural frequency-response function." *Experimental Mechanics*, Kluwer Academic Publishers, 28(1), 34–37.

Todd, M. D., Nichols, J. M., Pecora, L. M., and Virgin, L. N. (2001). "Vibration-based damage assessment utilizing state space geometry changes: local attractor variance ratio." *Smart Materials and Structures*, IOP Publishing, 10(5), 1000–1008.

Waszczyszyn, Z., and Ziemiański, L. (2001). "Neural networks in mechanics of structures and materials--new results and prospects of applications." *Computers & Structures*, 79(22),

2261–2276.

Wenzel, H., Veit-Egerer, R., and Widmann, M. (2012). *Project: D11-1 ANNEX B INTEGRATED EUROPEAN INDUSTRIAL RISK REDUCTION SYSTEM WP3 DEMONSTRATION REPORT – ANNEX B*.

Williams, and Salawu, O. S. (1997). "Damping as a damage indication parameter." *Proceedings of the 15th International Modal Analysis Conference*, 1531–1536.

Willsky, A. (1976). "A survey of design methods for failure detection in dynamic systems." *Automatica*, 12, 601–611.

Worden, K., Farrar, C. R., Manson, G., and Park, G. (2007). "The fundamental axioms of structural health monitoring." *Proceedings of the Royal Society A: Mathematical, Physical and Engineering Sciences*, 463, 1639–1664.

Worden, K., Manson, G., and Fieller, N. R. J. (2000). "Damage detection using outlier analysis." *Journal of Sound and Vibration*, 229(3), 647–667.

Wu, X., Ghaboussi, J., and Garrett Jr, J. H. (1992). "Use of neural networks in detection of structural damage." *Computers & Structures*, 42(4), 649–659.

Yan, A.-M., De Boe, P., and Golinval, J.-C. (2004). "Structural Damage Diagnosis by Kalman Model Based on Stochastic Subspace Identification." *Structural Health Monitoring*, 3(2), 103–119.

Yan, A.-M., Kerschen, G., De Boe, P., and Golinval, J.-C. (2005a). "Structural damage diagnosis under varying environmental conditions—Part I: A linear analysis." *Mechanical Systems and Signal Processing*, 19(4), 847–864.

Yan, A., and Golinval, J. C. (2005). "Structural damage localization by combining flexibility and stiffness methods." *Engineering Structures*, 27(12 SPEC. ISS.), 1752–1761.

Yan, A. M., Kerschen, G., De Boe, P., and Golinval, J. C. (2005b). "Structural damage diagnosis under varying environmental conditions - Part II: Local PCA for non-linear cases." *Mechanical Systems and Signal Processing*, 19(4), 865–880.

YANG, X. F., SWAMIDAS, A. S. J., and SESHADRI, R. (2001). "Crack Identification in Vibrating Beams Using the Energy Method." *Journal of Sound and Vibration*, 244(2), 339–357.

Zaurin, R., Khuc, T., and Catbas, F. N. (2016). "Hybrid Sensor-Camera Monitoring for Damage Detection: Case Study of a Real Bridge." *Journal of Bridge Engineering*, 21(6), 5016002.

Zhao, J., and DeWolf, J. T. (1999). "Sensitivity study for vibrational parameters used in damage detection." *Journal of Structural Engineering*, 125(4).

Zimmerman, D. C., and Kaouk, M. (1994). "Structural damage detection using a minimum rank update theory." *Journal of Vibration and Acoustics, Transactions of the ASME*, 116(2), 222–231.

Zou, Y., Tong, L., and Steven, G. P. (2000). "Vibration-Based Model-Dependent Damage (Delamination) Identification and Health Monitoring for Composite Structures — a Review." *Journal of Sound and Vibration*, 230(2), 357–378.

Zubaydi, A., Haddara, M. R., and Swamidas, A. S. J. (2002). "Damage identification in a ship's structure using neural networks." *Ocean Engineering*, 29(10), 1187–1200.

Appendix A Investigating the Relation between Measurement Noise and Residual Covariance

In order to investigate the effect of noise on the residual covariance, the noise effect on the data is defined as $\tilde{y} = y + v$, where, $\tilde{y}$ is the data with noise and v is the additional noise vector. The added noise would not have any effect on the expected value of the correlation matrix $\hat{R}_i$, assuming that the noise is white and with zero mean. Therefore, in view of (4) and (5), the expected value of the residual vector will not be also affected by the noise. However, the effect can be seen directly in the asymptotic covariance Σ^e which will be described in here.

The effect of noise on the covariance matrix of residual, i.e. Σ^e, is related directly to the covariance of the block Hankel matrix $\hat{\mathbf{H}}_{p+1}$, considering that the matrix $S(\theta_0)$ is independent of the noise effect. Moreover, $\hat{\mathbf{H}}_{p+1}$ is composed of output covariance matrices $\tilde{R}_i$ which, therefore, will be investigated for the effect of noise.

An element of $\tilde{R}_i$ corresponding to the covariance between sensor *a* and *b* is defined as $\tilde{R}_i^{a,b} = \frac{1}{N}\sum_{k=1}^{N} \tilde{y}_k^a \tilde{y}_{k-i}^b$. Subsequently, one general element of the covariance of $\hat{\mathbf{H}}_{p+1}$ is expressed between two elements of the output covariance matrix, for sensors *a*, *b*, *c* and *d* as

$$\mathrm{cov}(\tilde{R}_i^{a,b}, \tilde{R}_j^{c,d}) = \mathbf{E}\left[\tilde{R}_i^{a,b}\tilde{R}_j^{c,d}\right] - \mathbf{E}\left[\tilde{R}_i^{a,b}\right]\mathbf{E}\left[\tilde{R}_j^{c,d}\right] \qquad \textbf{(A-1)}$$

The noise is affecting only to the first part of (A-1), since

$$\mathbf{E}\left[\tilde{R}_i^{a,b}\right] = \mathbf{E}\left[\frac{1}{N}\sum_{k=1}^{N}\tilde{y}_k^a\tilde{y}_{k-i}^b\right] = \frac{1}{N}\sum_{k=1}^{N}\mathbf{E}\left[\tilde{y}_k^a\tilde{y}_{k-i}^b\right]$$

which can be expanded as

$$\mathbf{E}\left[\tilde{y}_k^a\tilde{y}_{k-i}^b\right] = \mathbf{E}\left[(y_k^a + v_k^a)(y_{k-i}^b + v_{k-i}^b)\right] = \mathbf{E}\left[y_k^a y_{k-i}^b + y_k^a v_{k-i}^b + v_k^a y_{k-i}^b + v_k^a v_{k-i}^b\right]$$

where

$$\mathbf{E}\left[y_k^a v_{k-i}^b \right] = \mathbf{E}\left[v_k^a y_{k-i}^b \right] = \mathbf{E}\left[v_k^a v_{k-i}^b \right] = 0 ,$$

and therefore

$$\mathbf{E}\left[\tilde{y}_k^a \tilde{y}_{k-i}^b \right] = \mathbf{E}\left[y_k^a y_{k-i}^b \right]$$

which is not affected by the additional output noise. Hence,

$$\mathbf{E}\left[\tilde{R}_i^{a,b} \right] \mathbf{E}\left[\tilde{R}_j^{c,d} \right] = \mathbf{E}\left[R_i^{a,b} \right] \mathbf{E}\left[R_j^{c,d} \right].$$

In order to investigate the effect of the noise, the first part is expanded as

$$\mathbf{E}\left[\tilde{R}_i^{a,b} \tilde{R}_j^{c,d} \right] = \mathbf{E}\left[\tfrac{1}{N^2} \sum_{k=1}^{N} \sum_{l=1}^{N} \tilde{y}_k^a \tilde{y}_{k-i}^b \tilde{y}_l^c \tilde{y}_{l-j}^d \right]$$

which can be rewritten as

$$\mathbf{E}\left[\tilde{R}_i^{a,b} \tilde{R}_j^{c,d} \right] = \tfrac{1}{N^2} \sum_{k=1}^{N} \sum_{l=1}^{N} \mathbf{E}\left[\tilde{y}_k^a \tilde{y}_{k-i}^b \tilde{y}_l^c \tilde{y}_{l-j}^d \right] .$$

Moreover, by expanding the measurement vectors $\tilde{y}$ to its components of y and v,

$$\mathbf{E}\left[\tilde{y}_k^a \tilde{y}_{k-i}^b \tilde{y}_l^c \tilde{y}_{l-j}^d \right] = \mathbf{E}\left[(y_k^a + v_k^a)(y_{k-i}^b + v_{k-i}^b)(y_l^c + v_l^c)(y_{l-j}^d + v_{l-j}^d) \right]$$

which is expanded to

$$\begin{aligned} \mathbf{E}[& y_k^a y_{k-i}^b y_l^c y_{l-j}^d + y_k^a y_{k-i}^b y_l^c v_{l-j}^d + y_k^a y_{k-i}^b v_l^c y_{l-j}^d + y_k^a y_{k-i}^b v_l^c v_{l-j}^d + \\ & y_k^a v_{k-i}^b y_l^c y_{l-j}^d + y_k^a v_{k-i}^b y_l^c v_{l-j}^d + y_k^a v_{k-i}^b v_l^c y_{l-j}^d + y_k^a v_{k-i}^b v_l^c v_{l-j}^d + \\ & v_k^a y_{k-i}^b y_l^c y_{l-j}^d + v_k^a y_{k-i}^b y_l^c v_{l-j}^d + v_k^a y_{k-i}^b v_l^c y_{l-j}^d + v_k^a y_{k-i}^b v_l^c v_{l-j}^d + \\ & v_k^a v_{k-i}^b y_l^c y_{l-j}^d + v_k^a v_{k-i}^b y_l^c v_{l-j}^d + v_k^a v_{k-i}^b v_l^c y_{l-j}^d + v_k^a v_{k-i}^b v_l^c v_{l-j}^d] \end{aligned} \qquad \textbf{(A-2)}$$

Since the measurements and noise vectors are independent, some of the components of (A-2) will be zero. As an example, in the second term, $y_k^a y_{k-i}^b y_l^c$ and noise element v_{l-j}^d are

independent, which results in $\mathbf{E}[y_k^a y_{k-i}^b y_l^c v_{l-j}^d] = \mathbf{E}[y_k^a y_{k-i}^b y_l^c]\mathbf{E}[v_{l-j}^d]$, and since $\mathbf{E}[v_{l-j}^d] = 0$, then $\mathbf{E}[y_k^a y_{k-i}^b y_l^c v_{l-j}^d] = 0$. This will bring (A-2) boiled down to

$$\begin{aligned}\mathbf{E}[&y_k^a y_{k-i}^b y_l^c y_{l-j}^d + y_k^a y_{k-i}^b v_l^c v_{l-j}^d + \\ &y_k^a v_{k-i}^b y_l^c v_{l-j}^d + y_k^a v_{k-i}^b v_l^c y_{l-j}^d + \\ &v_k^a y_{k-i}^b y_l^c v_{l-j}^d + v_k^a y_{k-i}^b v_l^c y_{l-j}^d + \\ &v_k^a v_{k-i}^b y_l^c y_{l-j}^d + v_k^a v_{k-i}^b v_l^c v_{l-j}^d]\end{aligned} \quad \textbf{(A-3)}$$

In addition, since $i \geq 1, j \geq 1$ the noise vectors with phase differences of i or j are always independent, i.e. $\mathbf{E}[v_l v_{l-j}] = \mathbf{E}[v_k v_{k-i}] = 0$, which makes (A-3) further simplified to $E_{k,l,i,j}$ defined as

$$\begin{aligned}E_{k,l,i,j} = \mathbf{E}[&y_k^a y_{k-i}^b y_l^c y_{l-j}^d + \\ &y_k^a v_{k-i}^b y_l^c v_{l-j}^d + y_k^a v_{k-i}^b v_l^c y_{l-j}^d + \\ &v_k^a y_{k-i}^b y_l^c v_{l-j}^d + v_k^a y_{k-i}^b v_l^c y_{l-j}^d + \\ &v_k^a v_{k-i}^b v_l^c v_{l-j}^d]\end{aligned} \quad \textbf{(A-4)}$$

Each component of $E_{k,l,i,j}$ can be evaluated by adjusting the indices in order to get nonzero values. These indices are adjusted based on the noise vectors, as they are assumed to be independent from each other and from measurements. The first term of $E_{k,l,i,j}$ contributes to the covariance matrix of the Hankel matrix without additional measurement noise. The second term is nonzero when $b = d$ and for $k - i = l - j$. By assuming that $i \geq j$

$$\mathbf{E}\left[y_k^a v_{k-i}^b y_l^c v_{l-j}^d \right] = \begin{cases} \mathbf{E}\left[y_k^a y_{k-(i-j)}^c v_{k-i}^b v_{k-i}^b \right] & b = d \text{ and } k - i = l - j \\ 0 & b \neq d \text{ or } k - i \neq l - j \end{cases}$$

in which

$$\mathbf{E}\left[y_k^a y_{k-(i-j)}^c v_{k-i}^b v_{k-i}^b \right] = \mathbf{E}\left[y_k^a y_{k-(i-j)}^c \right]\mathbf{E}\left[v_{k-i}^b v_{k-i}^b \right]. \quad \textbf{(A-5)}$$

The first part of (A-5) is the covariance between output measurements with $i-j$ phase difference. In view of (1), $y_k^a = H_a x_k + \varepsilon_k^a$ and therefore

$$\begin{aligned}\mathbf{E}\left[y_k^a y_{k-(i-j)}^c \right] &= \mathbf{E}\left[\left(H_a F^{i-j} x_{k-(i-j)} + \sum_{\iota=1}^{i-j} F^{\iota-1} w_{k-\iota}^a + \varepsilon_k^a \right) y_{k-(i-j)}^c \right] \\ &= H_a F^{i-j} \mathbf{E}\left[x_{k-(i-j)} y_{k-(i-j)}^c \right] + \sum_{\iota=1}^{i-j} F^{\iota-1} \mathbf{E}\left[w_{k-\iota}^a y_{k-(i-j)}^c \right] + \mathbf{E}\left[\varepsilon_k^a y_{k-(i-j)}^c \right]\end{aligned}.$$

Since the noise in a future time is independent of the output of the system in the past, $\mathbf{E}\left[w_{k-\iota}^a y_{k-(i-j)}^c \right] = 0$ for $\iota \le i-j$ and $\mathbf{E}\left[\varepsilon_k^a y_{k-(i-j)}^c \right] = 0$. Therefore,

$$\mathbf{E}\left[y_k^a y_{k-(i-j)}^c \right] = H_a F^{i-j} \mathbf{E}\left[x_{k-(i-j)} y_{k-(i-j)}^c \right] = H_a F^{i-j} \sigma_{x,y^c}$$

which gives

$$\mathbf{E}\left[y_k^a y_{k-(i-j)}^c v_{k-i}^b v_{k-i}^b \right] = H_a F^{i-j} \sigma_{x,y^c} \sigma_{v,b}^2 \qquad \text{if } b = d$$

and by defining δ_{bd} as the Kronecker delta function between *b* and *d*, it can be rewritten as

$$\mathbf{E}\left[y_k^a y_{k-(i-j)}^c v_{k-i}^b v_{k-i}^b \right] = H_a F^{i-j} \sigma_{x,y^c} \sigma_{v,b}^2 \delta_{bd}.$$

The third term of $E_{k,l,i,j}$ is nonzero only when $b = c$ and for $k - i = l$, which equals to

$$\mathbf{E}\left[y_k^a v_{k-i}^b v_l^c y_{l-j}^d \right] = \begin{cases} \mathbf{E}\left[y_k^a v_{k-i}^b v_{k-i}^b y_{k-(i+j)}^d \right] & b = c \text{ and } k-i = l \\ 0 & b \ne c \text{ or } k-i \ne l \end{cases}.$$

By considering the independence of noise and outputs

$$\mathbf{E}\left[y_k^a v_{k-i}^b v_{k-i}^b y_{k-(i+j)}^d \right] = \mathbf{E}\left[y_k^a y_{k-(i+j)}^d v_{k-i}^b v_{k-i}^b \right] = \mathbf{E}\left[y_k^a y_{k-(i+j)}^d \right] \mathbf{E}\left[v_{k-i}^b v_{k-i}^b \right].$$

In $\mathbf{E}\left[y_k^a y_{k-(i+j)}^d \right]$ the outputs are in $i+j$ phase difference. Similar to the evaluation of the second term of $E_{k,l,i,j}$, this term is evaluated as

$$\mathbf{E}\left[y_k^a y_{k-(i+j)}^d \right] = H_a F^{i+j} \sigma_{x,y^d}$$

and hence

$$\mathbf{E}\left[y_k^a y_{k-(i+j)}^d v_{k-i}^b v_{k-i}^b \right] = H_a F^{i+j} \sigma_{x,y^d} \sigma_{v,b}^2, \ if\ b = c$$

or

$$\mathbf{E}\left[y_k^a y_{k-(i+j)}^d v_{k-i}^b v_{k-i}^b \right] = H_a F^{i+j} \sigma_{x,y^d} \sigma_{v,b}^2 \delta_{bc} .$$

The fourth term of $E_{k,l,i,j}$ is nonzero for $a = d$ when $k = l - j$, and it can be defined as

$$\mathbf{E}\left[v_k^a y_{k-i}^b y_l^c v_{l-j}^d \right] = \begin{cases} \mathbf{E}\left[v_k^a y_{k-i}^b y_{k+j}^c v_k^a \right] & a = d \text{ and } k = l - j \\ 0 & a \neq d \text{ or } k \neq l - j \end{cases} .$$

Again by considering the independence of noise and outputs

$$\mathbf{E}\left[v_k^a y_{k-i}^b y_{k+j}^c v_k^a \right] = \mathbf{E}\left[y_{k+j}^c y_{k-i}^b v_k^a v_k^a \right] = \mathbf{E}\left[y_{k+j}^c y_{k-i}^b \right] \mathbf{E}\left[v_k^a v_k^a \right]$$

in which $\mathbf{E}\left[y_{k+j}^c y_{k-i}^b \right]$ is the covariance between outputs with $i + j$ phase difference. Therefore, it is evaluated as

$$\mathbf{E}\left[y_{k+j}^c y_{k-i}^b \right] = H_c F^{i+j} \sigma_{x,y^b} .$$

Hence, the fourth term can be computed as

$$\mathbf{E}\left[v_k^a y_{k-i}^b y_{k+j}^c v_k^a \right] = H_c F^{i+j} \sigma_{x,y^b} \sigma_{v,a}^2, \qquad if\ a = d$$

or

$$\mathbf{E}\left[v_k^a y_{k-i}^b y_{k+j}^c v_k^a \right] = H_c F^{i+j} \sigma_{x,y^b} \sigma_{v,a}^2 \delta_{ad} .$$

The fifth term is nonzero when $a = c$ and $k = l$. Therefore, it is evaluated as

$$\mathbf{E}\left[v_k^a y_{k-i}^b v_l^c y_{l-j}^d \right] = \begin{cases} \mathbf{E}\left[v_k^a y_{k-i}^b v_k^a y_{k-j}^d \right] & a = c \text{ and } k = l \\ 0 & a \neq c \text{ or } k \neq l \end{cases}$$

in which

$$\mathbf{E}\left[v_k^a y_{k-i}^b v_k^a y_{k-j}^d \right] = \mathbf{E}\left[y_{k-i}^b y_{k-j}^d v_k^a v_k^a \right] = \mathbf{E}\left[y_{k-i}^b y_{k-j}^d \right] \mathbf{E}\left[v_k^a v_k^a \right]$$

Due to the independence of noise and measurements. Moreover, $\mathbf{E}\left[y_{k-j}^d y_{k-i}^b \right]$ is the covariance between measurement outputs with $i-j$ phase difference. Similar to second term evaluation, by assuming $i \geq j$ it can be computed as

$$\mathbf{E}\left[y_{k-j}^d y_{k-i}^b \right] = H_d F^{i-j} \sigma_{x,y^b} .$$

Hence the fifth term of $E_{k,l,i,j}$ is evaluated as

$$\mathbf{E}\left[v_k^a y_{k-i}^b v_k^a y_{k-j}^d \right] = H_d F^{i-j} \sigma_{x,y^b} \sigma_{v,a}^2, \qquad if\ a = c$$

which can be rewritten as

$$\mathbf{E}\left[v_k^a y_{k-i}^b v_k^a y_{k-j}^d \right] = H_d F^{i-j} \sigma_{x,y^b} \sigma_{v,a}^2 \delta_{ac} .$$

Finally, the last term of $E_{k,l,i,j}$ is nonzero when $a = c$, $b = d$ and $i = j$ for $k = l$. These conditions are satisfied only for the diagonal elements. This term is computed as

$$\mathbf{E}\left[v_k^a v_{k-i}^b v_l^c v_{l-j}^d \right] = \begin{cases} \mathbf{E}\left[v_k^a v_{k-i}^b v_k^a v_{k-i}^b \right] & a = c \text{ and } b = d \text{ and } i = j \text{ and } k = l \\ 0 & a = c \text{ and } b = d \text{ and } i = j \text{ and } k = l \end{cases} .$$

Since the noise vectors are independent from each other and from themselves in different phases, $\mathbf{E}\left[v_k^a v_{k-i}^b v_k^a v_{k-i}^b \right] = \mathbf{E}\left[v_k^a v_k^a v_{k-i}^b v_{k-i}^b \right] = \mathbf{E}\left[v_k^a v_k^a \right] \mathbf{E}\left[v_{k-i}^b v_{k-i}^b \right] = \sigma_{v,a}^2 \sigma_{v,b}^2$.

By defining

$$\delta_{ab}^{cd} = \begin{cases} 1 & a = c \text{ and } b = d \\ 0 & \text{otherwise} \end{cases} ,$$

the last term can be evaluated as

$$\mathbf{E}\left[v_k^a v_{k-i}^b v_k^a v_{k-i}^b \right] = \sigma_{v,a}^2 \sigma_{v,b}^2 \delta_{ab}^{cd} .$$

By adding up all the evaluated components of $E_{k,l,i,j}$, an element of the covariance matrix of the block Hankel matrix is evaluated as

$$\mathrm{cov}(\tilde{R}_i^{a,b}, \tilde{R}_j^{c,d}) = \tfrac{1}{N^2} \sum_{k=1}^{N} \sum_{l=1}^{N} E_{k,l,i,j} - \mathbf{E}\left[R_i^{a,b} \right] \mathbf{E}\left[R_j^{c,d} \right]. \qquad \textbf{(A-6)}$$

Since the nonzero components of $E_{k,l,i,j}$ are constant with the change in *k* and *l*, their summation over $[k = 1...N, l = 1...N]$ equals to their value multiplied by the number of their repetitions. Therefore, each component needs to be counted based on its definition in terms of *k* and *l*. The first component of $E_{k,l,i,j}$ and the second part of (A-6) compose the covariance matrix element with no additional noise condition, i.e. $\mathrm{cov}(R_i^{a,b}, R_j^{c,d})$ which has a factor of $1/N$.

In view of the evaluation of other components of $E_{k,l,i,j}$, it can be seen that the factors *k* and *l* are in terms of each other. In all these components, factor *k* equals to factor *l* plus a constant in terms of *i* and or *j*. Therefore, number of repetitions for the two summations on *k* and *l* will be *N* times, which makes the final factor equal to $1/N^2 \times N = 1/N$.

By the addition of all the components of $E_{k,l,i,j}$, an element of the covariance matrix of the block Hankel matrix can be evaluated as

$$\begin{aligned} \mathrm{cov}(\tilde{R}_i^{a,b}, \tilde{R}_j^{c,d}) = \mathrm{cov}(R_i^{a,b}, R_j^{c,d}) &+ 1/N\, H_a F^{i-j} \sigma_{x,y^c} \sigma_{v,b}^2 \delta_{bd} + 1/N\, H_a F^{i+j} \sigma_{x,y^d} \sigma_{v,b}^2 \delta_{bc} \\ &+ 1/N\, H_c F^{i+j} \sigma_{x,y^b} \sigma_{v,a}^2 \delta_{ad} + 1/N\, H_d F^{i-j} \sigma_{x,y^b} \sigma_{v,a}^2 \delta_{ac} + 1/N\, \sigma_{v,a}^2 \sigma_{v,b}^2 \delta_{ab}^{cd} \end{aligned} \qquad \textbf{(A-7)}$$

where, $i \geq j$.

By assuming that the standard deviation of noise in channel $\odot$ is a ratio, i.e. noise ratio β, of the standard deviation of the output of that channel, $\sigma_{v,\odot}^2 = \beta^2 \sigma_{y,\odot}^2$, (A-7) is rewritten as

$$\begin{aligned}\operatorname{cov}(\tilde{R}_i^{a,b},\tilde{R}_j^{c,d}) = \operatorname{cov}(R_i^{a,b},R_j^{c,d}) + \frac{\beta^2}{N}\left(H_a F^{i-j}\sigma_{x,y^c}\delta_{bd} + H_a F^{i+j}\sigma_{x,y^d}\delta_{bc}\right)\sigma_{y,b}^2 \\ + \frac{\beta^2}{N}\left(H_c F^{i+j}\sigma_{x,y^b}\delta_{ad} + H_d F^{i-j}\sigma_{x,y^b}\delta_{ac}\right)\sigma_{y,a}^2 + \frac{\beta^4}{N}\sigma_{y,a}^2\sigma_{y,b}^2\delta_{ab}^{cd}\end{aligned} \quad \textbf{(A-8)}$$

It can be seen that the order of noise ratio is 2 for nonzero non-diagonal elements and 4 for diagonal elements. This relationship is simplified as

$$\operatorname{cov}(\tilde{R}_i^{a,b},\tilde{R}_j^{c,d}) = \operatorname{cov}(R_i^{a,b},R_j^{c,d}) + \Delta_{i,j}^{a,b,c,d}, \qquad \Delta_{\Sigma_R}^{v} = \beta^2\Im + \beta^4\aleph. \quad \textbf{(A-9)}$$

In which $\Delta_{\Sigma_R}^{v}$ is a matrix containing elements $\Delta_{i,j}^{a,b,c,d}$. It should be also noted that in the χ^2 value (9), the effect of the number of samples on the covariance matrix is neutralized by the factor $\sqrt{N}$ in the residual vector (5).

A.1 Positive definiteness of $\Delta_{\Sigma_R}^{v}$

In order to investigate the positive definiteness of $\Delta_{\Sigma_R}^{v}$, an element of $\tilde{R}_i^{a,b}$ is expanded as

$$\tilde{R}_i^{a,b} = R_i^{a,b} + \Re_i^{a,b}$$

in which $\Re_i^{a,b} = \frac{1}{N}\sum_{k=1}^{N}\left(y_k^a v_{k-i}^b + v_k^a y_{k-i}^b + v_k^a v_{k-i}^b\right)$. It was shown for (A-1) that $\mathbf{E}\left[\Re_i^{a,b}\right] = 0$ for $i > 1$.

By this definition, (A-1) can be rewritten as

$$\operatorname{cov}(\tilde{R}_i^{a,b},\tilde{R}_j^{c,d}) = \mathbf{E}\left[(R_i^{a,b} + \Re_i^{a,b})(R_j^{c,d} + \Re_j^{c,d})\right] - \mathbf{E}\left[R_i^{a,b}\right]\mathbf{E}\left[R_j^{c,d}\right] \quad \textbf{(A-10)}$$

considering that $\mathbf{E}\left[\tilde{R}_i^{a,b}\right] = \mathbf{E}\left[R_i^{a,b}\right]$ as mentioned in the beginning of this appendix. The first part of (A-10) is expanded as

$$\mathbf{E}\left[(R_i^{a,b} + \Re_i^{a,b})(R_j^{c,d} + \Re_j^{c,d})\right] = \mathbf{E}\left[R_i^{a,b}R_j^{c,d}\right] + \mathbf{E}\left[\Re_i^{a,b}\Re_j^{c,d}\right] + \mathbf{E}\left[R_i^{a,b}\Re_j^{c,d}\right] + \mathbf{E}\left[\Re_i^{a,b}R_j^{c,d}\right] \quad \textbf{(A-11)}$$

The two latter parts of (A-11) are evaluated similarly as

$$\mathbf{E}\left[R_i^{a,b}\Re_j^{c,d}\right]=\tfrac{1}{N^2}\mathbf{E}\left[\sum_{k=1}^{N}y_k^a y_{k-i}^b\right]\mathbf{E}\left[\sum_{l=1}^{N}\left(y_l^c v_{l-j}^d+v_l^c y_{l-j}^d+v_l^c v_{l-j}^d\right)\right]$$
$$=\tfrac{1}{N^2}\sum_{k=1}^{N}\sum_{l=1}^{N}\left(\mathbf{E}\left[y_k^a y_{k-i}^b y_l^c v_{l-j}^d\right]+\mathbf{E}\left[y_k^a y_{k-i}^b v_l^c y_{l-j}^d\right]+\mathbf{E}\left[y_k^a y_{k-i}^b v_l^c v_{l-j}^d\right]\right)=0$$

due to the independence of noise and output measurements and independence of noise in different steps for $j>0$. Therefore, (A-10) can be simplified as

$$\operatorname{cov}(\tilde{R}_i^{a,b},\tilde{R}_j^{c,d})=\operatorname{cov}(R_i^{a,b},R_j^{c,d})+\mathbf{E}\left[\Re_i^{a,b}\Re_j^{c,d}\right]. \quad \textbf{(A-12)}$$

By comparing (A-9) and (A-12) it can be seen that $\Delta_{i,j}^{a,b,c,d}=\mathbf{E}\left[\Re_i^{a,b}\Re_j^{c,d}\right]$ which is a member of the covariance matrix of vector $\Re$, i.e. $\Delta_{\Sigma_R}^{v}$. Therefore, $\Delta_{\Sigma_R}^{v}$ is semi-positive definite. Moreover, if $\beta\neq 0$ the diagonal elements are always nonzero and hence $\Delta_{\Sigma_R}^{v}$ is positive definite. The noise effect on the diagonal elements is investigated in the next section.

A.2 Effect on the diagonal elements

Since the diagonals of the covariance matrix dominate the calculations of the $\chi 2$ test, (A-8) is investigated in here for the diagonal elements which correspond to $a=c,b=d$ and $i=j$. Based on these assumptions, (A-8) is rewritten as

$$\operatorname{cov}(\tilde{R}_i^{a,b},\tilde{R}_i^{a,b})=\operatorname{cov}(R_i^{a,b},R_i^{a,b})+\frac{\beta^2}{N}\left(H_a\sigma_{x,y^a}+H_aF^{2i}\sigma_{x,y^b}\delta_{ab}\right)\sigma_{y,b}^2$$
$$+\frac{\beta^2}{N}\left(H_aF^{2i}\sigma_{x,y^b}\delta_{ab}+H_b\sigma_{x,y^b}\right)\sigma_{y,a}^2+\frac{\beta^4}{N}\sigma_{y,a}^2\sigma_{y,b}^2 \quad \textbf{(A-13)}$$

Because, $H_a\sigma_{x,y^a}=H_a\mathbf{E}\left[x_k y_k^a\right]=\mathbf{E}\left[H_a x_t y_t^a\right]=\mathbf{E}\left[y_t^a y_t^a\right]=\sigma_{y^a}^2$, (A-13) can be evaluated as

$$\operatorname{cov}(\tilde{R}_i^{a,b},\tilde{R}_i^{a,b})=\operatorname{cov}(R_i^{a,b},R_i^{a,b})+\frac{2\beta^2}{N}\left(\sigma_{y,a}^2\sigma_{y,b}^2+H_aF^{2i}\sigma_{x,y^a}\sigma_{y,a}^2\delta_{ab}\right)+\frac{\beta^4}{N}\sigma_{y,a}^2\sigma_{y,b}^2 \quad \textbf{(A-14)}$$

in which the effect of noise is in the order of 4 of β, the noise ratio applied on the standard deviation of the outputs. It can be inferred from (A-14) that in the diagonal elements, the parameter

with noise converges to a nonzero constant value by increasing *i*. In addition, all the diagonal elements of $\Delta^{v}_{\Sigma_R}$, in presence of noise, are non-zero, since the two last terms of (A-14) are positive as shown in the following.

The β^2 factor in (A-14) can be rewritten as

$$\sigma^2_{y,a}\sigma^2_{y,b} + H_a F^{2i}\sigma_{x,y^a}\sigma^2_{y,a}\delta_{ab} = \begin{cases} \sigma^2_{y,a}\sigma^2_{y,b} & a \neq b \\ \sigma^2_{y,a}\sigma^2_{y,a} + H_a F^{2i}\sigma_{x,y^a}\sigma^2_{y,a} & a = b \end{cases}.$$

Because $H_a F^{2i}\sigma_{x,y^a} = \mathbf{E}\left[y^a_k y^a_{k-2i} \right]$ and $\sigma^2_{y,a} = \mathbf{E}\left[y^a_k y^a_k \right]$, by using the Cauchy-Schwartz inequality

$$\left|\mathbf{E}\left[y^a_k y^a_{k-2i} \right]\right| \leq \mathbf{E}\left[y^a_k y^a_k \right]^{1/2} \mathbf{E}\left[y^a_{k-2i} y^a_{k-2i} \right]^{1/2}$$

in which $\mathbf{E}\left[y^a_{k-2i} y^a_{k-2i} \right] = \mathbf{E}\left[y^a_k y^a_k \right]$. Thus, the β^2 factor is always non-negative. The β^4 factor in (A-14) is also always positive and therefore the diagonals of $\Delta^{v}_{\Sigma_R}$ are always nonzero if $\beta \neq 0$.

A.3 Relation between $\Delta^{v}_{\Sigma_R}$ and the covariance matrix of the residual

In view of (3-18), matrix *T* can be defined that

$$vec(\tilde{\mathbf{H}}_p) = T vec(\tilde{R})$$

in which $\tilde{R}$ is a matrix containing $\tilde{R}_i$. By considering (3-23), the covariance of the residual vector $\tilde{\zeta}^e_N$ from the measurements with added noise can be evaluated as

$$\begin{aligned} \mathrm{cov}(\tilde{\zeta}^e_N, \tilde{\zeta}^e_N) = N\,\mathbf{E}\Big[\big(\mathbf{I}\otimes S(\theta_0)\big) T \mathrm{vec}(\tilde{R}) \mathrm{vec}(\tilde{R})^T T^T \big(\mathbf{I}\otimes S(\theta_0)\big)^T \Big] \\ -N\,\mathbf{E}\Big[\big(\mathbf{I}\otimes S(\theta_0)\big) T \mathrm{vec}(\tilde{R}) \Big] \mathbf{E}\Big[\big(\mathbf{I}\otimes S(\theta_0)\big) T \mathrm{vec}(\tilde{R}) \Big]^T \end{aligned} \qquad \textbf{(A-15)}$$

since $\mathrm{vec}(S(\theta_0)^T \tilde{\mathbf{H}}_p) = \big(\mathbf{I}\otimes S(\theta_0)\big) T\, \mathrm{vec}(\tilde{R})$ in which $\otimes$ represents the Kronecker product. (A-15) is rewritten as

$$\begin{aligned}\operatorname{cov}(\tilde{\zeta}_N^e, \tilde{\zeta}_N^e) &= N\left(\mathbf{I}\otimes S(\theta_0)\right) T\,\mathbf{E}\left[\operatorname{vec}(\tilde{R})\operatorname{vec}(\tilde{R})^T\right] T^T\left(\mathbf{I}\otimes S(\theta_0)\right)^T \\ &\quad -N\left(\mathbf{I}\otimes S(\theta_0)\right) T\,\mathbf{E}\left[\operatorname{vec}(\tilde{R})\right]\mathbf{E}\left[\operatorname{vec}(\tilde{R})\right]^T T^T\left(\mathbf{I}\otimes S(\theta_0)\right)^T \\ &= N\left(\mathbf{I}\otimes S(\theta_0)\right) T\left(\mathbf{E}\left[\operatorname{vec}(\tilde{R})\operatorname{vec}(\tilde{R})^T\right]-\mathbf{E}\left[\operatorname{vec}(\tilde{R})\right]\mathbf{E}\left[\operatorname{vec}(\tilde{R})\right]^T\right) T^T\left(\mathbf{I}\otimes S(\theta_0)\right)^T\end{aligned} .$$

In view of (A-9),

$$\mathbf{E}\left[\operatorname{vec}(\tilde{R})\operatorname{vec}(\tilde{R})^T\right]-\mathbf{E}\left[\operatorname{vec}(\tilde{R})\right]\mathbf{E}\left[\operatorname{vec}(\tilde{R})\right]^T = \operatorname{cov}(\tilde{R},\tilde{R}) = \Delta_{\Sigma_R}^v + \operatorname{cov}(R,R).$$

Therefore, the covariance matrix of the residual with additional noise can be defined as

$$\operatorname{cov}(\tilde{\zeta}_N^e, \tilde{\zeta}_N^e) = \operatorname{cov}(\zeta_N^e, \zeta_N^e) + \Delta_{\Sigma_\zeta}^v$$

in which

$$\Delta_{\Sigma_\zeta}^v = N\left(\mathbf{I}\otimes S(\theta_0)\right) T \Delta_{\Sigma_R}^v T^T\left(\mathbf{I}\otimes S(\theta_0)\right)^T.$$

It should be noted that since $\Delta_{\Sigma_R}^v$ is a positive definite matrix, $\Delta_{\Sigma_\zeta}^v$ is also positive definite based on its symmetric definition in terms of $\Delta_{\Sigma_R}^v$. Moreover, as mentioned before, the factor N removes the effect of number of samples in terms of $\frac{1}{N}$ in (A-8)and the final residual covariance matrix is independent on the number of samples.

Appendix B Basis of System Matrices

Lemma B.1: The acquired measurement y_k from a system such as (3-3) can be associated to other systems as well. In other words, the evaluated system matrices from a measured data, are not unique.

Proof: In order to demonstrate this non-uniqueness of the basis of the system matrices, assume measurement y_k is acquired from system (3-3). This measurement can be associated to any system with the formation

$$\begin{cases} \tilde{x}_{k+1} = \tilde{F}\tilde{x}_k + \tilde{w}_k \\ y_k = \tilde{H}\tilde{x}_k + \varepsilon_k \end{cases} \quad \textbf{(B-1)}$$

where

$$\tilde{x}_k = Tx_k, \quad \tilde{F} = TFT^{-1}, \quad \tilde{H} = HT^{-1} \qquad \text{and} \qquad \tilde{w}_k = Tw_k \quad \textbf{(B-2)}$$

in which T is any invertible matrix. By substituting the matrices of (B-2) into (B-1), the system (3-3) will be acquired and therefore the system matrices and measurements can be defined in any basis based on definition of T in (B-2).

Lemma B.2: Although the basis of the system matrices is not unique, the eigenstructure (λ, φ) of the state transition matrix is unique.

Proof: The eigenequation of F writes as

$$F\phi_j = \lambda_j \phi_j \qquad \text{for} \qquad j = 1 \cdots n \quad \textbf{(B-3)}$$

which in view of (B-2) is expanded as $(TFT^{-1})(T\phi_j) = \lambda_j (T\phi_j)$ or similarly as $\tilde{F}(T\phi_j) = \lambda_j (T\phi_j)$. By comparing the eigenequation of $\tilde{F}$, i.e. $\tilde{F}\tilde{\phi}_j = \tilde{\lambda}_j \tilde{\phi}_j$, with $\tilde{F}(T\phi_j) = \lambda_j (T\phi_j)$, it follows

$$\tilde{\phi}_j = T\phi_j \quad \text{and} \quad \tilde{\lambda}_j = \lambda_j . \quad \textbf{(B-4)}$$

The observed eigenvectors of the alternative basis are also written as

$$\tilde{\varphi}_j = \tilde{H}\tilde{\phi}_j = (HT^{-1})(T\phi_j) = H\phi_j = \varphi_j . \quad \textbf{(B-5)}$$

Hence, based on (B-4) and (B-5), the observed eigenstructure of the system is unique and independent of the system basis.

B.1 Modal basis

Since the system matrices are not unique, different basis can be assumed for the system from a specific measurement. One of the practical and appropriate basis of the system is the modal basis which is used often in the theoretical development of the method. The modal basis can be achieved by choosing the invertible matrix as

$$T^{-1} = \emptyset \text{, where } \emptyset = \begin{bmatrix} \phi_1 & \cdots & \phi_n \end{bmatrix}. \quad \textbf{(B-6)}$$

The eigenequation (B-3) is extended as

$$F\emptyset = \emptyset\Delta \quad \textbf{(B-7)}$$

where

$$\Delta = \begin{bmatrix} \lambda_1 & & 0 \\ & \ddots & \\ 0 & & \lambda_n \end{bmatrix}. \quad \textbf{(B-8)}$$

Based on definition $T^{-1} = \emptyset$, (B-7) is rewritten as $FT^{-1} = T^{-1}\Delta$ which by premultiplying with T results in the modal basis state transition matrix $\tilde{F}_\lambda$, where

$$\tilde{F}_\lambda = \Delta . \quad \textbf{(B-9)}$$

The observation matrix in the modal basis, i.e. $\tilde{H}_\lambda$, is similarly computed as

$$\tilde{H}_\lambda = HT^{-1} = H\emptyset = \Phi . \quad \textbf{(B-10)}$$

By this definition, the observability matrix (3-15) can be defined in modal basis as

$$O_{p+1} = \begin{bmatrix} \Phi \\ \Phi\Delta \\ \vdots \\ \Phi\Delta^{p} \end{bmatrix}. \qquad \textbf{(B-11)}$$

Appendix C Invariance Property of the χ^2-test

Lemma C.3: The χ^2-tests (3-33) and (3-35) will not change based on scaling of residual. Therefore, the non-uniqueness of the basis and the left singular vector $S(\theta_0)$.

Proof: By assuming the residual vector ζ scaled as $T\zeta$, where T is an invertible matrix, the Jacobian and Covariance matrices will be consistently TJ and $T\Sigma T^T$. Thus, the χ^2-test (3-33) writes as

$$\begin{aligned}\chi^2 &= (T\zeta)^T (T\Sigma T^T)^{-1} TJ \left((TJ)^T (T\Sigma T^T)^{-1} TJ\right)^{-1} (TJ)^T (T\Sigma T^T)^{-1} T\zeta \\ &= \zeta^T \Sigma^{-1} J \left(J^T \Sigma^{-1} J\right)^{-1} J^T \Sigma^{-1} \zeta\end{aligned} \quad \textbf{(C-1)}$$

which is equivalent to (3-33). Since the non-parametrical test is derived from the parametrical test, it inherits the invariance property.

Appendix D S101 Bridge Model Modeshapes

The modeshapes from the S101 bridge model are presented in the following figure.

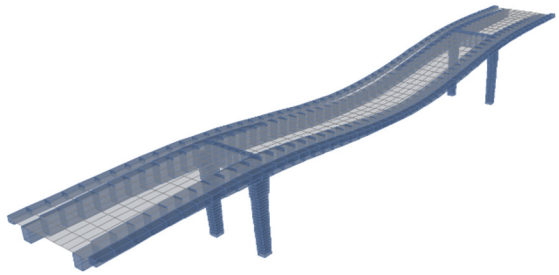

1st modeshape (bending 1)

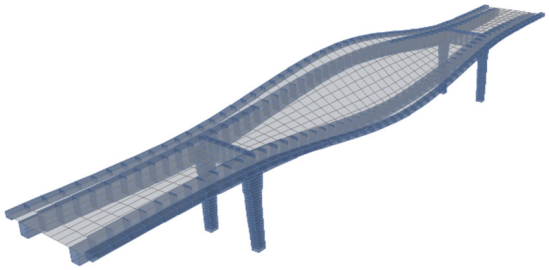

2nd modeshape (torsional 1)

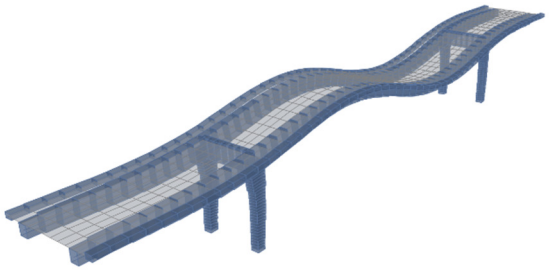

3rd modeshape (bending 2)

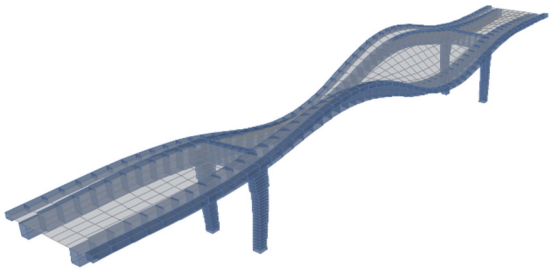

4th modeshape (torsioanl 2)

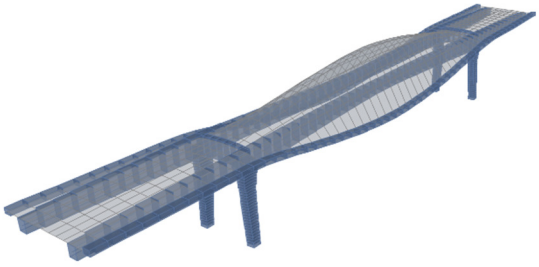

5th modeshape (local - not detected)

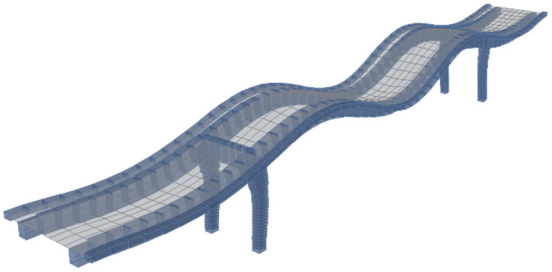

6th modeshape (bending 3)

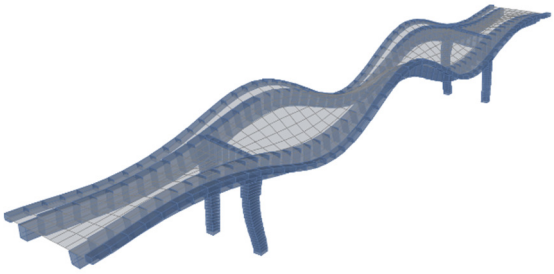

7th modeshape (torsional 3)

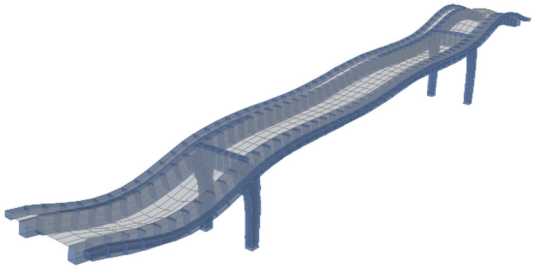

8th modeshape (bending 4, local on side spans)

Figure D.1 Modeshapes of the S101 bridge model

Appendix E The Data Acquisition System of the Yellow Frame

E.1 Data acquisition (DAQ) system

The DAQ system employed in this test is a hardware unit composed of IOTech®[2] data acquisition cards. The acquisition component is DAQ-Book/216. This system has an A/D converter of 16 bits with a maximum data transfer rate of 800Kbytes/sec. This system has 16 programmable input channels. The IOTech DBK13 card is used for the input with amplification capability of 10, 100 or 1000x. Moreover, there is an anti-aliasing filter from a DBK18 card included in this set. This system is shown in Figure E.1.

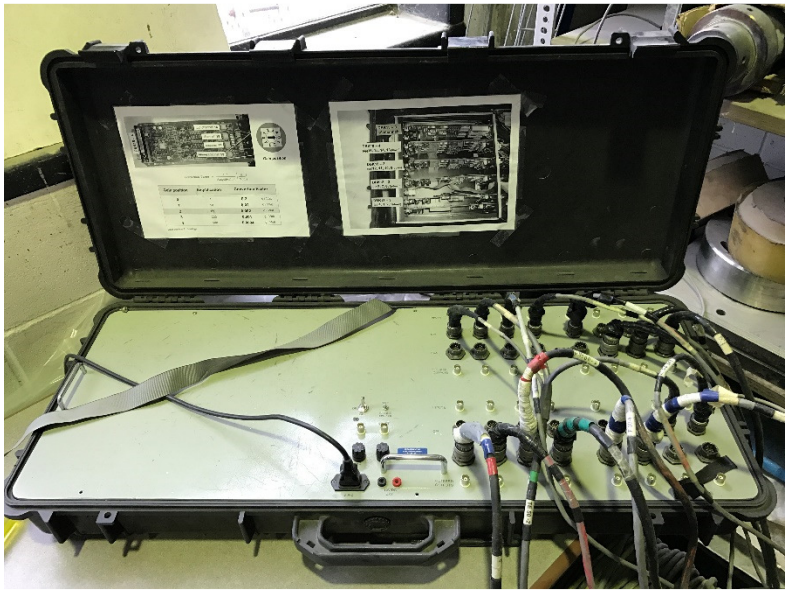

Figure E.1 DAQ system of the Yellow frame structure

E.2 Sensors and data acquisition software

There are two different types of force balanced accelerometers used in the testing of this structure. They are manufactured by Kinemetrics®[3]. One of these sensor types is FBA-11 which is a uniaxial accelerometer with the range of +/- 1.0 g. The other type is Epi-sensor which is a triaxial

[2] National Instruments http://www.ni.com/
[3] Kinemetrics http://www.kinemetrics.com/

accelerometer with the selectable range of +/-0.25g upto +/-4 g. In this structure, 9 FBA-11 sensors are used on the structure and 6 Epi-sensors are located on the ground (3 sensors) and on the structure (12 sensors). Two of these sensors are illustrated in Figure E.2.

(a) (b)

Figure E.2 Two sensors used in instrumenting the Yellow frame: (a) FBA-11 and (b) Epi-sensor

In order to acquire the data from the DAQ system, DaisyLab®[4], a graphical data acquisition software was used. Several programs and tools were used and further developed in the DaisyLab software to acquire the data from the sensors, scale them and write them to the hard disks.

[4] MC Measurement Computing http://www.mccdaq.com/

Appendix F Damage configurations of the Yellow frame

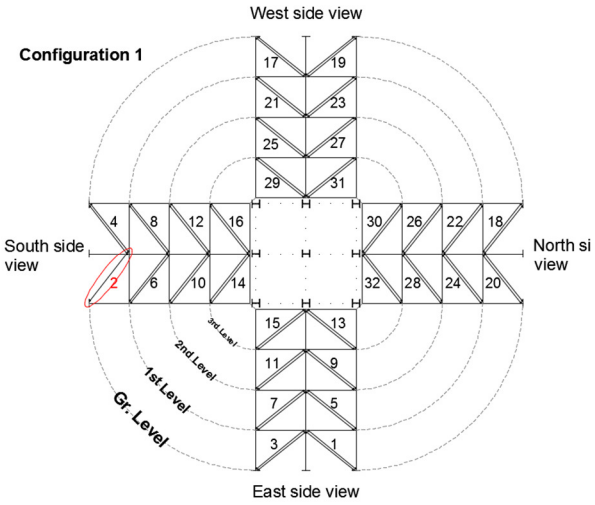

C1

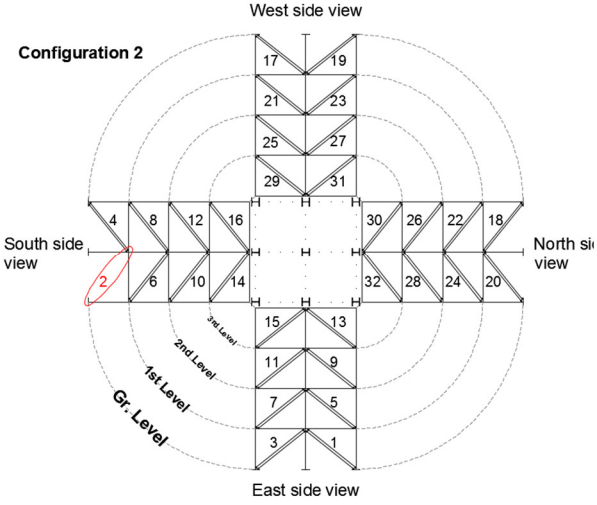

C2

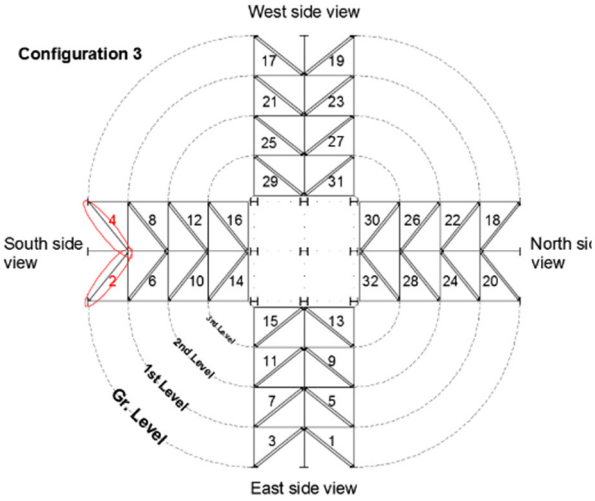

C3

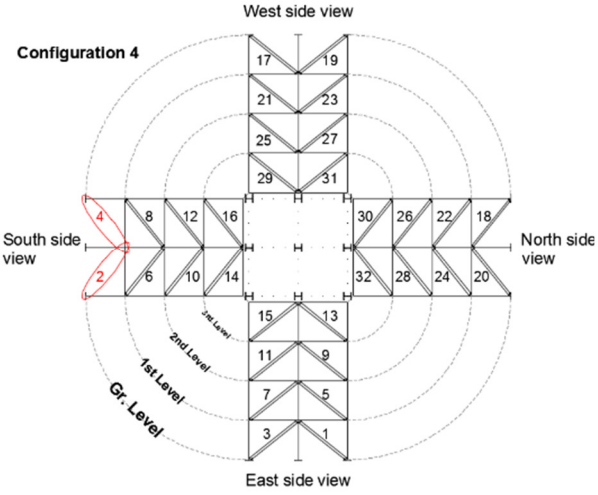

C4

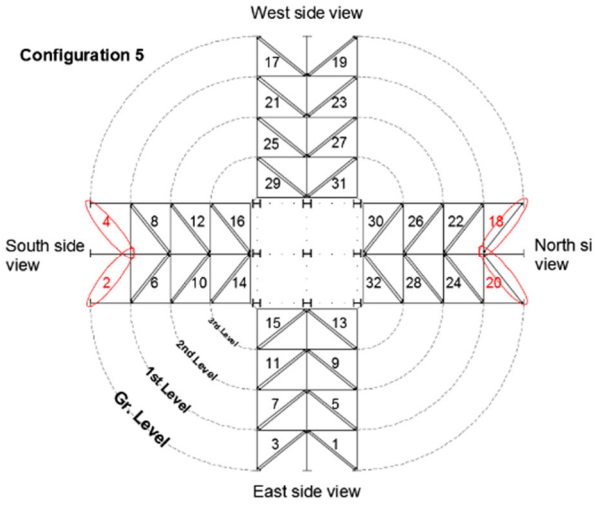

C5

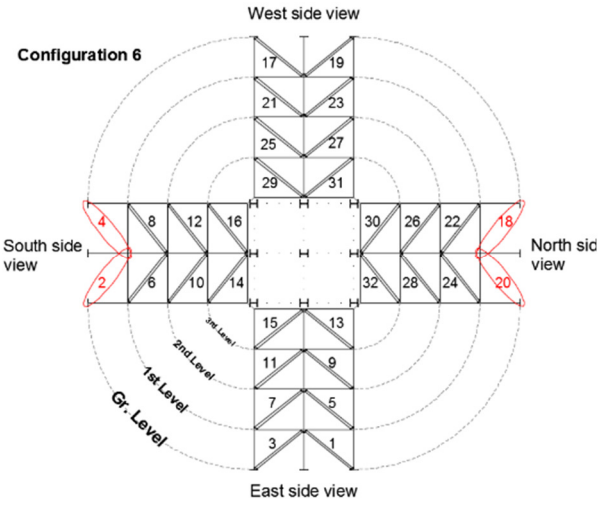

C6

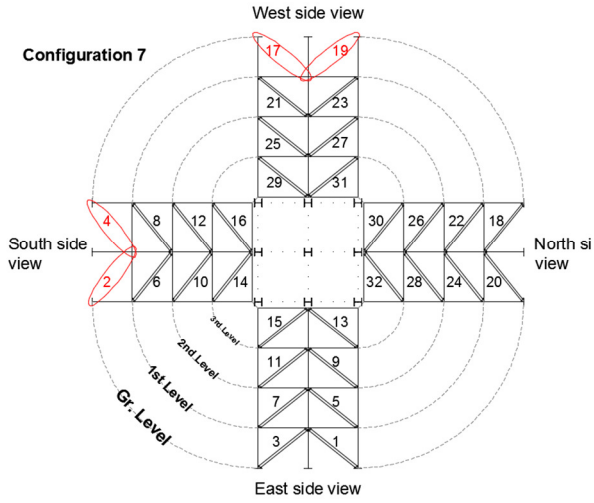

C7

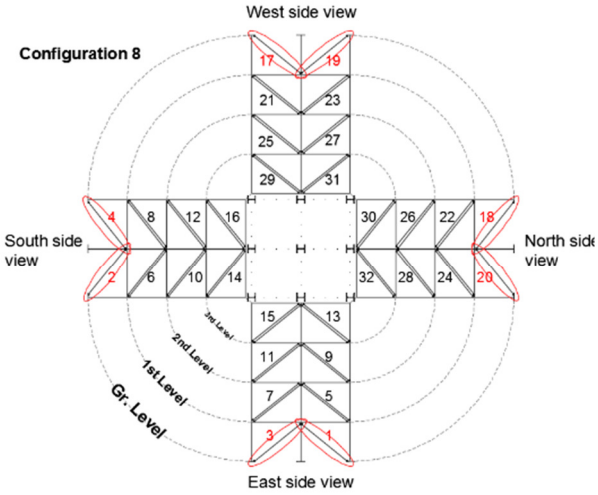

C8

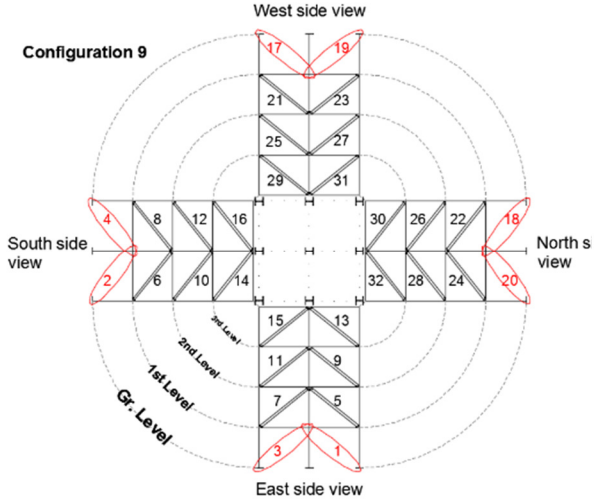

C9

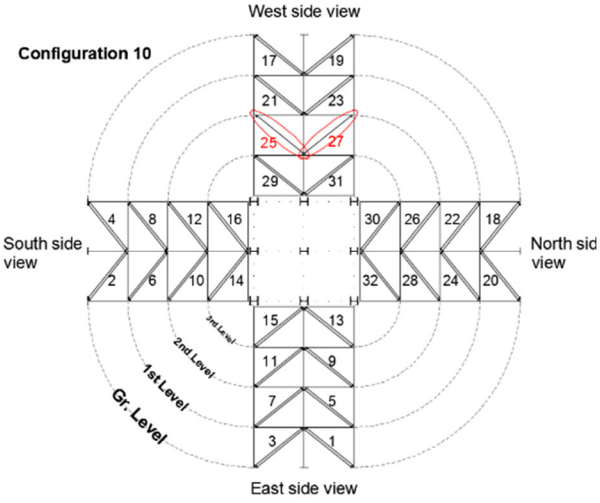

C10

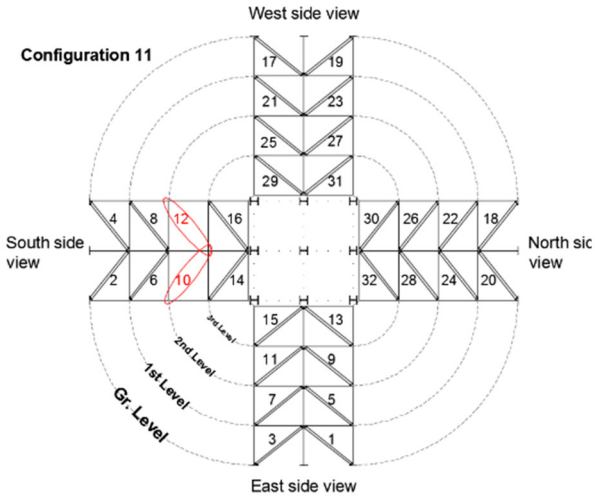

C11

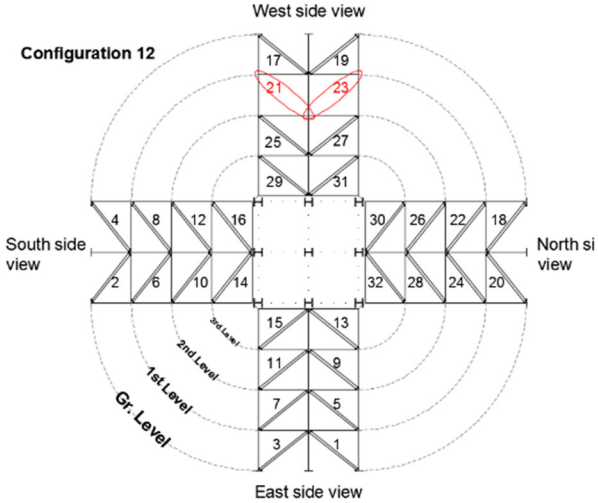

C12

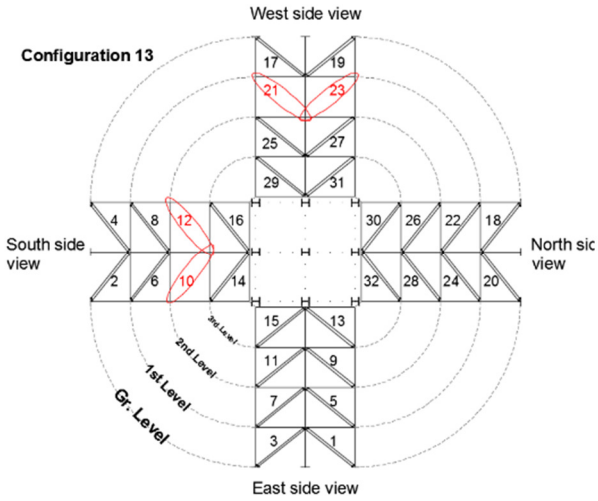

C13

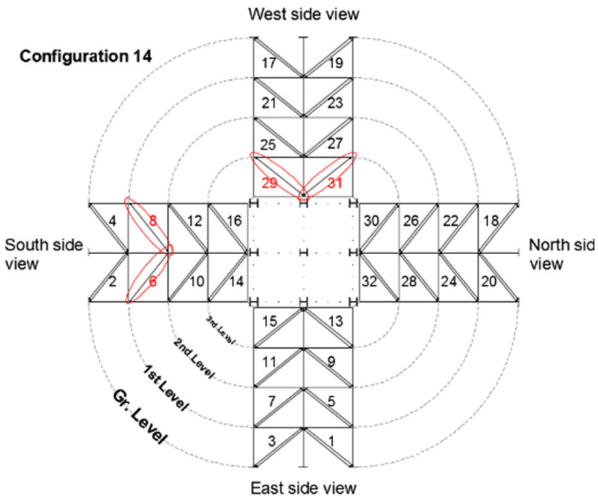

C14

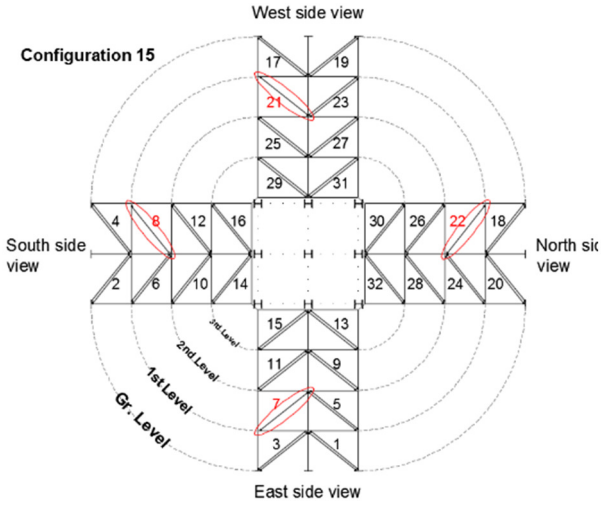

C15

Figure F.1 Damage configurations of the Yellow frame

Appendix G Flowchart of the SSDD and SSDL Technique

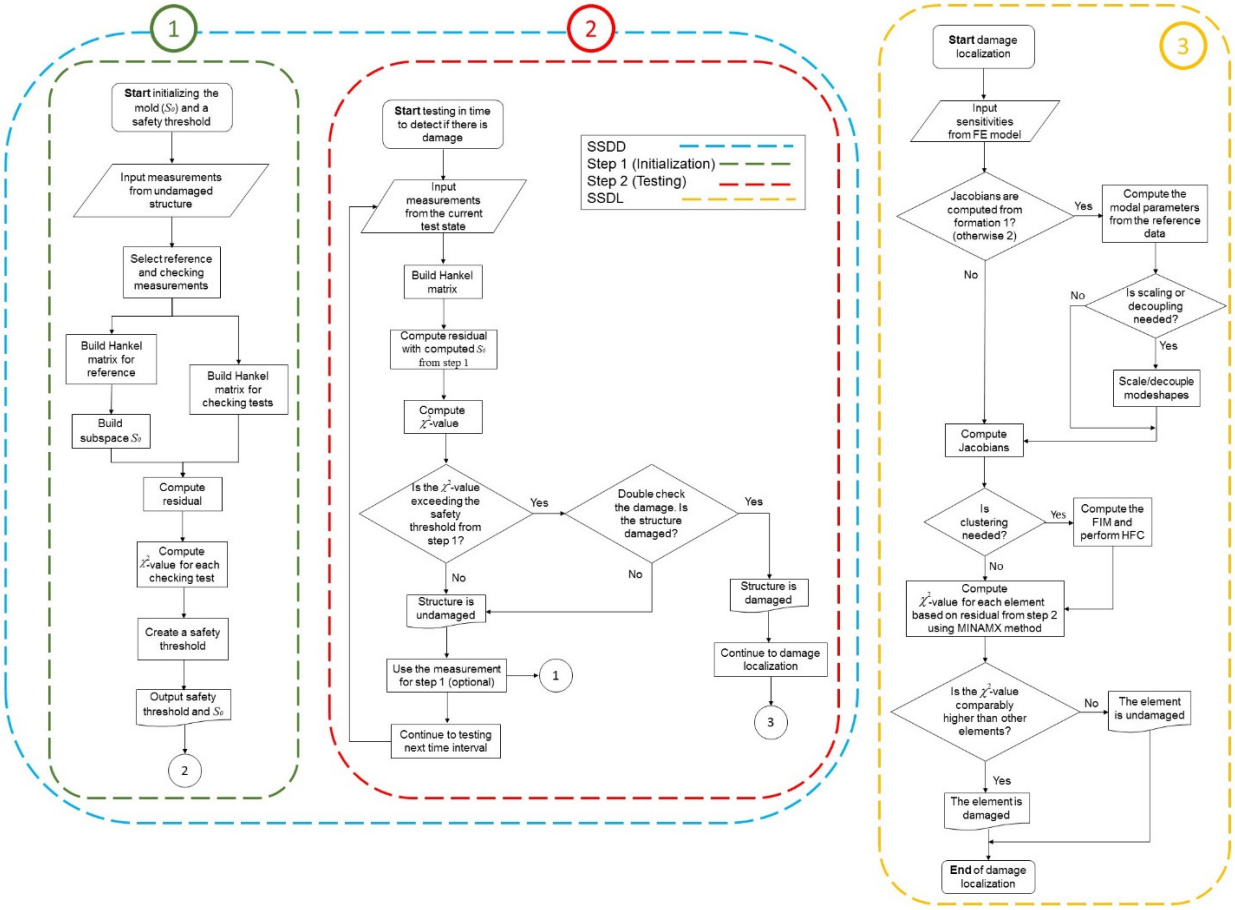

(a)

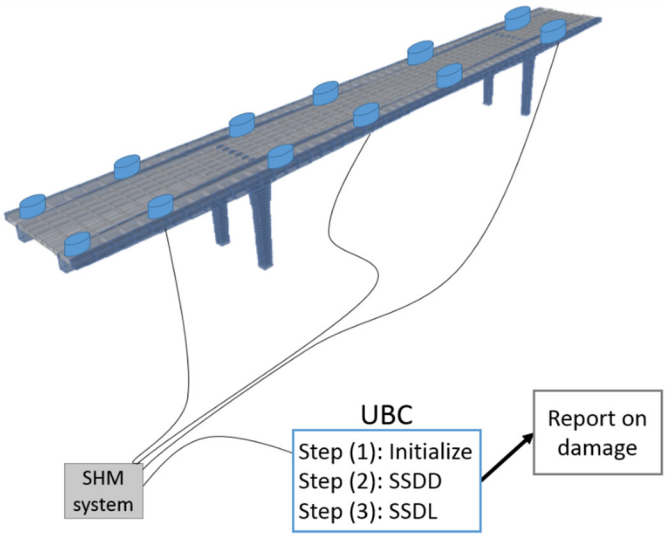

(b)

Figure G.1 (a) Flowchart of the SSDD and SSDL technique, (b) Schematic design of a basic structural health monitoring system of a bridge

G.1 Steps of the flowchart

In view of 5.5 and Figure G.1.a, the first step, i.e. step (1), is to create the subspace S_0 and a safety threshold from a set of measurements acquired from the undamaged structure. Firstly a period of measurement is chosen to serve as the reference state to build the subspace S_0. Subsequently, another set of measurements from the undamaged structure is chosen to create a safety threshold. In the next step, i.e. step (2) the real-time monitoring is performed for each time interval, e.g. 30 min, to test the current unknown condition of the structure using SSDD method. In this step, if the damage is identified, it will be rechecked and then the result will be reported. In case of detecting the damage, the next step is to localize the damage in the structure from step (3). However, if there is no damage detected, this measurement can be used in step (1) too, for creating the subspace S_0 or the safety threshold. Finally, the test continues to testing the next time interval in step (2).

Figure G.1.b shows a schematic design of a basic SHM system of a bridge. The data is collected by the sensors and sent to central system. This central system will send the data to a server located in University of British Columbia. In here, the steps (1) to (3) are performed and the results are reported.